



# 16ENV10 MetroRADON

Deliverable D2

Report on the influence of thoron on radon monitors used in Europe including (i) procedures for checking their sensitivity to thoron, (ii) recommendations on the construction of radon monitors that are not sensitive to thoron and (iii) technical approaches aimed at reducing thoron-related bias in the radon signal in existing monitors

Sofiiski Universitet Sveti Kliment Ohridski (SUBG)

Due date: February 2020  
Submission: June 2020

**EMPIR**



The EMPIR initiative is co-funded by the European Union's Horizon 2020 research and innovation programme and the EMPIR Participating States

## Table of contents

|  |    |
|--|----|
| LIST OF AUTHORS.....   | 3  |
| Introduction .....   | 4  |
| Task 2.1: Ensuring traceability of the secondary thoron reference instruments used in the experimental research to the primary thoron measurement system at IRSN ..... | 4  |
| Activity 2.1.1 .....   | 5  |
| Activity 2.1.2 .....   | 5  |
| Task 2.2: Investigation of the influence of thoron on radon measurements and calibrations .....  | 6  |
| Activity 2.2.1 .....   | 6  |
| Activity 2.2.2 .....   | 9  |
| Activity 2.2.3 .....   | 14 |
| Task 2.3: Development of techniques to reduce the influence of thoron on radon measurements and calibrations .....   | 20 |
| Activity 2.3.1 .....   | 20 |
| Activity 2.3.2 .....   | 23 |
| Activity 2.3.3 .....   | 29 |
| Activity 2.3.4 .....   | 30 |
| Activity 2.3.5 .....   | 34 |
| Summary .....  | 35 |
| References .....   | 37 |

## Annexes

## **LIST OF AUTHORS**

**SUBG:** D. Pressyanov, K. Mitev, I. Dimitrova, S. Georgiev, Ch. Dutsov

**IRSN:** N. Michielsen, S. Bondiguel, J. Malet

**CEA:** P. Cassette, B. Sabot

**STUK:** T. Turtiainen, O. Holmgren, R. Dehganzada

**BEV-PTP:** M. Stietka, H. Wiedner

## Introduction

This deliverable refers to WP2: Influence of thoron ( $^{220}\text{Rn}$ ) and its progeny on radon end-user measurements and radon calibrations. The aim of this work package is to investigate and to reduce the influence of thoron ( $^{220}\text{Rn}$ ) and its progeny on radon ( $^{222}\text{Rn}$ ) end-user measurements and radon calibrations.

The influence of thoron on the radon activity concentration measurements has already been observed with some radon monitors. This influence, if not properly corrected, can introduce bias in the radon risk estimates or can generate false alarms if the detectors are used to identify dwellings with radon concentrations that exceed reference/action levels. Both thoron and its progeny ( $^{212}\text{Pb}$ ,  $^{212}\text{Bi}$ + $^{212}\text{Po}$ / $^{208}\text{Tl}$ ) need to be taken into account, as the generated thoron progeny can remain within the detector volume long after the decay of the parent thoron atoms.

The work related to WP2 was structured in three tasks, each task being subdivided into several activities. This deliverable report summarizes the research and outcomes of each activity.

Within the report the influence of thoron and its progeny on active monitors and passive detectors was studied. The following definitions are used:

- *Active monitor* refers to a radon measuring instrument that runs on electric power.
- *Passive detector* refers to radon measuring instrument that runs without electric power.
- *Integrated activity concentration* refers to integrated activity concentration over time. This is the same as exposure and the unit commonly used in the report is  $\text{Bq h m}^{-3}$ .

Sampling employed by active monitors may be passive or active. The measurement method employed by active monitors may be continuous or integrated short term (IEC 61577-1, ISO 11665-1).

Sampling employed by passive detectors is passive. The measurement method is integrated long-term (see ISO 11665-1).

### **Task 2.1: Ensuring traceability of the secondary thoron reference instruments used in the experimental research to the primary thoron measurement system at IRSN**

*The aim of this task is to calibrate the secondary thoron reference instruments used in the laboratories at IRSN, BEV-PTP, SUBG and STUK against the existing primary thoron measurement system at IRSN and thus to ensure traceability to the IRSN primary system of the thoron measurements made by the partners. These calibrated instruments will be used in Task 2.2 to investigate the influence of thoron on radon measurement devices.*

This task provides a model for the first step in the procedures for testing the sensitivity of radon monitors to thoron: ensuring the traceability of the reference instruments used for thoron measurements during tests to the primary thoron measurement system at IRSN. In the same time the task provides procedures to assess the homogeneity of the thoron atmosphere in the exposure chambers used for test measurements.

### **Activity 2.1.1**

*IRSN and SUBG will establish and evaluate the reference thoron atmospheres in their reference test chambers. The range of thoron activity concentrations that can be created in both chambers will be assessed.*

*IRSN will assess the homogeneity of the thoron atmosphere in their BACCARA 1 m<sup>3</sup> test chamber using numerical simulation and experimentation. SUBG will study experimentally the inhomogeneity in their 50 L test chamber.*

The reference thoron atmospheres that can be created in the partners' test chambers were evaluated and tested. Two methods for experimental study of the thoron homogeneity in the calibration volumes have been proposed, tested and applied in the thoron calibration exercise that has been carried out at IRSN in the framework of this activity. The first method is based on capture of thoron decay products in silica aerogel powder and subsequent liquid scintillation counting of the aerogel activity. The second method is based on measurement of the density of tracks formed by <sup>220</sup>Rn and <sup>216</sup>Po in Kodak-Pathe LR-115/II solid state nuclear track detectors (SSNTDs).

Both methods were applied to study the <sup>220</sup>Rn homogeneity in an empty 50 L *AlphaGUARD* calibration container and showed that the differences in the <sup>220</sup>Rn concentration do not exceed 10 % (estimated as maximum deviation from the average value). The two methods were also applied in the thoron calibration exercise performed in the BACCARA chamber (1 m<sup>3</sup>) at IRSN with seven <sup>220</sup>Rn measuring instruments inside. The methods showed that the differences in the <sup>220</sup>Rn concentration at the center of the chamber, near the instruments' sampling points, do not exceed 10 %. However, higher differences were observed far from the instruments, for example the <sup>220</sup>Rn concentration near the upper wall of the chamber is up to 66 % higher than this at the center. The results of the studies on the methods and their applicability are described in a paper submitted for publication in *Applied. Radiat. Isot* [1], presented as Annex I. These methods have also been applied in tests of the thoron homogeneity of the STUK thoron exposure facility (Annex II).

To study the homogeneity of the thoron activity in the BACCARA radon chamber, IRSN performed a numerical study using the computational fluid dynamics code ANSYS/FLUENT. A fan was implemented in the model and the influence of the position of the thoron inlet as well as the position of instruments placed in the chamber was studied. Details of the equations used, the validation performed and the results are given in Annex III. Airflow velocities in the chamber explain the homogeneous thoron concentration in the center of the chamber as well as some higher concentrations close to the wall, in front of the fan and at the bottom of the chamber as observed during the experiment (Annex I).

### **Activity 2.1.2**

*IRSN, SUBG and STUK will jointly organise an exercise to calibrate their secondary thoron reference instruments for activity concentrations of 10<sup>2</sup>-10<sup>6</sup> Bq/m<sup>3</sup> at the IRSN radon/thoron calibration laboratory at Saclay, France. Information from A2.1.1 on the homogeneity of the thoron atmosphere will be taken into account.*

*SUBG will participate in the calibration with its reference thoron monitors – AlphaGUARD 2000 RnTn Pro and RAD 7, whilst STUK will participate with its thoron monitors: AlphaGUARDsand Lucas cells (Pylon Inc). In addition BEV-PTP will send their AlphaGUARD to IRSN for calibration.*

The calibration exercise was carried out in May 2018. Three different constant <sup>220</sup>Rn reference atmospheres, 10 kBq m<sup>-3</sup>, 46 kBq.m<sup>-3</sup> and 240 kBq m<sup>-3</sup>, were created, so that a wide range of <sup>220</sup>Rn activity concentrations was

covered and seven instruments, from BEV-PTP, IRSN, STUK and SUBG were calibrated (four AlphaGUARD detectors and three RAD 7 detectors). The ratios between the  $^{220}\text{Rn}$  activity concentration measured by the instrument and the reference activity concentration, measured by the thoron reference system at IRSN were close to 1 for the four AlphaGUARD detectors and around 0.6 for the three RAD7 detectors. The calibration factor of the AlphaGUARD detectors was found to change with the thoron activity concentration. The full report of the calibration exercise is given as Annex IV.

## Task 2.2: Investigation of the influence of thoron on radon measurements and calibrations

*The aim of this task is to investigate the influence of thoron on radon measurements and calibrations through the study of the sensitivity to thoron of a large sample group of radon monitors used in Europe, in order to understand and potentially correct for the influence of thoron on the performance of the radon monitors.*

A large number of radon monitors are available in the laboratories at BEV/PTP, CEA, IRSN, STUK and SUBG. Continuous (active) as well as integrated (passive) measurement devices will be investigated, with each partner addressing the instruments most commonly employed by end-users in their country. The experimental study will involve exposure of monitors to reference thoron and radon plus thoron concentrations and theoretical models and analysis will also be employed to determine, understand and potentially correct for the influence of thoron on the performance of the radon monitors.

### Activity 2.2.1

*IRSN, SUBG and STUK will study the influence of thoron on active radon monitors. Measurements will be performed in both thoron and radon plus thoron atmospheres using the secondary reference instruments calibrated in A2.1.2. At least 10 instruments available at IRSN, CEA, SUBG, STUK will be studied, for example AlphaGUARD (different types), DoseMan, radhomeHR3, BARASOL, monitors with Lucas cells, RAD7 etc.*

*Theoretical models and analysis will be employed by IRSN, SUBG and STUK to determine, understand and potentially correct for the influence of thoron on the performance of the radon monitors.*

STUK, SUBG and IRSN performed studies on the influence of thoron on active radon monitors. The studies were performed in both purely thoron and mixed radon plus thoron atmospheres, using the secondary reference instruments (AlphaGUARDs) calibrated in task A2.1.2. In total 16 instruments of different types were tested at the three laboratories. The results are summarized in Table 1. Detailed information about the methods, the experimental set-ups and the obtained results is given in Annex V and Annex VI. The influence of thoron on the radon signal was quantified by the cross-interference  $CI$ :

$$CI = \frac{E_{Rn}}{E_{Tn}} \times 100 \% \quad (1)$$

where  $E_{Rn}$  is the reported radon activity concentration (integrated activity concentration in the case of passive radon detectors), corrected for background and  $E_{Tn}$  is thoron activity concentration (integrated activity concentration in the case of passive radon detectors) during the exposure. In the case of active monitors two values of cross-interference are estimated (details in Annex V):

- Initial cross-interference  $CI$  (*initial*) which corresponds to the prompt response to thoron of the active monitors that is due to the sensitivity of the monitors to  $^{220}\text{Rn}$  and  $^{216}\text{Po}$ .  $CI$  (*initial*) would characterize the response of the monitor in case of a spike in thoron concentration;

- Final cross-interference  $CI$  (*final*) – in case of continuous thoron exposure  $CI$  increases due to the build-up of  $^{212}\text{Pb}$  and its decay products. After three days equilibrium is reached. Thus  $CI$  (*final*) represents the sensitivity of the monitors to thoron and all of its decay products and would characterize the response of the monitor in case of a continuous thoron exposure.

The cross-interference ( $CI$ ) results in Table 1 show that all tested active thoron monitors except for RadonEye, TSR4M and DoseMan comply with the IEC 61577-2 standard requirement for  $CI < 20\%$ .

The results suggest that, despite its short half-life, a certain amount of thoron diffuses in the detection chamber where thoron progenies can accumulate. Thoron and some alpha thoron progenies can be registered by the instrument as radon and its progenies and then give a false signal of a presence of radon. Due to the 10.64 h half-life of  $^{212}\text{Pb}$ , the full influence of thoron on a radon signal will be theoretically reached after 3 days. Also, when thoron is not present anymore in the atmosphere,  $^{212}\text{Pb}$  progenies accumulated in the detection chamber will take 3 days to disappear. Therefore, a minimum of a three day measurement period with a high thoron activity concentration (around  $10\text{ kBq}\cdot\text{m}^{-3}$  or more) is recommended to determine the final  $CI$ , instead of the 4 hours at  $1\ 000\text{ Bq}\cdot\text{m}^{-3}$  required in the IEC 61577-2 standard.

Table 1 – Results of the studies of the influence of thoron on active radon monitors.

| Instrument                                 | Tested at: | s/n           | Test dates                          | CI (initial)   | CI (final)     |
|--|------------|---------------|-------------------------------------|----------------|----------------|
| AlphaGUARD 2000 RnTn Pro                   | IRSN       | EF2283        | 18-22 May 2018<br>22-24 May 2018    |                | 1.1 %<br>0.6 % |
| DoseMan Fast Mode                          | IRSN       | DM357         | 18-22 May 2018<br>22-24 May 2018    | 11 %<br>18 %   | 36 %<br>39 %   |
| DoseMan Slow Mode                          | IRSN       | DM357         | 18-22 May 2018<br>22-24 May 2018    | 14 %<br>26 %   | 41 %<br>48 %   |
| AlphaE                                     | STUK       | 000260        | 5–10 Jun 2019<br>31 Jul–5 Aug 2019  | 6.5 %<br>8.9 % | 9.3 %<br>12 %  |
|  | STUK       | 000542        | 11–17 Jun 2019<br>31 Jul–5 Aug 2019 | 5.6 %<br>8.7 % | 9.2 %<br>13 %  |
|  | STUK       | 000499        | 5–9 Dec 2019                        | 5.7 %          | 8.6 %          |
|  |            |               |                                     |                |                |
| AlphaE                                     | SUBG       | 000499        | 14–17 Oct 2019                      | 4.5 %          | 13.7 %         |
|  |            |               | 22–28 Oct 2019                      | 11.5 %         | 17.0 %         |
|  |            |               | 16–20 Sep 2019                      | 10.0 %         | 17.1 %         |
|  |            |               | 26–30 Sep 2019                      | 12.7 %         | 18.7 %         |
|  |            |               | 04–08 Nov 2019                      | 15.5 %         | 20.2 %         |
| AlphaGUARD PQ2000 Pro<br>AlphaGUARD PQ2000 | STUK       | EF1641        | 6–9 Aug 2019                        | 5.1–11 %       | 7.2 %          |
|  | STUK       | EF0408        | 22–27 Jan 2020                      | 4.6-9.2 %      | 6.0 %          |
| RadonEye + <sup>2</sup>                    | STUK       | PE21812110009 | 20–23 August 2019                   | 28 %           | 42 %           |
|  | STUK       | PE21904100016 | 28 Nov–1 Dec 2019                   | 27 %           | 37 %           |
| RadonEye + <sup>2</sup>                    | SUBG       | PE21904100016 | 14–17 Oct 2019                      | 32.6 %         | 52.7 %         |
|  |            |               | 22–28 Oct 2019                      | 38.7 %         | 54.7 %         |
|  |            |               | 04–08 Nov 2019                      | 18.7 %         | 42.3 %         |
| Corentium Home                             | STUK       | 2403008304    | 20–24 Jun 2019                      |                | 1.8 %          |
|  |            |               | 24–29 Jul 2019                      |                | 2.5 %          |
| Airthings Wave                             | STUK       | 2900151289    | 28 Jun–2 Jul 2019<br>6–9 Aug 2019   |                | 1.3 %<br>2.3 % |
| Airthings Wave Plus                        | STUK       | 2930          | 24–28 Jun 2019                      |                | 2.7 %          |
|  |            |               | 24–29 Jul 2019                      |                | 3.6 %          |
| Corentium Pro                              | STUK       | 2700007355    | 3–5 Sep 2018                        | 0.2 %          | 1.2 %          |
|  |            | 2700007357    | 3–5 Sep 2018                        | 0.0 %          | 1.6 %          |
| TSR3 – Fast mode                           | SUBG       | 16014         | 16–20 Sep 2019                      | 1.0 %          | 7.7 %          |
|  |            |               | 26–30 Sep 2019                      | 1.2 %          | 12.3 %         |
| TSR3 – Slow mode                           | SUBG       | 16014         | 22–28 Oct 2019                      | 2.7 %          | 15.3 %         |
| TSR4M– Fast mode                           | SUBG       | 19015         | 22–28 Oct 2019                      | 6.2 %          | 125 %          |
|  |            |               | 16–20 Sep 2019                      | -              | 127 %          |
|  |            |               | 26–30 Sep 2019                      | -              | 186 %          |
|  |            |               | 04–08 Nov 2019                      | 11.2 %         | 114 %          |
| TSR4M– Slow mode                           | SUBG       | 19015         | 22–28 Oct 2019                      | 15.9 %         | 85.8 %         |
|  |            |               | 16–20 Sep 2019                      | -              | 69.5 %         |
|  |            |               | 26–30 Sep 2019                      | 7.9 %          | 115 %          |
|  |            |               | 04–08 Nov 2019                      | 18.7 %         | 76.4 %         |

### **Activity 2.2.2**

*CEA, IRSN, STUK, and SUBG will study the influence of thoron on passive integrating radon detectors. Measurements will be performed in both thoron and radon plus thoron atmospheres using the secondary reference instruments calibrated in A2.1.2. At least 10 detectors available at IRSN, CEA, SUBG and STUK will be studied, for example diffusion chambers with different alpha-track detectors, E-Perm electret chambers, compact disks/DVDs, etc.*

*Theoretical models and analysis will be employed by CEA, IRSN, STUK, and SUBG to determine, understand and potentially correct for the influence of thoron on the performance of the radon monitors.*

The influence of thoron on 17 types of passive integrating radon detectors was studied. The studied devices are based on solid state alpha track detectors, which is currently the most common type of detector used in radon surveys in Europe [2]. Eleven of the 17 studied devices are commercially available devices. In one of them the track detector is directly exposed to the atmosphere (bare detector), in the rest the track detector is placed in a non-hermetic housing (diffusion chamber). For most of them no data for the influence of thoron was found in literature or in the public documentation of the producer.

Two types detectors based on alpha track detection in DVD were also studied: a DVD etched at a depth greater than 80  $\mu\text{m}$  and a DVD coupled with an external radon absorber.

## Methodology

The influence of thoron on the radon signal was studied by exposure of the studied detectors to reference integrated activity concentration of thoron. The exposures were carried out at the exposure facilities of three of the project partners - STUK, Finland, SUBG, Bulgaria and IRSN, France. A detailed description of the study methodology applied by STUK is given in Annex VII, by SUBG in Annex VIII and by IRSN in Annex IX.

The most important aspects of the procedures for estimation of the sensitivity of passive radon detectors to thoron that were applied by STUK, SUBG and IRSN are the following:

- Reference integrated thoron activity concentration traceable to the thoron standard was used for exposures. In all exposure facilities the thoron activity was supplied by pumping air through a flow-through source. In the used exposure vessels a fan is situated near the inlet through which the activity is introduced, in order to achieve better homogeneity of the activity concentration of thoron.
- Homogeneity of the thoron activity concentration in the exposure chambers was tested by measurements with aerogel samplers (see Annex I). The thoron inhomogeneity at the positions for exposure of the detectors was estimated to be within 2 % for the exposure chamber at STUK and within 4 % for the exposure chamber at SUBG.
- More than one detector of each type was exposed in each exposure session (between two and ten identical detectors depending on the detector type).
- Most types of detectors were exposed in two independent exposure sessions at different activity concentrations.
- Thoron activity concentration was monitored throughout the exposure by a reference monitor. At STUK and SUBG *AlphaGUARD* PQ2000 RnTn monitors were used as reference monitors. These monitors were calibrated against the primary thoron system at IRSN in the frames of the calibration exercise organized within Activity 2.1.2 of the project (see Annex IV). At IRSN two RAD7 monitors calibrated by PTB were used. The same calibration factor was found for one of the RAD7 within Activity 2.1.2
- The exposures were carried out under typical indoor conditions. The temperature was stable in each exposure (between 21°C and 23°C in the different exposures).
- The detectors were analysed by the laboratory that provided them using the standard protocol for radon measurements.

There were some differences in the methodologies applied by the three laboratories:

- High integrated thoron activity concentration was used for the exposures at STUK and SUBG (between 2.5 MBq.h/m<sup>3</sup> and 14 MBq.h/m<sup>3</sup>) and low integrated thoron activity concentration was used at IRSN (170 kBq.h/m<sup>3</sup>).
- The exposure vessels used at STUK and SUBG are relatively small (with volumes of about 50 L and about 100 L, respectively). The exposure vessel at IRSN has a volume of 1 m<sup>3</sup>.
- For each of the detector types studied by STUK and SUBG transit detectors were used and were transported together with the exposed detectors (except when the detectors are provided and analysed at the exposure laboratory). The packaging of the transit detectors was removed at the end of the exposure of the other detectors from the same batch. In most cases the signal of the transit detectors was used to correct for the background radon exposure. No transit detectors were used for the devices studied at IRSN.

## Results

A summary of the results for the thoron cross interference (*CI*) on the signal of the passive radon detectors studied at SUBG is shown in Tables 2 and 3. The reported *CI* is estimated as the average of the *CI* of individual detectors. When the reported detector signal did not exceed the detection limit, an upper limit for the *CI* was estimated based on the estimated minimum detectable integrated activity concentration (MDAC). The *CI* uncertainties reported in Table 2 are estimated as a standard deviation of the individual *CI*. More details on the exposure conditions and results for the individual *CI* of the detectors are given in Annex VIII.

Table 2 – Cross interference (*CI*) of thoron on the radon signal for the diffusion chambers studied at SUBG. The average *CI*, the standard deviation and the *CI* range are given. When the signal is below the detection limit an upper limit for the *CI* is given, based on the minimal detectable integrated activity concentration (MDAC) of radon. The *CI* for the Raduet detector was estimated only for the low air exchange rate chamber (not taking into account the result from the high air exchange rate chamber in the pair).

| Manufacturer and detector type  | Detector description   | Number of detectors and exposures | Cross interference, % |                   |                 |
|---|--|-----------------------------------|-----------------------|-------------------|-----------------|
|   |  |                                   | av. <i>CI</i>         | <i>CI</i> st. dev | <i>CI</i> range |
| <b>Radosys, RSKS Risk</b>   | CR-39 in diffusion chamber, volume 29 cm <sup>3</sup> , height 5.5 cm                    | 8 detectors, 2 exposures          | 4.80                  | 0.65              | 4.00 – 6.23     |
| <b>„In-house“ by ISS, Italy (CR-39 by Intercast Spa, Italy in TASL holder)</b>            | PADC in diffusion chamber, diameter ≈ 5 cm, height ≈ 2 cm                                | 16 detectors, 2 exposures         | 9.35                  | 0.93              | 8.09 – 9.97     |
| <b>„In-house“ by ISS, Italy (CR-39 by Intercast Spa, Italy in Radout holder)</b>          | CR-39 in diffusion chamber, diameter 5 cm, height 2 cm                                   | 16 detectors, 2 exposures         | 4.48                  | 0.55              | 4.06 – 5.24     |
| <b>„In-house“ by ISS, Italy (CR-39 by Intercast Spa, Italy in Radout holder) (packed)</b> | CR-39 in diffusion chamber packed in 35-micron-thick LDPE, diameter 5 cm, height 2 cm    | 16 detectors, 2 exposures         | 0.23                  | 0.14              | < 0.13 - 0.48   |
| <b>Radonova, Radtrak<sup>2</sup></b>  | CR-39 in diffusion chamber, volume 25 cm <sup>3</sup> , diameter 5.4 cm                  | 4 detectors, 2 exposures          | 1.93                  | 0.39              | 1.38 – 2.08     |
| <b>Radonova, Rapidos</b>  | CR-39 in diffusion chamber, volume 65 cm <sup>3</sup> , diameter 5.4 cm                  | 3 detectors, 1 exposure           | < 0.57 (MDAC)         |                   |                 |
| <b>Radonova, Duotrak (ON)</b>   | CR-39 in diffusion chamber, volume 60 cm <sup>3</sup> , diameter 5.4 cm                  | 2 detectors, 1 exposure           | 7.8                   | 5.2               | 4.1 – 11.5      |
| <b>Radonova, Duotrak (OFF)</b>  | CR-39 in diffusion chamber, volume 60 cm <sup>3</sup> , diameter 5.4 cm                  | 2 detectors, 1 exposure           | 1.75                  | 0.32              | 1.71 – 1.79     |
| <b>Radosys, Raduet – low air exchange rate chamber only</b>                               | CR-39 in diffusion chamber, volume 25 cm <sup>3</sup> , diameter ≈ 5 cm, height ≈ 2.5 cm | 8 detectors, 2 exposures          | 1.76                  | 0.30              | 1.37 – 2.27     |
| <b>SUBG metal chambers</b>  | Kodak-Pathe LR-115/II in diffusion chamber, volume 290 cm <sup>3</sup>                   | 8 detectors,, 2 exposures         | < 0.29 (MDAC)         |                   |                 |

Table 3 – Cross interference (*CI*) of thoron on the radon signal for the DVD-based detectors studied at SUBG (more details of DVD detectors are provided in [3] and Deliverable 3). The average *CI*, the standard deviation and the *CI* range are given. When the signal is below the detection limit an upper limit for the *CI* is given, based on the minimal detectable integrated activity concentration (MDAC) of radon.

| Manufacturer and detector type  | Detector description  | Number of detectors and exposures | Cross interference ( <i>CI</i> ), % |                   |                 |
|---------------------------------|---|-----------------------------------|-------------------------------------|-------------------|-----------------|
|                                 |   |                                   | av. <i>CI</i>                       | <i>CI</i> st. dev | <i>CI</i> range |
| <b>DVDs at depth &gt; 80 µm</b> | DVD used as radon absorber and alpha track detector   | 7 detectors, 2 exposures          | < 1.6 (MDAC)                        |                   |                 |
| <b>DVDs + radon absorbers</b>   | DVD used as alpha track detector facing 2 foils of radon absorbing material (Markofol N), in a DVD case | 8 detectors, 2 exposures          | 6.3                                 | 2.5               | 3.3 – 10.5      |

A summary of the results for the thoron cross interference (*CI*) on the signal of the passive radon detectors studied at STUK is shown in Table 4. The reported *CI* is estimated as the average of the *CI* of individual detectors. The standard deviation and the range of observed *CI* for each detector type are also given. More details on the exposure conditions and results for the individual *CI* of the detectors are given in Annex VII.

Table 4 – Cross interference of thoron on the radon signal for the passive detectors studied at STUK. The average *CI*, the standard deviation and the *CI* range are given.

| Manufacturer and detector type                    | Detector description  | Number of detectors and exposures | Cross interference ( <i>CI</i> ), % |         |                 |
|---|---|-----------------------------------|-------------------------------------|---------|-----------------|
|   |   |                                   | av. <i>CI</i>                       | st. dev | <i>CI</i> range |
| <b>STUK (generic)</b>                             | Alpha-track detector in diffusion chamber                               | 6 detectors, 2 exposures          | 4.3                                 | 1.0     | 3.6 – 6.2       |
| <b>Radonova, Radtrak<sup>2</sup></b>              | CR-39 in diffusion chamber, volume 25 cm <sup>3</sup> , diameter 5.4 cm | 6 detectors, 2 exposures          | 1.5                                 | 0.5     | 0.8 – 2.2       |
| <b>AlphaRadon (generic)</b>                       | Alpha-track detector in diffusion chamber                               | 8 detectors, 2 exposures          | 7.2                                 | 0.8     | 6.5 – 8.8       |
| <b>Eurofins Radon Testing Sweden AB (generic)</b> | CR-39/PADC in diffusion chamber, diameter ≈ 6 cm, height 2 cm           | 6 detectors, 2 exposures          | 4.4                                 | 2.8     | 2.6 – 9.4       |

A summary of the results for the thoron cross interference (*CI*) on the signal of the passive radon detectors studied at IRSN is shown in Table 5. The reported *CI* is estimated as the arithmetic average of the *CI* of individual detectors. The standard deviation and the range of observed *CI* for ten devices and each detector type are also given. More details on the exposure conditions and results for the individual *CI* of the detectors are given in Annex IX.

Table 5 – Cross interference of thoron on the radon signal for the passive devices studied at IRSN. The average *CI*, the standard deviation and the *CI* range are given. “/” indicates that the detectors’ signal was below the detection limit.

| Detector type /<br>Manufacturer | Detector description  | Number of<br>detectors and<br>exposures | Cross interference ( <i>CI</i> ), % |         |                 |
|---------------------------------|---|---|-------------------------------------|---------|-----------------|
|                                 |   |   | av. <i>CI</i>                       | st. dev | <i>CI</i> range |
| <b>DPR2 / ALGADE</b>            | LR-115 in diffusion chamber (dome shape)                                | 10 detectors, 1 exposure                | /                                   | /       | /               |
| <b>DRF / ALGADE</b>             | LR-115 in diffusion chamber (dome shape)                                | 10 detectors, 1 exposure                | /                                   | /       | 7 – 7           |
| <b>EASYRAD / PEARL</b>          | CR-39 in diffusion chamber  | 10 detectors, 1 exposure                | 36                                  | 13      | 21 – 54         |
| <b>KODALPHA / ALGADE</b>        | LR-115 (bare detector)  | 10 detectors, 1 exposure                | 90                                  | 9       | 74 – 103        |
| <b>RADTRAK2 / Radonova</b>      | CR-39 in diffusion chamber, volume 25 cm <sup>3</sup> , diameter 5.4 cm | 10 detectors, 1 exposure                | 14                                  | 6       | 4 – 25          |
| <b>RAPIDOS / Radonova</b>       | CR-39 in diffusion chamber, volume 65 cm <sup>3</sup> , diameter 5.4 cm | 10 detectors, 1 exposure                | 11                                  | 2       | 7 – 15          |

### Summary of results

Except for EasyRAD and Kodalpha, the cross interference of thoron on the radon signal of all the instruments comply with the IEC 61577-2 standard requirement for *CI* < 20 %.

A low cross interference could be achieved with diffusion chambers with different constructions (in terms of volume, dimensions and inner compartments). As it is shown in Annex VIII, the cross interference cannot be predicted with a simple model of thoron penetration through an air gap.

When DVDs (or CDs) are used as a radon absorbers and detectors, the radon signal is not influenced by thoron. This is due to the fact that alpha tracks are analyzed at a depth greater than 80 μm at which no alpha-particles of thoron and its progeny could reach. When the DVD surface is used as a track detector that faces an external radon absorber (Makrofol N foils), some sensitivity to thoron is observed.

As expected by its measurement principle (bare detector) the Kodalpha shows that thoron is well registered by the detector as a radon signal.

The diffusion chambers packed in low-density polyethylene with a thickness of 35 μm showed very low thoron cross interference. Recommendations on the foils appropriate for protecting radon detectors are given in Activity 2.3.2.

No influence of thoron on the radon measurement could be seen in the mixed exposure of 170 kBq h m<sup>-3</sup> of thoron plus 421 kBq h m<sup>-3</sup> of radon. The thoron activity concentration was not high enough in comparison to the radon concentration. The potential thoron influence on the radon measurement might be hidden in the radon measurement uncertainties. For further tests with mixed thoron/radon atmosphere with the aim of

determining a cross-interference coefficient we recommend that the used concentration of thoron is similar or higher than that of radon.

For all types of detectors that were exposed to different thoron activity concentrations, a very good agreement between the average values of the *CI* obtained in the different exposures was observed. However, the standard deviation of the values of the *CI* of individual detectors was higher than the estimated individual uncertainties. This could be due to the local differences in the air circulation at different points in the exposure chamber which might influence the rate of thoron entrance in the detector volume. Another possible explanation lies in the difference in the dimensions of the housing of the individual detectors. Such differences can be incurred in the production process. A small difference in the air gap of the housing could lead to a different thoron entrance rate. The general tendency was that the passive monitors with larger air gaps showed larger variance in the *CI*.

There is a very good agreement between the results for the *CI* of the Raduet low air exchange rate chamber and the corresponding value that could be estimated from the literature.

There is very good agreement between the results for the *CI* of the Radtrak<sup>2</sup> radon detector obtained at STUK and SUBG. This shows that the methodologies applied by the two laboratories are comparable. On the other hand, the result for the *CI* of the Radtrak<sup>2</sup> detector obtained at IRSN is significantly higher than the results obtained at STUK and SUBG. The result for the *CI* of the Rapidos detector obtained at IRSN is also significantly higher than the upper limit for the *CI* of this detector estimated at SUBG. It is possible that the disagreement is due to an additional background exposure of the detectors studied at IRSN (e.g. during their transport back to the analyzing laboratory). Since in this study the exposure was at a relatively low thoron activity concentration and no transit detectors were used to estimate the background radon exposure, the thoron cross interference could possibly be overestimated. This hypothesis is supported by the fact that the Radtrak<sup>2</sup> and Rapidos detectors exposed at IRSN were transported together to the same analyzing laboratory and had very close signals. We recommend the usage of transit detectors, in order to obtain reliable results.

### **Activity 2.2.3**

*Using SUBG's laboratory facilities and the secondary reference instruments calibrated in A2.1.2, SUBG and BEV-PTP will study experimentally the response of radon/thoron measurement instruments/detectors available at SUBG and BEV-PTP at different environmental temperatures (between +5 °C and +45 °C) in both thoron and radon plus thoron atmospheres, under both static and dynamic regimes. SUBG and BEV-PTP will also study the response of radon/thoron measurement instruments under different radon/thoron concentrations ratios.*

*Theoretical models and analysis will be employed by SUBG and BEV PTP to determine, understand and potentially correct for the influence of thoron on the performance of the radon monitors.*

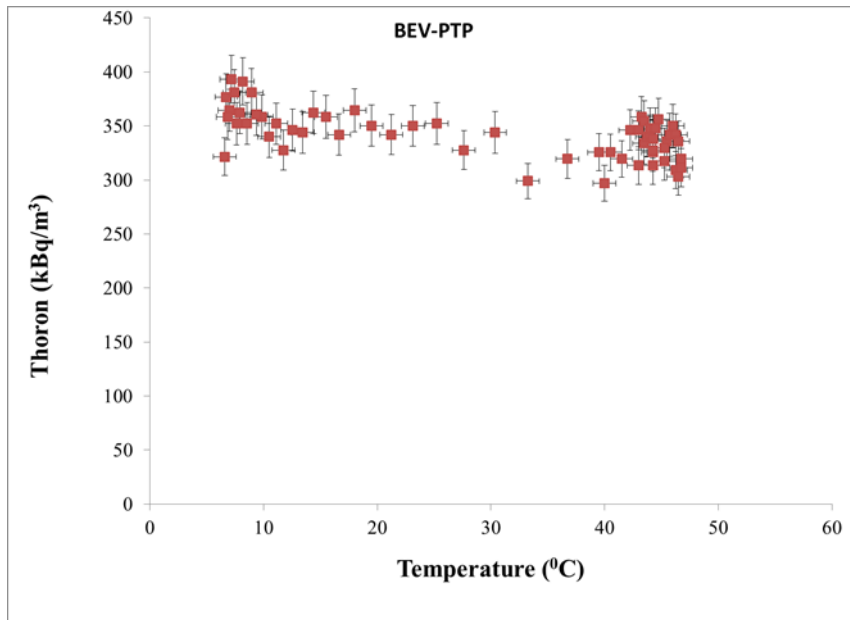


Figure 1 – Thoron activity concentration reported by the BEV-PTP instrument at different temperatures during exposure at stable activity concentration. A slight negative correlation has been observed ( $R^2=0.42$ ). Nevertheless, the calculated relative deviation over the temperature interval 5-45 °C remains within the  $\pm 10\%$  limit for the tests of the influence of the ambient temperature specified by standard IEC 61577-2.

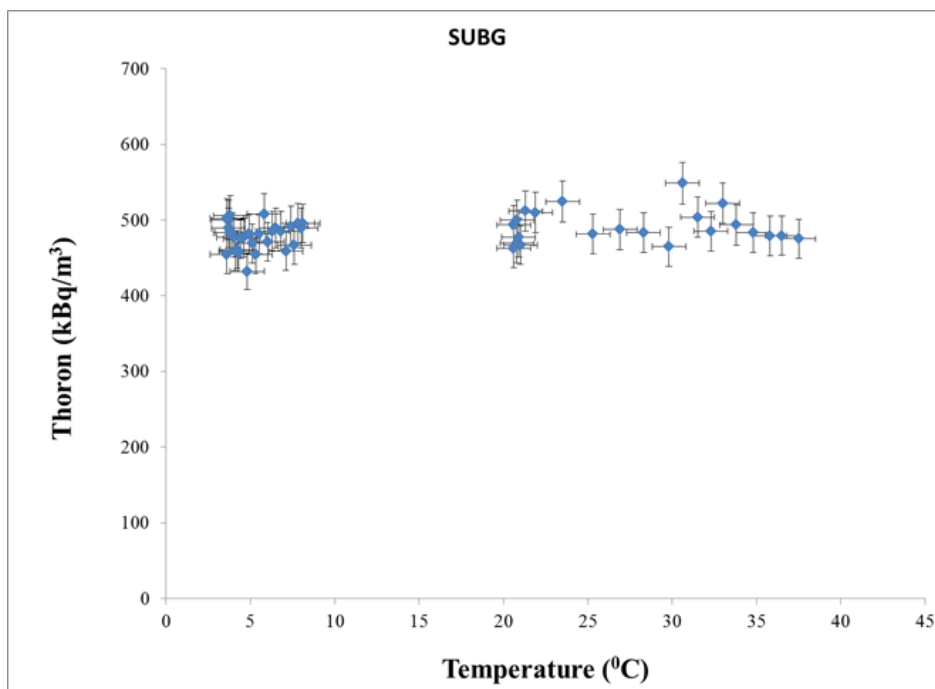


Figure 2 – Thoron activity concentrations obtained by the SUBG instrument at different temperatures in another exposure experiment at stable thoron activity concentration. The somewhat higher thoron levels than those in the experiment with BEV-PTP reference monitor are due to the reduced exposure volume, as other instruments were also placed in the exposure box during this exposure. Here, a slight positive correlation ( $R^2 = 0.08$ ) was observed, but the relative deviation remains well within the  $\pm 10\%$  limit for the tests of the influence of the ambient temperature specified by standard IEC 61577-2.

*Study of the influence of the temperature on active radon detectors*

The response of the SUBG and BEV-PTP secondary instruments was studied experimentally within the specified temperature interval in thoron, radon and mixed radon + thoron atmospheres (Annex X).

The results of the BEV-PTP reference instrument (AlphaGUARD PQ2000PRO RnTn) showed a slight negative correlation between the measured  $^{220}\text{Rn}$  activity concentration (Figure 1) and the temperature in the exposure box, while the SUBG reference instrument (also AlphaGUARD PQ2000PRO RnTn) showed a slight positive correlation (Figure 2). At this stage the results have no sufficient power to state that a correlation really exist and to speculate whether it is positive, negative or specific for the instrument. In spite of the slight correlation, over the temperature range 5-45 °C, the calculated relative deviation remains within the  $\pm 10\%$  limit for the tests of the influence of the ambient temperature specified by standard IEC 61577-2. At this stage when AlphaGUARD PQ2000 PRO RnTn monitors are used as reference instruments for thoron in exposure experiments over temperature range 5 – 45 °C a relative bias of maximum 10 % might be conservatively considered within the uncertainty budget.

The statistical analysis of the results shows no significant correlation between the  $^{222}\text{Rn}$  activity concentration and the temperature in the calibration container. Furthermore, no clear correlation between the activity concentration of  $^{222}\text{Rn}$  and  $^{220}\text{Rn}$  was observed. The calculated cross-interference of  $^{220}\text{Rn}$  on the  $^{222}\text{Rn}$  measurement is  $4\% \pm 3\%$  and therefore, well below the maximum of 20 % specified by standard IEC 61577-2. Although the calculated cross-interference of thoron on the  $^{222}\text{Rn}$  measurements is small, it could be shown clearly that  $^{220}\text{Rn}$  decay products which accumulate in the ionization chamber are the main reason for this cross-interference. The content of  $^{212}\text{Pb}$  and  $^{212}\text{Bi}+^{212}\text{Po}/^{208}\text{Tl}$  ( $^{212}\text{Po}$  is always in equilibrium with  $^{212}\text{Bi}$ ) in the ionization chamber increases during longer measurements. With an alpha energy of 6.1 MeV,  $^{212}\text{Bi}$  is supposed to have a slight interference on the number of detected  $^{222}\text{Rn}$  alpha particles with 5.6 MeV.

The technical details of this study are given in Annex X.

#### *Study of the influence of the temperature on passive radon detectors*

The influence of the temperature on the response of several kinds of diffusion chambers with two kinds of alpha track detectors (LR-115/II and CR-39) for  $^{222}\text{Rn}$  measurement was studied.

Two kinds of chambers with Kodak-Pathe LR-115/II detectors were studied and both kinds were metallic cylinders. In the first kind of chamber radon diffused in the volume of the chamber through polyethylene foils. In the second kind of diffusion chamber radon penetrates by diffusion through small gaps/holes around the chamber cap. Exposures to controlled  $^{222}\text{Rn}$  concentrations were made at temperatures of 2 °C, 21.5 °C and 45 °C using the laboratory facility at SUBG. Diffusion chambers covered by foils were metallic cylinders of 80 mm diameter and 75 mm height. At the bottom of the chamber a piece of detector Kodak-Pathe LR-115 type II was fixed. The chambers' openings were covered by different materials: filter paper, low density polyethylene (LDPE) of thickness 75  $\mu\text{m}$  or high density polyethylene (HDPE) of thickness 120  $\mu\text{m}$ . The diffusion chambers with "gaps/holes" had a diameter of 75 mm and a height of 75 mm with detector of Kodak-Pathe LR-115/II fixed in the same manner as in the first kind of chamber. A set of chambers that contained at least one chamber of each kind (covered by filter paper, metal foil, foil of LDPE or foil of HDPE) were loaded for exposure in a 50 L exposure vessel. For the foil-covered chambers the transmission ratio  $R$  was determined by  $R = C_{in}/C_{out}$ , where  $C_{in}$  is the radon concentration inside the detection volume and  $C_{out}$  is the radon concentration in the ambient air), assuming  $R = 1$  for chambers covered with filter paper. Results for the calibration factor  $CF$  are calculated by the ratio of net track density over integrated  $^{222}\text{Rn}$  concentration and shown in Figure 3. As shown, the  $CF$  of chambers with gaps/holes and of chambers covered by filter paper are practically identical.

Also, it is clearly shown that there are no signs for any temperature dependence within the temperature range 3-45 °C.

Experimentally determined values of  $R$  for the chambers covered by polyethylene foils are shown in Figure 4 (see also Annex XI). Clearly, the response of the diffusion chambers with polymer foil strongly depends on the temperature. Given the absence of temperature dependence in the response of chambers not covered by polymer foil, this temperature dependence is interpreted as due to the usage of polymer foil.

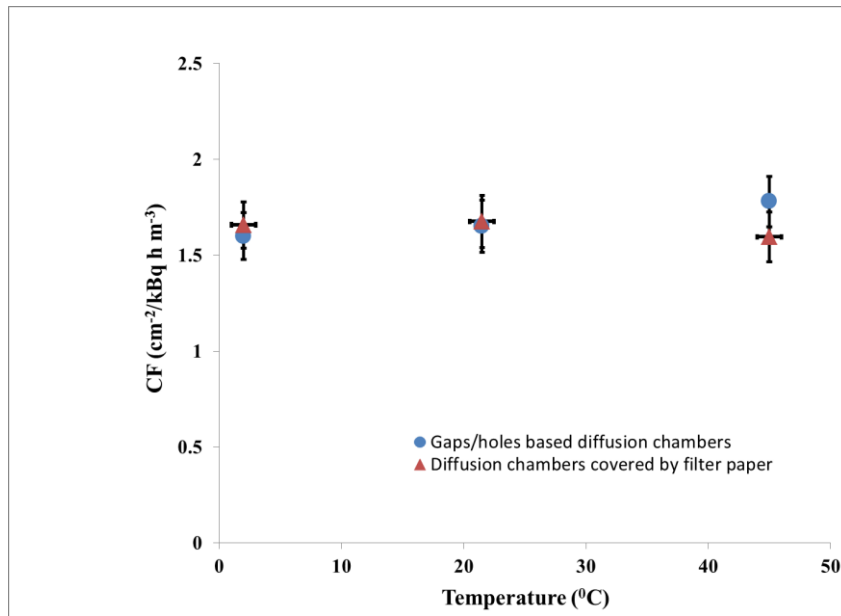


Figure 3 –CF of diffusion chambers in which radon diffuses through small gaps/holes (●) and through filter paper (▲). Both chambers show the same CF and there is no significant difference between the results at different temperatures.

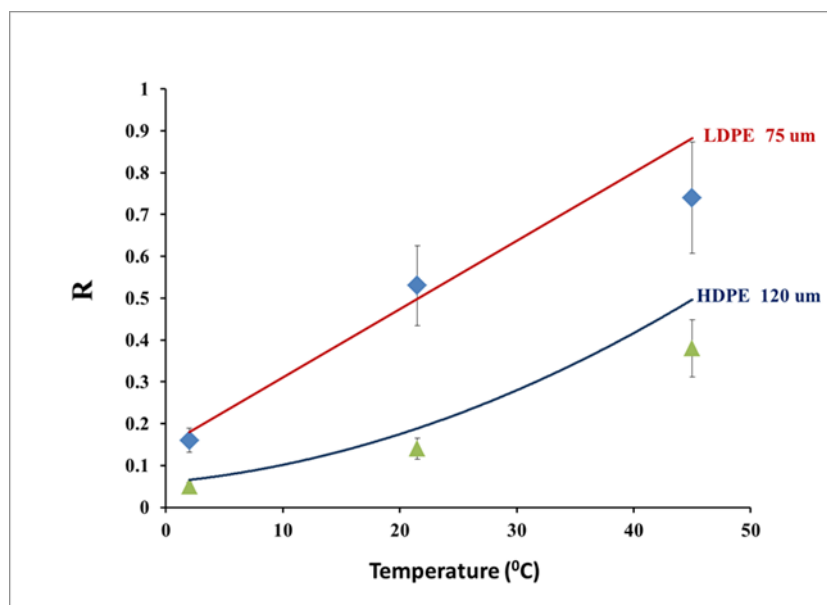


Figure 4 – The transmission ratio at different temperatures of the chambers of 80 mm diameter and 75 mm height, covered by 75 μm thick foil of LDPE (●) and 120 μm thick foil of HDPE (▲). The curves represent the estimates based on LDPE and HDPE data reported in [4].

Such temperature influence in the response of diffusion chambers covered by polymer foils has already been observed by other authors [5, 6]. According to the theoretical model [7] the expression for  $R$  is:

$$R = \frac{C_{in}}{C_{out}} = \frac{1}{1 + \lambda \frac{hV}{PS}}, \quad (2)$$

where  $h$  is the thickness of the polymer foil,  $V$  is the internal volume of the chamber,  $S$  is the surface of the polymer foil covering the chamber volume and  $P$  is the radon permeability in the polymer foil material. The permeability is  $P = KD$ , where  $D$  is the diffusion coefficient of radon in the material and  $K$  is its partition coefficient (dimensionless solubility). The temperature dependence is due to the temperature dependence of the permeability  $P$ . There is a good correspondence between the experimental points and the theoretical dependences which were calculated using the data for  $K$  and  $D$  published in [4].

Metal chambers of the same kind, but covered with low density polyethylene with thickness  $50 \mu\text{m}$  were also tested for thoron interference. Three such chambers were exposed to integrated  $^{220}\text{Rn}$  concentration of  $13.84 \pm 0.91 \text{ MBq h m}^{-3}$ . The estimated thoron interference was  $< 0.07 \%$ . This indicates that with chambers that use polyethylene foil as diffusion barriers almost absolute anti-thoron protection can be achieved, along with anti-humidity protection. However, the foil might cause temperature bias in the radon response.

Another set of radon chambers with CR-39 alpha track detectors were tested for temperature dependence of their radon response [8]. The set included three kinds of passive radon detectors commercially distributed by Radonova: Rapidos (A in Figure), Duotrak (B in Figure), Radtrak<sup>2</sup> (C in Figure). In all these chambers radon penetrates through small gaps/holes existing in their construction. The monitors were exposed in the SUBG exposure facility at controlled  $^{222}\text{Rn}$  concentrations at  $3^\circ\text{C}$  and  $45^\circ\text{C}$ .



Figure 5 – Three kinds of passive detectors produced by RADONOVA that were tested for temperature influence: Rapidos (A), Duotrak (B) and Radtrak<sup>2</sup> (C)

After exposure the chambers were processed at Radonova laboratory in Uppsala, Sweden, according to the standardized etching and track-counting protocol. The results are shown in Figures 6 and 7.

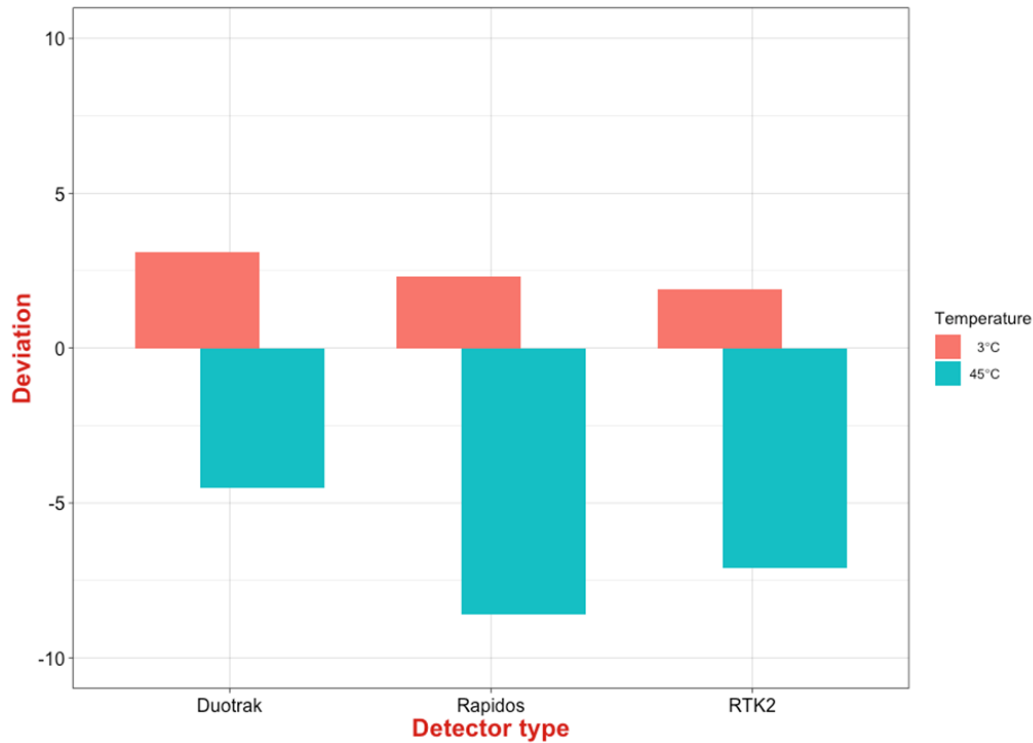


Figure 6 – Deviation of the calibration factor  $CF$  in % at temperatures 3 °C and 45 °C from its value at 20 °C. RTK2 is an abbreviation for Radtrak<sup>2</sup>.

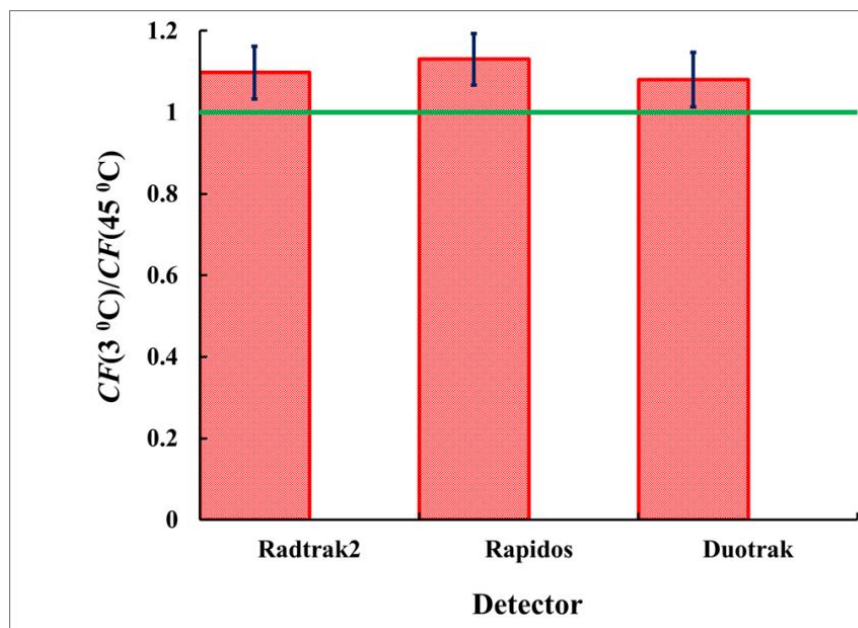


Figure 7 – Calibration factors ratio:  $CF(3\text{ °C})/CF(45\text{ °C})$ . In all detectors there is a drop of  $CF$  with 8-13 % at temperature 45 °C, compared to that at 3 °C.

In all Radonova monitors a drop of sensitivity at higher temperatures was observed. The drop is about 10 % from 3 °C to 45 °C. Most probably the reason for this drop is the fading of the CR-39 detectors, which has also been reported by other authors in the scientific literature [9].

Strong temperature dependence was also observed for detectors that employ radon absorption/adsorption in different materials: e.g. Makrofol N, activated charcoal [10], etc. In this case the bias within 5-35 °C exceeds 200 % and reliable quantitative measurements are possible only under controlled temperature conditions or by using the temperature compensation module, invented within the MetroRADON project (patent pending) [11].

## Task 2.3: Development of techniques to reduce the influence of thoron on radon measurements and calibrations

*The aim of this task is to develop techniques to reduce the influence of thoron on radon measurements and calibrations. Task 2.2 will investigate and develop a better understanding of the influence of thoron on radon measurements to potentially correct for this effect, whereas this task will develop practical techniques to reduce the influence of the thoron on radon measurements.*

*A literature review of potential methods to reduce the influence of thoron will be performed and systematic analysis of the different methods undertaken by STUK and SUBG. The properties of different filters/foils/membranes that might serve as selective thoron barriers (whilst not reducing radon penetration significantly) will be studied by SUBG and CEA. Recommendations will be proposed by SUBG, BEV-PTP, CEA, STUK and IRSN about the construction of radon monitors that are not sensitive to thoron and solutions aimed at reducing thoron-related bias in the radon signal in existing monitors (e.g. by using packaging/envelope as a thoron-barrier). Procedures to check the radon monitors for sensitivity to thoron will also be proposed.*

### Activity 2.3.1

*STUK and SUBG will undertake a literature review of potential techniques and materials to reduce the influence of thoron on radon measurements and calibrations.*

*Based on these findings, STUK and SUBG will perform an analytical analysis of the different techniques/materials and will identify the most promising ones, based on the effectiveness of the relative differentiation between thoron and radon.*

The review entitled: Review of potential techniques and materials to reduce the influence of thoron on radon measurements and calibrations was prepared and is published on the MetroRADON project web-site (Annex XII).

Within this activity, the following practical methods to discriminate against thoron interference were identified:

- Discriminative radon and thoron detectors that employ alpha-spectrometry
- Delay due to air flow in a buffer volume (pipe)
- Diffusion barriers:
  - Diffusion through polymer foils;
  - Diffusion through air gaps or pin holes

The discrimination by alpha-spectrometry is usually used with active monitors (RAD 7, AlphaGUARD PQ2000 PRO RnTn). Such monitors can measure radon and thoron separately. Additionally, the algorithm for data processing should take into account that the energies of alpha-particles of  $^{218}\text{Po}$  ( $^{222}\text{Rn}$  decay product) and  $^{212}\text{Bi}$  ( $^{220}\text{Rn}$  decay product) are very close to each other. Joint experiments made by SUBG and BEV-PTP within Activity 2.2.3 showed that radon/thoron interference with AlphaGUARD PQ2000 PRO RnTn is sufficiently eliminated.

Delay due to air flow in a buffer volume allows efficient thoron reduction practically not affecting radon concentration (Figure 8). The transmission ratio  $R$  in a detection volume where the air enters after delay  $t$ , ensured by a delay line of volume  $V$  through which the air is flushed with a flow-rate  $Q$  is:

$$R = e^{-\frac{\lambda V}{Q}} \quad (3)$$

Figure 8 shows the transmission ratio for thoron and radon.

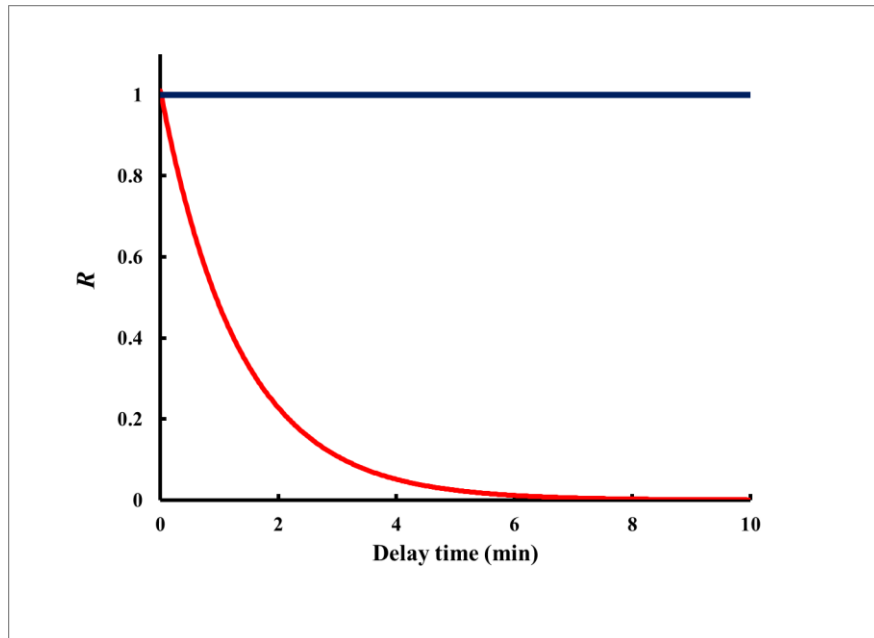


Figure 8 – The transmission ratio ( $R$ ) after a “delay line”. The red line corresponds to thoron, while the blue line corresponds to radon. The characteristic delay time is:  $V/Q$ , where  $V$  is the buffer volume of the delay line and  $Q$  is the air flow-rate through it.

As shown in Figure 8, a delay of 4-5 min may essentially eliminate thoron influence, practically not affecting radon concentration. Such delay is generally acceptable as it doesn’t significantly change the reaction of the instrument to fast changes in radon levels. The limitation of this approach is the need to keep the flow-rate constant through the delay line over the whole exposure time. This hampers applications with long exposure times and with passive instruments. The method is mostly useful for active instruments that do not use alpha-spectrometry discrimination between radon and thoron.

The use of diffusion barriers seems to be the most suitable approach to protect radon detectors for which fast reaction is not required. The used diffusion barriers are of two kinds:

- small gaps or pin holes;
- polymer foils.

Both processes can be parameterized by a unified expression for the transmission ratio:

$$R = \frac{C_{in}}{C_{out}} = \frac{1}{1+\lambda\tau} = \frac{1}{1+\frac{\lambda'}{x}} \quad (4)$$

where the characteristic diffusion time  $\tau$ , or the related parameter  $x$  ( $x = 1/\tau$ ) depends on the volume, the foil surface  $S$  or the pin-hole area and length.

Consider for instance, an alpha-track detector placed in a cup/chamber (“diffusion chamber”) in which radon gas diffuses from outside. To protect the detector from humidity and thoron influence, many such chambers are covered by, or packed with, a polymer foil [7]. The foil stops radon and thoron progeny, as well as the short-lived thoron ( $^{220}\text{Rn}$ ) and prevents moisture penetration. However,  $^{222}\text{Rn}$  diffuses through the foil and reaches concentration inside the chamber that is proportional to that outside. The transmission ratio  $R$  of the

$^{222}\text{Rn}$  concentration inside the chamber ( $C_{in}$ ) to that in the ambient air ( $C_{out}$ ) is given in Equation (2). For “gap/pin-holes” diffusion barriers the expression is:

$$R=C_{in}/C_{out}=1/(1+\lambda dV/D_{air}A), \quad (5)$$

where  $A$  is the total area of gaps/holes,  $d$  is the length of one hole and  $D_{air}$  is the coefficient of diffusion of radon in air.

The diffusion barrier reduces both thoron and radon concentrations. However, due to the great difference between the decay constants of thoron and radon, it is possible to achieve a substantial reduction of thoron while the reduction of radon is much smaller (Figure 9).

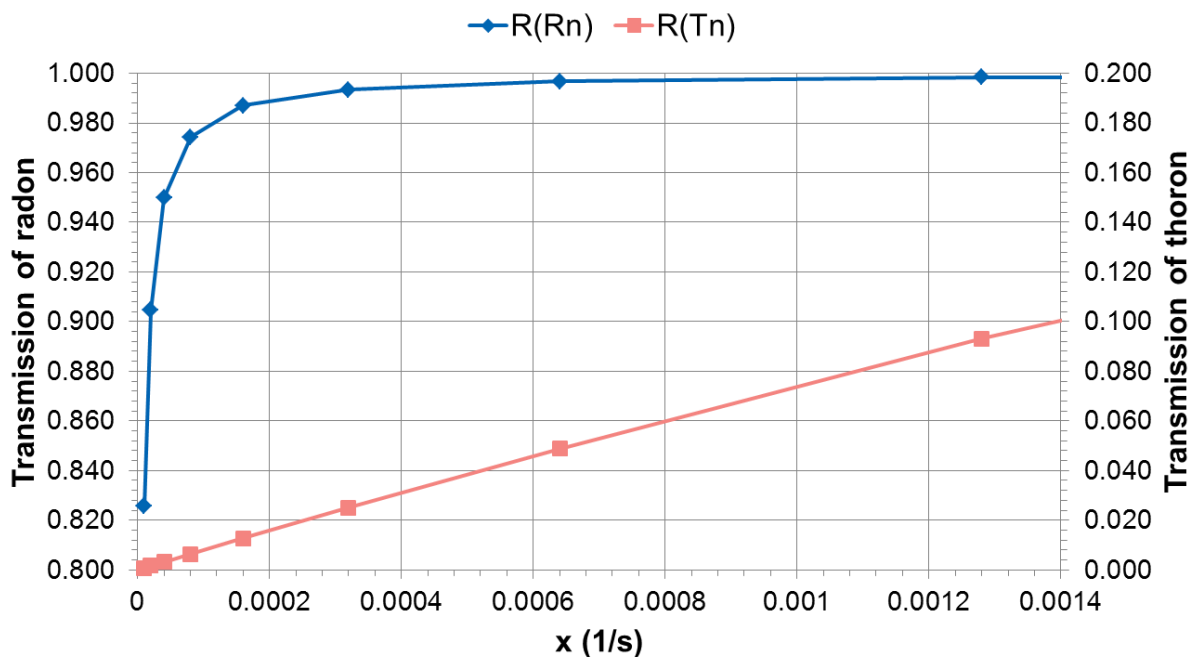


Figure 9 – The transmission ratio  $R$  of radon or thoron as dependent on the parameter  $x$  ( $x = 1/\tau$ ) of the diffusion barrier (see Equations 3-5). As seen, it is possible to reduce the thoron transmission to 1-2 % in the same time keeping the transmission of radon close to 100 %.

The diffusion barrier approach is usable with passive detectors for long-term exposure, as well as with active monitors used in a passive (diffusion) sampling mode. However, it shows specific limitations:

- Pin holes and gaps do not isolate the detector volume from the ambient air. When used at high humidity some of these detectors may be not reliable because of the water condensation on the detector surface or the blocking of the gaps by drops of water. Reports in the scientific literature [12] demonstrate also that thoron interference of such barriers is affected by air turbulence/air streams around the detector.
- Polymer foils employ diffusion through the polymer material. This is a physico-chemical process that depends on temperature. The temperature dependence is attributed to the temperature dependence of the permeability  $P(T)$ , which in turn depends on the partition and diffusion coefficients  $P(T)=K(T)D(T)$ . As a result, although the polymer foil may ensure close to absolute anti-thoron and anti-humidity protection, it may introduce a temperature bias in the radon response [5, 6, 13]. Therefore, a

dedicated study was planned and carried-out to overcome this problem of polymer foil packaging without losing the great benefits it may provide (Annex XI and Annexes XIII-XVI).

Even though passive radon detectors with gap/pin-holes based barriers dominate the market, they face difficulties to perform well at high humidity (see [http://metro-radon.eu/wp-content/uploads/2019/07/Tommasino\\_Sofia2019.pdf](http://metro-radon.eu/wp-content/uploads/2019/07/Tommasino_Sofia2019.pdf)). On the other hand, reference radon levels for work places are set in the legislation of many countries, which requires reliable radon monitoring of working places. Therefore, within MetroRADON the research on polymer foils was planned to search for options that are free of or sufficiently compromise the shortcomings of both kinds of diffusion barriers: air gaps/pin-holes and polymer membranes.

### Activity 2.3.2

*SUBG will evaluate the properties of different filters/foils/ membranes identified in A2.3.1 that could potentially serve as selective thoron barriers and will evaluate their radon permeability.*

*SUBG will initially undertake a literature survey of radon ( $^{222}\text{Rn}$ ) permeability data.*

*SUBG will then perform an experimental study of the permeability of radon ( $^{222}\text{Rn}$ ), using it as a thoron ( $^{220}\text{Rn}$ ) surrogate, because both isotopes have the same solubility and diffusion coefficient. Using the radon permeability data, the thoron permeability of the various materials will be evaluated and the most promising materials identified.*

The radon absorption properties of six different polymer foils were determined at SUBG. An experimental set-up and methodology were developed in order to characterize thin polymer foils.

The studied foils are:

- Makrofol DE
- Makrofol N
- polypropylene (PP)
- high-density polyethylene (HDPE)
- low-density polyethylene (LDPE) —plain and anti-slip covered.

The partition coefficients  $K$  and the diffusion lengths  $L_D$  ( $L_D = \sqrt{D/\lambda}$ ) of radon in these polymers are experimentally determined for several temperatures in the range  $T = 5\text{--}31\text{ }^\circ\text{C}$  (see Table 6). Some of the obtained values are compared to published data available for the given temperatures. It should be noted here that the radon and thoron absorption properties of polyethylene might vary between different producers or different batches. Therefore, a test of the radon transport properties is recommended. This could be done using the methodologies developed in the framework of this project, which are described in Annex XIII.

Thus far, it is shown that the temperature dependencies of the partition coefficients  $K(T)$ , the diffusion lengths  $L_D(T)$ , and the permeability  $P(T)$  could be described analytically for the studied temperature range  $5\text{--}31\text{ }^\circ\text{C}$  (see Table 7). The results of this study are published in [4], which is also given in Annex XIII. These results allow full characterization of the radon absorption and transmission through the studied polymers in the temperature range  $5\text{--}31\text{ }^\circ\text{C}$ .

Overall, the temperature variation of the permeability within the studied range is highest for PP and LDPE and lowest for Makrofol N and Makrofol DE while LDPE-A and HDPE are in the medium area. However, LDPE and LDPE-A are best suited for practical handling. Possibly, the material LDPE-A is the best compromise from the point of view of the ease of usage and the temperature influenced variation of the permeability.

As noted, the major problem when polymer membranes are used as anti-thoron barriers is the introduced temperature bias in the response to radon. The transmission ratio increases with temperature in the studied temperature intervals (Figure 4). The temperature variation in radon transmission factor within 5 – 40 °C is assessed as the difference  $R_{Rn}(40\text{ °C}) - R_{Rn}(5\text{ °C})$ . As seen in Figure 10, the temperature variation in radon transmission can be reduced by reducing the value of  $hV/S$  (e.g. by reducing the volume and/or increasing the foil surface and/or reducing the foil thickness). However, this raises the thoron transmission, which may also vary significantly with the temperature (Figure 10).

Table 6 – Partition coefficients, diffusion lengths, diffusion coefficients and permeability of <sup>222</sup>Rn in polyethylene at various temperatures.

|       | PP   | LDPE      | LDPE-A   | HDPE     | Mak N      | Mak DE     |
|-------|--|-----------|----------|----------|------------|------------|
| T°C   | Partition coefficient K                                      |           |          |          |            |            |
| 5(1)  | 6.13(55)   | 4.18(39)  | 4.05(42) | 3.63(33) | 211(16)    | 77.5(67)   |
| 10(1) |  |           |          |          | 183(12)    | 72.8(58)   |
| 21(1) | 3.69(38)   | 3.66(38)  | 3.13(41) | 2.51(22) | 103.3(79)  | 34.6(30)   |
| 31(1) | 3.25(43)   | 3.70(43)  | 2.96(30) | 2.44(21) | 70.2(51)   | 27.8(24)   |
| T°C   | Diffusion length L <sub>D</sub> , um                         |           |          |          |            |            |
| 5(1)  | 67.6(51)   | 605(30)   | 646(36)  | 460(19)  | 18.0(10)   | 20.8(10)   |
| 10(1) |  |           |          |          | 23.9(10)   | 26.8(10)   |
| 21(1) | 198(10)  | 1210(64)  | 1204(85) | 880(22)  | 36.2(10)   | 43.3(13)   |
| 31(1) | 300(15)  | 1880(140) | 1722(54) | 1252(23) | 52.1(15)   | 62.9(16)   |
| T°C   | Diffusion coefficient D, 10 <sup>-14</sup> m <sup>2</sup> /s |           |          |          |            |            |
| 5(1)  | 0.96(14)   | 76.9(77)  | 87.4(97) | 44.3(37) | 0.0677(79) | 0.0911(84) |
| 10(1) |  |           |          |          | 0.120(10)  | 0.151(11)  |
| 21(1) | 8.20(85)   | 307(33)   | 304(43)  | 162(8)   | 0.275(15)  | 0.394(25)  |
| 31(1) | 18.9(19)   | 739(111)  | 623(39)  | 329(12)  | 0.570(32)  | 0.831(43)  |
| T°C   | Permeability P, 10 <sup>-13</sup> m <sup>2</sup> /s          |           |          |          |            |            |
| 5(1)  | 0.59(10)   | 32.1(44)  | 35.4(54) | 16.1(20) | 1.43(20)   | 0.706(89)  |
| 10(1) |  |           |          |          | 2.20(24)   | 1.10(12)   |
| 21(1) | 3.03(44)   | 113(17)   | 95.1(18) | 40.7(41) | 2.84(27)   | 1.36(15)   |
| 31(1) | 6.1(10)  | 273(52)   | 184(22)  | 80.4(75) | 4.00(37)   | 2.31(23)   |

Table 7 – Estimated dependence of the diffusion coefficient (*D*), partition coefficient (*K*) and permeability (*P*) on the temperature (*T*).

| Polymer     | ln(D)=a <sub>D</sub> + b <sub>D</sub> T |                | ln(K)=a <sub>K</sub> + b <sub>K</sub> T |                | ln(P)=a <sub>P</sub> + b <sub>P</sub> T |                |
|-------------|---|----------------|---|----------------|---|----------------|
|             | a <sub>D</sub>                          | b <sub>D</sub> | a <sub>K</sub>                          | b <sub>K</sub> | a <sub>P</sub>                          | b <sub>P</sub> |
| PP          | -32.76(35)                              | 0.1159(51)     | 1.93(11)                                | -0.0262(59)    | -30.87(23)                              | 0.092(10)      |
| LDPE        | -28.33(16)                              | 0.0869(80)     | 1.45(11)                                | -0.0053(56)    | -26.88(19)                              | 0.0815(96)     |
| LDPE-A      | -28.13(16)                              | 0.0755(64)     | 1.45(12)                                | -0.0123(56)    | -26.69(19)                              | 0.0635(82)     |
| HDPE        | -28.81(13)                              | 0.0771(55)     | 1.33(12)                                | -0.0158(56)    | -27.49(16)                              | 0.0619(68)     |
| Makrofol N  | -35.22(12)                              | 0.0791(57)     | 5.603(82)                               | -0.0441(43)    | -29.61(13)                              | 0.0347(59)     |
| Makrofol DE | -35.00(11)                              | 0.0844(54)     | 4.62(14)                                | -0.0443(73)    | -30.39(14)                              | 0.0410(69)     |

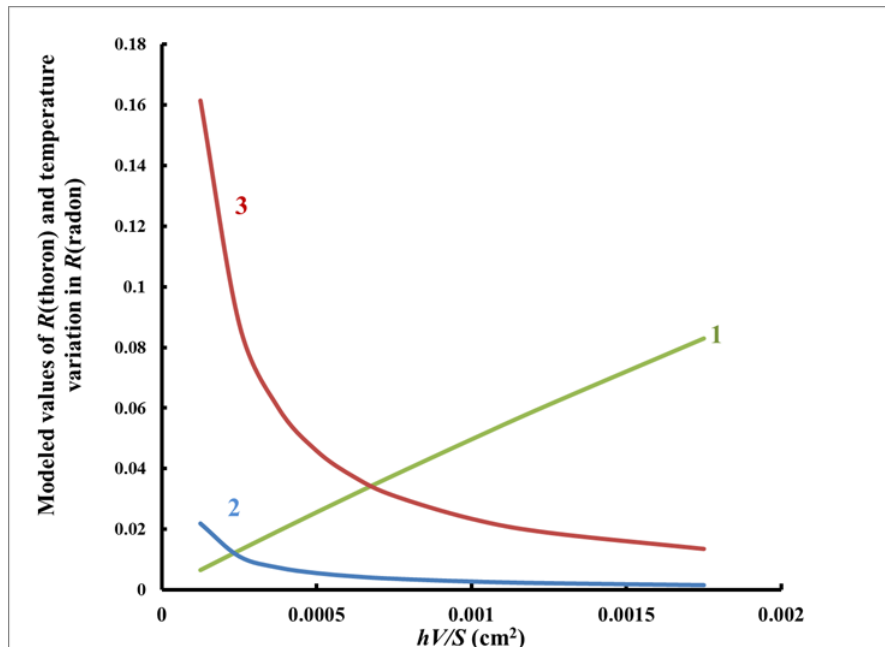


Figure 10 –Temperature variation in radon transmission factor within 5-40 °C (1); values of the thoron transmission factor at 5 °C (2) and 40 °C (3), as dependent on  $hV/S$ . The dependences are shown for low density polyethylene.

The dependences illustrated in Figure 10 show that finding the best balance between the reduction of the thoron influence by a polymer foil and the increase of the temperature bias in radon transmission can be a challenge. One possible approach, especially for detectors that are scheduled to work at high humidity and high thoron levels is to use two barriers: a gap/pin holes based chamber that is additionally packed in a polymer-foil package of small  $hV/S$ . This may keep the temperature bias small, in the same time providing an additional (to that provided by gaps/pin holes) anti-thoron protection.

Surprisingly, for many widely used detectors it turned out that the temperature dependence of the detector’s response is reciprocal to that introduced by the polymer foil. This led to a novel technical concept [11] with a potential to overcome the temperature dependence problem of many types of detectors. It is possible to design a “compensation module” in which the detector is placed, that facilitates reduction or elimination of the temperature dependence of the detector (see Figure 11) by proper selection of the foil material and the parameters  $h$ ,  $V$ ,  $S$  of the module. In the same time such module can provide an efficient protection against the thoron interference and humidity. This novel concept led to a patent application submitted within MetroRADON project [11].

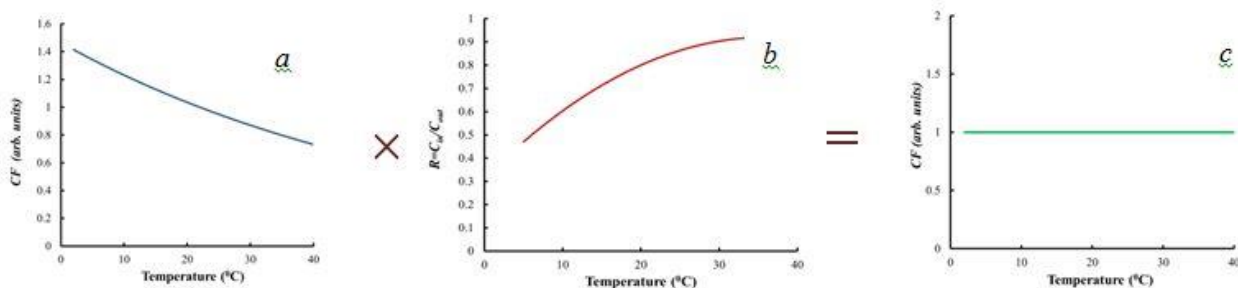


Figure 11 – The concept of the compensation module design (patent pending) [3, 11]: The temperature dependence of many radon detectors (a) and that introduced by polymer anti-thoron barriers (b) are reciprocal. This can be used to reduce/eliminate the temperature dependence (c), the thoron influence and also the humidity influence.

At this stage SUBG conducted a proof-of-concept study based on data available for the radon permeability of polyethylene at different temperatures. Using the experimental results for  $R$  at three different temperature levels for chambers covered by LDPE or HDPE and by interpolating between the experimental points [11] different compensation modules were designed. Photos of some of them are shown in Figure 12.



Figure 12 – Compensation modules used for pilot, “proof-of-concept” experiments.

For proof-of-concept experiments detectors with strong temperature influence were selected. They are based on a concept first proposed by Tommasino et al. [14] that employ coupling of alpha-track detector with an external radon absorber/adsorber that serves as radiator (Figure 13). The  $CF$  of these detectors drops by 250-270 % when the temperature increases from 5 to 35 °C.



Figure 13 – Radon detectors with Makrofol N absorbers (up) and sheet of activated carbon adsorber (down) used as radiators for Kodak-Pathe LR-115/II alpha track detectors coupled with the radiators.

The results obtained by specially designed modules with foils of low density polyethylene of 75  $\mu\text{m}$  thickness and high density polyethylene of 120  $\mu\text{m}$  thickness are shown in Figure 14. As seen, the temperature bias over the interval 5- 35  $^{\circ}\text{C}$  is reduced from 250-270 % to less than 10 %. This means that the temperature bias can be practically compensated within the measurement uncertainty.

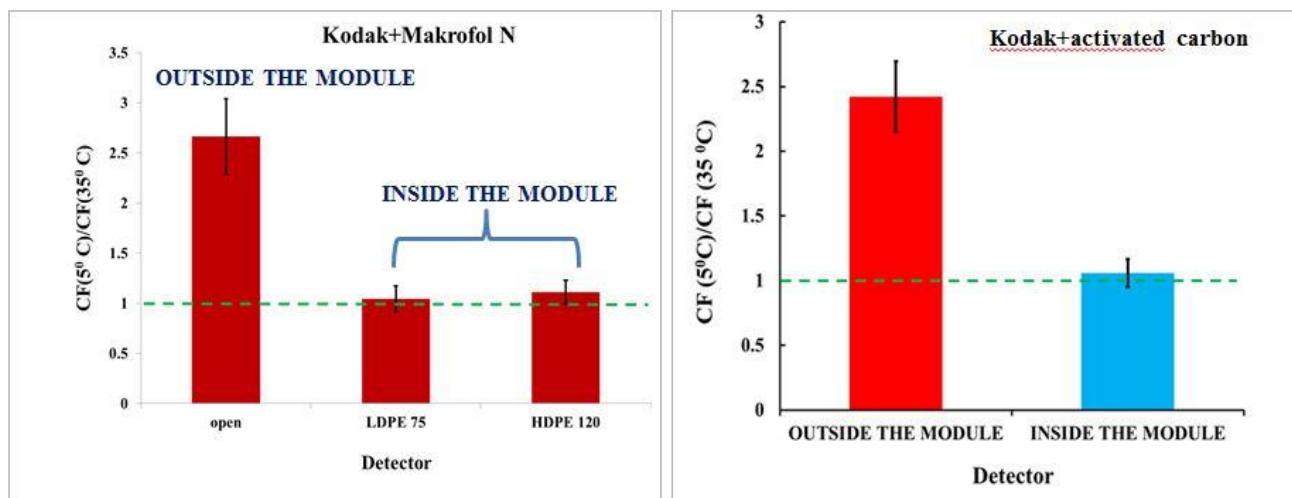


Figure 14 – Results for the temperature dependence of detectors shown in Figure 13 over temperature range 5-35  $^{\circ}\text{C}$ . As shown, the temperature bias of the detectors placed inside the compensation module is practically compensated.

The major findings related to the performance of the compensation module have been published [3, 13] and are attached as Annex XI and Annex XIV.

### Activity 2.3.3

*SUBG and CEA will develop and then characterize one or more selective barriers for  $^{220}\text{Rn}$  identified in A2.3.2.*

*It is well known that radon is soluble in some polymers and this solubility can be used to design/select a polymer membrane that allows diffusion of radon and not thoron. Using data from A2.3.2, the nature and thickness of the membranes will be carefully chosen so that the diffusion time is much greater than the thoron half-life, but much less than the half-life of radon.*

*The performance of such barriers will be experimentally tested on the CEA and SUBG facilities and expressed, for example, as attenuation factors for both gases.*

In the framework of this task, the SUBG team organized a workshop on *Transport of Radon and Thoron in Polymers*, which was held on 21- 22 March 2019 at the Faculty of Physics, Sofia University “St. Kliment Ohridski”, Sofia, Bulgaria. The objective of the workshop was to systemize the available knowledge and data for the radon absorption and transmission properties of various polymers and to identify the most promising materials for thoron barriers. The presentations of the workshop are available on the MetroRadon web site [<http://metroradon.eu/index.php/documents/>].

During the workshop the rubbery, low density polyethylene was identified as a particularly appropriate material for the development of selective thoron barriers, because it is a hydrophobic and bioinert polymer which can easily be used for temperature welding and has appropriate radon absorption properties (i.e. large radon permeability).

In order to characterize the radon absorption properties of polyethylene in a systematic manner, the French primary thoron detector developed at CEA was installed at SUBG and series of experiments were performed to characterize the polyethylene’s radon and thoron absorption properties. The results of these studies are presented in Annex XV and demonstrate an excellent agreement between the results obtained with the French primary standard and the radon absorption properties determined in task A2.3.2.

Consider a volume  $V$  placed in a radon atmosphere with radon concentration  $C_{out}$ . Assume also that radon and/or thoron can enter in the volume by diffusion through a polyethylene foil of surface  $S$  and thickness  $d$ . The radon and thoron concentrations inside the volume ( $C_{in}$ ) will depend on the outside concentration  $C_{out}$ , the surface to volume ratio ( $S/V$ ), the thickness of the polymer ( $d$ ) and the temperature ( $T$ ). In order to illustrate the  $^{222}\text{Rn}$  and  $^{220}\text{Rn}$  transmission ratios, Tables 8, 9 and 10 show the calculated equilibrium  $C_{in}/C_{out}$  ratios for different  $S/V$  ratios and  $T = 10, 20$  and  $30^\circ\text{C}$ , respectively. For more details see Annex XV. The results in Tables 8, 9 and 10 demonstrate that the low density polyethylene material is very appropriate for thoron barriers – it has low thoron and high radon permeability, which results in low thoron and high radon transmission factors.

Table 8 – Dependence of the equilibrium  $C_{in}/C_{out}$  on the  $S/V$  ratio for  $T=20^\circ\text{C}$  and various polyethylene thicknesses.

| T=20 °C |                  |                  |                  |                  |                  |                  |
|---------|------------------|------------------|------------------|------------------|------------------|------------------|
|         | S/V =2           |                  | S/V =0.8         |                  | S/V =0.2         |                  |
| d, um   | Rn               | Tn               | Rn               | Tn               | Rn               | Tn               |
|         | $C_{in}/C_{out}$ | $C_{in}/C_{out}$ | $C_{in}/C_{out}$ | $C_{in}/C_{out}$ | $C_{in}/C_{out}$ | $C_{in}/C_{out}$ |
| 30      | 97 %             | 0.72 %           | 93 %             | 0.29 %           | 77 %             | 0.07 %           |
| 50      | 95 %             | 0.43 %           | 89 %             | 0.17 %           | 67 %             | 0.04 %           |
| 70      | 93 %             | 0.31 %           | 85 %             | 0.12 %           | 59 %             | 0.03 %           |
| 100     | 91 %             | 0.22 %           | 80 %             | 0.09 %           | 50 %             | 0.02 %           |

Table 9 – Dependence of the equilibrium  $C_{in}/C_{out}$  on the S/V ratio for T=10 °C and various polyethylene thicknesses.

| T=10 °C |                  |                  |                  |                  |                  |                  |
|---------|------------------|------------------|------------------|------------------|------------------|------------------|
|         | S/V =2           |                  | S/V =0.8         |                  | S/V =0.2         |                  |
| d, um   | Rn               | Tn               | Rn               | Tn               | Rn               | Tn               |
|         | $C_{in}/C_{out}$ | $C_{in}/C_{out}$ | $C_{in}/C_{out}$ | $C_{in}/C_{out}$ | $C_{in}/C_{out}$ | $C_{in}/C_{out}$ |
| 30      | 94 %             | 0.32 %           | 86 %             | 0.13 %           | 60 %             | 0.03 %           |
| 50      | 90 %             | 0.19 %           | 78 %             | 0.08 %           | 48 %             | 0.02 %           |
| 70      | 86 %             | 0.14 %           | 72 %             | 0.05 %           | 39 %             | 0.01 %           |
| 100     | 81 %             | 0.10 %           | 64 %             | 0.04 %           | 31 %             | 0.01 %           |

Table 10 – Dependence of the equilibrium  $C_{in}/C_{out}$  on the S/V ratio for T=30 °C and various polyethylene thicknesses.

| T=30 °C |                  |                  |                  |                  |                  |                  |
|---------|------------------|------------------|------------------|------------------|------------------|------------------|
|         | S/V =2           |                  | S/V =0.8         |                  | S/V =0.2         |                  |
| d, um   | Rn               | Tn               | Rn               | Tn               | Rn               | Tn               |
|         | $C_{in}/C_{out}$ | $C_{in}/C_{out}$ | $C_{in}/C_{out}$ | $C_{in}/C_{out}$ | $C_{in}/C_{out}$ | $C_{in}/C_{out}$ |
| 30      | 99 %             | 1.62 %           | 97 %             | 0.65 %           | 89 %             | 0.16 %           |
| 50      | 98 %             | 0.97 %           | 95 %             | 0.39 %           | 82 %             | 0.10 %           |
| 70      | 97 %             | 0.69 %           | 93 %             | 0.28 %           | 77 %             | 0.07 %           |
| 100     | 96 %             | 0.49 %           | 90 %             | 0.19 %           | 70 %             | 0.05 %           |

#### Activity 2.3.4

Based on the results from A2.3.1-A2.3.3, SUBG, IRSN, STUK, CEA and BEV-PTP will develop recommendations on the construction of radon monitors that are not sensitive to thoron including the technical concepts / solutions aimed at reducing thoron-related bias in the radon signal in existing monitors.

SUBG, IRSN, STUK, CEA and BEV-PTP will also develop recommendations for tests to check the sensitivity of radon monitors and detectors to thoron.

The recommendation on the test procedures for studying thoron sensitivity of active radon monitors is to follow the protocol developed in this work. It is as follows:

- A traceability of the readings of the reference monitor which will be used to measure the thoron concentration should be ensured;
- The homogeneity of the thoron activity concentration during the exposure should be verified or measured;
- An exposure to constant thoron activity concentration for at least 96 hours is recommended.
- The initial and final cross-interference (CI) should be calculated where applicable.
- It is advisable to record the air velocities during the tests.
- The air pressure, temperature and humidity should be measured and recorded during the exposure.

The recommendation on the procedures for studying thoron sensitivity of passive radon detectors are:

- The homogeneity of thoron activity concentration inside the exposure vessel should be tested during the exposure or in another exposure set-up with a similar geometry (in terms of positions of detectors, fans, reference monitor, etc.)

- More than one detector of each type should be exposed in each session, in order to reduce the influence of differences in the housing and in the air circulation. Detectors of the same type should be placed apart from each other. Correspondingly, it is better to conduct more than one independent exposure of each type of detector.
- To obtain reliable results for the thoron cross-interference, exposures should be carried out at high integrated thoron activity concentration (of the order of MBq.h/m<sup>3</sup>). In addition, transit (blank) detectors should be used that have to be unpacked at the same time as the exposed detectors and transported together with them.

In addition, the following general recommendations could be made:

- No single construction of radon diffusion chamber could be recommended over the others. In general, the chambers with smaller width of the air gaps (of the order of tenths of a millimeter) show lower thoron sensitivity.
- The thoron sensitivity should be studied experimentally for each specific detector type. The results of such studies (including those presented in this report) should be viewed as an estimate for the thoron *C<sub>I</sub>* and not as a correction factor to be applied for measurements under diffusion mode.
- In places where significant thoron levels are not excluded detectors can be packed in polymer membranes to reduce the thoron sensitivity of the detectors. At the same time such packing eliminates the influence of moisture/humidity. Such packages should be well designed, as shown in Activity 2.3.2 or below in this section, in order to minimize the combined bias due to the temperature and thoron influence. In addition, when detectors show decreasing response with the increase of the temperature, the design of the package as a proper “compensation module” [11] may reduce or eliminate the temperature bias as well as the thoron interference.
- If polyethylene packaging is used for protection against thoron, it is recommended to calibrate the packed detectors and to perform the calibration at temperatures, which are close to the expected mean temperature during the exposure. This is to ensure, as much as possible, same conditions during the calibration and the measurement.

Using diffusion barriers (gap/pin-holes as well as polymer foils) always introduces an additional inertia in the response. Figure 15 shows the introduced characteristic inertia time (the time needed for the concentrations in the protected volume to reach 63 % (i.e.:  $1-e^{-1}$ ) of the equilibrium level, after sudden change of the ambient concentration from zero to constant non-zero value. As shown, if thoron interference of less than 5 % is targeted, the additional inertia introduced by the diffusion process may approach 1 hour.

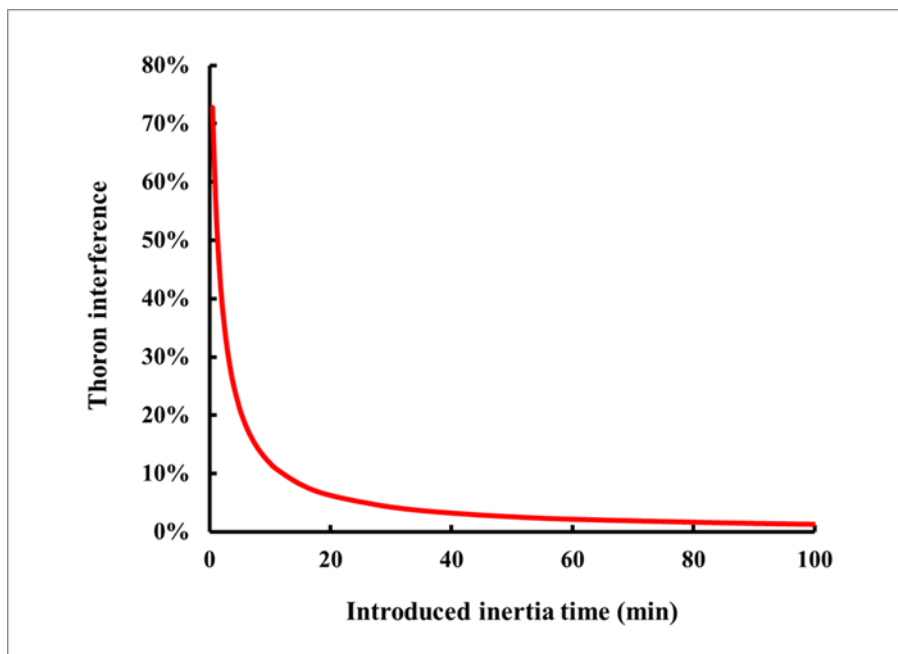


Figure 15 – Characteristic “inertia time” introduced by diffusion barriers versus the thoron interference in volumes protected by such barriers.

Therefore, for the active monitors for which a fast reaction to changing concentrations is of importance (e.g. for short-term measurements), spectrometry discrimination may be recommended. This mode is suitable for active monitors only and might not be cost-efficient. For active monitors that allow fast air sampling and counting in different time intervals, counting in two different time intervals can also be used to determine the activity concentrations of  $^{222}\text{Rn}$  and  $^{220}\text{Rn}$  isotopes separately. Alternatively, delay lines (see Figure 8) may be used. An example of such a mode is for instance reducing the thoron interference of the old version of AlphaGUARD PQ2000 PRO in which no spectrometry discrimination between radon and thoron is used. Experimentally it was found that in flow mode (with flow rate of 1 L/min) the thoron interference is  $(28.0 \pm 8.8) \%$ . It can be reduced 20 times (e.g. to about 1.4 %) by using a delay line with a delay time of 4 min. With a flow rate of 1 L/min the air should pass through a 4 L buffer volume before reaching the detection volume of the instrument. The delay of 4 min does not substantially change the ability of the instrument for fast reaction to changing radon concentration.

For active monitors working in a passive (diffusion) sampling mode, which do not require a fast reaction (e.g. for long-term measurements), using/adding diffusion barriers might be the best option, since it is cost efficient and easy to use. It can be illustrated again with the old version of AlphaGUARD PQ2000 PRO operating in diffusion mode. Experimentally, it was found that in this mode with a 10 min measuring cycle the thoron interference of the studied instrument is  $(8.8 \pm 1.3) \%$ . By adding an additional diffusion barrier (hole based) of aluminum foil with a hole in the center as shown in Figure 16, the thoron interference is reduced about twice – to  $(4.23 \pm 0.84) \%$ .



Figure 16 – Reducing thoron interference of radon monitor in a passive sampling mode by adding an additional diffusion barrier.

Packing monitors in hermetic polyethylene packs is another diffusion barrier option. For monitors with response not dependent on the temperature and which may operate at a wide temperature range, the package should be designed by choosing a proper material and  $hV/S$  value of the package, to ensure sufficient anti-thoron protection with minimum temperature bias introduced by the package (see Figure 10). However, if the radon response of the monitor decreases along with the increase of the temperature, a package can be designed as a compensation module as described above and in [11]. In this case packing such monitors according to the “compensation module design” may compensate or significantly reduce both thoron interference and the temperature influence (Figure 17).



Figure 17 – Packing a passive detector with (small) thoron interference and (small) temperature influence that reduces the detector response along with the increase of the temperature, designed as “compensation module” may improve its performance both against thoron and temperature influence. In addition, packing detectors in polymer foil will ensure protection against high moisture/humidity levels. Therefore, we recommend this option for monitors scheduled for use under high humidity and severe environmental conditions: e.g. working places in mines, caves, water works etc.

Another option to reduce the thoron influence on radon monitors and detectors is to pack them in polyethylene and use the known temperature dependence of the permeability of polyethylene to take account for the temperature induced bias. The idea is to account for the possible bias due to the temperature dependent diffusion of radon in the polymer, using the  $P(T)$  dependence, which was investigated in Task A.2.3.2 (shown in Annex XIII). From Equation 2 one can calculate the thoron transmission factor of the packaging for different temperatures and the bias in the radon readings due to the temperature-dependent radon diffusion. An example of the results of such calculations is shown in Figure 18.

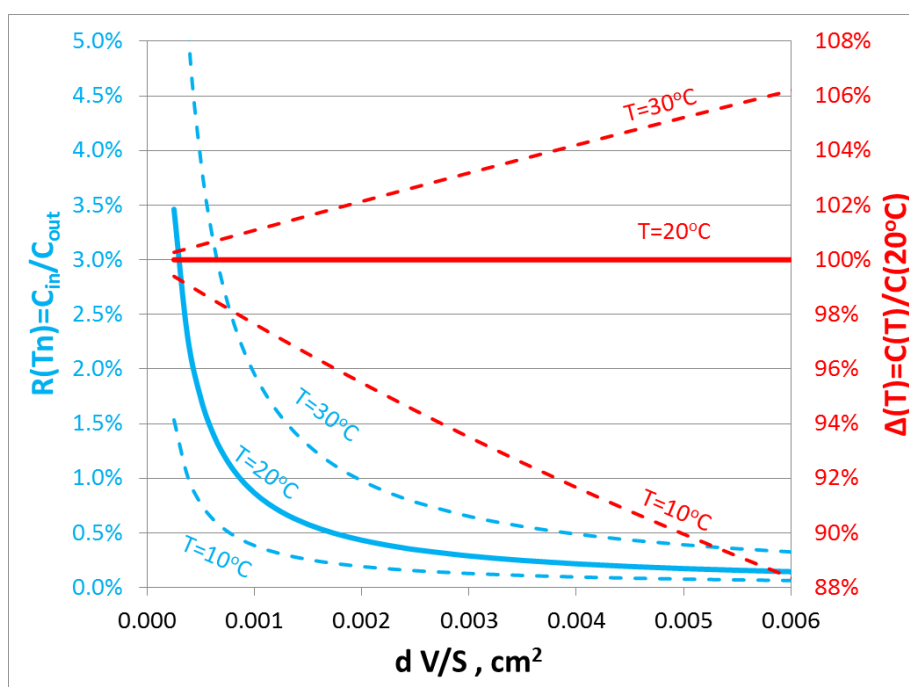


Figure 18 – Thoron transmission factors (blue) and temperature-induced radon bias (red) relative to  $T = 20^\circ\text{C}$  for  $T = 10, 20$  and  $30^\circ\text{C}$  vs.  $dV/S$  (cm<sup>2</sup>) of the polyethylene packaging. Here and in the Figure  $d$  is the thickness of the polyethylene foil used for the packaging.

The blue lines in Figure 18 show the ratio of the thoron concentrations inside and outside the packaging which is actually the reduction of the thoron  $CI$  on the detector due to the packing. The red lines show the radon concentration inside the packaging at different temperatures relative to the radon concentration inside the packaging at a fixed temperature  $T = 20^\circ \text{C}$ . If the packed detectors are calibrated at that temperature, the red lines give the potential bias due to the different average temperature during the exposure. Based on the known temperature behavior of the radon and thoron diffusion through the polymer, three methods for the reduction of thoron influence and taking into account the possible bias in the radon readings are proposed. These are:

- Reduction of the thoron influence by packing in polyethylene foils and evaluation of the possible bias in the radon readings due to temperature variations.
- Reduction of thoron influence by packing in polyethylene foils and performing differential measurements.
- Reduction of thoron influence by packing in polyethylene foils and performing temperature correction (for radon monitors with temperature record).

The above methods employ the known temperature dependence of the radon transmission through the polyethylene and provide simple and effective means for reduction of temperature-related bias. The methods are described in detail in Annex XVI.

### **Activity 2.3.5**

*Based on the results from A2.1.1-A2.1.2, A2.2.1-A2.2.3 and A2.3.1-A2.3.4, SUBG, IRSN, STUK, CEA, and BEV-PTP will write a report on the influence of thoron on radon monitors used in Europe including proposals for checking their sensitivity to thoron, and recommendations on the construction of radon monitors that are not sensitive to thoron together with technical approaches aimed at reducing thoron-related bias in the radon signal in existing monitors.*

The present report constitutes A2.3.5.

## Summary

- The testing of radon monitors for thoron sensitivity should include reference (secondary) thoron monitor that is calibrated with, or traceable to a primary thoron measuring system. We recommend a stable reference  $^{220}\text{Rn}$  atmosphere to be created in an exposure chamber by flushing air with constant flow-rate consecutively through the  $^{220}\text{Rn}$  source and the exposure chamber. To ensure thoron homogeneity fan(s) should operate in the exposure chamber during exposure. We recommend the reference instrument to be placed inside the exposure chamber throughout the exposure. Thoron homogeneity in the chamber should be checked during exposure or in another experiment under the same exposure conditions. The air pressure, temperature, humidity and air velocities (if applicable) during the tests should be recorded;
- The calibration exercise which was carried out in IRSN with seven thoron measuring instruments (four AlphaGUARDs and three RAD 7s), showed that the ratios between the  $^{220}\text{Rn}$  activity concentrations measured by the instrument and the reference activity concentration measured by the IRSN reference instrument is close to 1 for the four AlphaGUARDs and around 0.6 for the three RAD7s. The calibration factor of the AlphaGUARDs was found to change with the thoron activity concentration.
- The following radon monitors were tested for thoron cross-interference (CI): AlphaE, *AlphaGUARD* PQ2000 Pro, *AlphaGUARD* PQ2000, *AlphaGUARD* 2000 RnTh Pro, RadonEye +2, Corentium Home, Airthings Wave, Airthings Wave Plus, Corentium Pro, TSR3 – Fast and slow mode and TSR4M– Fast and slow mode, DoseMan – Fast and slow mode. All tested active thoron monitors except for RadonEye, TSR4M and DoseMan comply with the IEC 61577-2 standard requirement for  $CI < 20\%$ .
- A minimum of three days test with a high thoron activity concentration (around  $10\text{ kBq}\cdot\text{m}^{-3}$  or more) is recommended to determine an accurate final CI of the active monitors, instead of the 4 hours at  $1000\text{ Bq}\cdot\text{m}^{-3}$  required in the IEC 61577-2 standard.
- The following passive radon detectors were tested: RSKS and Raduet by Radosys, Radtrak<sup>2</sup>, Rapidos and Duotrak by Radonova, DPR2, DRF and Kodalpha by Algade, Easyrad by Pearl, 1 detector by STUK, 1 detector by AlphaRadon, 1 detector by Eurofins Radon Testing, 3 types of in-house detectors (1 designed by SUBG and 2 by ISS, Italy) and two types of detectors based on alpha track detection in DVD (CD). Except for EasyRAD and Kodalpha, the cross interference of thoron on the radon signal of all the instruments comply with the IEC 61577-2 standard requirement for  $CI < 20\%$ . No single construction of the studied radon monitors based on diffusion chambers could be recommended over the others. A low cross interference could be achieved with diffusion chambers with different constructions (in terms of volume, dimensions and inner compartments). In general, the chambers with smaller width of the air gaps (of the order of tenths of millimeter) show lower thoron sensitivity.
- The manufacturers of radon monitors should perform cross-interference testing for their radon instruments and should include this information in the specifications of the instrument.
- For instruments for which fast reaction to rapidly changing concentrations is required a spectrometric discrimination between radon and thoron is probably the best option. For active monitors with active sampling, counting in two different time intervals can also be used. With a proper data processing such instruments can measure radon and thoron separately still keeping capacity for fast reaction to rapidly changing concentrations.
- If spectral discrimination is not used but the instruments are expected to have a fast reaction, a proper approach is to incorporate a delay line either within the instrument design or as supplementary module. The parameters of such delay line (buffer volume and flow-rate) should correspond to the instrument's technical characteristics.
- For continuous radon monitors which do not perform spectral discrimination, but record the temperature and for which a fast reaction is not necessarily required, the thoron influence may be reduced by packing the monitors (or their sensitive volume) in polyethylene foils. The temperature-

induced bias in the radon readings can be corrected from the temperature record and using the known dependence of the radon permeability of the foil on the temperature.

- For instruments for which fast reaction to rapidly changing concentrations is not required, and which work in a diffusion mode, additional diffusion barrier can be used, e. g. as those shown in Figures 16 and 17.
- For passive detectors diffusion barriers might be considered in the design and tested in the prototypes. If instruments are scheduled to work at high humidity we recommend diffusion barriers based on polyethylene foils of low density polyethylene.
- For detectors in which the usage of polyethylene packing is planned to reduce the thoron interference, it is recommended to calibrate the packed detectors and to perform the calibration at temperatures which is close to the expected mean temperature during the measurement. This is to comply with the general principle that the conditions during the calibration and the measurement should be as close as possible.
- For detectors in which the usage of polyethylene packing is planned to reduce the thoron interference, a possible temperature bias may be introduced. Three methods for simple and effective handling and taking account of this bias are proposed in Annex XVI.
- For detectors that have response decreasing with the increase of the temperature, the temperature bias can be compensated if the anti-thoron polymer packing is designed as a compensation module, according to [11].

## References

1. Mitev K., Cassette P., Pressyanov D., Georgiev S., Dutsov Ch., Michielsen N., Sabot B., 2019. Methods for the experimental study of  $^{220}\text{Rn}$  homogeneity in calibration chambers. Manuscript submitted to Applied Radiation and Isotopes.
2. G Pantelic et al, Literature review of Indoor radon surveys in Europe, Publications Office of the European Union, Luxembourg, 2018, ISBN 978-92-79-97643-8(online), doi 10.2760/977726 (online), JRC114370, JRC Technical Report.
3. Pressyanov, D. 2019. Highly sensitive passive detectors for short-term pre- and post- mitigation measurements. Proc. 33<sup>rd</sup> AARST 2019 International Symposium, Denver, CO, USA.
4. Georgiev S., Mitev, K., Dutsov, Ch., Boshkova, T., Dimitrova I., 2019. Partition coefficients and diffusion lengths of  $^{222}\text{Rn}$  in some polymers at different temperatures. Int. J. Env. Res. Publ. Health, 16, 4523.
5. Fleischer, R.L., Giard, W.R., Turner, L.G., 2000. Membrane-based thermal effects in  $^{222}\text{Rn}$  dosimetry. Radiat. Meas. 32, 325-328.
6. Tommasino, L., 2016. Concealed errors in radon measurements and strategies to eliminate them. Presented at the 8th Int. Conf. on Protection against Radon at Home and Work, Prague, 12-16 September 2016.
7. Ward III, W. J., Fleischer, R. L., Mogro-Campero, A., 1977. Barrier technique for separate measurements of radon isotopes. Rev. Sci. Instrum. 48, 1440-1441.
8. Pressyanov, D., Rönqvist, T., Gutiérrez-Villanueva, J-L., 2019. Temperature dependence CR39. Presentation on MetroRADON Workshop, Paris, September 2019.
9. Caresana, M., Ferrarini, M., Garlati L., Parravicini A., 2010. About ageing and fading of CR-39 PADC track detectors used as air radon concentration measurement devices. Radiat. Meas. 45, 183–189.
10. Cooper, A., Le, T. N., Iimoto, T., Kosako, T., 2011. Temperature calibration formula for activated charcoal radon collectors. J. Env. Radioact. 102, 60-63.
11. Pressyanov, D., 2019. Bulg. Pat. Appl. Reg. Nr. 112897, priority: 19.03.2019 (assignee: Sofia University “St. Kliment Ohridski”), WIPO Appl. Reg. Nr. PCT/BG2020/000003.
12. Sahoo, B. K., Sapra, B. K., Kanse, S. D., Gaware, J. J., & Mayya, Y. S., 2013. A new pin-hole discriminated  $^{222}\text{Rn}/^{220}\text{Rn}$  passive measurement device with single entry face. Radiat. Meas. 58, 52-60.
13. Pressyanov, D, Dimitrov, D., 2020. The problem with temperature dependence of radon diffusion chambers with anti-thoron barrier. Rom. J. Phys. 65, art. 801.
14. Tommasino, L., Tommasino, M.C., Viola, P., 2009. Radon-film-badges by solid radiators to complement track detector-based radon monitors. Radiat. Meas. 44, 719-723.



16ENV10 MetroRADON

Deliverable D2

Annexes

**EMPIR**



The EMPIR initiative is co-funded by the European Union's Horizon 2020 research and innovation programme and the EMPIR Participating States

# List of Annexes

- Annex I. Methods for the experimental study of  $^{220}\text{Rn}$  homogeneity in calibration chambers
- Annex II. Homogeneity testing of Tn-220 atmosphere at STUK
- Annex III. Thoron simulation in BACCARA
- Annex IV. Ensuring traceability of the secondary thoron reference instruments
- Annex V. Study on the influence of thoron on active radon monitors
- Annex VI. Study of the influence of thoron on radon activity concentration measurement of continuous radon monitors at IRSN
- Annex VII. Cross-interference tests performed on track-etch detectors
- Annex VIII. Study of the influence of thoron on passive radon detectors
- Annex IX. Investigation of the influence of thoron on passive integrated radon detectors
- Annex X. Investigation of the response of radon/thoron measurement instruments at different temperatures
- Annex XI. The problem with temperature dependence of radon diffusion chambers with anti-thoron barrier
- Annex XII. Review of potential techniques and materials to reduce the influence of thoron on radon measurements and calibrations
- Annex XIII. Partition Coefficients and Diffusion Lengths of  $^{222}\text{Rn}$  in Some Polymers at Different Temperatures

Annex XIV. Highly sensitive passive detectors for short-term pre- and post- mitigation

Annex XV. Characterization of polyethylene as a selective barrier for  $^{220}\text{Rn}$

Annex XVI. Methods for reduction of thoron-related bias in the radon signal of existing radon monitors

**EMPIR**



The EMPIR initiative is co-funded by the European Union's Horizon 2020 research and innovation programme and the EMPIR Participating States



16ENV10 MetroRADON

Deliverable D2  
Annex I

Activity A.2.1.1

Methods for the experimental study of  
 $^{220}\text{Rn}$  homogeneity in calibration  
chambers

K. Mitev, P. Cassette, D. Pressyanov, S. Georgiev,  
Ch. Dutsov, N. Michielsen, B. Sabot

(manuscript submitted for publication in Applied  
Radiation and Isotopes)

# Methods for the experimental study of $^{220}\text{Rn}$ homogeneity in calibration chambers

**K. Mitev<sup>a,\*</sup>, P. Cassette<sup>b</sup>, D. Pressyanov<sup>a</sup>, S. Georgiev<sup>a</sup>, Ch. Dutsov<sup>a</sup>, N. Michielsen<sup>c</sup>, B. Sabot<sup>b</sup>**

<sup>a</sup> Sofia University “St. Kliment Ohridski”, Faculty of Physics, 1164 Sofia, Bulgaria.

<sup>b</sup> CEA, LIST, Laboratoire National Henri Becquerel (LNE-LNHB), 91191 Gif-sur-Yvette Cedex, France.

<sup>c</sup> Institut de Radioprotection et de Sûreté Nucléaire (IRSN), 92262 Fontenay aux Roses, France.

## Abstract

This work presents two experimental methods for the evaluation of  $^{220}\text{Rn}$  homogeneity in calibration chambers. The first method is based on LSC of the  $^{220}\text{Rn}$  decay products captured in silica aerogel. The second method is based on application of solid state nuclear track detectors facing the air of the calibration chambers. The performances of the two methods are evaluated by dedicated experiments. The repeatability of the method, estimated as relative standard deviation of the LSC measurements of ten silica aerogel samplers exposed under the same conditions is found to be 1.6%. Both methods are applied to study thoron homogeneity in a 50 L empty AlphaGuard emanation and calibration container with its fan turned on, and it was found that the  $^{220}\text{Rn}$  distribution is homogeneous within 10%. Both methods are also applied to test the thoron homogeneity in the BACCARA chamber at IRSN during a thoron calibration exercise. The results show that, at the centre of the

---

\* Corresponding author. Tel.: + 359 889 714 226.  
E-mail address: kmitev@phys.uni-sofia.bg (K. Mitev).

chamber where the inputs of the sampling systems of the instruments were put close to each other, the thoron inhomogeneity is less than 10%. However, regions of higher thoron concentrations are clearly identified near the walls and the upper part of the chamber, with  $^{220}\text{Rn}$  concentrations being up to 60% higher compared to the concentration at the reference point. These results highlight the importance of the control and assessment of thoron homogeneity in thoron calibrations and in the cases when radon monitors are checked for thoron influence.

**Keywords:** Thoron ( $^{220}\text{Rn}$ ), Thoron calibration, Thoron homogeneity, LSC, nuclear track detectors.

## 1. Introduction

Thoron ( $^{220}\text{Rn}$ ) is an isotope of the noble gas radon with 55.8 s half-life. Studies in the last decade demonstrate that doses from thoron decay series cannot be considered negligible and there is a need for improvement of passive methods to measure thoron progeny and of the associated metrological assurance (McLaughlin, 2010; Hosoda et. al., 2017). The quality assurance of thoron measuring instruments and the studies of the influence of  $^{220}\text{Rn}$  on the radon measurement devices are areas of active research (Sabot et. al., 2016; Röttger et. al., 2009; Röttger et. al., 2010; Röttger et. al., 2014; Tokonami, 2005; He et. al., 2017; Michielsen and Bondiguel, 2015). However, the short half-life of  $^{220}\text{Rn}$  makes it difficult to ensure that it is homogeneously distributed in the chamber volume when thoron exposures are performed. Therefore, experimental methods able to probe thoron homogeneity are highly necessary.

The objective of this work is to present two newly proposed methods for evaluation of thoron homogeneity and their application in the thoron calibration exercise that has been carried out at IRSN in the framework of the MetroRADON Euramet EMPIR joint research project. The first method is based on a capture of thoron decay products in silica aerogel grains and subsequent liquid scintillation counting (LSC) of the silica aerogel. The second method is based on the measurement of the density of tracks formed by  $^{220}\text{Rn}$  and  $^{216}\text{Po}$  in Kodak Pathe LR-115/II solid state nuclear track detectors (SSNTDs). The two methods are applied successfully for the evaluation of  $^{220}\text{Rn}$  homogeneity in small (50 L) calibration vessels as well as in the BACCARA chamber (1 m<sup>3</sup>) at IRSN with seven  $^{220}\text{Rn}$  measuring instruments inside.

## 2. Evaluation of thoron homogeneity by LSC of silica aerogel

This method makes use of a silica aerogel as thoron sampler and its subsequent mixing with a LS cocktail for LSC counting. The idea of the sampler is to allow thoron to enter freely from the environmental air into the cylindrical volume through the filters and to stop the thoron decay products on the filters. Thus, when  $^{220}\text{Rn}$  decays inside the sampler, its decay products ( $^{216}\text{Po}$ ,  $^{212}\text{Pb}$ ,  $^{212}\text{Bi}$ ,  $^{212}\text{Po}$  and  $^{208}\text{Tl}$ ) will attach to the silica aerogel and their activity in the silica aerogel will be proportional to the  $^{220}\text{Rn}$  activity that has entered in the cylinder. The latter is proportional to the ambient  $^{220}\text{Rn}$  activity concentration in the air surrounding the sampler. The usage of silica aerogel provides a large / sufficient amount of free space in the sampler for thoron to diffuse in and at the same time allows the effective capture of its decay products.

The  $^{220}\text{Rn}$  transport inside the sampler (assumed to have a cylindrical geometry) can be described by the diffusion equation with a term accounting for radioactive decay. As the thoron half-life is 55.8 s, for constant thoron concentration and exposures longer than 10 min, a steady state diffusion can be assumed:

$$D \frac{\partial^2 C}{\partial x^2} - \lambda C = \frac{\partial C}{\partial t}, \text{ with } \frac{\partial C}{\partial t} = 0 \quad (1)$$

where  $C$  is the  $^{220}\text{Rn}$  activity concentration,  $D$  is the diffusion coefficient of  $^{220}\text{Rn}$  in the material,  $\lambda$  is the  $^{220}\text{Rn}$  decay constant,  $x$  is the space coordinate along the cylinder axis and  $t$  is the time variable. The solution of the above equation in plate parallel geometry along the axis of the sampler is:

$$C(x) = C_{out} \frac{\cosh\left(\frac{2x-L}{2L_D}\right)}{\cosh\left(\frac{L}{2L_D}\right)} \quad (2)$$

and the  $^{220}\text{Rn}$  activity in the sampler ( $A_{Tn}$ ) is given by

$$A_{Tn} = 2C_{out}V\frac{L_D}{L}\tanh\left(\frac{L}{2L_D}\right), \quad (3)$$

where  $C_{out}$  is the outside  $^{220}\text{Rn}$  activity concentration (assuming that the filters are transparent to thoron),  $L$  and  $V$  are the height and the volume of the cylinder and  $L_D=(D/\lambda)^{1/2}$  is the diffusion length of  $^{220}\text{Rn}$  in the material (air or silica aerogel). Taking into account that the diffusion coefficient of  $^{220}\text{Rn}$  in air is  $D=10^{-5}\text{ m}^2/\text{s}$  (Ishimori et. al., 2013) which gives  $L_D=3.0\text{ cm}$ , from Eq. 2 it follows that one can expect non-homogeneous thoron distribution inside the sampler. Thus, it is important, as shown hereafter, to choose carefully the thickness of the samplers to ensure best performance.

Specially designed thoron samplers were developed as shown in Fig 1. The sampler consists of a cylindrical body and two end caps, which serve to fix and support two air filters (bottom and top) at the ends of the cylinder (Fig. 1a). The inner and the outer diameters of the cylinder are 4.4 cm and 4.7 cm, respectively. The diameters were chosen to fit the diameter of the filters ( $d=4.7\text{ cm}$ ). The silica aerogel was crushed and sieved (from  $\sim 0.5\text{ mm}$  to  $3.0\text{ mm}$ ) to get grains with suitable size – small enough so they can fit in the sampler without punctuating the closing filters and, at the same time, large enough (e.g. larger than dust particles) to allow the aerogel to absorb the LS cocktail quickly in order to perform the LSC measurement as soon as possible after the exposure. The silica aerogel is placed in the cylinder (Fig. 1b) and the sampler is closed tight (Fig. 1c). All plastic parts of the thoron sampler are locally made with a 3D printer.

In order to evaluate the thoron homogeneity during the calibration exposures the thoron samplers can be positioned at any point of interest in the calibration chamber. After the end of the thoron exposure, the samplers are removed and the silica aerogel

from each sampler is carefully transferred in a high performance LS glass vial. The mass of the transferred silica aerogel is determined by weighing the LS vials. The vials are then filled with 15 mL Ultima Gold LLT LS cocktail and placed for 10 min in an ultrasonic bath in order to facilitate the full penetration of the scintillation cocktail in the silica aerogel and to remove air bubbles from it (Fig. 3).

Different types of filters were tested - glass microfiber filter with an equivalent pore size of 1.2  $\mu\text{m}$  and thickness 260  $\mu\text{m}$  (LLG-Labware 9045867), mixed cellulose ester membrane filter with an equivalent pore size of 0.2  $\mu\text{m}$  and thickness 130  $\mu\text{m}$  (ADVANTEC A20A047A) and mixed cellulose ester membrane filter with 0.3  $\mu\text{m}$  equivalent pore size and thickness 150  $\mu\text{m}$  (Millipore PHWP04700). The performance criterion for the choice of the filter is the agreement between the measured net LS counting rate and the expected net LS counting rate from the activity, absorbed in the aerogel, which is determined from Eq. 3.

The results from the tests showed that net LS counting rate obtained with the glass microfiber filters is always higher than the net LS counting rate expected from the absorbed activity (Eq. 3). Therefore, we conclude that the used glass microfiber filters do not completely stop the thoron progeny from penetrating in the samplers. The best agreement between the measured and the expected net LS counting rate was obtained with two membrane filters placed on each entry of the sampler. Both types of filters ADVANTEC A20A047A and Millipore PHWP04700 show excellent performance. Scanning electron microscope images of the used membrane filters are shown in Fig. 2.

In order to choose the optimal thickness, three different samplers were produced with  $L=1.0$  cm, 1.5 cm and 2.0 cm. Six samplers (two of each thickness) were exposed to thoron in a 50 L AlphaGuard calibration container with an AlphaGuard

PQ2000 PRO (Rn/Tn) reference monitor placed inside. The  $^{220}\text{Rn}$  activity concentration during the exposure was  $C_{out}=612(61)\text{ kBq/m}^3$  and the exposure duration was 68.2 h. The samplers were placed at the bottom of the vessel close to each other with a special focus on  $^{220}\text{Rn}$  freely reaching each sampler and passing through the filters. After the exposure the silica aerogel from each sampler was transferred in a high performance glass vial and the vials were measured on a RackBeta 1219 LS counter (Wallac, Finland). The results are shown in Table 1 and indicate that the thinnest samples have the highest net counting rate per unit mass. Considering the results in Table 1 and noting that the net LS counting rate is due to several thoron progenies ( $^{212}\text{Pb}$ ,  $^{212}\text{Bi}$ ,  $^{212}\text{Po}$  and  $^{208}\text{Tl}$ ) it can be concluded that samplers with thickness  $L=1\text{ cm}$  which contain around 5 g of silica aerogel provide sufficiently good sensitivity of the method to be applied for the evaluation of  $^{220}\text{Rn}$  homogeneity.

The most important characteristic of the proposed method from the point of view of practical applications is its repeatability. It is studied in this work with the experimental set-up shown schematically in Fig. 4 and on the photo in Fig. 5. The set-up consists of a powerful fan (gas-flow  $2.5\text{ m}^3/\text{min}$ ) mounted to a tube. Inside the tube there are 10 thoron samplers divided in two groups (AG1 to AG5 mounted closer to the fan and AG6 to AG10 just behind them, see Fig. 4a and Fig 5a). The samplers are positioned with their filter-sides parallel to the air-flow (see Fig. 4b and Fig 5b). The entire system is placed in a 50 L calibration container (Fig. 6) with one thoron sampler placed at the exit of the tube perpendicular to the gas-flow (AG11) and another sampler placed outside beside the tube (AG12), see Fig. 4a and Fig. 6. The thoron inlet is positioned right in front of the fan and the container is closed hermetically. The gas-flow of the fan ( $150\text{ m}^3/\text{h}$ ) is chosen large enough to guarantee

that all the samplers in the tube (AG1-AG10) are exposed to the same thoron concentration and the volume refresh rate (50 times per min) is sufficient to assume that AG11 and AG12 are also exposed to the same concentration. The duration of the  $^{220}\text{Rn}$  exposure was 66 h and the thoron activity concentration in the container was 474(47) kBq/m<sup>3</sup>. After the exposure, the silica aerogel from the samplers was transferred and measured on the RackBeta 1219 LS counter as described above. The net counting rate of each sample was followed for 60 h and the net counting rates at the moment of the end of exposure are evaluated. The results, presented in Table 2, show that the relative standard deviation of the net counting rates per unit mass of the samplers in the tube (AG1-AG10) is 1.6% and their variations are fully within the estimated uncertainties. Moreover, the sampler AG11, which is in front of the tube and is perpendicular to the air stream also agrees well with the mean value within its estimated uncertainty. The same is also true for the sampler AG12, which is behind the tube (see Fig. 4a and Fig. 6). These results suggest a repeatability of the method of the order of 1.6%, which is an excellent repeatability for the evaluation of thoron homogeneity in  $^{220}\text{Rn}$  calibrations.

### **3. Evaluation of thoron homogeneity by SSNTDs**

The other approach we investigated to evaluate the homogeneity of  $^{220}\text{Rn}$  in chambers is based on the use of bare SSNTDs, placed at different points inside the chamber. These detectors register alpha particles that reach the detector surface with energy and incident angle within certain registration window specific for each type of SSNTDs. Normally, the air contains a mixture of isotopes (in this case  $^{220}\text{Rn}$  and its progeny atoms  $^{216}\text{Po}$ ,  $^{212}\text{Pb}$ ,  $^{212}\text{Bi}+^{212}\text{Po}/^{208}\text{Tl}$ ,  $^{212}\text{Po}$  is always in equilibrium with  $^{212}\text{Bi}$ ). However, in an exposure chamber volume a substantial part of the progeny

atoms is deposited on the internal walls (George et al., 1983). The deposited fraction is higher when a fan creates air turbulence inside the chamber (Cheng et al., 1990) (the described experiments were made in this mode). Parallel measurements (Pressyanov, 2002) of the activity concentrations of  $^{222}\text{Rn}$  and its progeny in 200 L spherical volume with a fan operating inside showed that the deposited fractions are 94.0%, 99.7% and 99.9% for  $^{218}\text{Po}$  (half-life 3.05 min),  $^{214}\text{Pb}$  (half-life 26.8 min) and  $^{214}\text{Bi}$  (half-life 19.9 min), respectively. When  $^{220}\text{Rn}$  + progeny is created in the chamber, due to the longer half-life of  $^{212}\text{Pb}$  (half-life 10.64 h) and  $^{212}\text{Bi}$  (half-life 60.55 min) one can expect that practically all of the  $^{212}\text{Pb}$  and  $^{212}\text{Bi}+^{212}\text{Po}$  atoms are deposited on the walls and their air fraction is negligible. Results of other authors (Harley et. al., 2010) also show extreme disequilibrium in air between  $^{220}\text{Rn}$  and its decay products  $^{212}\text{Pb}$  and  $^{212}\text{Bi}$ , even for much larger volumes (e.g. rooms) than the volumes of 200 L or 1 m<sup>3</sup>. Therefore, within the present approach, we assume that the isotopes in the air are  $^{220}\text{Rn}$  and  $^{216}\text{Po}$  and that  $^{216}\text{Po}$ , due to its short half-life of 0.15 s, it has of the same volume distribution as  $^{220}\text{Rn}$ .

In our experiments SSNTDs of Kodak-Pathe LR-115 type II were used. They register alpha particles within an energy and angular window of registration that depends on the etching conditions and the mode of counting. These conditions in our case were etching with 10% NaOH at 60 °C for 100 min, washing with water for 30 min and washing for 2 min in still 50% ethanol and visual counting by microscope - only of tracks that created holes through the 12 μm sensitive layer of this type of detectors were counted. As described elsewhere (Pressyanov, 2012), under these conditions the detectors register alpha particles of energy within 1.5 – 4.0 MeV and incident angle <55° to the normal. The air volumes from which the alpha particles of different isotopes can be detected are schematically shown in Fig.7. What is essential

for this application is that the alpha particles from the  $^{220}\text{Rn}$  progeny atoms deposited on the detector surface cannot be detected, as their energy is well above the upper energy threshold of the window for registration. From Fig.7 it follows that, to avoid contribution from the atoms deposited on the chamber internal surface, the SSNTD face should look to air being at a distance of at least 8 cm from any surface – i.e. outside the range of  $^{212}\text{Po}$  alphas. Under these conditions the tracks will be due only to the alpha particles from the sources in the air ( $^{220}\text{Rn}$  and  $^{216}\text{Po}$ ) and the registered tracks will originate from the isotopes that are in a small volume within a distance of 2.4 – 5.0 cm from the detector surface (“detection volumes”, see Fig. 7).

Respecting the above rule, Kodak-Pathé LR-115/II detectors were used in two experiments. The first was in 50 L cylindrical exposure chamber in which 33 pieces of detectors were placed. The map of the “detection volumes” is shown in Fig. 8. The exposure was made at the laboratory facility, described elsewhere (Pressyanov et. al., 2017). The exposure was made at an average  $^{220}\text{Rn}$  concentration of 800(50) kBq m<sup>-3</sup> for 220 min. During exposure the  $^{220}\text{Rn}$  concentrations were followed by a reference instrument AlphaGUARD PQ2000 PRO (Rn/Tn). The analysis of the results showed that the distribution of  $^{220}\text{Rn}$  in the air is homogeneous within 10%. The variations between the results can be explained by the detector reading uncertainty and sub-volumes of significantly higher or lower concentrations cannot be identified. Similar homogeneity (i.e. within 10%) of the empty 50 L AlphaGuard calibration volume with its own fan turned on is obtained by the LS counting of the silica aerogel (not shown).

#### **4. Application of the methods during the thoron calibration exercise, performed at BACCARA chamber at IRSN**

A thoron calibration exercise was carried out in May 2018 in the framework of the MetroRADON Euramet project using the IRSN reference radon chamber called BACCARA. The BACCARA chamber is a 1 m<sup>3</sup> stainless steel chamber with a thoron reference instrument attached to it (Sabot et. al., 2016), which is used to create reference radon and thoron atmospheres for calibration of radon and thoron measuring devices. During the thoron calibration exercise, four AlphaGuards and three RAD7 instruments were placed in the chamber and their thoron measurement performance was checked against the reference instrument (Fig. 9). The thoron calibration exercise and its results will be described in detail elsewhere. In order to test the thoron homogeneity in the BACCARA chamber during the calibration exercise 12 silica aerogel thoron samplers and 22 pieces of SSNTDs were placed at different positions in the chamber (Fig. 9). The SSNTDs were placed in all parts of BACCARA internal volume, but respecting the stated above rule for detector position. The thoron exposure duration was 48 h and the <sup>220</sup>Rn activity concentration in the chamber was 46 kBq/m<sup>3</sup>. In order to avoid the effect of possible <sup>220</sup>Rn inhomogeneity during the calibration, the inputs of the instruments sampling systems were put close to each other as much as possible to the extent of forming a sampling point in the chamber (Fig. 10). The silica aerogel samples and the SSNTDs were placed around the sampling and all other parts of the chamber, trying to cover the upper part of the chamber (Figures 11 and 12) as well as the space around the sampling points and around and between the detectors (Fig. 13).

After the end of the exposure, the silica aerogel samples were treated as described above. The activity in the samples is measured on a Wallac Guardian LS counter at LNHB and the results are shown in Table 3. For better visualization, the values obtained with the different samplers are shown relative to the reference point in

Figures 11-13. The results in Table 3 and Fig. 11 show that the differences between the  $^{220}\text{Rn}$  concentrations in positions “C”, near the center of the chamber, close to the instruments’ sampling points, do not exceed 10%. But, one can observe higher differences for positions “W”, far from the center of the chamber, for example the  $^{220}\text{Rn}$  concentrations near the upper wall of the chamber (AT7) are up to 61% higher than those in the center (Fig. 11). Similarly, the thoron concentration near the walls of the chamber are higher than those at the reference point (see, for example AT4, AT5, AT11 and AT7 in Fig. 11 and 12). The  $^{220}\text{Rn}$  concentration below the instruments (AT8) are also higher than those in the reference point (Fig. 13). Overall, it seems that the  $^{220}\text{Rn}$  concentration near the sampling point of the instruments is homogeneous, but there are volumes in the chamber near the walls, the entry point of the thoron and in front of the fan where much higher  $^{220}\text{Rn}$  concentrations are observed.

The SSNTD results reveal signs of inhomogeneity with up to about 60% deviation from the reference point (Fig. 14). It should be noted also that the silica aerogel sampling method and the SSNTD method give consistent results for the points where the two methods can be applied (see Fig. 12). For example, the detection volume of the highest deviation ratio 1.61(0.18) corresponds to SSNTD No 4 and it is close to the space where LSC of silica aerogel (AT5) also showed high deviation (ratio of 1.55). Similarly, SSNTD No 7 and AT11, which are close at the back of the chamber, give very close results (Fig. 12). The two methods clearly demonstrate that there can be high thoron inhomogeneity near the walls of the chamber.

## 5. Conclusions

Two experimental methods for evaluation of  $^{220}\text{Rn}$  homogeneity in calibration chambers are presented. The first method is based on LSC of thoron short-lived decay

products captured in silica aerogel and the second method is based on application of SSNTDs. The performance of the two methods is evaluated in several dedicated experiments where it is shown that the repeatability of the method based on LSC of silica aerogel is within 1.6%. Both methods are applied to study thoron homogeneity in a 50 L empty AlphaGuard emanation and calibration container with its fan turned on, and it was found that thoron distribution is homogeneous within 10%.

Both methods are applied successfully to test the thoron homogeneity in the BACCARA chamber during the thoron calibration exercise that was carried out at IRSN, France in the framework of the MetroRADON Euramet EMPIR project. The results show that, at the centre of the chamber, where the inputs of the instruments sampling systems were put close to each other, the thoron inhomogeneity is less than 10%. However, regions of higher thoron concentrations are clearly identified near the walls and the upper part of BACCARA, with  $^{220}\text{Rn}$  concentrations being up to 60% higher compared to the concentration at the reference point. These results highlight the importance of the control and assessment of thoron homogeneity in thoron calibrations and in the case when radon monitors are checked for thoron influence. The assessment of  $^{220}\text{Rn}$  homogeneity will be particularly important in the case of checking passive radon monitors for thoron influence. That is because, contrary to the case of active monitors, there are no inputs of the passive detectors, so they cannot be put together near a common sampling point in the calibration chamber. Thus, an experimental method for checking thoron homogeneity as those described in this work will be highly necessary.

## **Acknowledgements**

This work is supported by the European Metrology Programme for Innovation and Research (EMPIR), JRP-Contract 16ENV10 MetroRADON ([www.euramet.org](http://www.euramet.org)). The EMPIR initiative is co-funded by the European Union's Horizon 2020 research and innovation programme and the EMPIR Participating States.

## References

- Cheng, Y. S., Su, Y. F., Chen, B. T., 1990. Plate-out rates of radon progeny and particles in a spherical chamber. Proc. XXIX Hanford Symposium on Health and the Environment, pp. 65-79.
- George, A. C., Knutson, E. O., Tu, K. W., 1983. Radon daughter plateout – I measurements. Health Phys. 45, 439-444.
- Harley, N., Chitaporn, P., Medora, R., Merrill, R., 2010. Measurement of the indoor and outdoor  $^{220}\text{Rn}$  (thoron) equilibrium factor: Application to lung dose. Radiat. Prot. Dosimetry 141, 357-362.
- He, Z., Xiao, D., Lv, L., Zhou, Q., Wu, X., Shan, J., 2017. Stable control of thoron progeny concentration in a thoron chamber for calibration of active sampling monitors, Radiation Measurements. 102, 27-33.
- Hosoda, M., Kudo, K., Iwaoka, K., Yamada, R., Suzuki, T., Tamakuma, Y., Tokonami, S., 2017. Characteristic of thoron ( $^{220}\text{Rn}$ ) in environment, Appl. Radiat. Isot. 120, 7-10.
- Ishimori, Y., Lange, K., Martin, P., Mayya, Y.S., Phaneuf, M., 2013. Measurement and calculation of radon releases from NORM residues, IAEA technical reports series No. 474.
- Kobayashi, Y., Tokonami, S., Takahashi, H., Zhuo, W., Yonehara, H., 2005. International Congress Series, 1276, 281-282.
- McLaughlin, J., 2010. An overview of thoron and its progeny in the indoor environment, Radiat. Prot. Dosimetry. 141, 316-321.
- Michielsen, N., Bondiguel, S., 2015. The influence of thoron on instruments measuring radon activity concentration, Radiat. Prot. Dosimetry. 141, 289-292.

- Pressyanov, D., 2002. Evaluation of the radiological hazards in houses and working places by integrated measurements of the individual  $^{222}\text{Rn}$  progeny in air. Research contract between the Ghent University and Sofia University “St. Kliment Ohridski” (DOB/HB/RS/02), final report.
- Pressyanov, D., 2012. Radon and Radon Progeny: Methodological Points and Case Studies. Lambert Academic Publishing GmbH & Co. KG, Saarbruecken, Germany. ISBN: 978-3-8484-8604-5
- Pressyanov D., Mitev K., Georgiev S., Dimitrova I., Kolev J. (2017) Laboratory facility to create reference radon + thoron atmosphere under dynamic exposure conditions. J. Env. Radioact.166, 181-187.
- Röttger, A., Honig, A., Arnold, D., 2009. The German thoron progeny chamber – Concept and application, Appl. Radiat. Isot. 67, 839-842.
- Röttger, A., Honig, A., Dersch, R., Ott, O., Arnold, D., 2010. A primary standard for activity concentration of  $^{220}\text{Rn}$  (thoron) in air, Appl. Radiat. Isot. 68, 1292-1296.
- Röttger, A., Honig, A., Linzmaier, D., 2014. Calibration of commercial radon and thoron monitors at stable activity concentrations, Appl. Radiat. Isot. 87, 44-47.
- Sabot, B., Pierre, S., Michielsen, N., Bondiguel, S., Cassette, P., 2016. A new thoron atmosphere reference measurement system, Appl. Radiat. Isot. 109, 205-209.

### **Figure captions:**

- Fig. 1.** A photograph of a thoron sampler. a) – Empty sampler, with bottom air filter, ready to be filled with silica aerogel and the top end cap with top air filter mounted; b) the sampler filled with silica aerogel; c) closed sampler ready to be placed in thoron chamber.
- Fig. 2.** Scanning electron microscope images of the Millipore membrane filters used for the samplers. a) and b) –surface view, c) and d) – cross-sectional view.
- Fig. 3.** High performance LS glass vials (20 ml) filled with silica aerogel and Ultima Gold LLT LS cocktail. The photograph is taken after the vials had been placed for 10 min in a ultrasonic bath. When filled with LSC cocktail, the aerogel becomes translucent.
- Fig. 4.** Schematic view of the geometry used to test the repeatability of the silica aerogel method. a) Schematic view of the exposure vessel, the  $^{220}\text{Rn}$  inlet, the fan and the tube with the thoron samplers; b) Illustration of the arrangement of the thoron samplers in the tube.
- Fig. 5.** Photographs of the experimental arrangement used to test the repeatability of the silica aerogel method: the fan, the tube and the thoron samplers can be seen in the picture.
- Fig. 6.** Photograph of the exposure set-up used to test the repeatability of the silica aerogel method. The fan and the tube with the samplers are placed in a 50 L vessel. Additional samplers are placed in front and near the tube.
- Fig. 7.** Air-volumes from which alpha particles can be detected by LR-115/II SSNTD. The volumes are shaped taking into account the fact that energy

window for track registration get narrow when the incident angle is increasing.

**Fig. 8.** The picture shows the spots in the chamber volume from where activity can be detected by the placed in a grid Kodak Pathe LR-115/II SSNTD (“detection” volumes).

**Fig. 9.** A photograph of the BACCARA chamber showing the experimental set-up used in the thoron calibration exercise. The thoron inlet nozzle and the fan used to homogenize the air in the chamber are indicated as well as the positions of some of the thoron samplers and the SSNTDs.

**Fig. 10.** Photograph showing the sampling point, where the inlets of the thoron measuring instruments are located. There are thoron samplers (AT1, AT2 and AT6) and a SSNTD (No 16) around the sampling point. The percent in the boxes with the sampler number indicate the sampler’s readings relative deviation with respect to the reference (AT1).

**Fig. 11.** Position and relative deviation with respect to the reference position of the readings of the thoron samplers in the upper half of the BACCARA.

**Fig. 12.** Position and relative deviation with respect to the reference position of the readings of the thoron samplers in the upper half of the BACCARA and near the sampling point.

**Fig. 13.** Position and relative deviation with respect to the reference position of the readings of the thoron samplers located below and between the  $^{220}\text{Rn}$  measuring instruments.

**Fig. 14.** The ratio of the SSNTD signal (net track density) to the signal of the detector that is at closest distance to the reference point (detector No 16).

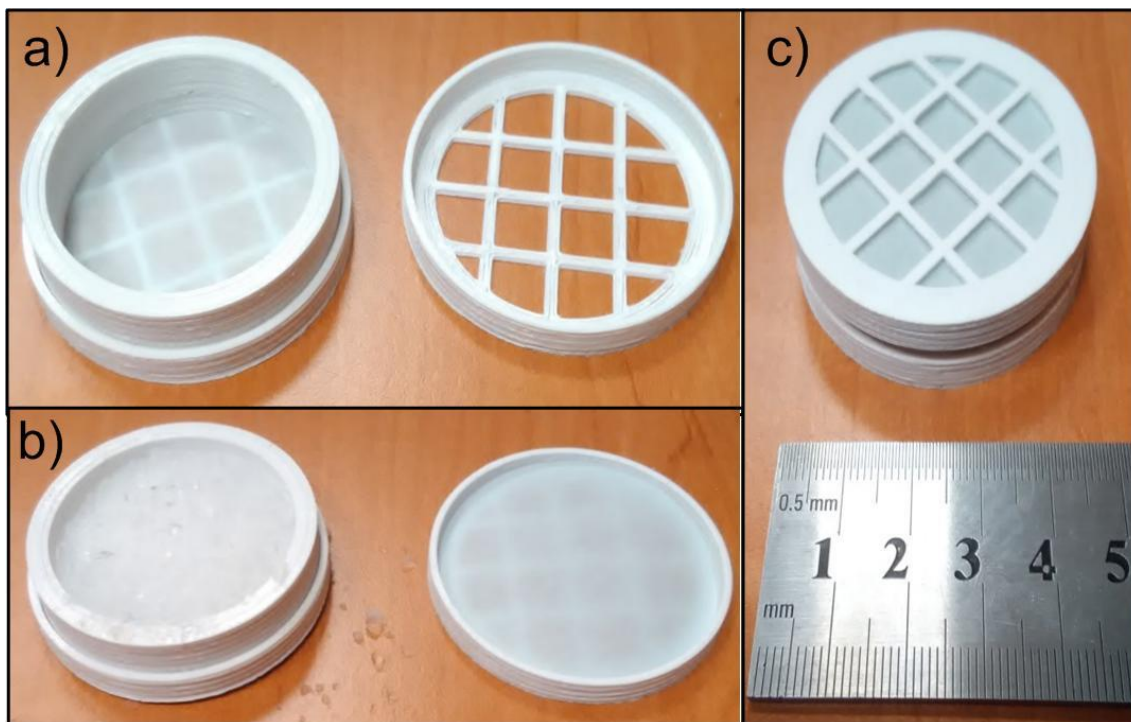


**Fig. 1**

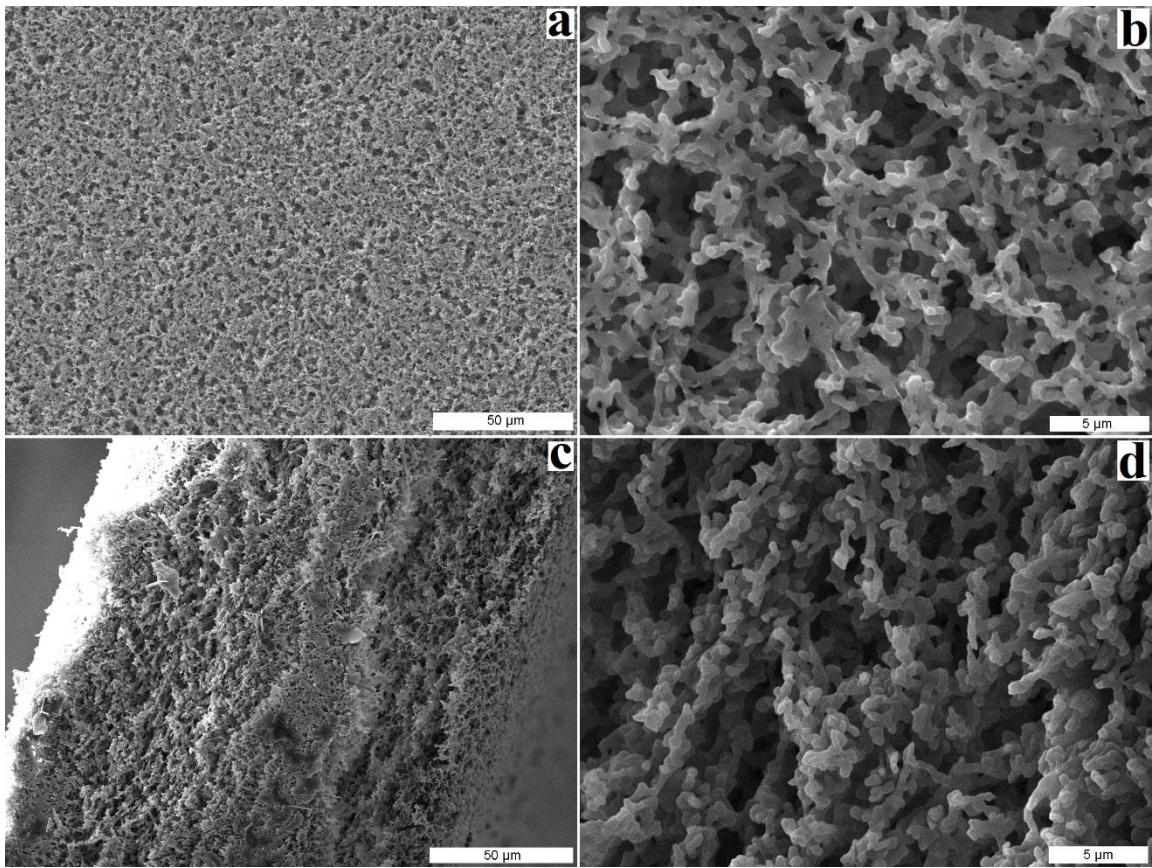


**Fig. 2**



**Fig. 3**

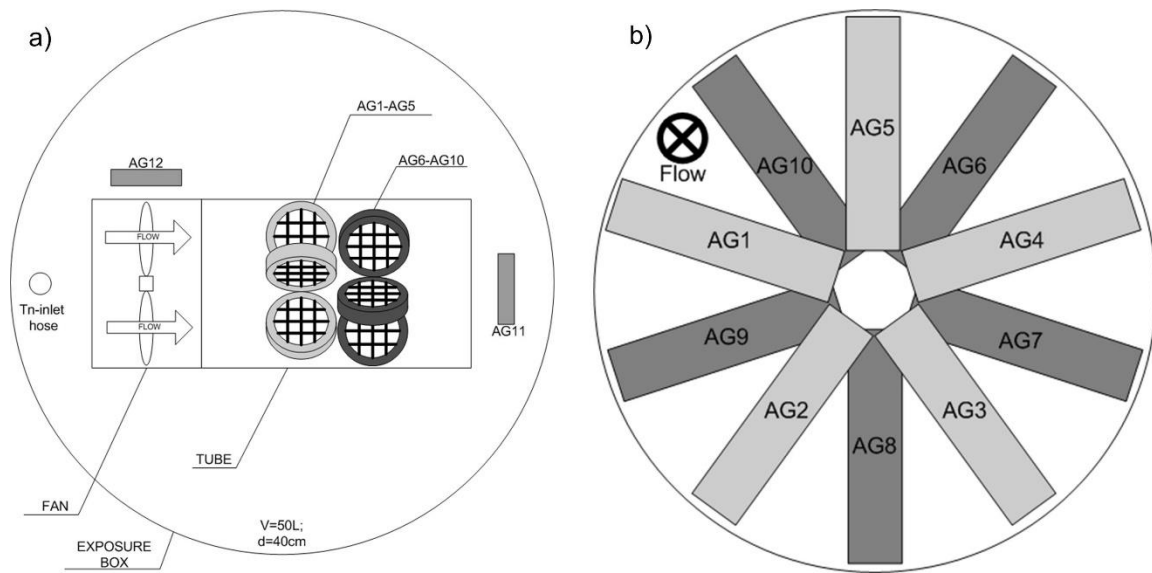


**Fig. 4**



**Fig. 5**

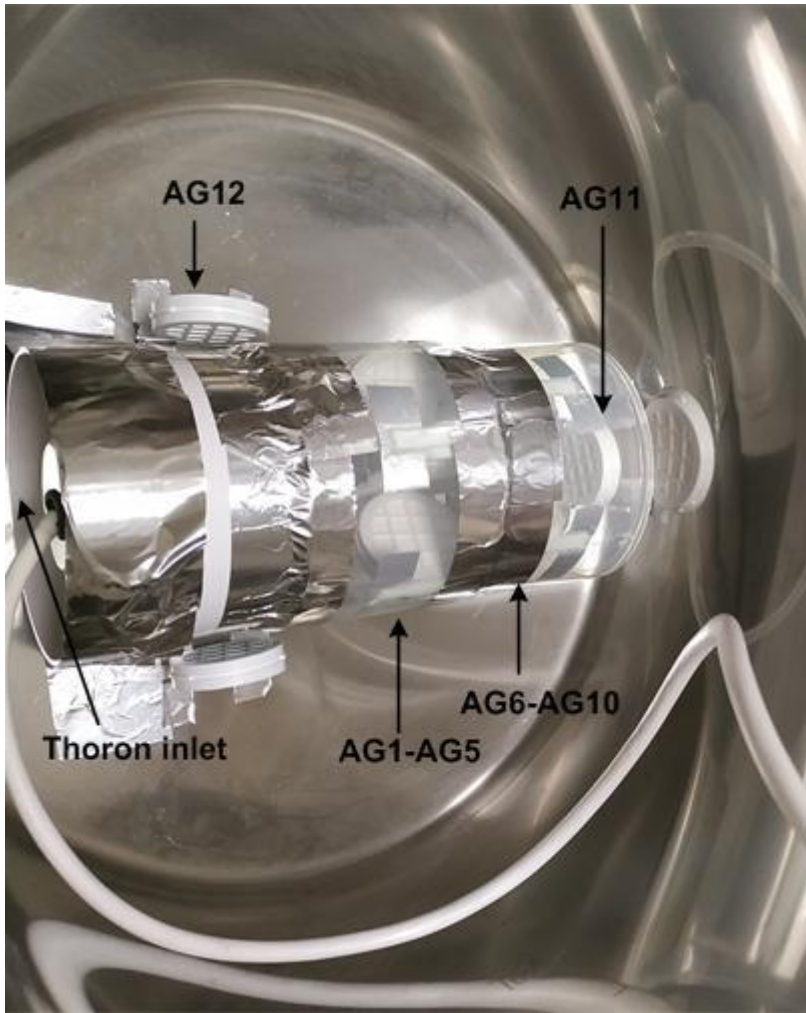


**Fig. 6**

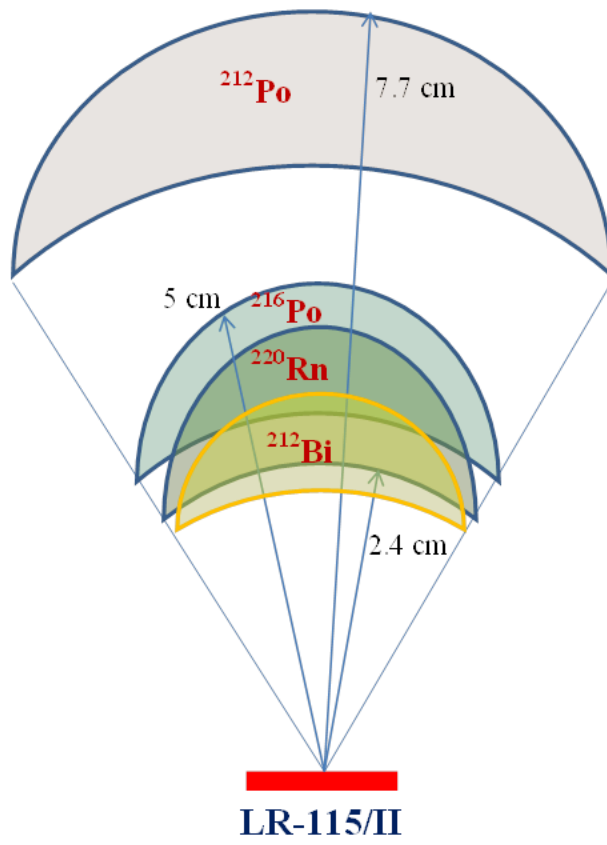


**Fig. 7**

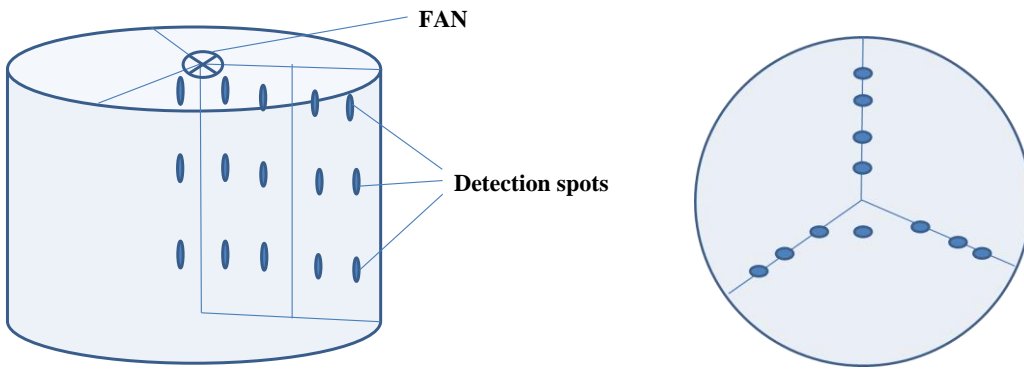


**Fig. 8**

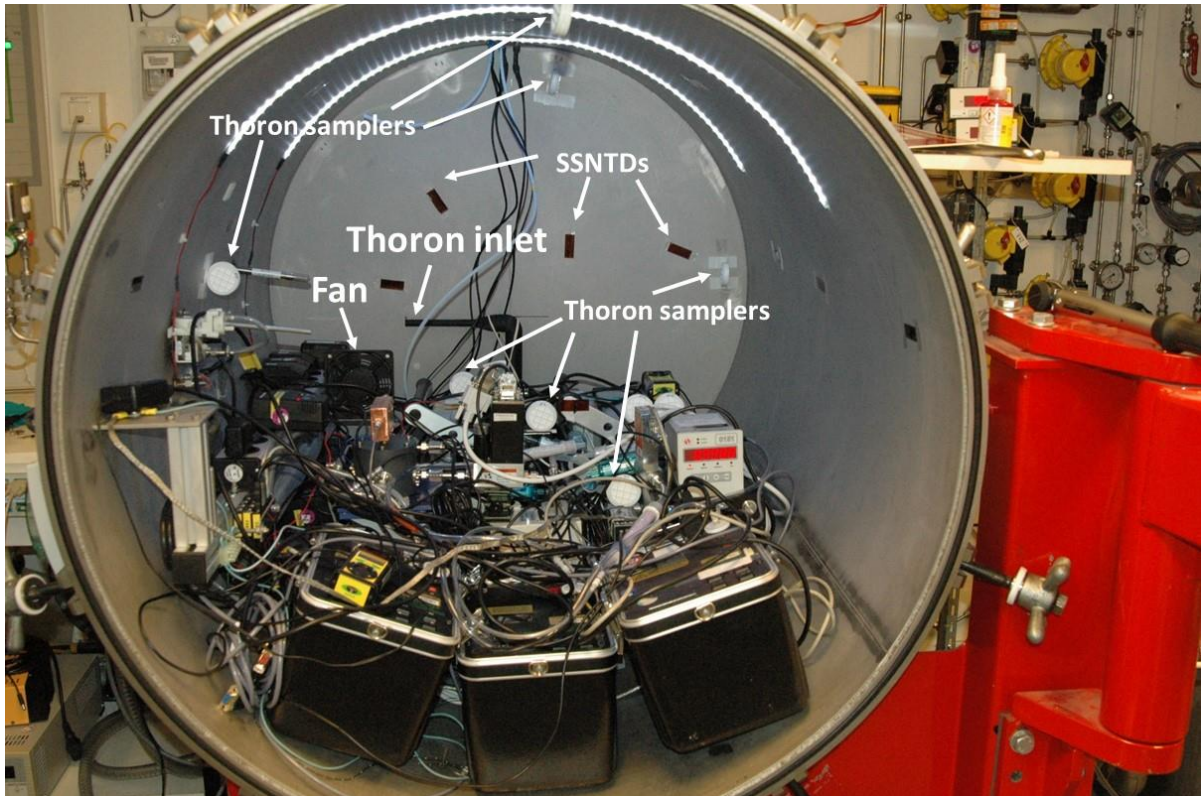


**Fig. 9**

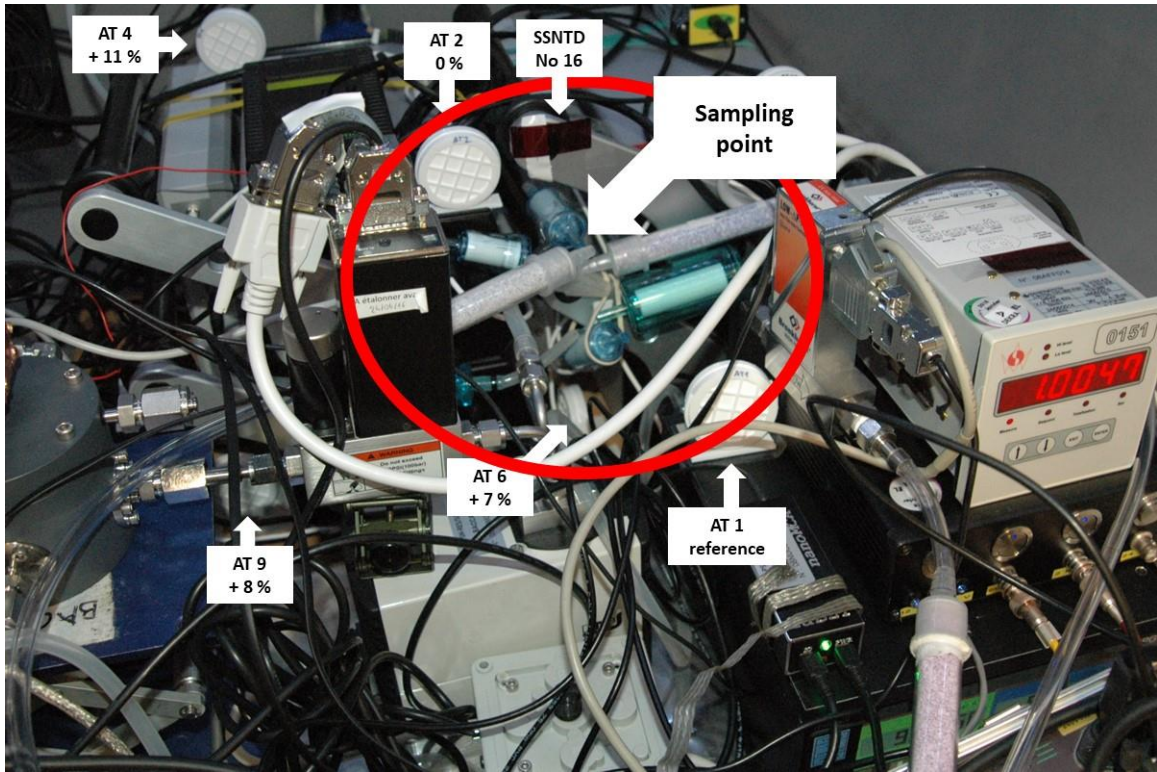


**Fig. 10**

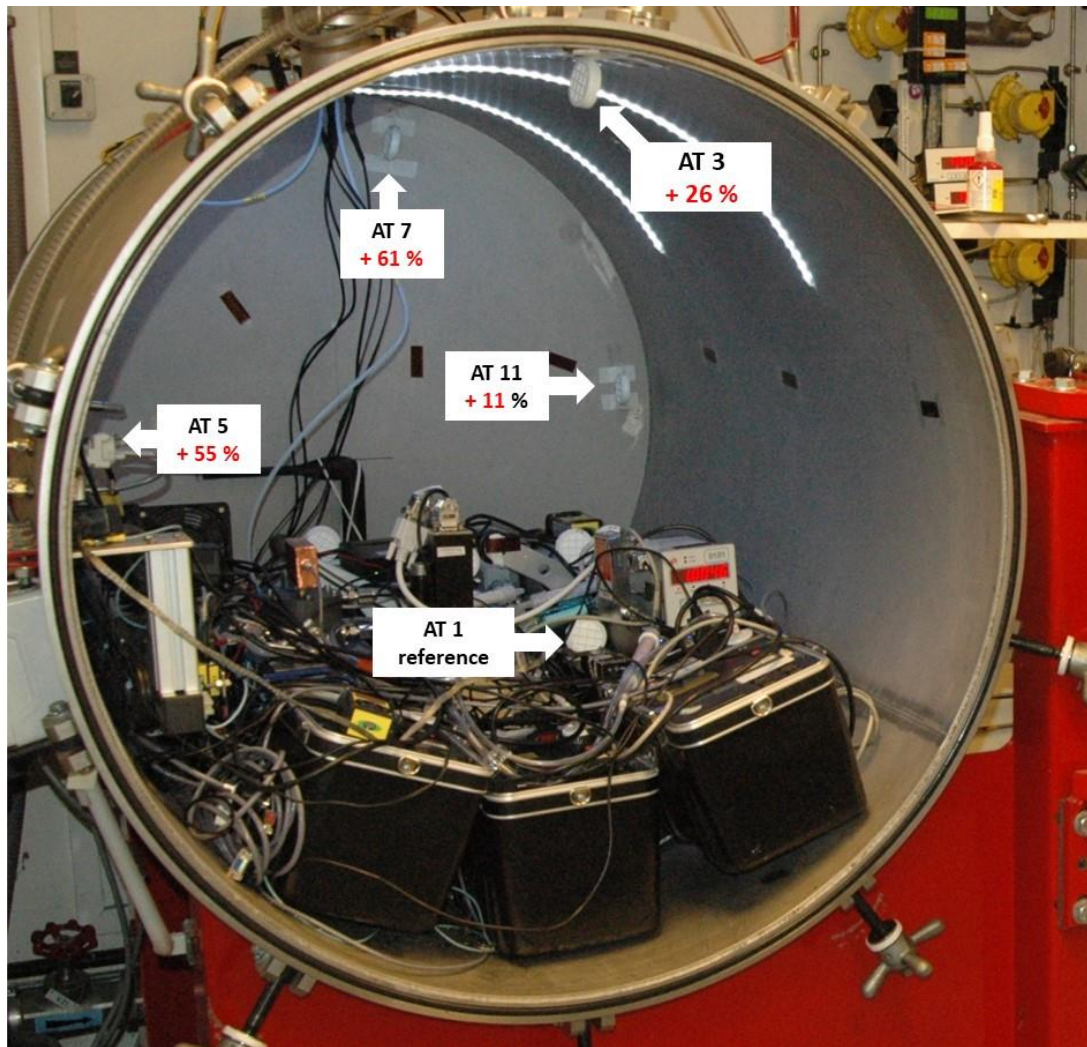


Fig. 11

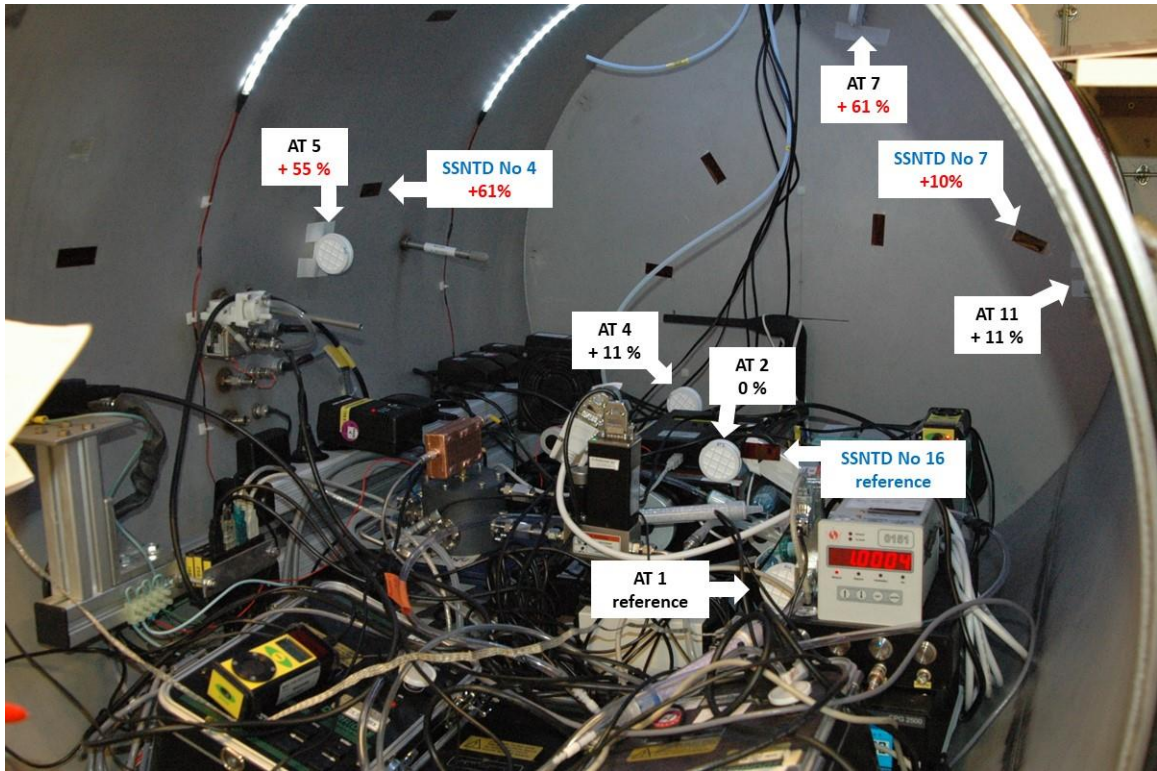
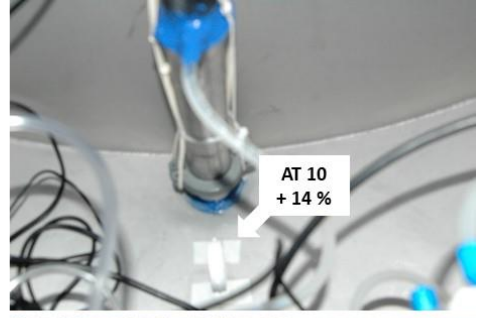
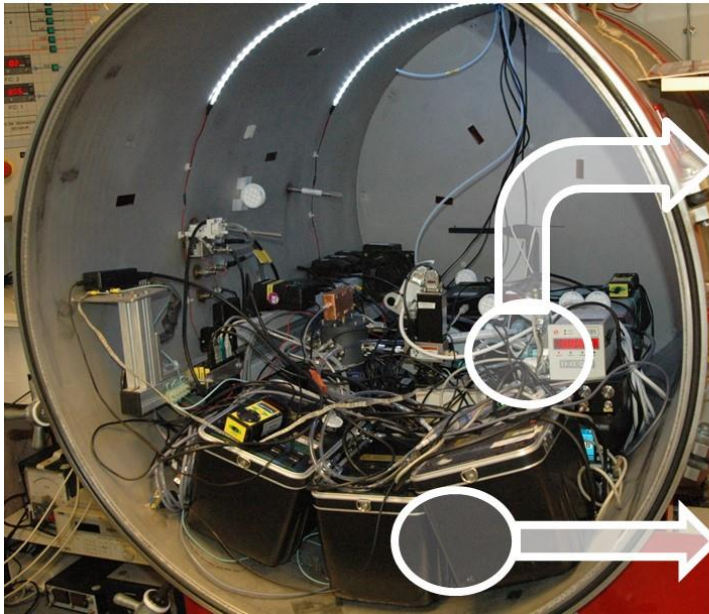


Fig. 12



**Fig. 13.**

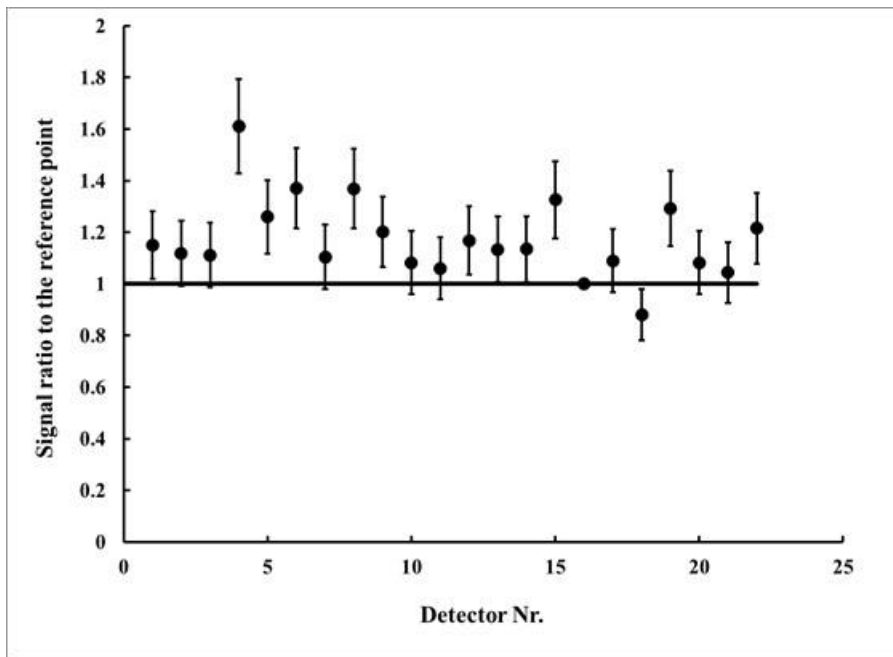


Fig. 14

**Table 1:** Net counting rates per unit mass of thoron samplers with different heights exposed together to  $^{220}\text{Rn}$  in air.

| Sampler | L, cm | V, cm <sup>3</sup> | Mass of the silica aerogel in the samplers, g | Net LS counting rate per unit mass of the silica aerogel, s <sup>-1</sup> g <sup>-1</sup> |
|---------|-------|--------------------|---|---|
| S1      | 1.0   | 15.21              | 5.421(5)                                      | 10.290(58)  |
| S2      | 1.0   | 15.21              | 5.202(5)                                      | 10.415(60)  |
| M1      | 1.5   | 22.81              | 8.649(5)                                      | 9.119(56)   |
| M2      | 1.5   | 22.81              | 8.472(5)                                      | 9.054(58)   |
| L1      | 2.0   | 30.41              | 11.932(5)                                     | 7.761(56)   |
| L2      | 2.0   | 30.41              | 11.920(5)                                     | 7.714(55)   |

**Table 2:** Study of the repeatability of  $^{220}\text{Rn}$  readings with thoron samplers. The numbers in the brackets indicate the overall estimated standard uncertainties.

| Thoron sampler                                  | Mass of the silica aerogel in the LS vial (g) | Net LS counting rate per unit mass of the silica aerogel at the end of the exposure( $\text{s}^{-1}\text{g}^{-1}$ ) | Difference from the mean (%) |
|---|---|---|------------------------------|
| AG 1  | 5.014(5)                                      | 6.44(26)  | 1.3%                         |
| AG 2  | 5.064(5)                                      | 6.24(22)  | -1.9%                        |
| AG 3  | 5.054(5)                                      | 6.40(14)  | 0.6%                         |
| AG 4  | 4.914(5)                                      | 6.31(16)  | -0.8%                        |
| AG 5  | 5.055(5)                                      | 6.43(16)  | 1.0%                         |
| AG 6  | 5.050(5)                                      | 6.51(18)  | 2.3%                         |
| AG 7  | 5.040(5)                                      | 6.21(21)  | -2.3%                        |
| AG 8  | 5.042(5)                                      | 6.26(12)  | -1.6%                        |
| AG 9  | 5.043(5)                                      | 6.37(19)  | 0.1%                         |
| AG 10   | 5.021(5)                                      | 6.44(20)  | 1.3%                         |
| AG 11   | 5.062(5)                                      | 6.48(25)  | 1.8%                         |
| AG 12   | 4.884(5)                                      | 6.22(14)  | -2.2%                        |
| mean AG1-AG10 $\bar{x}$                         | 5.030   | 6.36  |                              |
| std. dev. $s$                                   | 0.059   | 0.10  |                              |
| $u_{bb} = \text{rel. std. dev. } s/\bar{x}$ (%) | 1.2 %   | 1.6 %   |                              |

**Table 3:** Homogeneity study with thoron samplers during the thoron calibration exercise performed in the BACCARRA chamber. The numbers in the brackets indicate the overall estimated standard uncertainties.

| Sample | Decay corrected net counting rate, cpm | Mass of the silica aerogel in the LS vial (g) | Specific net LS counting rate at the end of the exposure( $s^{-1}g^{-1}$ ) | Center (C) / Walls (W) | Normalized to AT1 |
|--------|--|---|--|------------------------|-------------------|
| AT1    | 108.2(17)                              | 5.346(5)                                      | 20.24(32)  | C                      | 1.00              |
| AT2    | 111.9(18)                              | 5.546(5)                                      | 20.17(33)  | C                      | 1.00              |
| AT3    | 139.1(20)                              | 5.444(5)                                      | 25.56(37)  | W                      | 1.26              |
| AT4    | 122.6(20)                              | 5.471(5)                                      | 22.41(37)  | C                      | 1.11              |
| AT5    | 169.6(24)                              | 5.402(5)                                      | 31.39(44)  | W                      | 1.55              |
| AT6    | 116.2(22)                              | 5.361(5)                                      | 21.68(41)  | C                      | 1.07              |
| AT7    | 179.2(26)                              | 5.503(5)                                      | 32.57(48)  | W                      | 1.61              |
| AT8    | 119.6(24)                              | 5.550(5)                                      | 21.54(44)  | W                      | 1.06              |
| AT9    | 119.5(26)                              | 5.454(5)                                      | 21.91(47)  | C                      | 1.08              |
| AT10   | 127.7(27)                              | 5.550(5)                                      | 23.00(50)  | C                      | 1.14              |
| AT11   | 125.8(29)                              | 5.598(5)                                      | 22.47(51)  | W                      | 1.11              |



16ENV10 MetroRADON

Deliverable D2

Annex II

Activity A.2.1.1

Homogeneity testing of Tn-220  
atmosphere at STUK

T. Turtiainen, R. Dehqanzada  
STUK

Turtiainen T, Dehqanzada R

## Homogeneity testing of Tn-220 atmosphere at STUK

Tn-220 atmosphere at STUK is a 101.1-litre container the operation of which has been described in other documentation under WP2 of MetroRadon project. In order to carry out reliable calibrations and cross-interference testing, Tn-220 gas must be homogeneously distributed inside the container. As Tn-220 has a short half-life (55.6 sec), mixing of air inside the container is essential. Therefore, thoron-rich gas from the source is directed in front of the fan that is placed on the lid of the container (Fig.1). Flow velocity at the reference point is  $(0.24 \pm 0.03)$  m/s and the height of the container is 0.57 m.

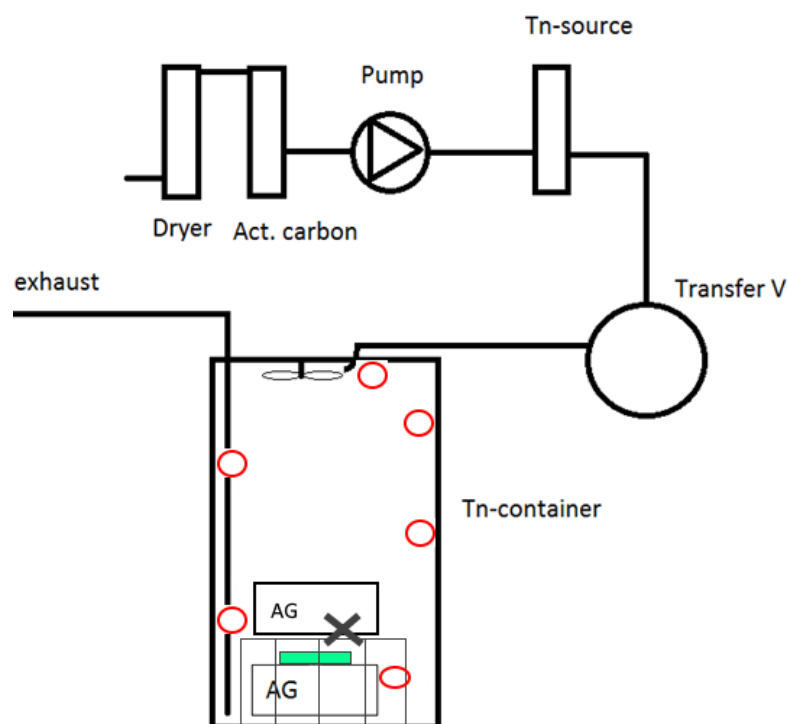


Figure 1. Tn-220 atmosphere and placement of Aerogel samplers marked in red circles. "AG" stands for AlphaGuard radon instrument and "X" is the point of flow velocity measurement.

### Test method

The method employed for testing homogeneity of the atmosphere was aerogel sampling that has been described in detail by Mitev et al. (see Annex I). In short, thoron gas dissolves in aerogel and the dissolved Tn-220 decays into thoron progeny. Of thoron progeny, Pb-212 has a half-life of 10.64 hours and can thus be measured for a couple of days after the exposure.

Turtiainen T, Dehqanzada R

In total, 6 samplers were placed inside the container with adhesive tape. Two AlphaGuard instruments were placed inside the chamber, in order to emulate flow conditions during cross-interference testing (Fig. 1). The chamber operated for 120 hours in mean Tn-220 concentration of  $(44\ 100 \pm 700)$  Bq/m<sup>3</sup> (Fig. 2). During this time Pb-212 had reached equilibrium with Tn-220.

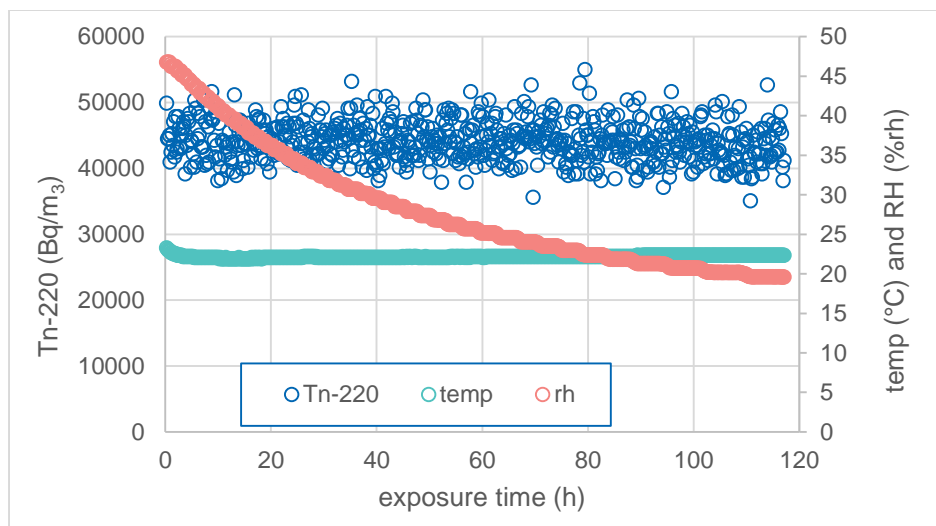


Figure 2. Tn-220 concentration, temperature and relative humidity during the homogeneity testing.

After the exposure, the aerogel samplers were opened, and the aerogel was carefully transferred into tared glass liquid scintillation vials (22 mL). After this, the transferred mass of aerogel from each sampler was measured.

17 mL of UltimaGold LLT LS liquid scintillation cocktail was added into each vial in two batches (10 mL and 7 mL). The vials were closed and shaken, in order to remove air bubbles. The remaining air was removed with an ultrasonic bath for 1 hour. A background sample from unexposed aerogel was also prepared.

The samples were cooled for 4 hours and then measured with Guardian 1414 liquid scintillation spectrometer. The counting time was 30 minutes and decay-correction was made for the end time of the exposure using half-life of Pb-212.

## Results and conclusion

All specific count rates obtained from the samples were the same within uncertainty expressed with  $k=2$  (Table 1). Furthermore, recorded Tn-220 concentration remained stable. These findings indicate that the Tn-220 atmosphere at STUK is homogenous and suitable for calibrations and cross-interference testing.

Turtiainen T, Dehqanzada R

Table 1. Measured mass and specific count rates from the Aerogel samplers. Uncertainty is given  $k=1$ .

| Sampler ID | Mass (g) | Count rate (cpm/g) |
|------------|----------|--------------------|
| TAS1       | 4.973    | 30.1 $\pm$ 0.4     |
| TAS2       | 4.972    | 30.6 $\pm$ 0.5     |
| TAS9       | 4.968    | 30.6 $\pm$ 0.5     |
| TAS10      | 4.955    | 30.4 $\pm$ 0.5     |
| TAS11      | 4.965    | 29.2 $\pm$ 0.5     |
| TAS12      | 4.958    | 30.9 $\pm$ 0.5     |



16ENV10 MetroRADON

Deliverable D2

Annex III

Activity 2.1.1

Thoron simulation in BACCARA

J. Malet  
IRSN

The objective of this study is to evaluate the homogeneity of the thoron activity in the BACCARA test chamber. A numerical study has been performed using a Computational Fluid Dynamics code ANSYS/FLUENT.

## Description of the modelling

### Equations

The air flow inside the chamber is considered to be steady-state, incompressible and the temperature homogeneous. The flow is modelled by solving the Navier-Stokes equation and a RANS (Reynolds-Average Navier-Stokes) turbulence model, the  $k$ - $\epsilon$  model, where  $k$  is the turbulent kinetic energy and  $\epsilon$  represents its rate of dissipation ; this model is the most common one to simulate turbulent flow conditions. Basically,  $k$ - $\epsilon$  models assume that turbulent characteristics are isotropic (the same in all directions). Thoron  $^{220}\text{Rn}$  is modelled by a convection-diffusion equation in which a sink term has been added to represent the radioactive decay. In Fluent, this equation is solved as a mass fraction of the gas in the air.

### Initial and boundary conditions

Wall boundary conditions are no-slip condition with standard wall function. Thoron is considered with a zero flux on walls. A 0-velocity and 0-thoron initial conditions in the whole domain were considered.

Two standard inlet and outlet boundary conditions are used (see Figure 1):

- one inlet (in blue on Figure 1), so-called Thoron inlet, in which the thoron gas is injected horizontally, with a constant mass flow-rate of 0.001 kg/s : the velocity as well as the gas concentration are constant over the whole section of this inlet ; this can be assumed since the injection tube is quite long, about 10 times the diameter, allowing to consider a good mixing of the flow ;
- an outlet condition (in red on Figure 1), so-called chamber outlet : this condition is modelled by applying a constant outlet mass flow-rate, so that the velocity will be simulated on the outlet section.

Two other inlet and outlet boundary conditions are used in order to simulate the fan located inside the chamber (in yellow on Figure 1). The geometry of the fan is modelled as an annular flow section placed in a square body (Figure 2).

- A 'fan -inlet' condition on one side : a special treatment is performed to simulate the fan : the velocity is taken constant and equal to 7 m/s over the whole section representing the fan, the turbulence intensity is considered to be of 5% and the length scale is 12.5 cm, the diameter of the fan ; the fan is modelled by a circular ring ; the value of 7 m/s has been extrapolated from experimental measurements : the velocity profile of the flow in front of the fan has been measured with a hot wire anemometer at different distances from the fan ; several simulations with different inlet velocities have been initially performed in order to find for which inlet velocity values the simulated profiles at 3 and 10 cm distance were similar in the simulations and in the measurements ; the inlet condition for the thoron concentration is the outlet concentration obtained on the last cell in front of the so-called 'fan outlet' ;
- A 'fan-outlet' condition is imposed on the other side of the fan, considered as a pressure-outlet section on which the thoron concentration is calculated on the last cell for being re-used in the fan-inlet conditions.

## Discretization

The finite volume method (FVM) was used for the discretization of the relevant equations, with the SIMPLE algorithm. Second-order upwind schemes were chosen for the simulation of pressure, momentum and turbulent kinetic energy and dissipation rate.

The mesh is generated with ANSYS Meshing and a hexahedral modelling of the space has been used (Figure 3). Different mesh densities have been tested in order to check the mesh convergence. Meshes from 1 to 8 millions of nodes have been used, with different local refinements. The latter are located close to the inlet and outlet sections, as well as in the lower part of the chamber where the different monitoring devices are installed. Concerning the monitoring devices, the first ones are the RAD7 devices located on the left of Figure 3 ; in the middle of the chamber are located some specific thoron equipment as well as all sampling lines ; at least, on the right, four Alphaguards are installed.

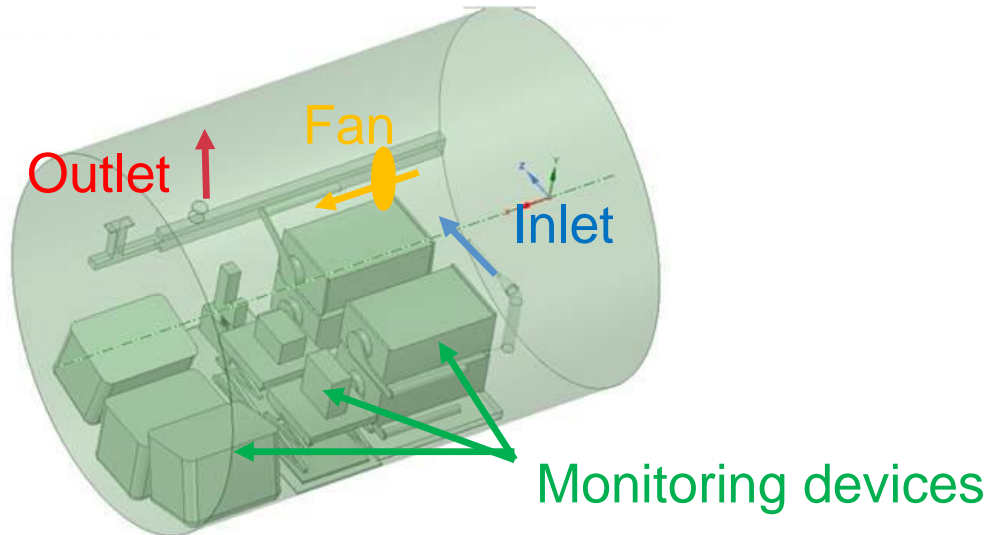


Figure 1 : Inlet and outlet positions for the CFD simulations

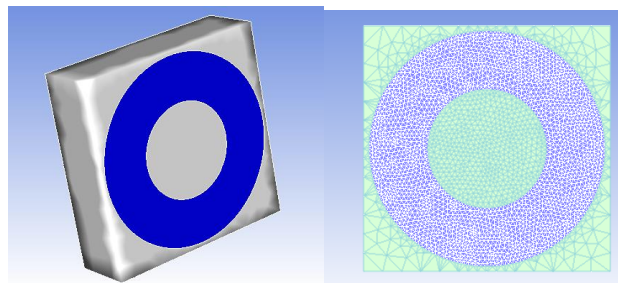


Figure 2 : Geometrical discretization of the fan inlet : dark blue : cells where velocity is imposed, green-blue cells or grey material : fan walls

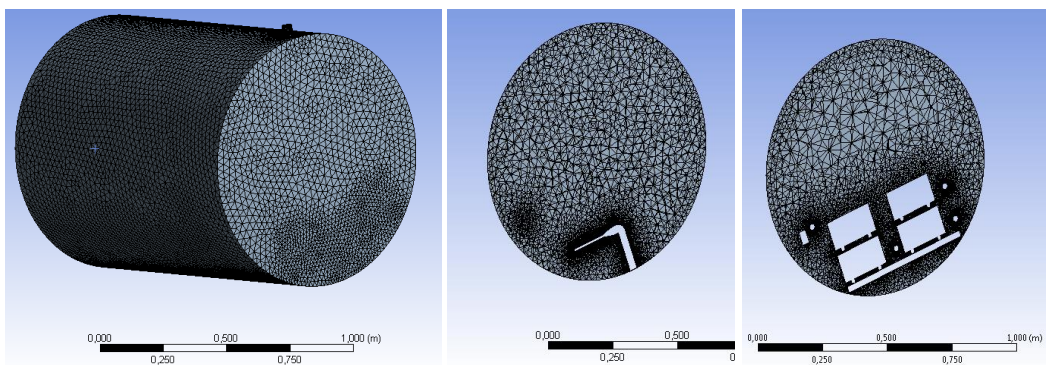


Figure 3 : Different view of the mesh

## Validation

Each CFD simulation needs to be validated on different well-chosen cases in order to get some confidence to the results. In that case, two main validations have been done: one simulating the mixing flow, i.e. the way a gas is mixed inside a volume in which a constant ventilation is maintained, and another one simulating the radioactive decay of the thoron gas. These validations have been achieved successfully so that the phenomena are assumed to be well considered.

Another important point when performing numerical simulation is to verify the results' mesh independency. This has also been performed here on three different mesh densities. Lastly, the influence of turbulence modelling has been investigated using different RANS turbulence models. No major difference in the results was observed.

## Results

Different simulations have been performed in order to assess the impact of each geometrical component on the flow. Figure 4 shows the impact of the different monitoring devices inside the chamber: it can be seen that, since the monitoring devices are not directly in the front of the fan, and since the jet induced by the fan does not spread as much over such a short distance, the flow is mainly similar in all configurations. Furthermore, the mixing induced by the fan is important, as illustrated in Figure 4. A more detailed presentation is proposed by looking on the velocity field over different sections of the chamber, as presented on Figure 5 and Figure 6. It can be seen that the monitoring devices are not located in a plane where strong convection occurs.

A transitory calculation has also been performed to illustrate how fast the steady-state is reached. Results are presented on Figure 7 for different views at 5 s (left) and 12 s (center) and 112 s. It can be seen that the convective flow-steady-state is reached in a short time (it is already reached at 5s), much lower than the radioactive decay of the thoron (55s).

The thoron concentration is presented on Figure 8, where it can be seen that the homogeneity is achieved, especially due to the presence of the fan, as already presented on Figure 5.

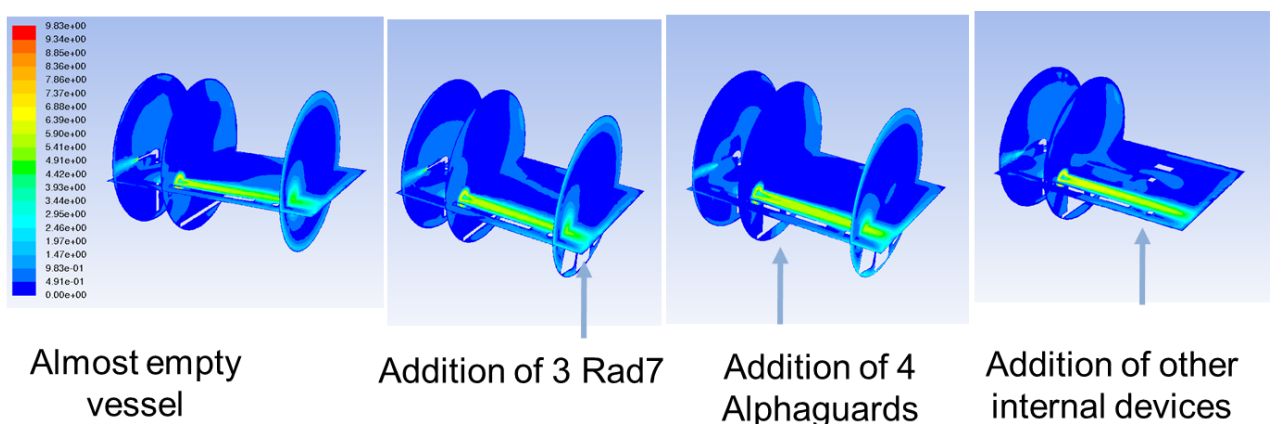


Figure 4 : Velocity field for different simulations with different internal monitoring devices, from the « most empty chamber » on the left, to the “most filled chamber” on the right.

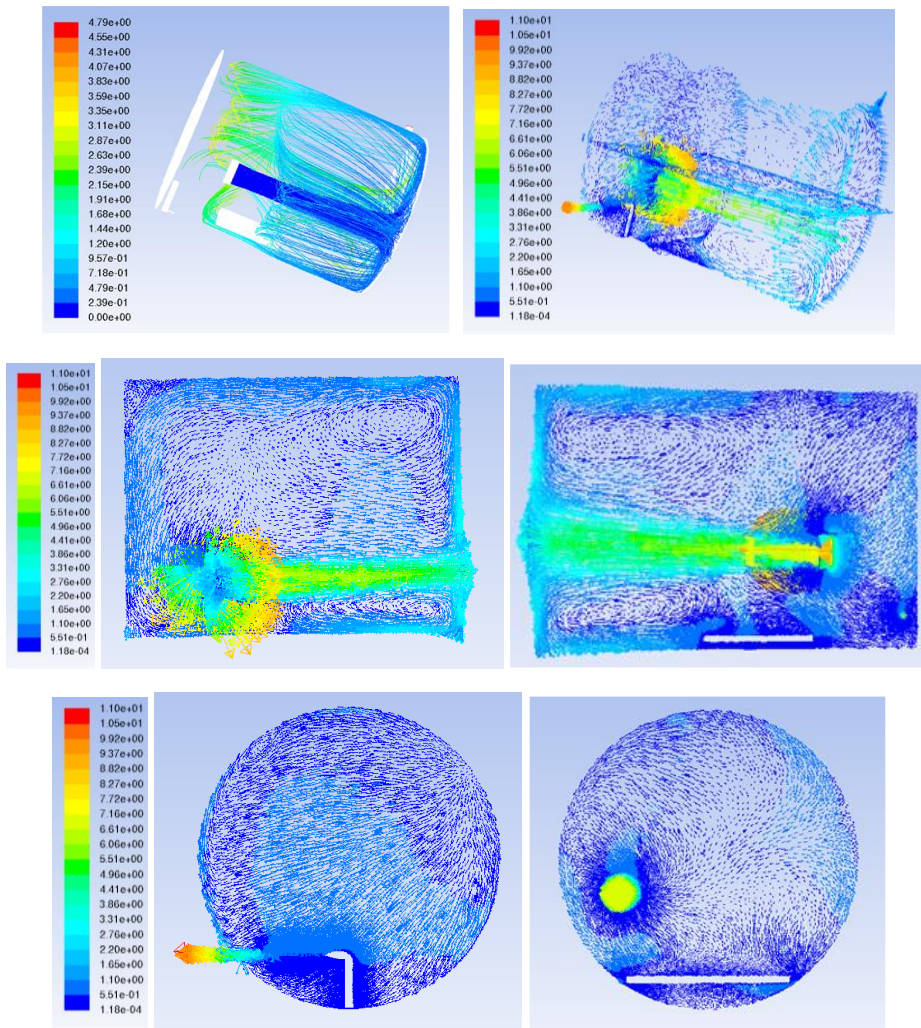


Figure 5 : Pathlines from the fan action and 3D velocity field on the first line, upper view and side view of the velocity field in the fan planes on the middle lines, and the thoron injection zones on the last line

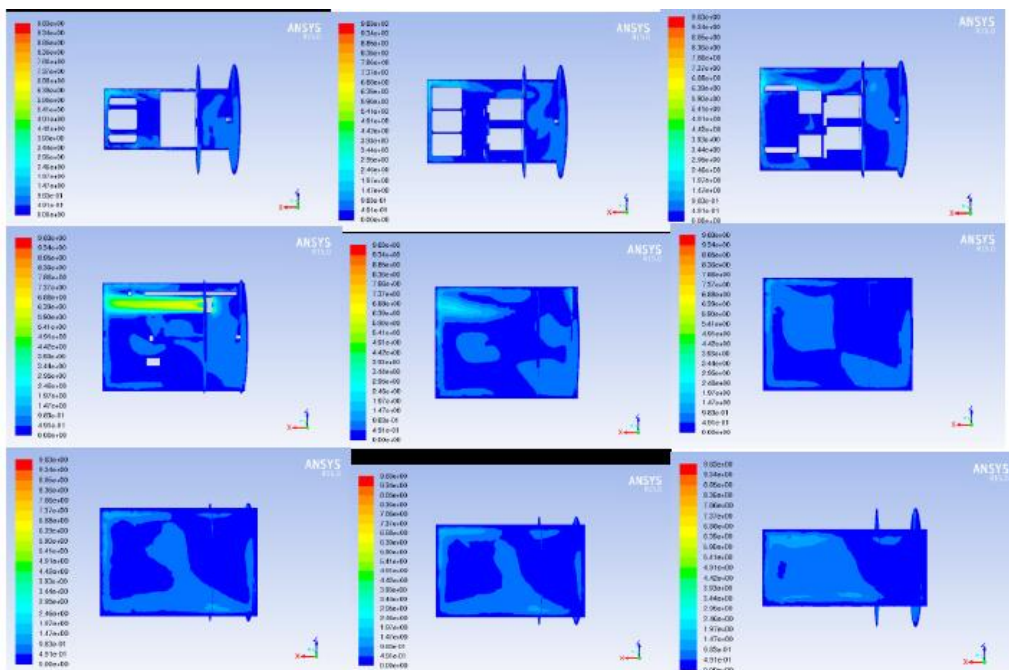


Figure 6 : Velocity field over different horizontal cross section of the chamber: the monitoring devices are not located in a plane where strong convection occurs

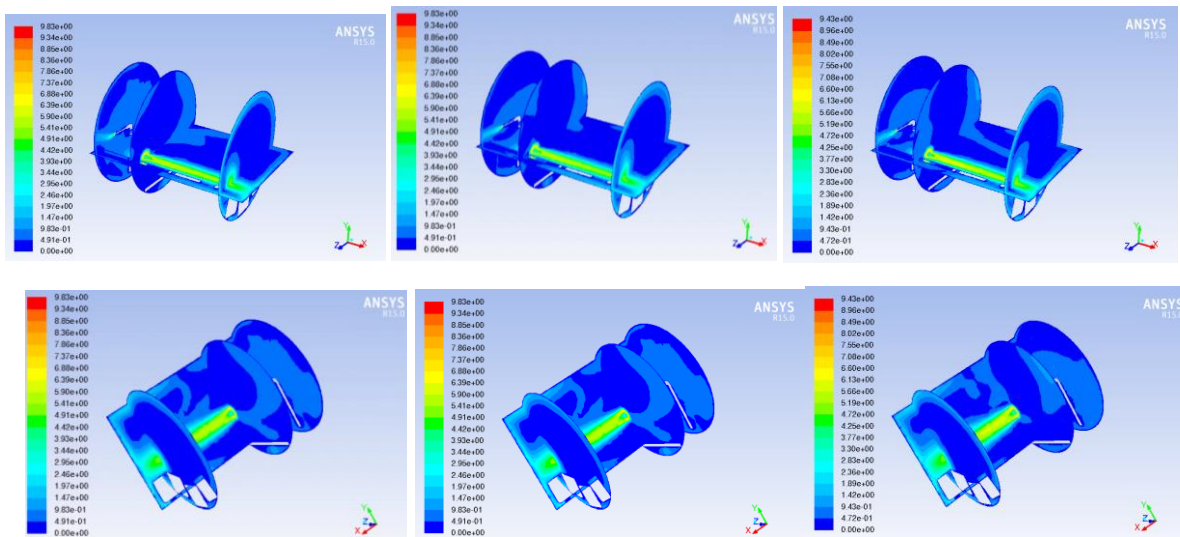


Figure 7 : Information on the steady-state: Comparison of the results at three times: 5 s (left) and 12 s (center) and 112 s (right) for the case with 3 Rad7 and no Alphaguards

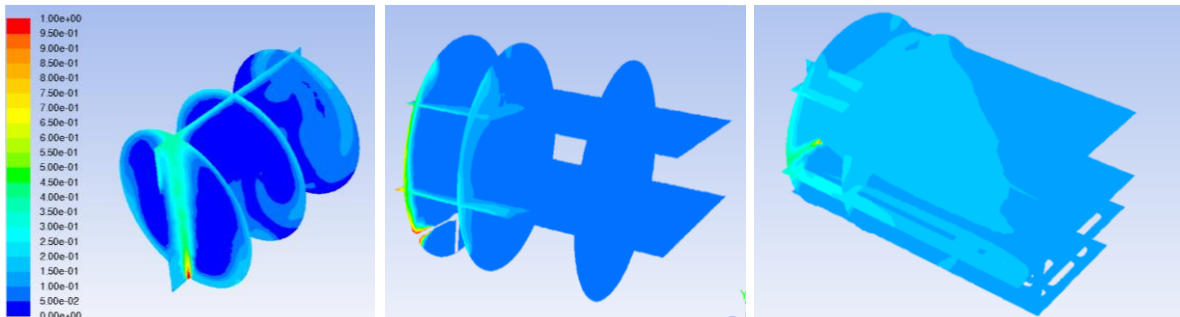


Figure 8 : Thoron concentration, on the left part : simulation without fan, having the thoron injection directed upwards, on the central and right part, lower and upper lateral thoron injection, in a case when the fan is activated : the role of the fan in the mixing is confirmed



16ENV10 MetroRADON

Deliverable D2

Annex IV

Task A.2.1.2

Ensuring traceability of the secondary  
thoron reference instruments

Nathalie Michielsen  
IRSN



# Ensuring traceability of the secondary thoron reference instruments

---

WP2: Influence of thoron ( $^{220}\text{Rn}$ ) and its progeny on radon end-user measurements and radon calibrations

Task 2.1: Ensuring traceability of the secondary thoron reference instruments used in the experimental research to the primary thoron measurement system at IRSN

Document version: January 2020

Contact person: Nathalie Michielsens

PSE-ENV/SEREN/BERAD

B.P. 17 - 92262 Fontenay-aux-Roses - France

email: [nathalie.michielsens@irsn.fr](mailto:nathalie.michielsens@irsn.fr)

tel 33(0)1 58 35 72 27

## CONTENTS

|     |   |    |
|-----|---|----|
| 1   | OBJECT .....                                  | 3  |
| 2   | INTRODUCTION .....                            | 3  |
| 3   | INSTRUMENTS SET UP .....                      | 3  |
| 4   | MATERIAL AND METHODS.....                     | 5  |
| 5   | RESULTS .....                                 | 9  |
| 5.1 | Environmental conditions.....                 | 9  |
| 5.2 | Background .....                              | 9  |
| 5.3 | Thoron activity concentration .....           | 10 |
| 5.4 | Thoron reference activity concentrations..... | 12 |
| 5.5 | Calibration factor.....                       | 12 |
| 6   | CONCLUSION .....                              | 15 |

## 1 OBJECT

This work is done in the frame of the EMPIR project 16ENV10 MetroRADON: “Metrology for radon monitoring”, it is a part of the working package 2 (Influence of thoron ( $^{220}\text{Rn}$ ) and its progeny on radon end-user measurements and radon calibrations); and task 2.1 (Ensuring traceability of the secondary thoron reference instruments used in the experimental research to the primary thoron measurement system at IRSN).

The aim of this task is to calibrate the secondary thoron reference instruments used in the partners laboratories against the existing primary thoron measurement system at IRSN and thus to ensure traceability of the thoron measurements made by the partners. These calibrated instruments will be used in Task 2.2 to investigate the influence of thoron on radon measurement devices.

## 2 INTRODUCTION

The thoron calibration exercise has been organized by the IRSN. The experiments were held from the 16<sup>th</sup> to the 31<sup>th</sup> of May 2018 in the IRSN test chamber BACCARA in Saclay with the help of SUBG. Five laboratories, BEV-PTP, IRSN, STUK and SUBG, from four countries participated with seven instruments. As agreed between the partners, the calibration exercise covers three levels of thoron activity concentration around 10 kBq/m<sup>3</sup>, 50 kBq/m<sup>3</sup> and 250 kBq/m<sup>3</sup>.

## 3 INSTRUMENTS SET UP

The participating laboratories (IRSN, SUBG, STUK and BEV-PTP) have sent their  $^{220}\text{Rn}$  secondary reference instruments to IRSN (Fig.1).



*Figure 1 - Preparation of the secondary reference instruments for the calibration*

Four AlphaGUARD and three RAD7 have been calibrated against the IRSN thoron reference system (Sabot et al., 2015). Details on the apparatus and the accessories used for the calibration are given in table 1. The colour code (blue, yellow, green and red) is related to a laboratory.

Table 1 - Instruments identification

| Instrument               | Identification | pump identification            | flowmeter                                    |
|--------------------------|----------------|--------------------------------|--|
| AlphaGUARD 2000 RnTh PRO | EF 2312        | AP 1527                        |  |
| RAD7                     | RAD7-2964      | inside                         |  |
| AlphaGUARD 2000 RnTh PRO | EF 2104        | AP 1367                        |  |
| RAD7                     | RAD7-2030      | inside                         |  |
| AlphaGUARD 2000 RnTh PRO | EF 1338        | AP no number BEV               |  |
| AlphaGUARD 2000 RnTh PRO | EF 2283        | AP 1507                        |  |
| RAD7                     | RAD7-0517      | inside                         | Bronkhorst SNM8204166A<br>N° BACCARA DMQ 012 |
| reference system         | IRSN prototype | Kif-Lab<br>BACCARA<br>08POM010 | N°<br>n°                                     |

The connection between the different parts of the instruments was done according to the partner's use, which means that the tubes for the connections of the alphaGUARD to the pump or the Rad7 to the dryer were the owner tubing. So the lengths of the tubes were not exactly the same for one apparatus to another but the difference can be considered negligible (the difference of arrival time in the detectors are negligible compared to the thoron half-life).

Dry air was used during all the experiments so only one dryer was used for the all set of experiments except for the Rad7 (SUBG).

The protocol setup for each apparatus is given in tables 2 and 3. Those protocols correspond to the manufacturer configuration.

Table 2 - AlphaGUARD set-up

| Instrument Identification | Flow pump (l/min) | Set up configuration      | Measurement cycle |
|---------------------------|-------------------|---------------------------|-------------------|
| EF 2312                   | 1                 | thoron mode, flow through | 10 min            |
| EF 2104                   | 1                 | thoron mode, flow through | 10 min            |
| EF 1338                   | 1                 | thoron mode, flow through | 10 min            |
| EF 2283                   | 1                 | thoron mode, flow through | 10 min            |

Table 3 - RAD7 set-up

| Instrument Identification | mode                               | protocol | pump |
|---------------------------|------------------------------------|----------|------|
| RAD7-2964                 | Normal mode, thoron on small dryer | none     | auto |
| RAD7-2030                 | Normal mode, thoron on small dryer | none     | auto |
| RAD7-0517                 | Normal mode, thoron on small dryer | none     | auto |

The measurement cycle of the Rad7 has been chosen to one hour for the low and medium activity while it has been fixed to 10 min for the high activity experiments.

The date and time of the active devices were synchronized and flow rate checked.

The flow rate of each instrument has been measured before and after the exposition with a calibrated mass flow controller. The flow rate of the reference system and the RAD7 517 were continuously measured during the experiments and were stable through the all exposures.

Results of the flow measurement are given in table 4. The flow rates before and after the exposure can be considered the same for all apparatus.

Table 4 - results of the flow rate measurement before and after the exposure

| AlphaGUARD                |                            | 17/05/2018                             |              |
|---------------------------|----------------------------|--|--------------|
| Instrument Identification | Flow rate (standard l/min) | temperature                            | 23,5 °C      |
| EF 2312                   | 0,96                       | pressure                               | 999 mbar     |
| EF 2104                   | 0,94                       |  |              |
| EF 1338                   | 0,89                       | noisy (vibration inside the alphapump) |              |
| EF 2283                   | 1,04                       |  |              |
|                           |                            | 30/05/2018                             |              |
|                           | Flow rate (standard l/min) | temperature                            | 25,8 °C      |
| EF 2312                   | 0,96                       | pressure                               | 996 mbar     |
| EF 2104                   | 0,94                       |  |              |
| EF 1338                   | 0,89                       | noisy (vibration inside the alphapump) |              |
| EF 2283                   | 1,02                       |  |              |
| RAD7                      |                            | 17/05/2018                             |              |
| Instrument Identification | Flow rate (standard l/min) | temperature                            | 23,4 °C      |
| RAD7-2964                 | 0,72                       | pressure                               | 1004,01 mbar |
| RAD7-2030                 | 0,62                       |  |              |
| RAD7-0517                 | 0,80                       |  |              |
|                           |                            | 30/05/2018                             |              |
|                           | Flow rate (standard l/min) | temperature                            | 25,8 °C      |
| RAD7-2964                 | 0,70                       | pressure                               | 996 mbar     |
| RAD7-2030                 | 0,62                       |  |              |
| RAD7-0517                 | 0,77                       |  |              |

## 4 MATERIAL AND METHODS

Thoron atmosphere was created in the IRSN reference radon chamber called BACCARA. It consists of a one cubic meter stainless steel cylinder in which instruments to be calibrated can be placed together. This volume is connected to a  $^{220}\text{Rn}$  flow-through source (Pylon Electronic, Inc.) and a  $^{220}\text{Rn}$  reference measurement system, developed recently in the framework of the MetroNORM project (Sabot et al., 2016). This system allows a direct measurement of the  $^{220}\text{Rn}$  alpha decays with a geometrical efficiency calculated with a Monte Carlo method and is traceable to a radon gas

primary standard. Three different constant  $^{220}\text{Rn}$  reference atmospheres, i.e.  $10 \text{ kBq}\cdot\text{m}^{-3}$ ,  $46 \text{ kBq}\cdot\text{m}^{-3}$  and  $240 \text{ kBq}\cdot\text{m}^{-3}$ , have been established to cover a wide range of  $^{220}\text{Rn}$  activity concentrations.

The thoron and dilution air circulate through the chamber, in order to establish a constant thoron activity concentration inside BACCARA (fig. 2). Clean pressurized air going through the  $^{220}\text{Rn}$  flow-through source at a constant flow rate of  $1 \text{ L}/\text{min}$  is mixed and diluted with a constant flow rate of  $3 \text{ m}^3/\text{h}$  clean pressurized air. This high flow rate allows a quick air turnover in the chamber, around 20 min. This inlet air mixed with thoron arrives at one side at the bottom chamber and exits at the other side on the top of BACCARA. A fan is used to ensure homogeneity in the cylinder. Activity concentration of thoron and climatic parameters are measured continuously.

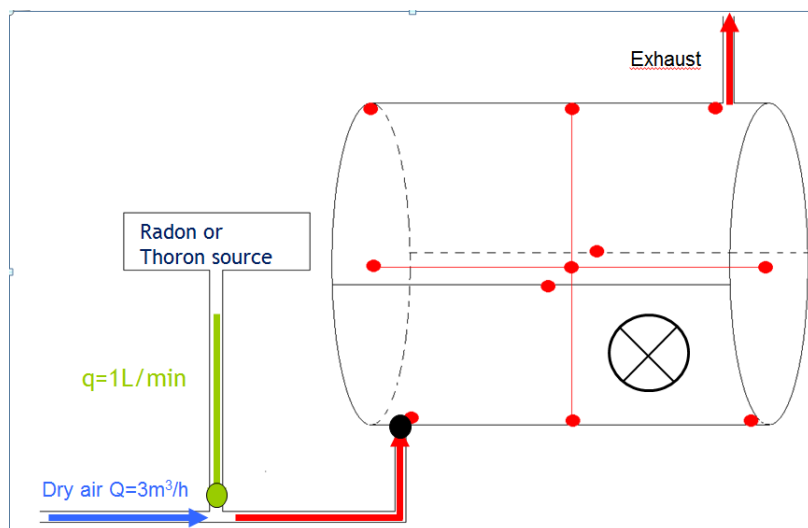


Figure 2 - Schematic diagram of BACCARA

Seven  $^{220}\text{Rn}$  monitors have been placed inside and the reference system connected outside the chamber (on the left side, fig. 3). Four of the monitors are the AlphaGUARDS type and the three other are RAD7. All the sampling points of these active devices including the  $^{220}\text{Rn}$  reference system were placed in close proximity in order to avoid adverse effect of possible inhomogeneity of the  $^{220}\text{Rn}$  distribution in the chamber (fig. 4).

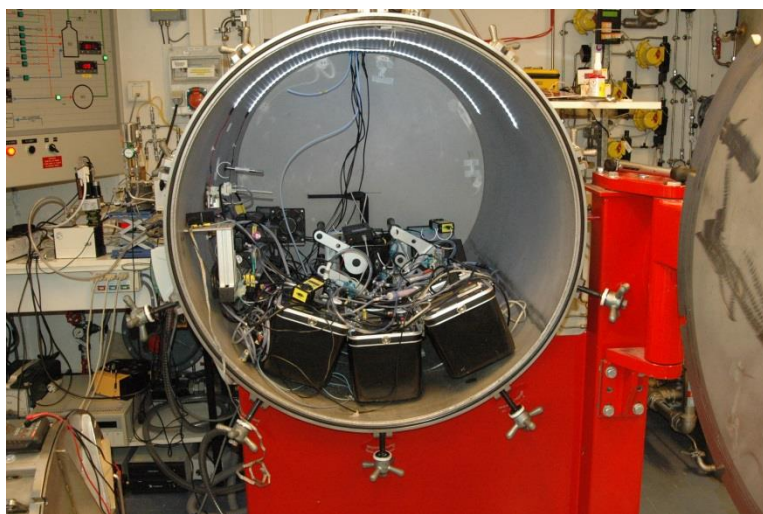


Figure 3 - Photo of the instruments in BACCARA

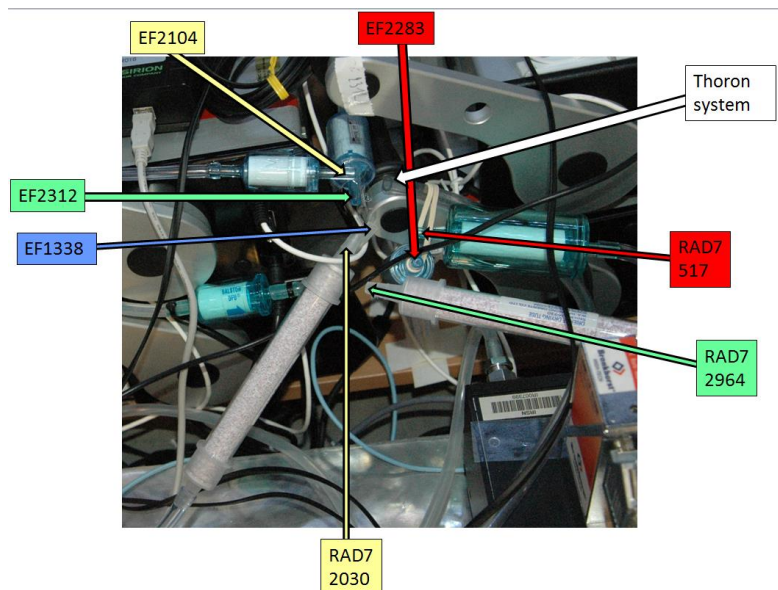


Figure 4 - Sampling points for the low and medium level

#### Experiment with only air (No thoron)

From 17<sup>th</sup> to 18<sup>th</sup> of May, the background of the instruments was checked. Therefore, only air without thoron was circulated through BACCARA and the thoron concentration was registered. All the instruments reported a low background and the thoron reference system shows no contamination of  $^{210}\text{Po}$ .

#### Experiments with thoron

From May 24<sup>th</sup> to 25<sup>th</sup> a medium level (around  $50 \text{ kBq}\cdot\text{m}^{-3}$ ) atmosphere was set up followed by a low level (five time less) exposure, from 25<sup>th</sup> to 28<sup>th</sup>. For the low level exposure an ageing volume (long stainless steel tube of 5L) was inserted between the thoron source and the air inlet of the chamber, in order to lower the thoron activity.

For the high level exposure another set-up was used. While instruments were left in the chamber, the mixture of thoron and air was directly connected to a buffer volume inside the chamber (fig. 5). A constant flow rate of 15 L/min was circulated through this buffer. This buffer volume was equipped of a shared sampling probe (inner diameter of 4 mm, length of 30 cm) allowing the instruments to sample the air to be measured (fig. 5). Taking into account the higher residence time in the sampling probe, the ratio between the activity concentration at the last point of sampling to the activity concentration at the inlet is 99.9%, therefore the sampling place should not affect the results by more than 0.1%. Nevertheless this assumption was also verified experimentally by placing the thoron system at two different places; i.e. first at the inlet of the tube and, in a second time, at the end of the tube (by shifting with the Rad7 517, fig. 5).

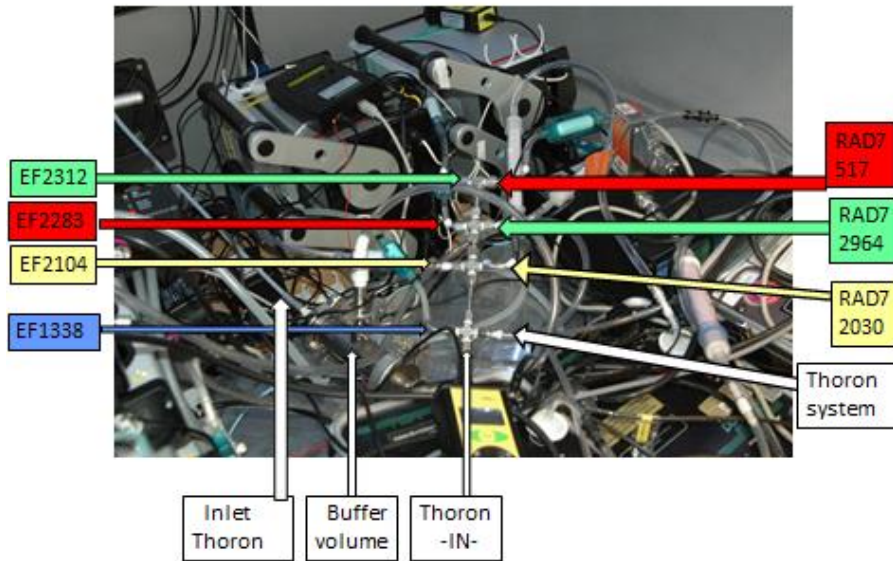


Figure 5 - Thoron inlet and sampling probe for the high level experiments

Two experiments of three hours were conducted on May 29<sup>th</sup> with this configuration.

During this two experiments, an influence of the start and stop pump of the alphaGuards on the Rad7s flow rate was observed, so a last experiment with only the Rad7s and the reference system connected to the shared sampling probe has been running during the night (29 to 30 of May) (fig. 6). Note that the unused sampling points were plugged.

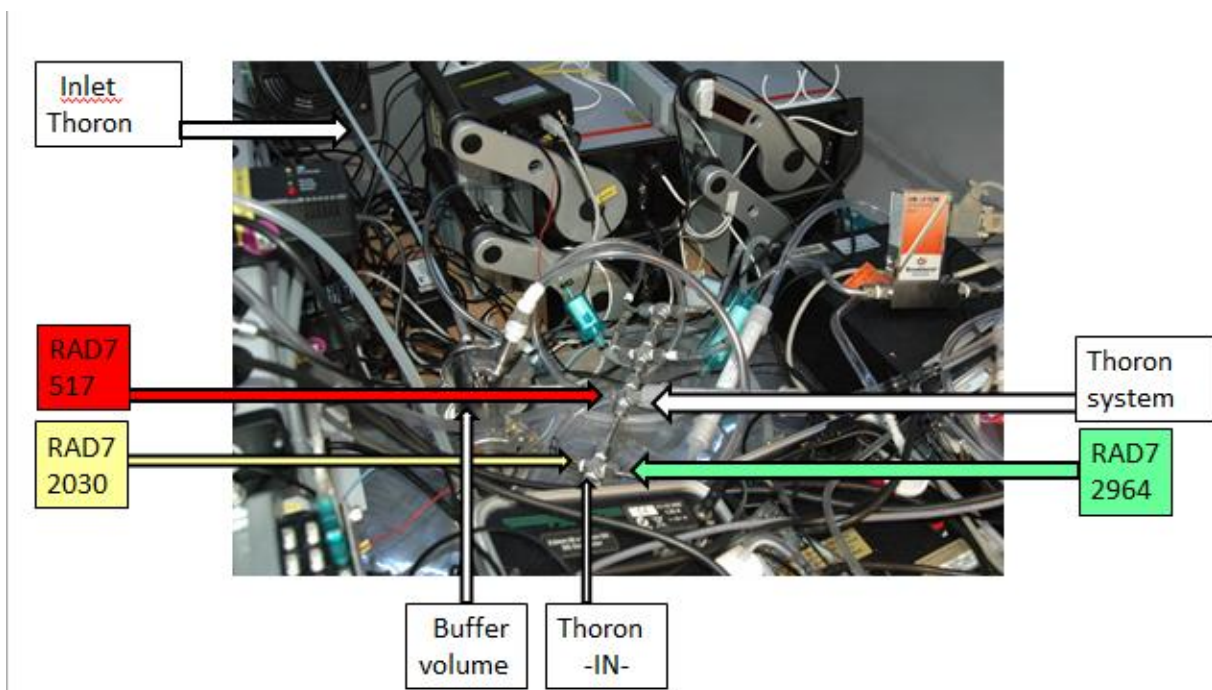


Figure 6 - Sampling point for the Rad7

## 5 RESULTS

### 5.1 Environmental conditions

The relative humidity for all the experiments were under 5 %.

The arithmetic mean and the uncertainty of the temperature, T, and the pressure, P, in the test bench are reported in table 5 for each experiments.

*Table 5 - Environmental conditions data*

| Experiments                     | Date and time                           | Temperature<br>in °C | uncertainty<br>in °C | Pressure<br>in<br>mbar | uncertainty<br>in<br>mbar |
|---------------------------------|---|----------------------|----------------------|------------------------|---------------------------|
| Background                      | 17 May 18h30 to<br>18 May 10h00         | 27.4                 | 0.2                  | 993.5                  | 0.4                       |
| Low activity                    | 25 May 15h20 to<br>28 May 14h40         | 28.4                 | 0.5                  | 996.3                  | 0.8                       |
| Medium<br>activity              | 24 May 18h30 to<br>25 May 14h30         | 27.2                 | 0.2                  | 997.2                  | 0.2                       |
| High activity                   | 29 May 9h20 to<br>12h<br>and 13h to 15h | 26.4                 | 0.2                  | 995.1                  | 0.1                       |
| High activity<br>with only rad7 | 29 May 16h10 to<br>30 May 9h40          | 27.1                 | 0.3                  | 993.1                  | 0.5                       |

### 5.2 Background

The activity concentration of thoron,  $A_{VTh}$ , measured by the apparatus during the background experiment is reported in table 6 (arithmetic mean and standard deviation of this mean).

*Table 6 - Activity concentration of thoron measured during the background experiment*

| Instrument identification | $A_{VTh}$ in Bq.m <sup>-3</sup> | $\sigma(A_{VTh})$ in Bq.m <sup>-3</sup> |
|---------------------------|---------------------------------|---|
| EF 1338                   | 14                              | 10                                      |
| EF 2104                   | 4                               | 2                                       |
| EF 2283                   | 0                               | 4                                       |

|           |   |    |
|-----------|---|----|
| EF 2312   | 1 | 24 |
| RAD7-0517 | 3 | 1  |
| RAD7-2030 | 2 | 1  |
| RAD7-2964 | 3 | 1  |

The spectrum of the thoron reference system was checked for non-contamination of polonium-210.

The background can be considered negligible for all instruments.

### 5.3 Thoron activity concentration

Activity concentrations of thoron,  $A_{vTh}$ , measured by the apparatus during the low and medium activity concentration test are reported in table 7 (arithmetic mean and standard deviation of this mean) and those obtained during the three experiments at high concentration are reported in table 8.

*Table 7 - Measured thoron activity concentration for low and medium atmosphere*

| Instrument identification | Low activity                    |   | Medium activity                 |   |
|---------------------------|---------------------------------|---|---------------------------------|---|
|                           | $A_{vTh}$ in Bq.m <sup>-3</sup> | $\sigma(A_{vTh})$ in Bq.m <sup>-3</sup> | $A_{vTh}$ in Bq.m <sup>-3</sup> | $\sigma(A_{vTh})$ in Bq.m <sup>-3</sup> |
| EF 1338                   | 8969                            | 42                                      | 49512                           | 246                                     |
| EF 2104                   | 8835                            | 42                                      | 48166                           | 270                                     |
| EF 2283                   | 9642                            | 44                                      | 52649                           | 287                                     |
| EF 2312                   | 9561                            | 44                                      | 51126                           | 243                                     |
| RAD7-0517                 | 5037                            | 31                                      | 25325                           | 116                                     |
| RAD7-2030                 | 6170                            | 44                                      | 30583                           | 102                                     |
| RAD7-2964                 | 5777                            | 46                                      | 25958                           | 119                                     |

The value of the thoron activity concentration depends strongly on the type of instrument. Two populations are observed: values obtained by the alphaGUARDS and those measured by the RAD7s. The higher relative difference (i.e. (max-min)/min) for each population is 9% with the alphaGUARDS for both levels, and 22% and 21% with the Rad7 for low and medium level respectively. This suggests that results differences between instruments are lower with the alphaGUARD than with the RAD7. The higher concentrations are measured by the EF2283 and the Rad7-2030 and the lower by the EF2104 and the Rad7-517 for both levels.

Table 8 - Measured thoron activity concentration for high activity

| Instrument identification | first                           |   | second                          |   | third                           |   |
|---------------------------|---------------------------------|---|---------------------------------|---|---------------------------------|---|
|                           | $A_{VTh}$ in Bq.m <sup>-3</sup> | $\sigma(A_{VTh})$ in Bq.m <sup>-3</sup> | $A_{VTh}$ in Bq.m <sup>-3</sup> | $\sigma(A_{VTh})$ in Bq.m <sup>-3</sup> | $A_{VTh}$ in Bq.m <sup>-3</sup> | $\sigma(A_{VTh})$ in Bq.m <sup>-3</sup> |
| EF 1338                   | 297621                          | 3739                                    | 297433                          | 3456                                    | NA                              | –                                       |
| EF 2104                   | 253350                          | 2346                                    | 238671                          | 4006                                    | NA                              | –                                       |
| EF 2283                   | 273107                          | 2632                                    | 258678                          | 2993                                    | NA                              | –                                       |
| EF 2312                   | 266120                          | 2514                                    | 251825                          | 3174                                    | NA                              | –                                       |
| RAD7-0517                 | 141118                          | 623                                     | 142769                          | 574                                     | 142632                          | 273                                     |
| RAD7-2030                 | 167941                          | 756                                     | 167000                          | 615                                     | 176594                          | 393                                     |
| RAD7-2964                 | 132412                          | 1315                                    | 134077                          | 1769                                    | 146434                          | 589                                     |

As for the previous levels, a difference of value is observed between the alphaGUARDs and the Rad7. But the behaviour of the instruments between the three experiments is not as consistent for this high level. A higher relative difference (i.e. (max-min)/min) of 25% is observed for the alphaGUARDs compare to the 9% observed for the low and medium level.

The only difference between the first and the second experiment is the sampling point of the reference system and the Rad7-517. For the first experiment the sampling point of the Rad7 was at the right end of the sampling probe (fig.5) while it was at the right entrance of the probe (at the place of the reference system fig.5) for the second experiment. As expected, the value of thoron activity concentration was slightly higher at the entrance than at the end of the probe (98.8%); the same behaviour was observed for the thoron reference system. The Rad7-2030 and 2964 as well as the alphaGUARD EF1338 recorded the same value for both experiments as expected, since their sampling point stayed the same. But the second experiment values were 94% of the first experiment values for the three alphaGUARDs EF2104, EF2283 and EF2312. Compare to the EF1338 placed at the entrance of the probe, the other alphaGUARDs might have difficulty to sample. Also the pump of the alphaGUARD is not running continuously and the working on/off regime might have some influence on other apparatus placed downstream.

In the third experiments only 4 sampling points were used with the RAD7 and the reference system (fig.6). The higher relative difference (i.e. (max-min)/min) is 23%, comparable to those obtained for low and medium levels.

In conclusion, a change of thoron concentration is observed along the sampling probe used for the high level experiment which needs to be taken into account for the comparison with the reference thoron system.

## 5.4 Thoron reference activity concentrations

The thoron reference activity concentrations for each experiment are given in table 9

*Table 9 - Thoron reference activity concentrations*

| experiments                             | Date and time                   | Reference $A_{Th}$ in Bq.m <sup>-3</sup> | Uncertainty (k=1) in Bq.m <sup>-3</sup> |
|---|---------------------------------|--|---|
| Low activity                            | 25 May 15h20 to<br>28 May 14h40 | 9856                                     | 228                                     |
| Medium activity                         | 24 May 18h30 to<br>25 May 14h30 | 46169                                    | 649                                     |
| High activity (first)                   | 29 May 9h20 to 12h              | 244304                                   | 3290                                    |
| High activity (second)                  | 29 May 13h to 15h               | 239922                                   | 3713                                    |
| High activity (third)<br>with only rad7 | 29 May 16h10 to<br>18 May 9h40  | 247825                                   | 2242                                    |

As previously noticed the only difference between the first and the second experiment for the high activity was a change of the sampling point, first, at the right entrance of the probe then, at the right end (fig.5). A slightly lower value is observed at the end of the probe.

## 5.5 Calibration factor

The calibration factor, R, is calculated as the ratio between the average measurement of the instrument and the thoron reference system. The uncertainty on R takes into account the uncertainty of the expected true value and the standard deviation of the mean result of the instrument to be calibrated. Results are presented in figure 7 and table 10.

In the high level case, the results of the first experiment were taking into account for the instruments and compare to the closest sampling point result of the reference instrument in order to take into account the change of the thoron activity concentration along the sampling probe. Moreover a rectangular interval relative uncertainty of 10.6% (this value corresponds to the maximum difference of the Rad7-2964 readings) was added to the uncertainty component of the expected true value activity concentration.

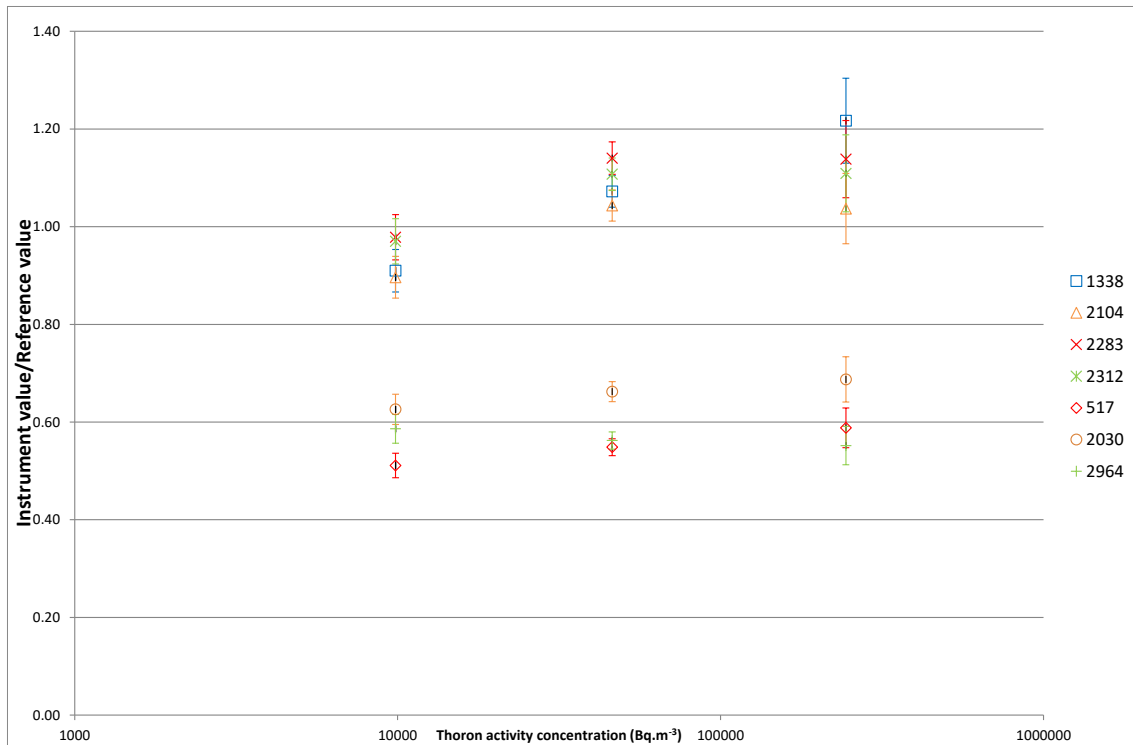


Figure 7 - Calibration factor

The Rad7s calibration factors are found around 0.6, even though two of the instruments (517 and 2964) had been send to the manufacturer UK affiliated company for a “calibration” just before this exercise. For each Rad7 the calibration factors are comparable for the all activity range.

The alphaGUARDs calibration factors are close to 1 with a lower value for the lower activity concentration. The calibration factor of the alphaGUARD EF1338 depends on the activity concentration.

Table 10 - Calibration results

| alphaGUARD                                   | EF1338                                     |                                     |  |   |                   |
|--|--|-------------------------------------|--|---|-------------------|
| Expected true value<br>in Bq.m <sup>-3</sup> | Uncertainty (k=1)<br>in Bq.m <sup>-3</sup> | Mean value<br>in Bq.m <sup>-3</sup> | $\sigma$ (mean)<br>in Bq.m <sup>-3</sup> | Calibration factor<br>(Instrument/true) | Uncertainty (k=2) |
| 9856   | 228  | 8969                                | 42                                       | <b>0.91</b>                             | <b>0.04</b>       |
| 46169  | 649  | 49512                               | 246                                      | <b>1.07</b>                             | <b>0.03</b>       |
| 244304                                       | 8161                                       | 297321                              | 3739                                     | <b>1.22</b>                             | <b>0.09</b>       |
| alphaGUARD                                   | EF2104                                     |                                     |  |   |                   |
| Expected true value<br>in Bq.m <sup>-3</sup> | Uncertainty (k=1)<br>in Bq.m <sup>-3</sup> | Mean value<br>in Bq.m <sup>-3</sup> | $\sigma$ (mean)<br>in Bq.m <sup>-3</sup> | Calibration factor<br>(Instrument/true) | Uncertainty (k=2) |
| 9856   | 228  | 8835                                | 42                                       | <b>0.90</b>                             | <b>0.04</b>       |
| 46169  | 649  | 48166                               | 270                                      | <b>1.04</b>                             | <b>0.03</b>       |
| 244304                                       | 8161                                       | 253350                              | 2346                                     | <b>1.04</b>                             | <b>0.07</b>       |
| alphaGUARD                                   | EF2283                                     |                                     |  |   |                   |
| Expected true value<br>in Bq.m <sup>-3</sup> | Uncertainty (k=1)<br>in Bq.m <sup>-3</sup> | Mean value<br>in Bq.m <sup>-3</sup> | $\sigma$ (mean)<br>in Bq.m <sup>-3</sup> | Calibration factor<br>(Instrument/true) | Uncertainty (k=2) |
| 9856   | 228  | 9642                                | 44                                       | <b>0.98</b>                             | <b>0.05</b>       |
| 46169  | 649  | 52649                               | 287                                      | <b>1.14</b>                             | <b>0.03</b>       |
| 239922                                       | 8221                                       | 273107                              | 2632                                     | <b>1.14</b>                             | <b>0.08</b>       |
| alphaGUARD                                   | EF2312                                     |                                     |  |   |                   |
| Expected true value<br>in Bq.m <sup>-3</sup> | Uncertainty (k=1)<br>in Bq.m <sup>-3</sup> | Mean value<br>in Bq.m <sup>-3</sup> | $\sigma$ (mean)<br>in Bq.m <sup>-3</sup> | Calibration factor<br>(Instrument/true) | Uncertainty (k=2) |
| 9856   | 228  | 9561                                | 44                                       | <b>0.97</b>                             | <b>0.05</b>       |
| 46169  | 649  | 51126                               | 243                                      | <b>1.11</b>                             | <b>0.03</b>       |
| 239922                                       | 8221                                       | 266120                              | 2514                                     | <b>1.11</b>                             | <b>0.08</b>       |
| RAD7   | 517  |                                     |  |   |                   |
| Expected true value<br>in Bq.m <sup>-3</sup> | Uncertainty (k=1)<br>in Bq.m <sup>-3</sup> | Mean value<br>in Bq.m <sup>-3</sup> | $\sigma$ (mean)<br>in Bq.m <sup>-3</sup> | Calibration factor<br>(Instrument/true) | Uncertainty (k=2) |
| 9856   | 228  | 5037                                | 31                                       | <b>0.51</b>                             | <b>0.03</b>       |
| 46169  | 649  | 25325                               | 116                                      | <b>0.55</b>                             | <b>0.02</b>       |
| 239922                                       | 8221                                       | 141118                              | 623                                      | <b>0.59</b>                             | <b>0.04</b>       |
| RAD7   | 2030                                       |                                     |  |   |                   |
| Expected true value<br>in Bq.m <sup>-3</sup> | Uncertainty (k=1)<br>in Bq.m <sup>-3</sup> | Mean value<br>in Bq.m <sup>-3</sup> | $\sigma$ (mean)<br>in Bq.m <sup>-3</sup> | Calibration factor<br>(Instrument/true) | Uncertainty (k=2) |
| 9856   | 228  | 6170                                | 44                                       | <b>0.63</b>                             | <b>0.03</b>       |
| 46169  | 649  | 30583                               | 102                                      | <b>0.66</b>                             | <b>0.02</b>       |
| 244304                                       | 8161                                       | 167941                              | 756                                      | <b>0.69</b>                             | <b>0.05</b>       |
| RAD7   | 2964                                       |                                     |  |   |                   |
| Expected true value<br>in Bq.m <sup>-3</sup> | Uncertainty (k=1)<br>in Bq.m <sup>-3</sup> | Mean value<br>in Bq.m <sup>-3</sup> | $\sigma$ (mean)<br>in Bq.m <sup>-3</sup> | Calibration factor<br>(Instrument/true) | Uncertainty (k=2) |
| 9856   | 228  | 5777                                | 46                                       | <b>0.59</b>                             | <b>0.03</b>       |
| 46169  | 649  | 25958                               | 119                                      | <b>0.56</b>                             | <b>0.02</b>       |
| 239922                                       | 8221                                       | 132412                              | 1315                                     | <b>0.55</b>                             | <b>0.04</b>       |

## 6 CONCLUSION

Three different constant  $^{220}\text{Rn}$  reference atmospheres, i.e.  $10 \text{ kBq}\cdot\text{m}^{-3}$ ,  $46 \text{ kBq}\cdot\text{m}^{-3}$  and  $240 \text{ kBq}\cdot\text{m}^{-3}$ , have been established to cover a wide range of  $^{220}\text{Rn}$  activity concentrations and calibrate seven instruments.

Ratios between the  $^{220}\text{Rn}$  activity concentrations measured by the instrument and the reference activity concentration have been found close to 1 for the four AlphaGUARD and around 0.6 for the three RAD7. The calibration factor of an alphaGUARD changes with the thoron activity concentration.

The results obtained in this work reveal some discrepancies in the readings of certain types of  $^{220}\text{Rn}$  measurement instruments and emphasize the importance of the metrological assurance of  $^{220}\text{Rn}$  measurements.



# Deliverable D2

## Annex V

### TASK A.2.2.1

Study on the influence of thoron on active radon monitors

T. Turtiainen<sup>1</sup>, R. Dehganzada<sup>1</sup>, O. Holmgren<sup>1</sup>,  
S. Georgiev<sup>2</sup>, K. Mitev<sup>2</sup>

<sup>1</sup>) Sateilyturvakeskus (STUK), Laippatie 4, P.O. Box 14, FI-00881 Helsinki, Finland

<sup>2</sup>) Sofiiski Universitet Sveti Kliment Ohridski (SUBG), Bul Tzar Osvoboditel 15, 1504, Sofia, Bulgaria

## Contents

|   |    |
|---|----|
| I. Summary.....   | 3  |
| II. Theory.....   | 5  |
| III. Cross-interference testing of radon monitors at STUK.....  | 9  |
| III.1 Exposure set-up and reference instruments at STUK.....  | 9  |
| III.2 Tests of Alpha E, Saphymo GmbH (now Bertin instruments).....  | 11 |
| III.3 Tests of AlphaGuard PQ2000 Pro, Saphymo GmbH (now Bertin instruments).....  | 16 |
| III.4 Tests of RadonEye 2+, RadonFTLab.....   | 18 |
| III.5 Tests of Corentium Home, Airthings AS.....  | 20 |
| III.6 Tests of Airthings Wave, Airthings AS.....  | 22 |
| III.7 Tests of Airthings Wave Plus, Airthings AS.....   | 24 |
| III.8 Tests of Corentium Pro, Airthings AS.....   | 26 |
| III.9 Additional test: response time.....   | 28 |
| IV. Cross-interference testing of radon monitors at SUBG.....   | 30 |
| IV.1 Exposure set-up and reference instruments at SUBG.....   | 30 |
| IV.2 Tests of Alpha E, Saphymo GmbH (now Bertin instruments).....   | 31 |
| IV.3 Tests of RadonEye 2+, RadonFTLab.....  | 36 |
| IV.4 Tests of TSR3.....   | 39 |
| IV.5 Tests of TSR4M.....  | 42 |
| V. Intercomparison of cross-interference testing of radon monitors at STUK and SUBG.....                                    | 50 |
| VI. On the possible altitude dependence of the AlphaE readings due to sensitivity to radiation produced by cosmic rays..... | 51 |

T. Turtiainen, R. Dehganzada, O. Holmgren, S. Georgiev, K. Mitev

## I. Summary

A study of the influence of thoron on active radon monitors was performed in the framework of Task A2.2.1 of the MetroRadon project. Influence of thoron was investigated by measuring the radon (Rn-222) signal acquired by a radon monitor during thoron (Rn-220) exposure. The ratio of false Rn-222 signal to Rn-220 concentration is the instrument's cross-interference (CI) to thoron. The study was performed in the exposure facilities of STUK and SUBG.

The theoretical model for the evaluation of the thoron influence on active radon monitors was developed at STUK and adopted at SUBG. In total 14 different instruments have been tested in both labs in various exposures conditions, including exposures to pure Thoron in air atmospheres as well as exposure to mixed Radon and Thoron atmosphere. Two of the instruments (one AlphaE and one RaonEye2+) were tested in both laboratories.

The results of the tests are summarized in Table A1. These results show that all tested monitors except for RadonEye and TSR4M comply with the IEC 61577-2 standard requirement for CI <20%.

In the case of the TSR4M monitor, we suspect that there is a technical problem with the analysis of the spectrum (ROI selection and analysis, etc.).

The RadonEye 2+ data shows higher than 20% cross-interference in most of the experiments. In normal measurement environment, little thoron is present. Low cross-interference signal may therefore not be a desired feature. The lower the cross-interference, the slower the diffusion into the detection volume. This reduces the temporal response of the instrument. Continuous radon measurement is mostly used for detecting temporal variations in radon concentration and long response time may lead to false interpretation of the data sets.

The theoretical model developed for the CI evaluation is shown in Chapter II. The cross-interference tests performed at STUK are described in Chapter III and those in SUBG in Chapter IV. Chapter V presents the comparison of CI results of two instruments, which are performed at STUK and SUBG. In Chapter VI we comment on the possible sensitivity of the AlphaE readings to cosmic radiation.

| Instrument                                 | Tested at: | s/n                      | Test dates  | CI (initial)            | CI (final)             |
|--|------------|--------------------------|---|-------------------------|------------------------|
| AlphaE                                     | STUK       | 000260                   | 5–10 Jun 2019                                       | 6.5 %                   | 9.3 %                  |
|  | STUK       | 000542                   | 31 Jul–5 Aug 2019                                   | 8.9 %                   | 12 %                   |
|  | STUK       | 000499                   | 11–17 Jun 2019<br>31 Jul–5 Aug 2019<br>5–9 Dec 2019 | 5.6 %<br>8.7 %<br>5.7 % | 9.2 %<br>13 %<br>8.6 % |
| AlphaE                                     | SUBG       | 000499                   | 14–17 Oct 2019                                      | 4.5 %                   | 13.7 %                 |
|  |            |                          | 22–28 Oct 2019                                      | 11.5 %                  | 17.0 %                 |
|  |            |                          | 16–20 Sep 2019                                      | 10.0 %                  | 17.1 %                 |
|  |            |                          | 26–30 Sep 2019<br>4-8 Nov 2019                      | 12.7 %<br>15.5 %        | 18.7 %<br>20.2 %       |
| AlphaGuard PQ2000 Pro<br>AlphaGuard PQ2000 | STUK       | EF1641                   | 6–9 Aug 2019  | 5.1–11 %                | 7.2 %                  |
|  | STUK       | EF0408                   | 22–27 Jan 2020                                      | 4.6–9.2%                | 6.0 %                  |
| RadonEye + <sup>2</sup>                    | STUK       | PE21812110009            | 20–23 August 2019                                   | 28 %                    | 42 %                   |
|  | STUK       | PE21904100016            | 28 Nov–1 Dec 2019                                   | 27 %                    | 37 %                   |
| RadonEye + <sup>2</sup>                    | SUBG       | PE21904100016            | 14–17 Oct 2019                                      | 32.6 %                  | 52.7 %                 |
|  |            |                          | 22–28 Oct 2019                                      | 38.7 %                  | 54.7 %                 |
|  |            |                          | 4-8 Nov 2019  | 18.7 %                  | 42.3 %                 |
| Corentium Home                             | STUK       | 2403008304               | 20–24 Jun 2019                                      |                         | 1.8 %                  |
|  |            |                          | 24–29 Jul 2019                                      |                         | 2.5 %                  |
| Airthings Wave                             | STUK       | 2900151289               | 28 Jun–2 Jul 2019                                   |                         | 1.3 %                  |
|  |            |                          | 6–9 Aug 2019  |                         | 2.3 %                  |
| Airthings Wave Plus                        | STUK       | 2930                     | 24–28 Jun 2019                                      |                         | 2.7 %                  |
|  |            |                          | 24–29 Jul 2019                                      |                         | 3.6 %                  |
| Corentium Pro                              | STUK       | 2700007355<br>2700007357 | 3–5 Sep 2018  | 0.2 %                   | 1.2 %                  |
|  |            |                          | 3–5 Sep 2018  | 0.0 %                   | 1.6 %                  |
| TSR3 – Fast mode                           | SUBG       | 16014                    | 16–20 Sep 2019                                      | 1.0 %                   | 7.7 %                  |
|  |            |                          | 26–30 Sep 2019                                      | 11.5 %                  | 12.3 %                 |
| TSR3 – Slow mode                           | SUBG       | 16014                    | 22–28 Oct 2019                                      | 2.7%                    | 15.3 %                 |
| TSR4M– Fast mode                           | SUBG       | 19015                    | 22–28 Oct 2019                                      | 6.2 %                   | 125 %                  |
|  |            |                          | 16–20 Sep 2019                                      | -                       | 127 %                  |
|  |            |                          | 26–30 Sep 2019                                      | -                       | 186 %                  |
|  |            |                          | 4-8 Nov 2019  | 11.2%                   | 114 %                  |
| TSR4M– Slow mode                           | SUBG       | 19015                    | 22–28 Oct 2019                                      | 15.9 %                  | 85.8 %                 |
|  |            |                          | 16–20 Sep 2019                                      | -                       | 69.5 %                 |
|  |            |                          | 26–30 Sep 2019                                      | 7.9%                    | 115 %                  |
|  |            |                          | 4-8 Nov 2019  | 18.7%                   | 76.4 %                 |

Table A1. Summary of the CI tests performed at STUK and SUBG.

## II. Theory

The sampling of radon instruments is either active or passive. In active sampling, sample air is pumped into the detection volume. In most cases, Tn-220 enters the detection volume regardless of its short half-life of 55.6 seconds. In passive sampling, sample air is passively transported to the detector by diffusion. In order to prevent thoron from entering the detection volume, a diffusion barrier is normally applied either in form of a filter or a small gap, if no other separation technique is applied. Depending on the diffusion time at the barrier various amounts of Tn-220 gas may enter the detection volume.

Thoron progeny generally does not diffuse into the detector but is retained at the diffusion barrier. The instrument has been designed to measure activity concentration of Rn-222 gas, not its progeny aerosol. Requirement for preventing decay products from entering the sensitive volume of the detection unit is given in standard IEC 61577-2. Tn-220 gas that enters the detection volume attains equilibrium with its first daughter Po-216 very rapidly (in about 1 second). Formation of full equilibrium in the Tn-220 progeny decay chain is then regulated by Pb-212, whose half-life is 10.64 hours. The next decay product Bi-212 has both alpha and beta decays and branching occurs. In full equilibrium with Tn-220, the final alpha activity is 270 % and the final beta activity is 230 % of that of the constant Tn-220 activity. Alpha active isotopes are Tn-220, Po-216, Bi-212 and Po-212. Beta active isotopes are Pb-212, Bi-212 and Tl-208 (Fig A1).

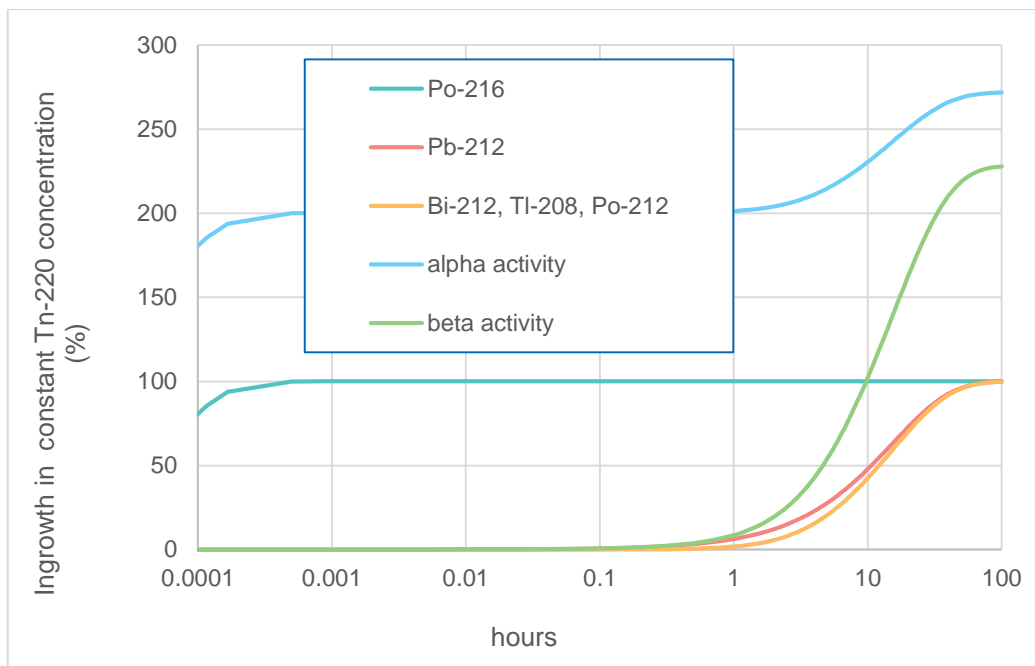


Figure A1. Formation of Tn-220 progeny in the detection volume in constant Tn-220 concentration.

If electrostatic collection is applied in the detection volume, and the detector is a semi-conductor capable of energy separation of alpha decays, the instrument can record a spectrum in which separate peaks for each alpha active decay product can be obtained (Fig. A2). If spectroscopy is applied, Tn-220 progeny can be identified, and they have little effect on the calculated Rn-222 concentration. Manufacturers of Rn-222 monitors seldom report if their inexpensive instruments apply spectroscopy, this information is reported mainly for expensive professional models.

T. Turtiainen, R. Dehganzada, O. Holmgren, S. Georgiev, K. Mitev

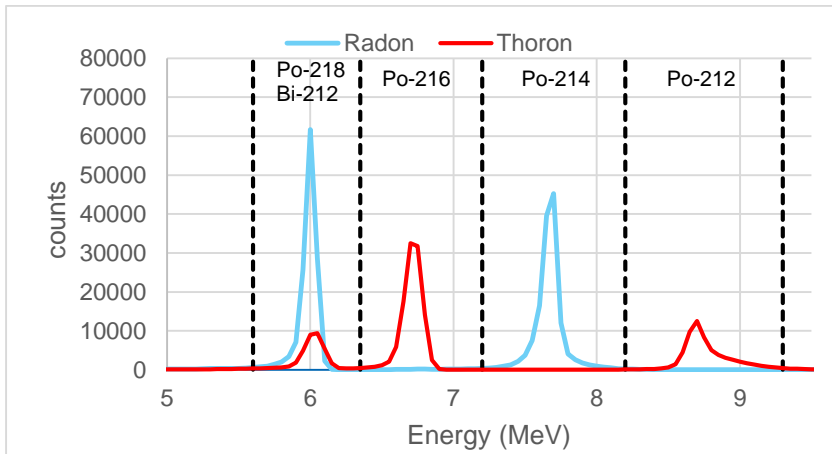


Figure A2. Radon (with progeny) and thoron (with progeny) spectrum recorded with alpha spectrometer RAD 7 (DurrIDGE).

Many of the Rn-222 monitors are based on silicon diodes. In figure A3, we have assessed four scenarios for formation of thoron cross-interference signal (Fig A3). First, all alpha counts are regarded as radon progeny signals and are included in the calculation of Rn-222 concentration (no spectroscopy is carried out). Second, only Bi-212 alpha counts are included, third, only Po-216 signals are rejected, and fourth, only Po-212 signals are rejected.

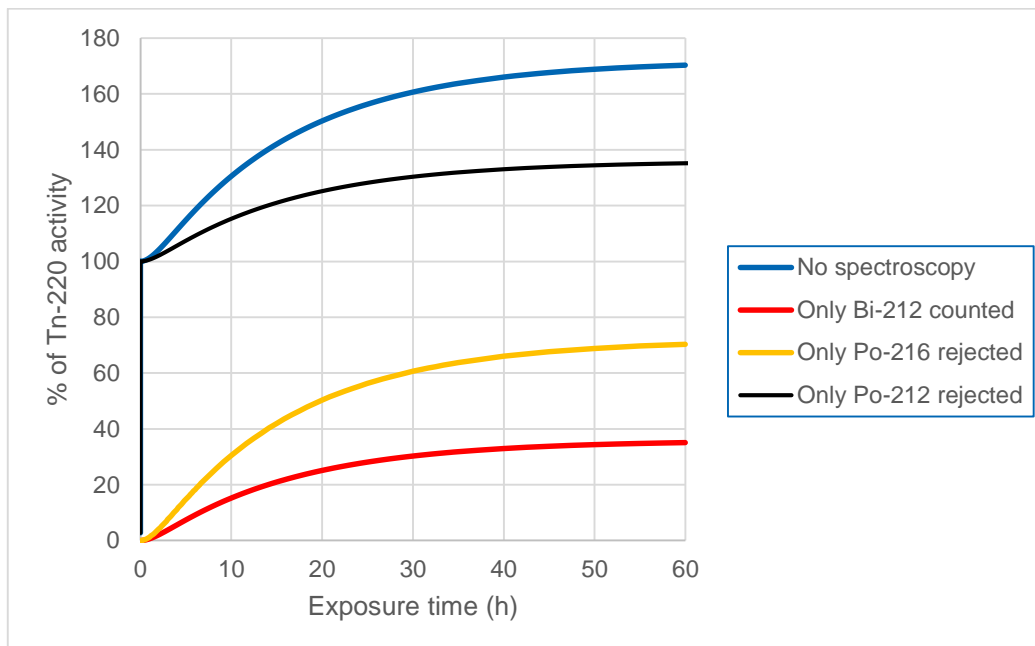


Figure A3. Formation of cross-interference signal from constant Tn-220 exposure over time.

The formation curves, however, have common features. There is (or is not) a fast response for Tn-220. This cross-interference signal represents a case where there is a short-term, pulse-like thoron concentration around the instrument. We call this signal *initial cross-interference*. If thoron exposure continues, the cross-interference signal increases for the first three days. After this, an equilibrium is attained. We call this signal *final cross-interference*.

T. Turtiainen, R. Dehganzada, O. Holmgren, S. Georgiev, K. Mitev

We can approximate a function to which we can fit the recorded cross-interference signal,  $\mu$ :

$$\mu(t) = \mu_i + \mu_s(1 - e^{-\lambda_{Pb-212}t}) \quad [1]$$

The initial cross-interference is then calculated

$$CI_i = \frac{\mu_i}{C_{Tn}} \times 100\% \quad [2]$$

The final cross-interference is calculated

$$CI_f = \frac{\mu_i + \mu_s}{C_{Tn}} \times 100\% \quad [3]$$

Interpretation of the signal may, however, not be this straight-forward. The region of interest (ROI) on the spectrum may be set in such a way that only part of a specific thoron decay product signals are counted. The ROI settings or amplification may vary between instruments of the same model. There may also be an averaging algorithm for making the data set less scattered. This type of correction will cause delays in the formation of cross-interference signal.

In addition to silicon diodes, there are instruments where the detector is an ionization chamber or a Lucas cell. Ionization chambers also record the alpha and beta decays of the Rn-222/Tn-220 progeny as well as the alpha-active gasses. Alpha/beta coincidence summing is also often present in the spectrum. Resolution of alpha peaks in a pulse ionization spectrum is wider than in semiconductor detectors and therefore, probably only Po-212 with high alpha energy can be rejected by spectroscopy (Fig. A4). Lucas cells only detect alpha particles and cannot separate decay products according to their energy.

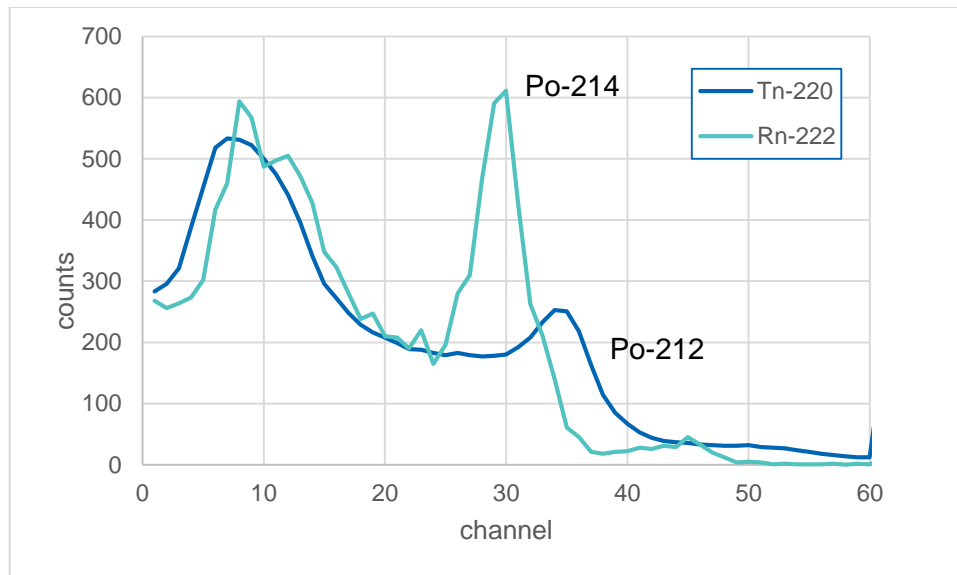


Figure A4. Radon (with progeny) and thoron (with progeny) spectrum recorded with the same pulse ionization chamber (AlphaGuard PQ2000). Tn-220 spectrum has been reduced by a factor of 80.

T. Turtiainen, R. Dehganzada, O. Holmgren, S. Georgiev, K. Mitev

In the exposures at low activity concentrations performed at SUBG we failed to maintain constant thoron concentration in the exposure system. These are the exposures performed in the periods: 14–17 Oct 2019, 22–28 Oct 2019 and 4-8 Nov 2019. It is found that the thoron concentration in these exposures can be approximated with a linear dependence of the type:

$$C_{Tn}(t) = \alpha t + \beta. \quad [4]$$

Therefore, for these exposures at SUBG we have modified the theoretical model proposed by STUK. In this case, in order to account for the linear variation of the thoron concentration, the radon readings of the instruments  $C_{Rn}$  are fitted with the function:

$$C_{Rn}(t) = CI_i C_{Tn}(t) + CI_f (1 - e^{-\lambda_{Pb-212} t}) C_{Tn}(t). \quad [5]$$

Substituting  $C_{Tn}$  from Eq. 4 in Eq. 5 one gets:

$$C_{Rn}(t) = CI_i (\alpha t + \beta) + CI_f (\alpha t + \beta) (1 - e^{-\lambda_{Pb-212} t}). \quad [6]$$

Equation [6] was used to find  $CI_i$  and  $CI_f$  in the exposures from 14–17 Oct 2019, 22–28 Oct 2019 and 4-8 Nov 2019 performed at SUBG. Hereafter this model (Eq. 6) is referred to as *the modified model*.

### III. Cross-interference testing of radon monitors at STUK

#### III.1 Exposure set-up and reference instruments at STUK

Thoron atmosphere was created in a 101.1-litre Emanation Calibration Container (s/n EV03117, Saphymo GmbH). Air exchange through the container was created with Qdos60 peristaltic pump (Watson Marlow) and monitored from the air outlet with Thermo GFM Pro flow meter (s/n TS561043). The inlet air was first desiccated with Laboratory Drying Unit (DurrIDGE) filled with freshly regenerated Drierite and second, radon was removed with a 1-litre activated carbon unit (Saphymo) before the thoron source. A flow-through thoron source TH-1025 from Pylon Electronics Inc. was used and its certified activity on 14 Sep 2018 is  $(100,83 \pm 0.63)$  kBq (certificate I4751) (see Figure A5). The thoron-rich air was directed (after a 175 mL transfer volume) in front of a small fan situated under the lid of the container (Figure A6).

Homogeneity of thoron gas inside the container has been validated with aerogel samplers before. Reference instrument for thoron concentration measurement was AlphaGuard PQ2000 RnTn (s/n EF2104, Saphymo GmbH) which has been calibrated against the LNHB primary thoron standard at IRSN (May 2018). The instrument was operated with AlphaPump (s/n AP1367), the flow rate of which was checked before and after exposures with Aalborg GFM 17 mass flow meter (calibration certificate M-18D020). Humidity and temperature were measured with HygroClip HC2A-S -probe (Rotronic AG, s/n 0020300479, certificate 9-0366029443). Air velocity measurements were carried with Swema 3000MD (s/n 681989) and SWA31 probe (s/n 421629) calibrated at Pietikko Oy (certificate 201801231).

In most experiments, humidity was not regulated and therefore it decreased when dried thoron-bearing air was pumped into the container. In three tests, humidity in air was regulated with a bottle of supersaturated  $MgCl_2$  aqueous solution placed inside the container. Temperature and air pressure were not regulated, and they followed the those in the laboratory.

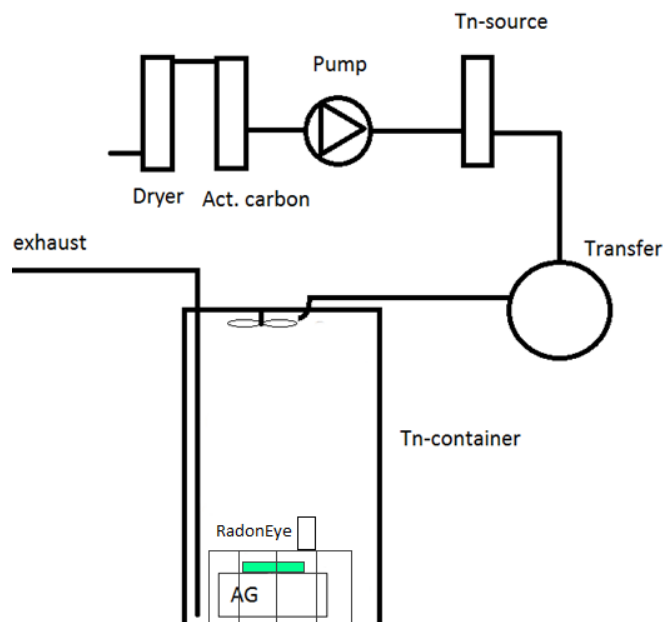


Figure A5. Set-up of the cross-interference test. The instrument under testing (in this example RadonEye) was placed on a grid above the reference instrument (AG).

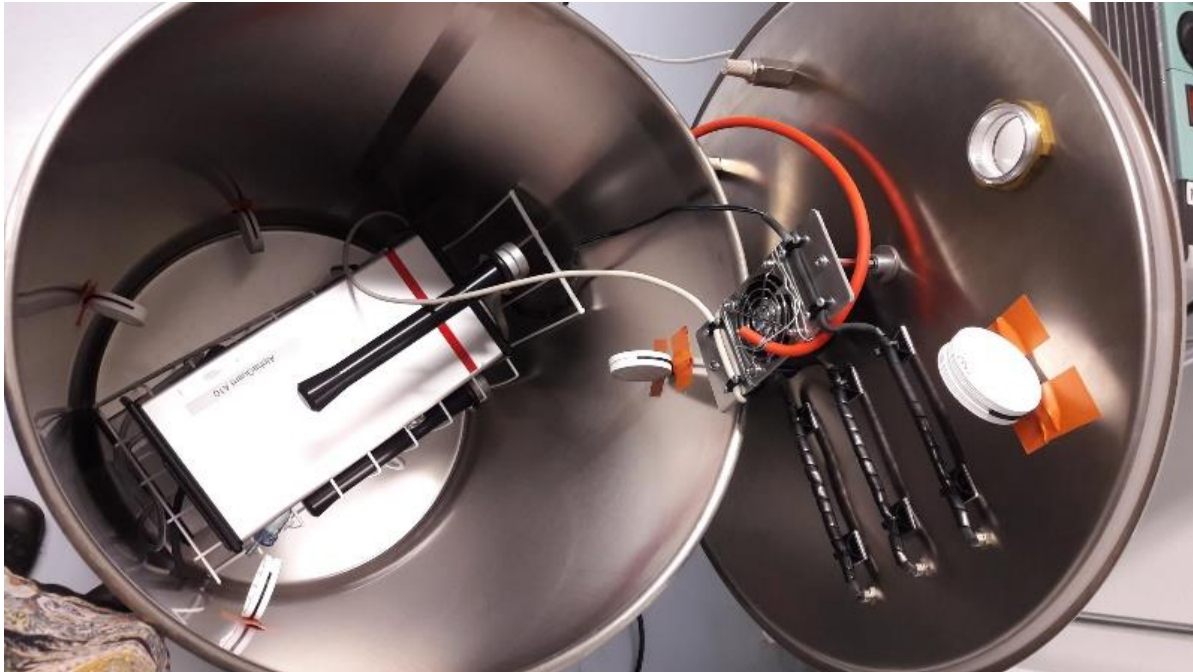


Figure A6. Snapshot of the STUK experimental system with the reference instrument (on the bottom) and instrument under testing (on top). Attached white discs are aerogel samplers for assessing homogeneity of thoron gas during the exposure.

Air flow velocity measurements were performed in the container without an instrument intended testing but with the reference instrument placed on the bottom. Flow velocity logger was placed next to the reference instrument. The flow rate at the grid level, in the middle was recorded as  $(0.24 \pm 0.03)$  m/s and it was normal to the grid plane. The uncertainty of flow velocity measurements is given with 1 SD.

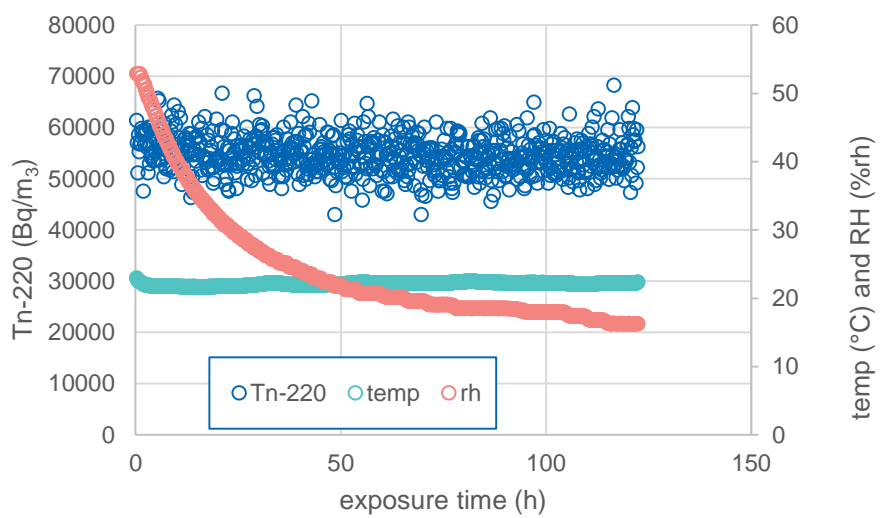
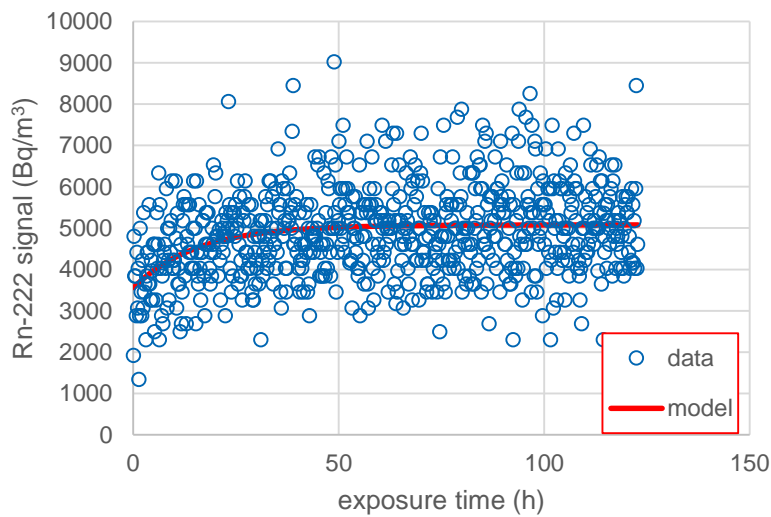
Rn-222 concentration in the laboratory is  $<20$  Bq/m<sup>3</sup>, mostly in the range 10–20 Bq/m<sup>3</sup>. This signal was considered negligible as Tn-220 exposure concentrations were normally between 25–70 kBq/m<sup>3</sup> and the recorded cross-interference signal  $>500$  Bq/m<sup>3</sup>. At the beginning of the exposure, ambient air radon is sealed into the thoron atmosphere. After operating the atmosphere for four days with flow rate of 60 mL/min (equivalent Tn-220 concentration of 25 kBq/m<sup>3</sup>), only 2 % of the original Rn-222 remains in the atmosphere.

Several unsuccessful tests are not included in this report. In many cases, Tn-220 concentration did not remain constant enough for reliable assessment of CI or Tn-220 could not be calculated. This could be due to leakage in tube fittings, wrong valve positions, reference instrument pump settings etc. Unfortunately, all tests on RadonEye RD200 model at STUK were unsuccessful and are hence not reported.

T. Turtiainen, R. Dehganzada, O. Holmgren, S. Georgiev, K. Mitev

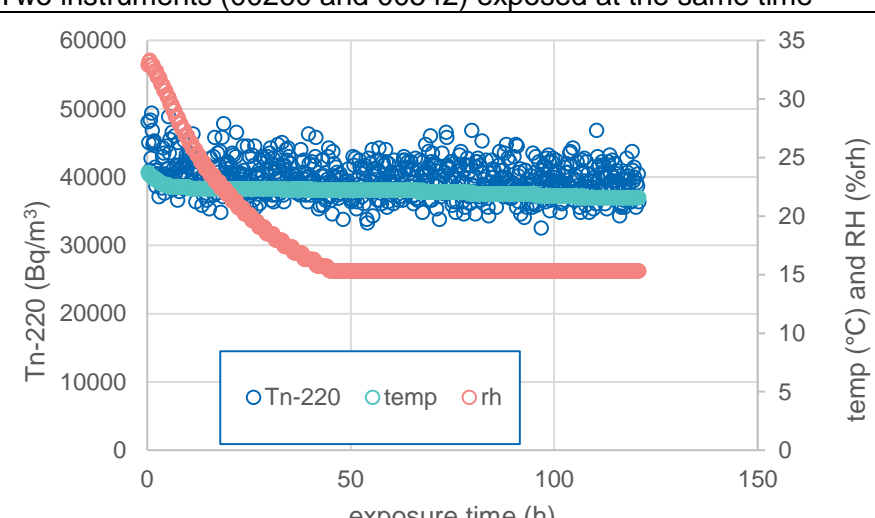
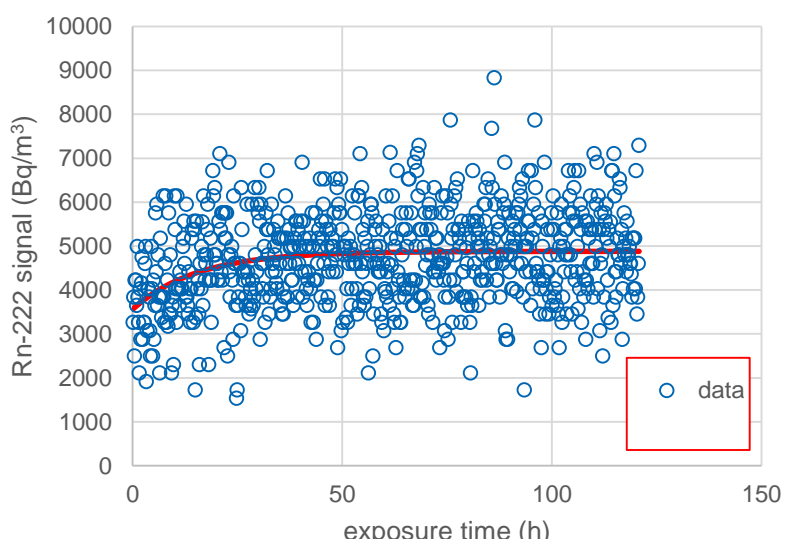
### III.2 Tests of Alpha E, Saphymo GmbH (now Bertin instruments)

AlphaE is a small, portable radon monitor that can be used for measuring personal radon exposure. The detector is a silicon diode.

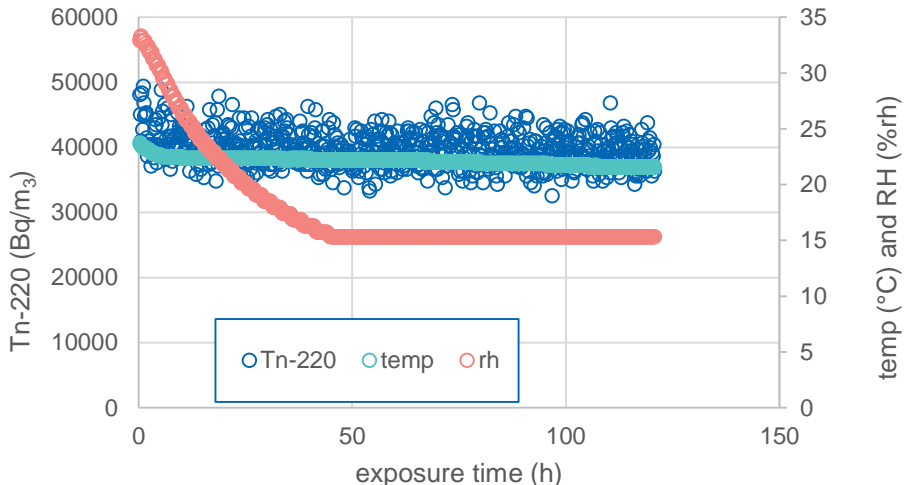
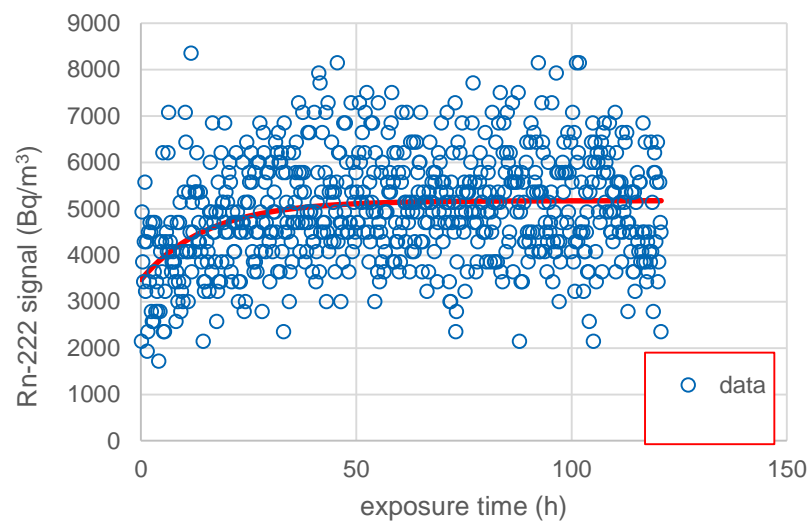
|                           |  |
|---------------------------|--|
| Test date                 | 5–10 June 2019   |
| Instrument                | Alpha E  |
| Instrument s/n            | 000260   |
| Air velocity/geometry     | 0.24 m/s sideways to the air inlet   |
| C(Tn-220) mean            | $(54\,700 \pm 1\,000) \text{ Bq/m}^3$  |
| CI (initial)              | 6.5 %  |
| CI (final)                | 9.3 %  |
| NB                        | 10-min time integral   |
| Exposure conditions       |   |
| Cross-interference signal |  |



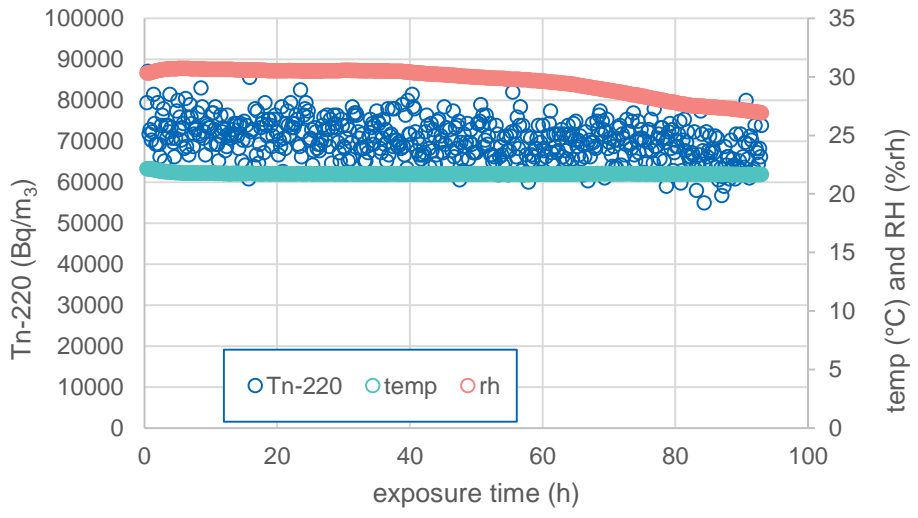
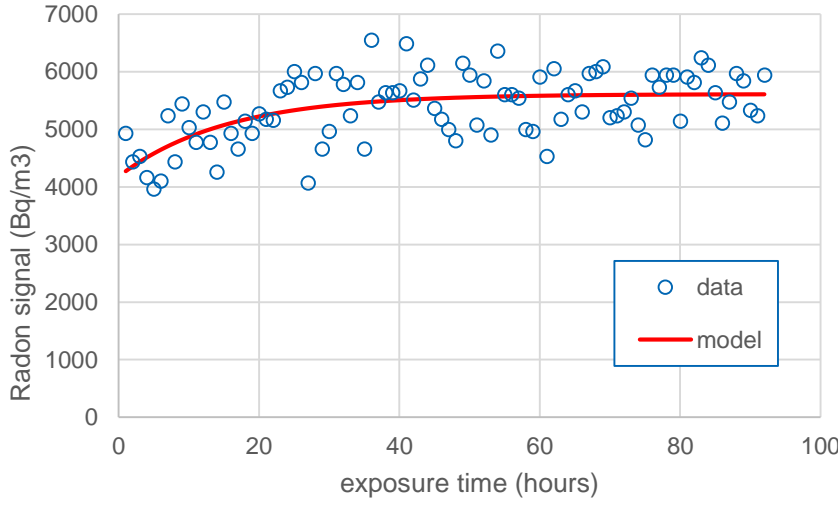
T. Turtiainen, R. Dehganzada, O. Holmgren, S. Georgiev, K. Mitev

|                           |  |
|---------------------------|--|
| Test date                 | 31 July–5 August 2019  |
| Instrument                | Alpha E  |
| Instrument s/n            | 000260   |
| Air velocity/geometry     | 0.24 m/s sideways to air inlet   |
| C(Tn-220) mean            | $(39\,800 \pm 700)$ Bq/m <sup>3</sup>  |
| CI (initial)              | 8.9 %  |
| CI (final)                | 12 %   |
| NB                        | Two instruments (00260 and 00542) exposed at the same time                           |
| Exposure conditions       |   |
| Cross-interference signal |  |

T. Turtiainen, R. Dehganzada, O. Holmgren, S. Georgiev, K. Mitev

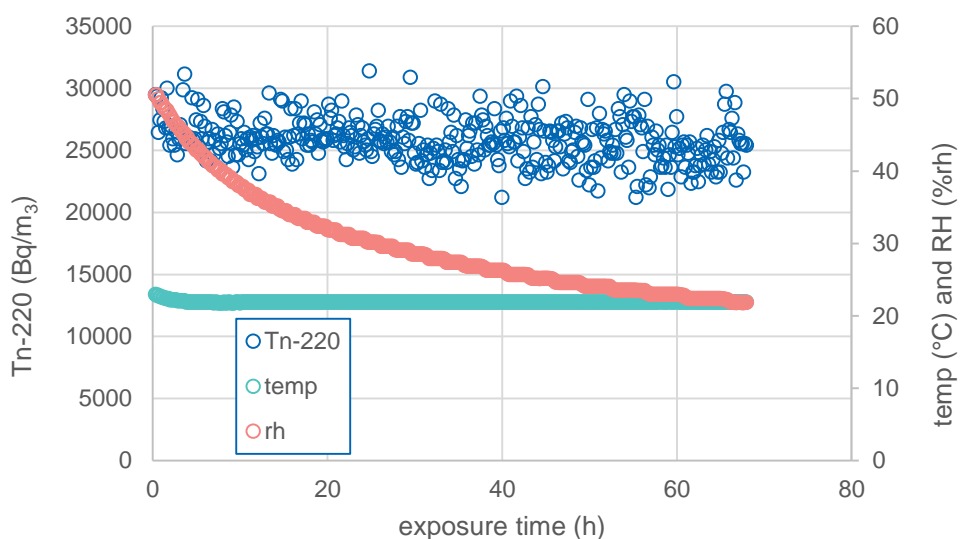
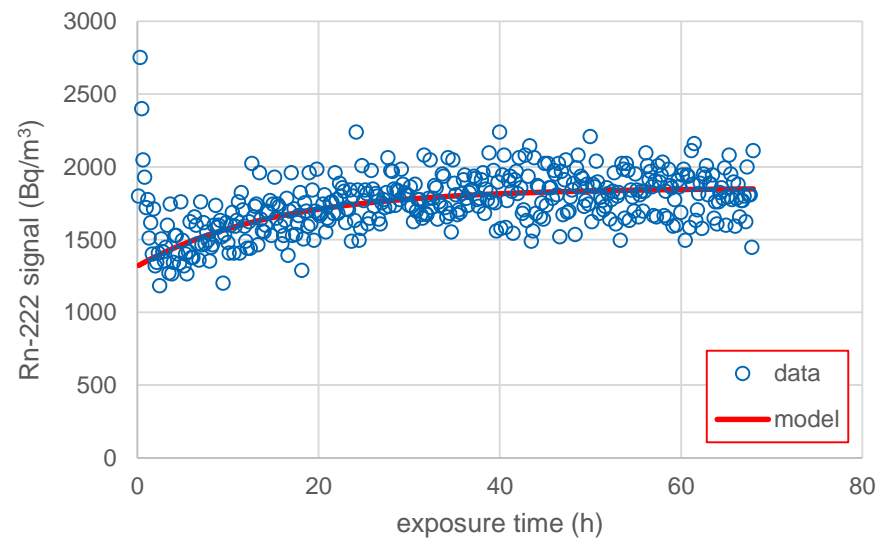
|                           |  |
|---------------------------|--|
| Test date                 | 31 July–5 August 2019  |
| Instrument                | Alpha E  |
| Instrument s/n            | 000542   |
| Air velocity/geometry     | 0.24 m/s sideways to air inlet   |
| C(Tn-220) mean            | $(39\,800 \pm 700)$ Bq/m <sup>3</sup>  |
| CI (initial)              | 8.7 %  |
| CI (final)                | 13 %   |
| NB                        | Two instruments (00260 and 00542) exposed at the same time                           |
| Exposure conditions       |   |
| Cross-interference signal |  |

T. Turtiainen, R. Dehganzada, O. Holmgren, S. Georgiev, K. Mitev

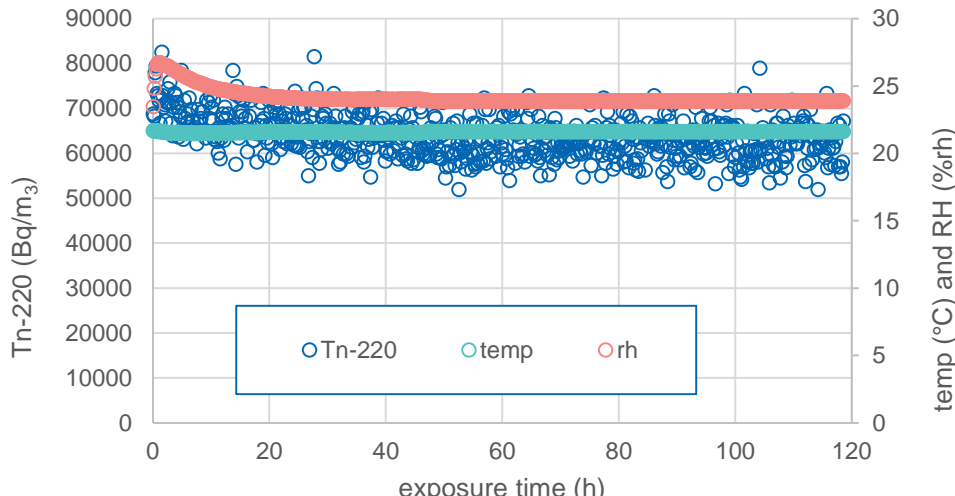
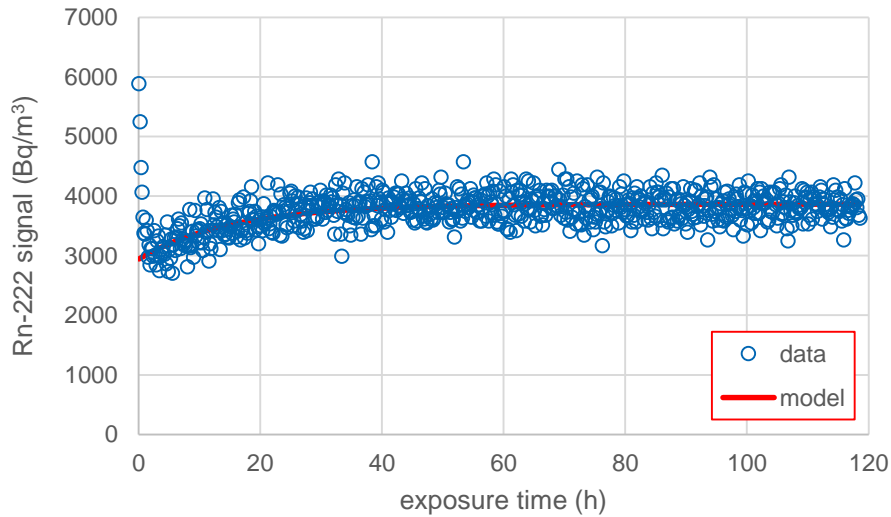
|                           |  |
|---------------------------|--|
| Test date                 | 5–9 December 2019  |
| Instrument                | Alpha E  |
| Instrument s/n            | 000499   |
| Air velocity/geometry     | 0.24 m/s towards air inlet   |
| C(Tn-220) mean            | $(70\,400 \pm 1000) \text{ Bq/m}^3$  |
| CI (initial)              | 5.7 %  |
| CI (final)                | 8.6 %  |
| NB                        | Inter-comparison to Sofia University tests; 60 min time integral                     |
| Exposure conditions       |   |
| Cross-interference signal |  |

### III.3 Tests of AlphaGuard PQ2000 Pro, Saphymo GmbH (now Bertin instruments)

AlphaGuard is a professional radon instrument. The detector is an ionization chamber.

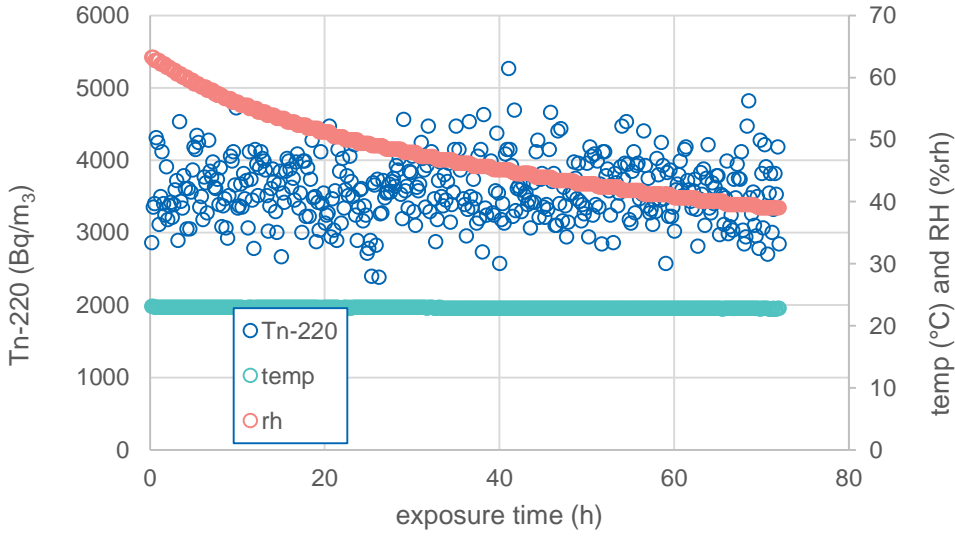
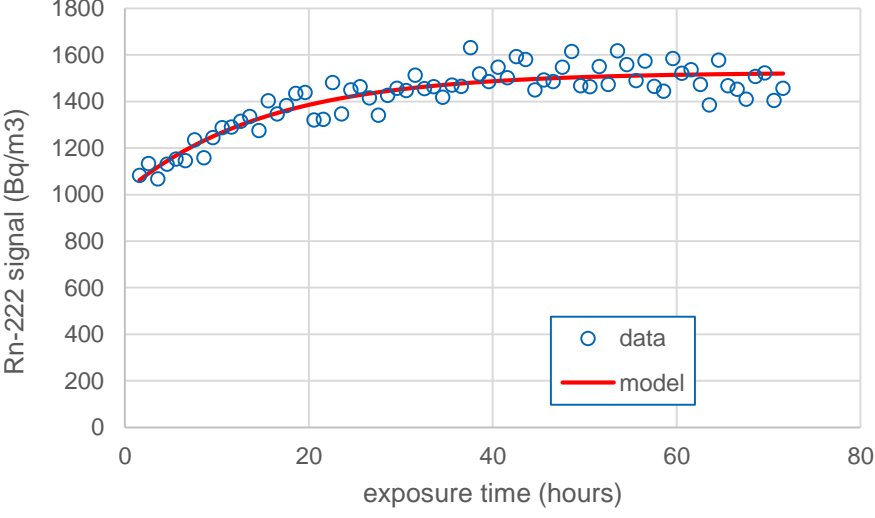
|                           |  |
|---------------------------|--|
| Test date                 | 6–9 August 2019  |
| Instrument                | AlphaGuard PQ2000 Pro  |
| Instrument s/n            | EF1641   |
| Air velocity/geometry     | 0.24 m/s sideways to air inlet   |
| C(Tn-220) mean            | (25 800 ± 500) Bq/m <sup>3</sup>   |
| CI (initial)              | 5.1–11 %   |
| CI (final)                | 7.2 %  |
| NB                        | Two instruments were exposed at the same time (see Airthings Wave). Diffusion 10-min mode was used in the test. High initial CI signals were obtained during the first hour of exposure. |
| Exposure conditions       |   |
| Cross-interference signal |    |

T. Turtiainen, R. Dehganzada, O. Holmgren, S. Georgiev, K. Mitev

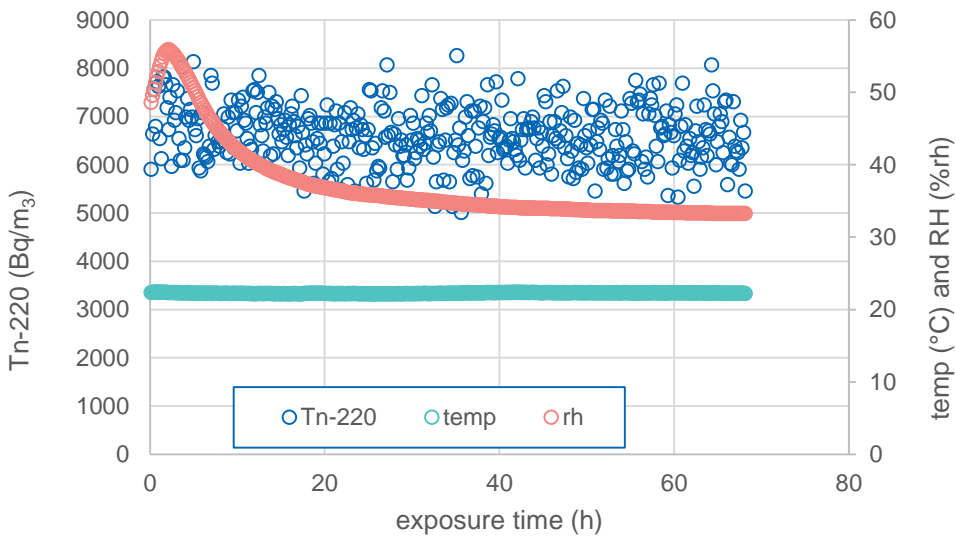
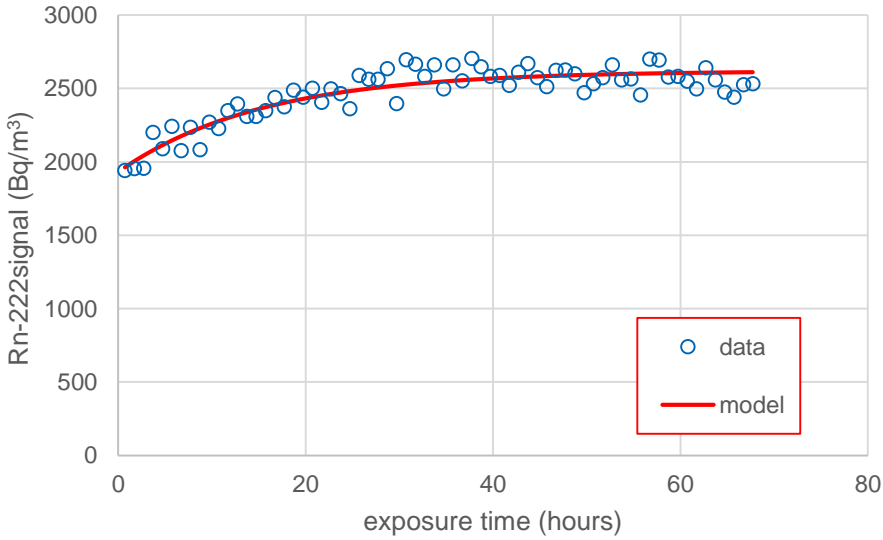
|                           |  |
|---------------------------|--|
| Test date                 | 22–27 January 2019   |
| Instrument                | AlphaGuard PQ2000 Pro  |
| Instrument s/n            | EF0408   |
| Air velocity/geometry     | 0.24 m/s sideways to air inlet   |
| C(Tn-220) mean            | (63 900 ± 1 000) Bq/m <sup>3</sup>   |
| CI (initial)              | 4.6–9.2 %  |
| CI (final)                | 6.0 %  |
| NB                        | Diffusion 10-min mode was used in the test. High initial CI signals were obtained during the first hour of exposure. |
| Exposure conditions       |                                   |
| Cross-interference signal |                                  |

### III.4 Tests of RadonEye 2+, RadonFTLab

RadonEye 2+ is an ionization chamber. Its response time in changing radon concentration is short.

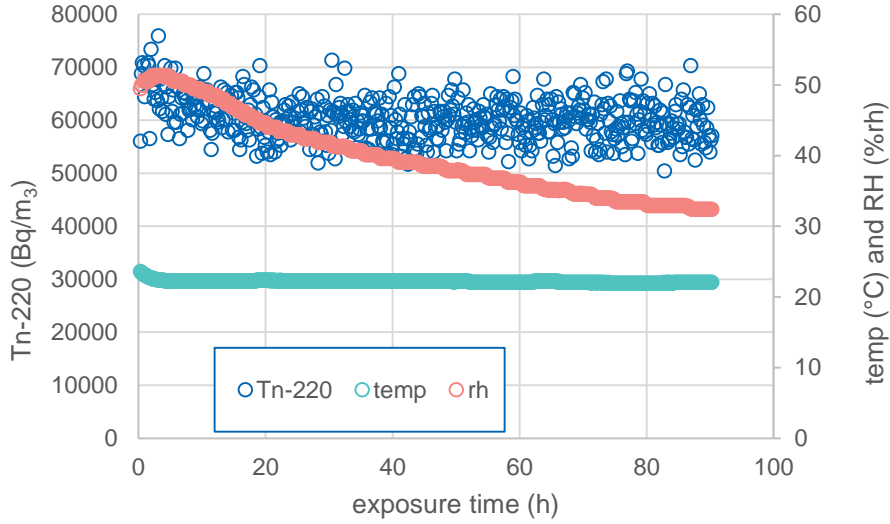
|                           |   |
|---------------------------|---|
| Test date                 | 20–23 August 2019   |
| Instrument                | RadonEye 2+   |
| Instrument s/n            | PE21812110009   |
| Air velocity and geometry | 0.24 m/s sideways to air inlet  |
| C(Tn-220) mean            | $(3590 \pm 100) \text{ Bq/m}^3$   |
| CI (initial)              | 28 %  |
| CI (final)                | 42 %  |
| NB                        | Maximum detectable signal is $9400 \text{ Bq/m}^3$ . Tn-220 exposure concentration was adjusted accordingly |
| Exposure conditions       |                          |
| Cross-interference signal |                         |

T. Turtiainen, R. Dehganzada, O. Holmgren, S. Georgiev, K. Mitev

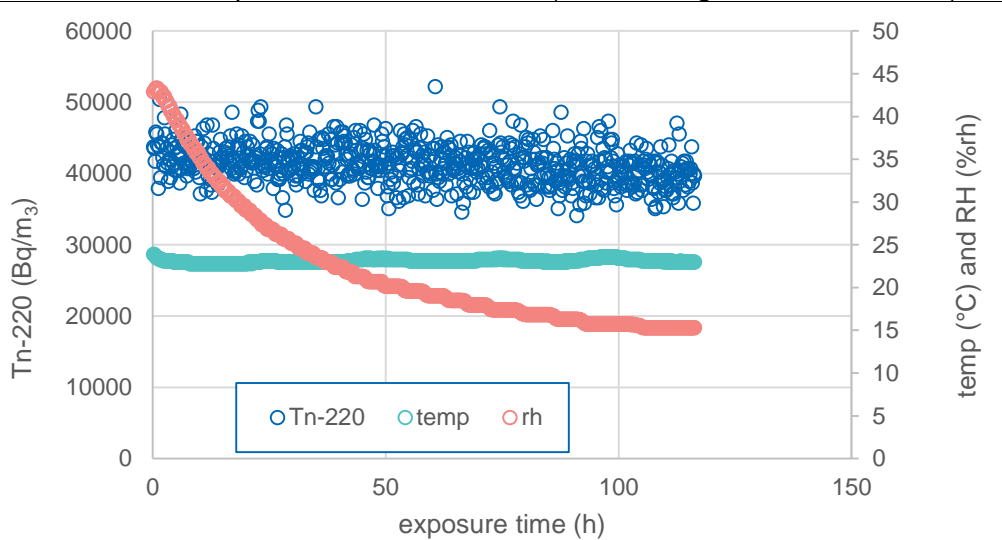
|                           |  |
|---------------------------|--|
| Test date                 | 28 Nov–1 Dec 2019  |
| Instrument                | RadonEye 2+  |
| Instrument s/n            | PE21904100016  |
| Air velocity and geometry | 0.24 m/s sideways to air inlet   |
| C(Tn-220) mean            | $(6640 \pm 130) \text{ Bq/m}^3$  |
| CI (initial)              | 27 %   |
| CI (final)                | 37 %   |
| NB                        | Inter-comparison to Sophia University tests  |
| Exposure conditions       |   |
| Cross-interference signal |  |

### III.5 Tests of Corentium Home, Airthings AS

Corentium home is intended for radon measurements in homes. The detector is a PIN diode. The shortest time integral available from Corentium Home is 1 day. Therefore, only final CI is reported.

|  |  |
|--|--|
| Test date  | 20–24 June 2019  |
| Instrument   | Corentium Home   |
| Instrument s/n                                       | 2403008304   |
| Air velocity/geometry                                | 0.24 m/s against front panel   |
| C(Tn-220) mean                                       | (60 200 ± 900) Bq/m <sup>3</sup>   |
| Rn-222 signal from instrument at the end of exposure | Long term average: 964 Bq/m <sup>3</sup><br>Short term average (1 day): 1071 Bq/m <sup>3</sup> |
| CI (final)   | 1.8 %  |
| Exposure conditions                                  |             |

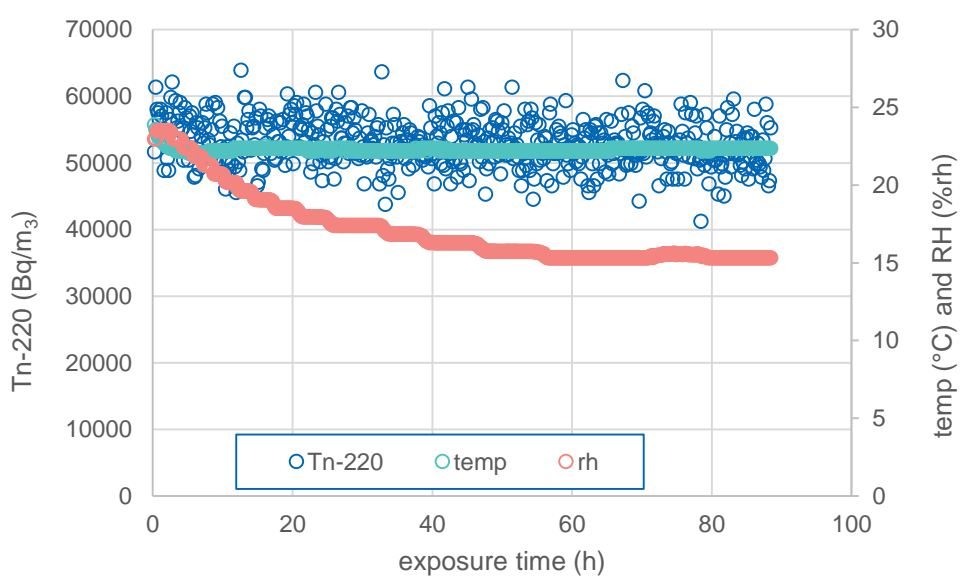
T. Turtiainen, R. Dehganzada, O. Holmgren, S. Georgiev, K. Mitev

|  |   |
|--|---|
| Test date  | 24–29 July 2019   |
| Instrument   | Corentium Home  |
| Instrument s/n                                       | 2403008304  |
| Air velocity/geometry                                | 0.24 m/s against front panel  |
| C(Tn-220) mean                                       | $(41\,300 \pm 600) \text{ Bq/m}^3$  |
| Rn-222 signal from instrument at the end of exposure | Long term average: $1079 \text{ Bq/m}^3$<br>Short term average (1 day): $1036 \text{ Bq/m}^3$ |
| CI (final)   | 2.5 %   |
| NB   | Two instruments exposed at the same time (see Airthings Wave Plus 2930)                       |
| Exposure conditions                                  |            |

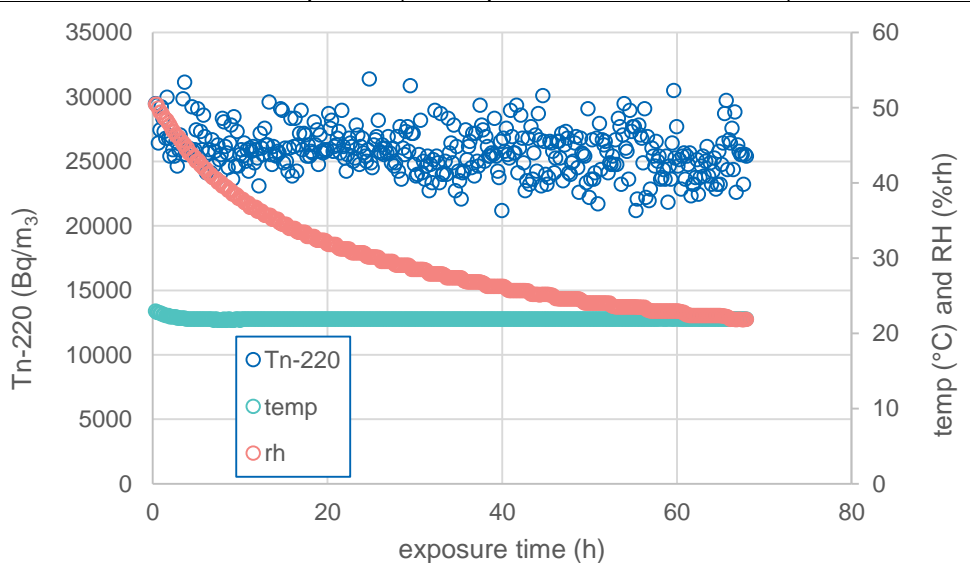
T. Turtiainen, R. Dehganzada, O. Holmgren, S. Georgiev, K. Mitev

### III.6 Tests of Airthings Wave, Airthings AS

Airthings Wave is intended for domestic use and its detector is a PIN diode. The shortest time integral available from Corentium Home is the mean for the last 48 hours. Therefore, only final CI is reported.

|  |   |
|--|---|
| Test date  | 28 June–2 July 2019   |
| Instrument   | Airthings Wave  |
| Instrument s/n                                       | 2900151289  |
| Air velocity/geometry                                | 0.24 m/s against top panel  |
| C(Tn-220) mean                                       | $(53\,000 \pm 800) \text{ Bq/m}^3$  |
| Rn-222 signal from instrument at the end of exposure | 48-hour average: 660 Bq/m <sup>3</sup>  |
| CI (final)   | 1.3 %   |
| NB   |   |
| Exposure conditions                                  |  |

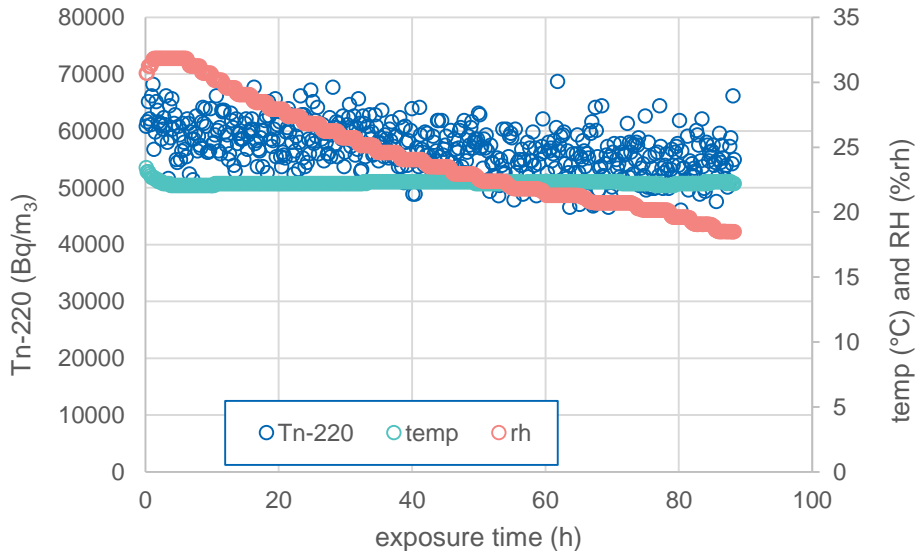
T. Turtiainen, R. Dehganzada, O. Holmgren, S. Georgiev, K. Mitev

|  |   |
|--|---|
| Test date  | 6–9 August 2019   |
| Instrument   | Airthings Wave  |
| Instrument s/n                                       | 2900151289  |
| Air velocity/geometry                                | 0.24 m/s against top panel  |
| C(Tn-220) mean                                       | $(25\,800 \pm 500)$ Bq/m <sup>3</sup>   |
| Rn-222 signal from instrument at the end of exposure | 48-hour average: 584 Bq/m <sup>3</sup>  |
| CI (final)   | 2.3 %   |
| NB   | Two instruments were exposed (see AlphaGuard PQ2000 Pro)                            |
| Exposure conditions                                  |  |

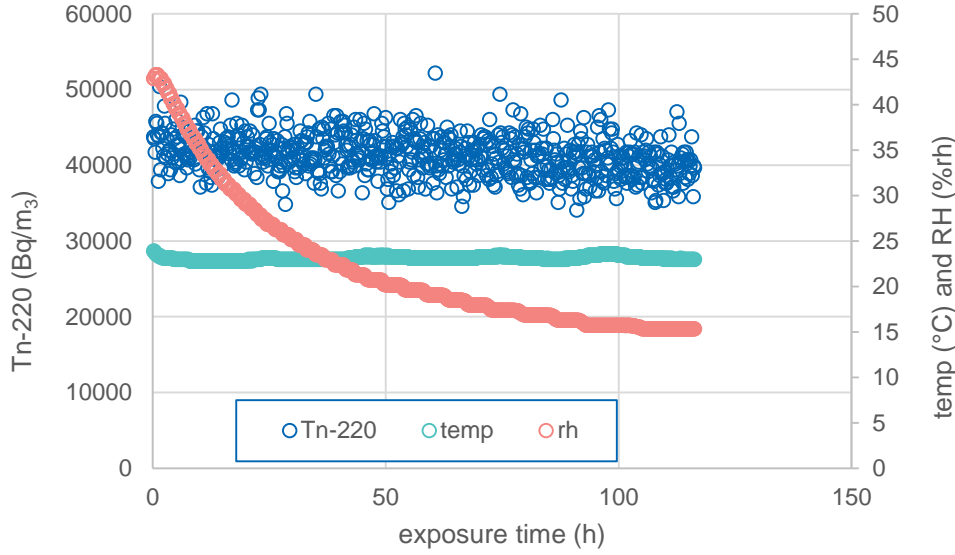
T. Turtiainen, R. Dehganzada, O. Holmgren, S. Georgiev, K. Mitev

### III.7 Tests of Airthings Wave Plus, Airthings AS

Airthings Wave Plus is intended for domestic use and its detector is a PIN diode. The shortest time integral available from Corentium Home is the mean for the last 48 hours. Therefore, only final CI is reported.

|                               |   |
|-------------------------------|---|
| Test date                     | 24–28 June 2019   |
| Instrument                    | Airthings Wave Plus   |
| Instrument s/n                | 2930  |
| Air velocity/geometry         | 0.24 m/s against top panel  |
| C(Tn-220) mean                | (56 900 ± 900) Bq/m <sup>3</sup>  |
| Rn-222 signal from instrument | 2 day: 622 Bq/m <sup>3</sup><br>3 day: 910 Bq/m <sup>3</sup><br>4 day: 1520 Bq/m <sup>3</sup> |
| CI (final)                    | 2.7 %   |
| NB                            |   |
| Exposure conditions           |            |

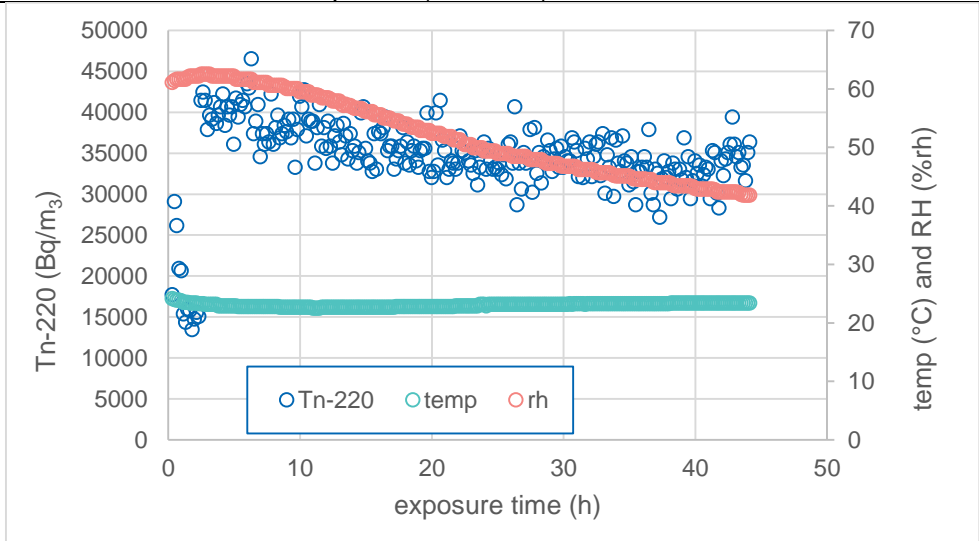
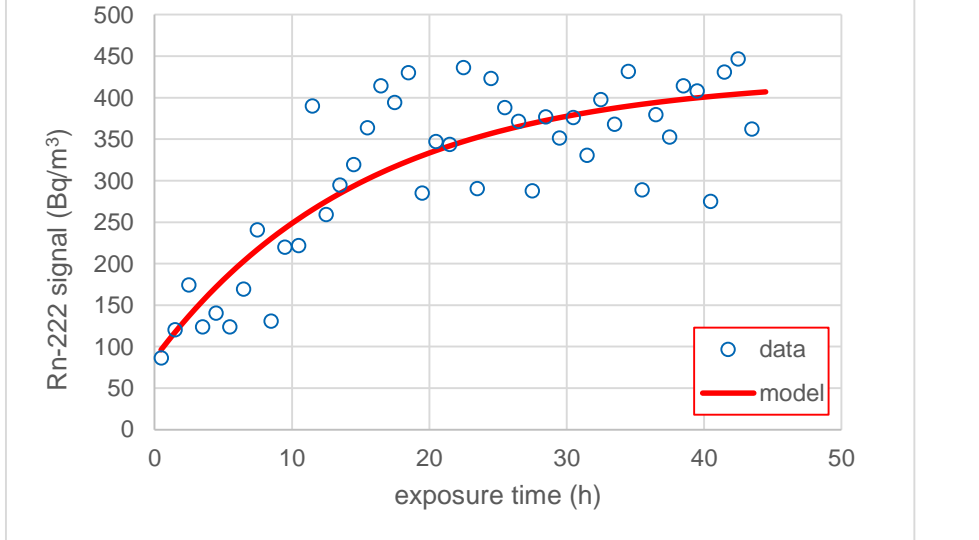
T. Turtiainen, R. Dehganzada, O. Holmgren, S. Georgiev, K. Mitev

|                               |  |
|-------------------------------|--|
| Test date                     | 24–29 July 2019  |
| Instrument                    | Airthings Wave Plus  |
| Instrument s/n                | 2930   |
| Air velocity/geometry         | 0.24 m/s against top panel   |
| C(Tn-220) mean                | $(41\,300 \pm 600) \text{ Bq/m}^3$   |
| Rn-222 signal from instrument | 2 day: $1307 \text{ Bq/m}^3$<br>3 day: $1436 \text{ Bq/m}^3$<br>4 day: $1468 \text{ Bq/m}^3$<br>5 day: $1473 \text{ Bq/m}^3$ |
| CI (final)                    | 3.6 %  |
| NB                            | Two instruments exposed at the same time (see Corentium Home)  |
| Exposure conditions           |   |

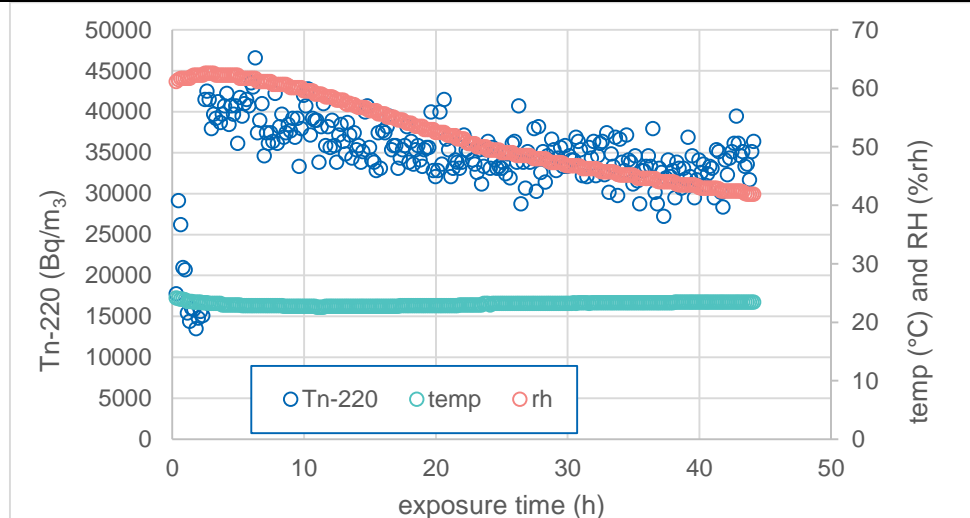
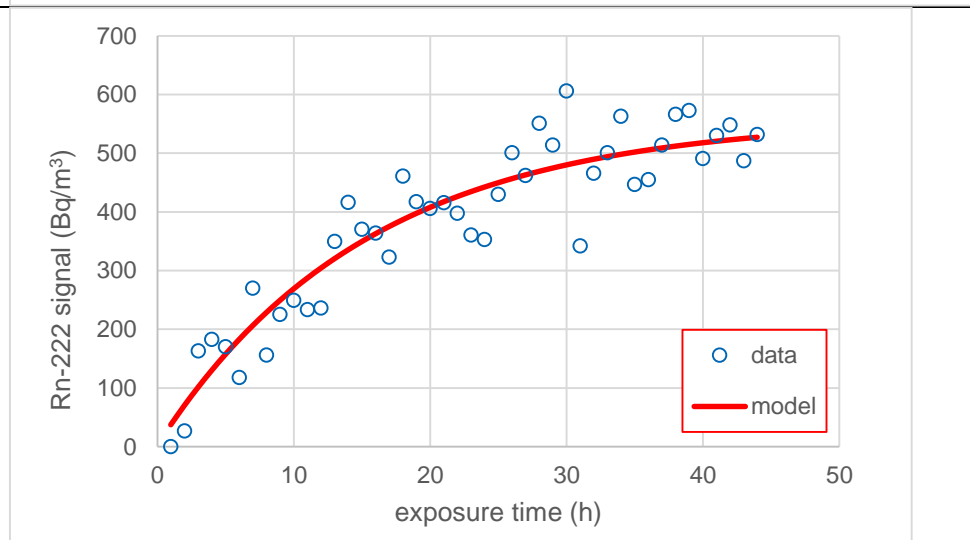
T. Turtiainen, R. Dehganzada, O. Holmgren, S. Georgiev, K. Mitev

### III.8 Tests of Corentium Pro, Airthings AS

Corentium Pro is a professional radon instrument, which has four PIN diode chambers.

|                           |  |
|---------------------------|--|
| Test date                 | 3–5 September 2018   |
| Instrument                | Corentium Pro  |
| Instrument s/n            | 2700007355   |
| Air velocity/geometry     | 0.24 m/s against top of the unit (diffusion holes on the bottom of the unit)         |
| C(Tn-220) mean            | $(34\,600 \pm 600) \text{ Bq/m}^3$   |
| CI (initial)              | 0.2 %  |
| CI (final)                | 1.2 %  |
| NB                        | Two instruments were exposed (see next).   |
| Exposure conditions       |   |
| Cross-interference signal |  |

T. Turtiainen, R. Dehganzada, O. Holmgren, S. Georgiev, K. Mitev

|                           |   |
|---------------------------|---|
| Test date                 | 3–5 September 2018  |
| Instrument                | Corentium Pro   |
| Instrument s/n            | 2700007357  |
| Air velocity/geometry     | 0.24 m/s against top of the unit (diffusion holes on the bottom of the unit)  |
| C(Tn-220) mean            | $(34\,600 \pm 600) \text{ Bq/m}^3$  |
| Cl (initial)              | 0.0 %   |
| Cl (final)                | 1.6 %   |
| NB                        | Two instruments were exposed (see previous).  |
| Exposure conditions       |  <p>The graph displays three data series over a 50-hour exposure period. The left y-axis represents Tn-220 activity in Bq/m³, ranging from 0 to 50,000. The right y-axis represents temperature in °C and relative humidity (%rh), ranging from 0 to 70. The x-axis is exposure time in hours, from 0 to 50. Blue circles represent Tn-220 activity, which starts at approximately 45,000 Bq/m³ and gradually decreases to about 30,000 Bq/m³. A red line shows the relative humidity, which remains constant at approximately 60%. A green line shows the temperature, which remains constant at approximately 20°C. A legend at the bottom identifies the series: blue circles for Tn-220, green circles for temp, and red circles for rh.</p> |
| Cross-interference signal |  <p>The graph shows the Rn-222 signal in Bq/m³ on the y-axis (0 to 700) against exposure time in hours on the x-axis (0 to 50). Blue circles represent the measured data points, and a solid red line represents a model fit. The signal starts at 0 at time 0 and increases rapidly, following a curve that levels off towards the end of the exposure period, reaching approximately 550 Bq/m³ at 45 hours. A legend at the bottom identifies the series: blue circles for data and a red line for model.</p>   |

T. Turtiainen, R. Dehganzada, O. Holmgren, S. Georgiev, K. Mitev

### III.9 Additional test: response time

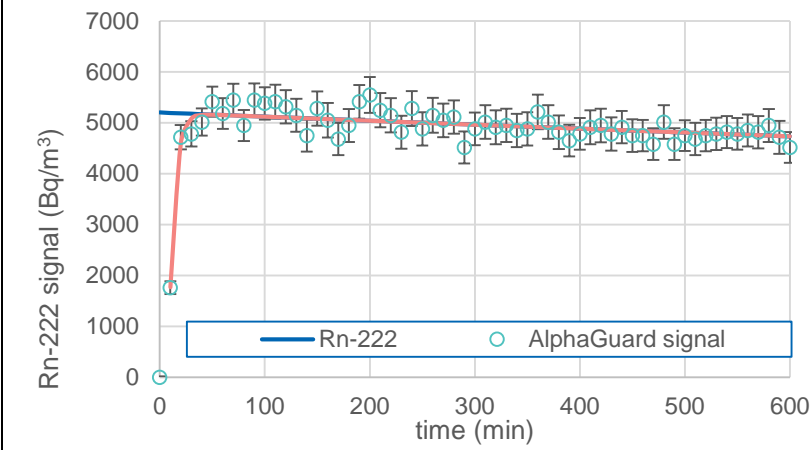
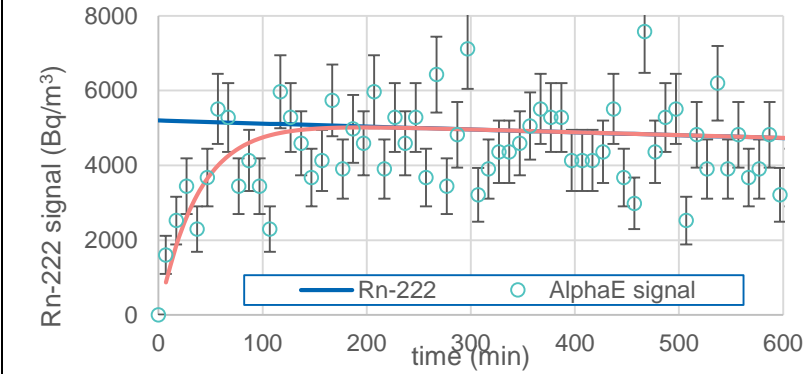
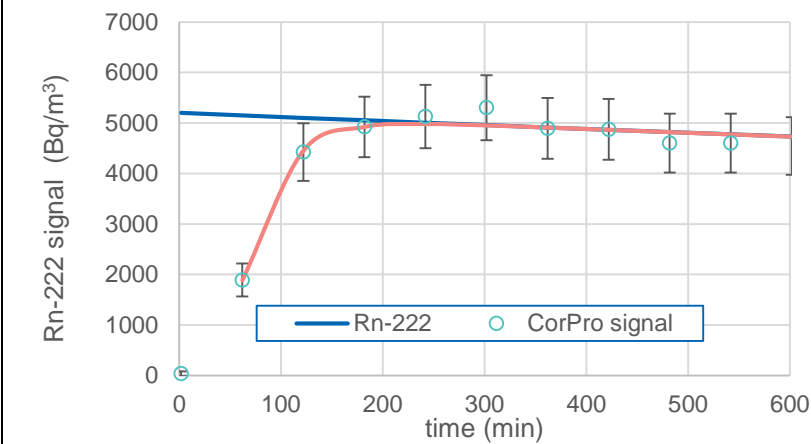
The cross-interference signal from Corentium Pro was different from the other units. The initial cross-interference signal was very small and therefore we wanted to compare the response time of the following instruments: Corentium Pro, AlphaE and AlphaGuard P30. In standard IEC 61577-2:2014, response time has been defined as the duration between the instant of a step change and the instant when the output signal reaches for the first time 90 % of its final value.

The 101.1-litre container was evacuated from radon with activated carbon adsorption. Within one minute, the Rn-222 concentration inside the container was increased to  $(5100 \pm 200)$  Bq/m<sup>3</sup> by directing radonous air from a radon source into the container.

AlphaGuard and AlphaE operated in 10-minute diffusion mode. Corentium Pro operated in 60-min diffusion mode, because no shorter integral can be selected. The gross signals were corrected with respective background signal and calibration coefficient.

From the results we can see that the response time of Corentium Pro radon monitor is long, about 130 minutes. This may partly explain, why the final cross-interference signal (and thoron diffusion into the chamber) was very low. Also, the initial cross-interference signal was very small. This suggests that Corentium Pro is applying spectroscopy and at least partly rejects Po-216 counts. Another explanation could be that the instrument applies averaging to the results. According to the test, we cannot conclude the reason for the very low initial cross-interference signal.

Low cross-interference signal, however, is not necessarily a desired one. The lower the cross-interference, the slower the diffusion into the detection volume. This reduces the temporal response of the instrument. Continuous radon measurement is mostly used for detecting changing radon concentration. The measuring location could be e.g. work place, where timed mechanical ventilation is in use. After the working hours, the ventilation automatically reduces into a small value or stops completely. In the morning, the ventilation starts again. This results in changing radon concentration and the difference between nightly maximum and daily minimum can be more than an order of magnitude. If the measurement is carried out with a monitor with poor temporal response, the first hours in the morning may falsely indicate radon signals, that are above reference value.

|                         |  |
|-------------------------|--|
| Instrument              | AlphaGuard P30, s/n EF2280   |
| Estimated response time | 20 min   |
| Response signal         |    |
| Instrument              | AlphaE, s/n 00260  |
| Estimated response time | 90 min   |
| Response signal         |   |
| Instrument              | Corentium Pro, s/n 2700006845  |
| Estimated response time | 130 min  |
| Response signal         |  |

#### IV. Cross-interference testing of radon monitors at SUBG

##### IV.1 Exposure set-up and reference instruments at SUBG

Thoron atmosphere was created in a 50.4-litre Emanation Calibration Container (s/n EV035112, Saphymo GmbH). Air exchange through the container was created with Mastreflex peristaltic pump (Cole-Palmer). A closed system was used in all experiments, as shown in Figure A7. A flow-through thoron source TH-1025 from Pylon Electronics Inc. was used and its certified activity on 02 May 2015 is  $(106.275 \pm 0.344)$  kBq (certificate I003866). The thoron-rich air was directed in front of a small fan situated under the lid of the container (Figure A8).

Homogeneity of thoron gas inside the container has been validated with aerogel samplers before. Reference instrument for thoron concentration measurement was AlphaGuard PQ2000 RnTn (s/n EF2312, Saphymo GmbH) which has been calibrated against the LNHB primary thoron standard at IRSN (May 2018). The instrument was operated with AlphaPump (s/n AP1527). The humidity and temperature were measured with the AlphaGuard sensors.

Rn-222 concentration in the laboratory is typically below  $30 \text{ Bq/m}^3$ , mostly in the range  $10\text{--}30 \text{ Bq/m}^3$ . This concentration was considered negligible to the Tn-220 exposure concentrations which were created in the tests.

The temperature, humidity and air pressure were not regulated, and they followed the those in the laboratory.

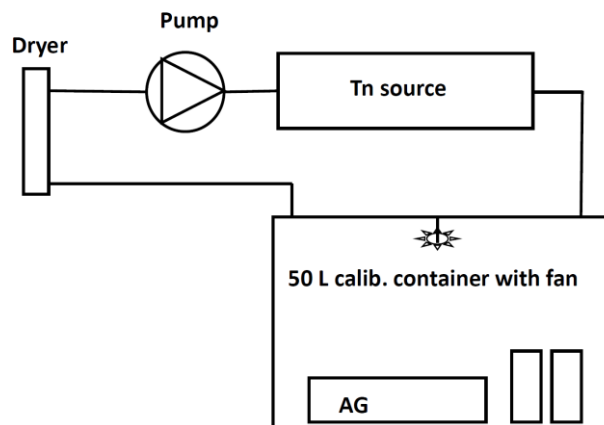


Figure A7. Set-up of the cross-interference test. The instrument under testing (in this example RadonEye) was placed on a grid above the reference instrument (AG).

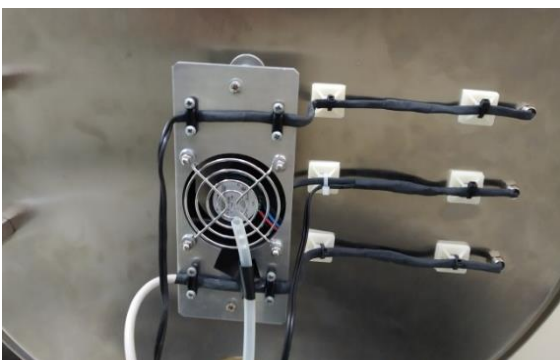
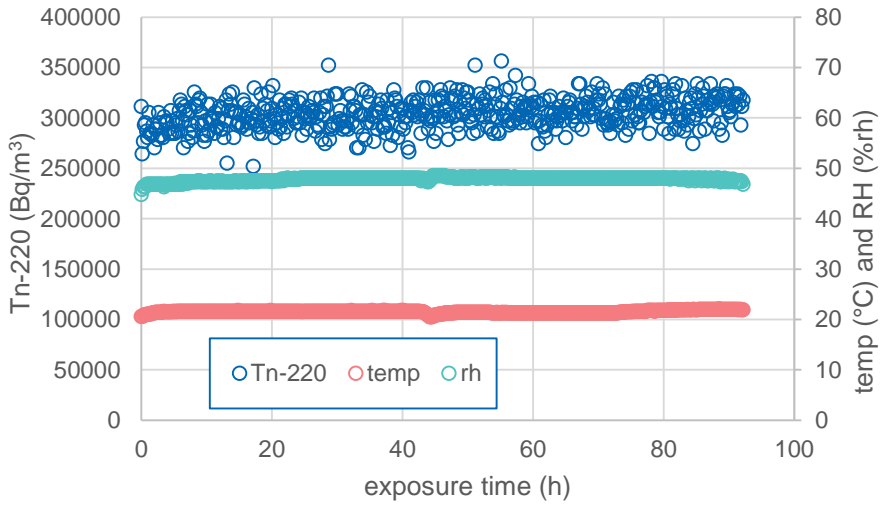
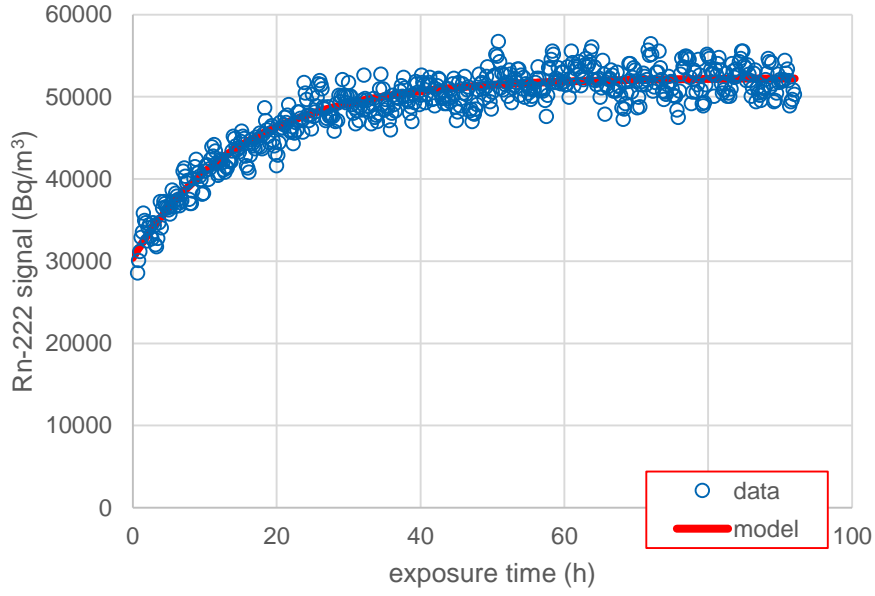
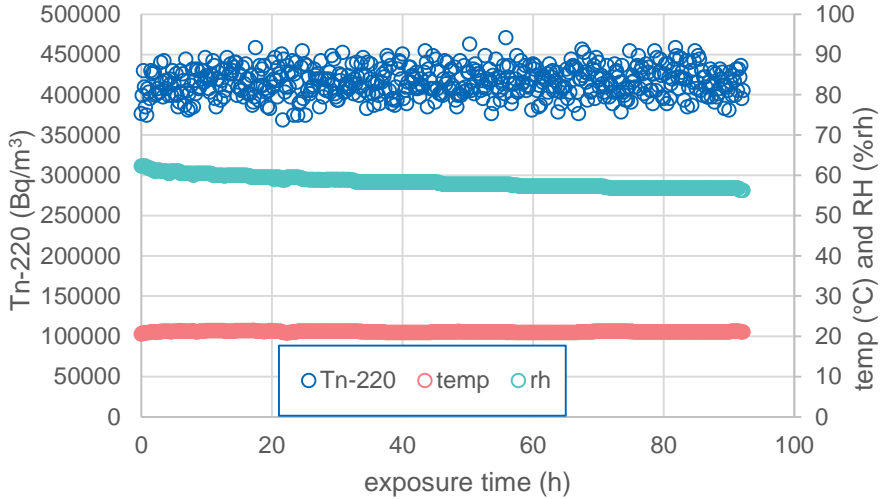
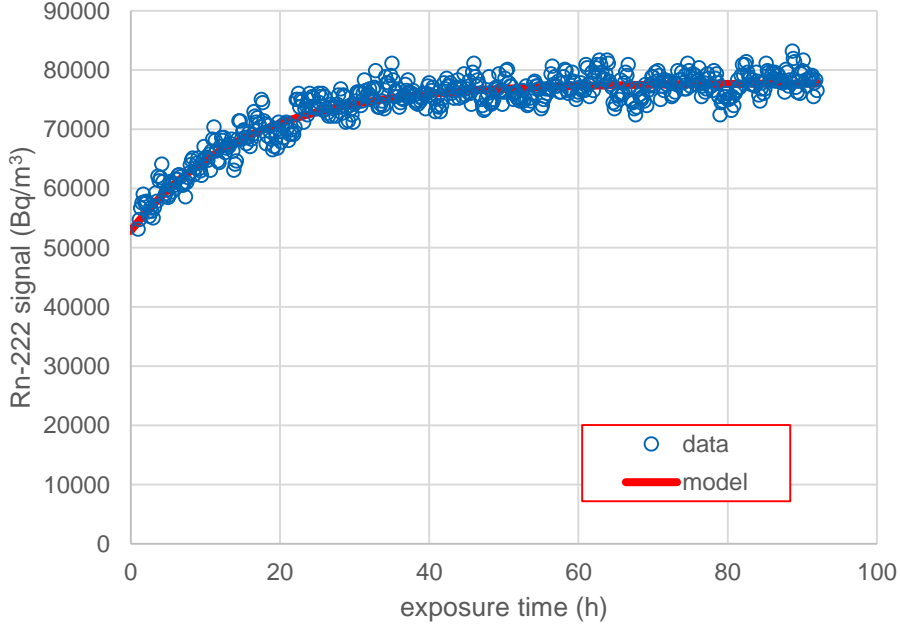


Figure A8. Snapshot of the SUBG experimental system with the reference instrument (AG).

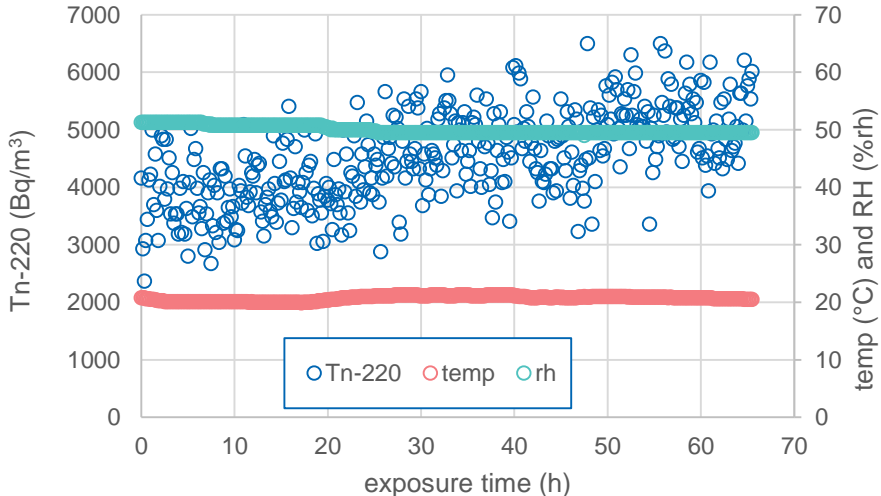
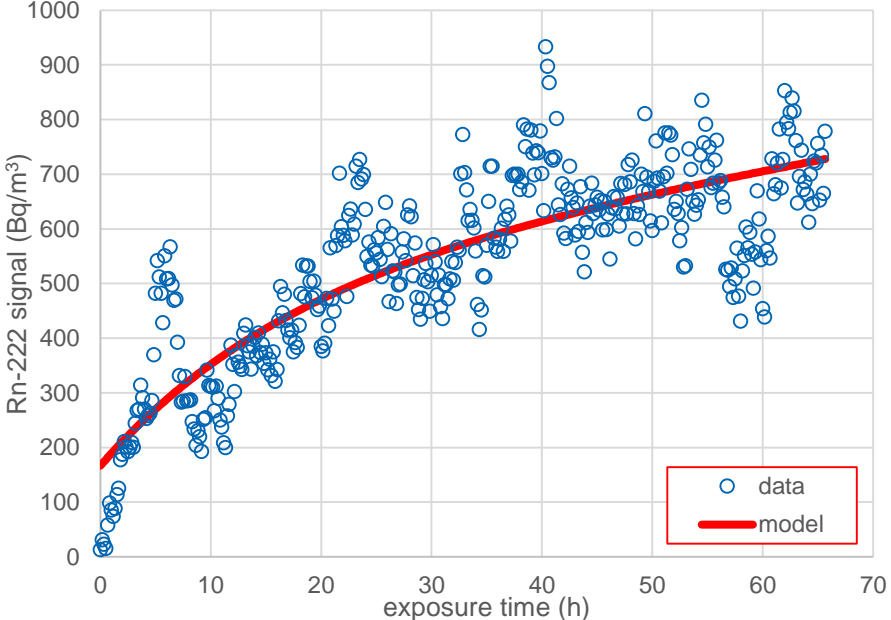
#### IV.2 Tests of Alpha E, Saphymo GmbH (now Bertin instruments)

|                           |  |
|---------------------------|--|
| Test date                 | 16–20 September 2019   |
| Instrument                | Alpha E  |
| Instrument s/n            | AE000499   |
| C(Tn-220) mean            | $(304\,000 \pm 15\,000) \text{ Bq/m}^3$  |
| CI (initial)              | 10 %   |
| CI (final)                | 17.1 %   |
| NB                        |  |
| Exposure conditions       |   |
| Cross-interference signal |  |

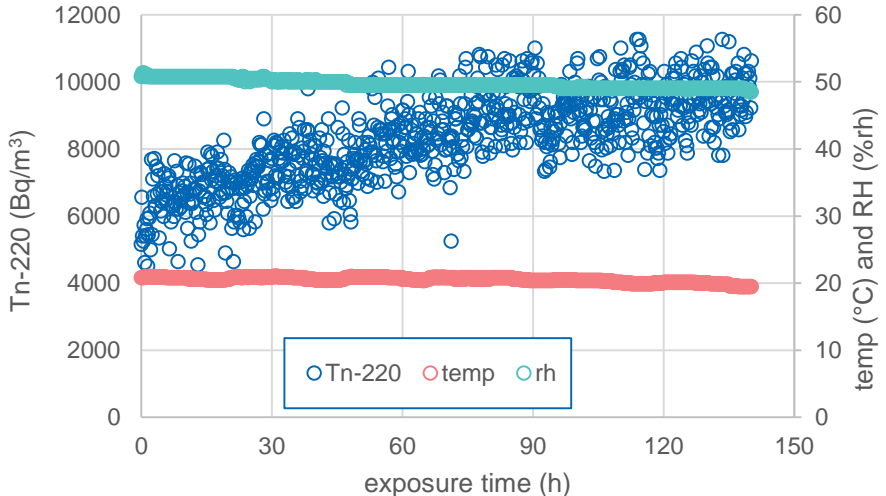
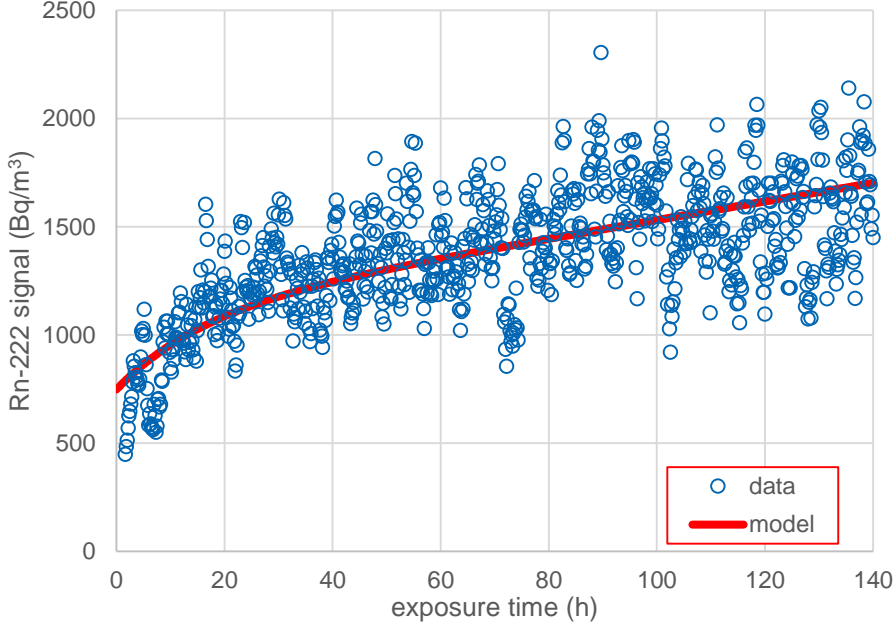
T. Turtiainen, R. Dehganzada, O. Holmgren, S. Georgiev, K. Mitev

|                           |  |
|---------------------------|--|
| Test date                 | 26–30 September 2019   |
| Instrument                | Alpha E  |
| Instrument s/n            | AE000499   |
| C(Tn-220) mean            | (416 000 ± 18 000) Bq/m <sup>3</sup>   |
| CI (initial)              | 12.7 %   |
| CI (final)                | 18.7 %   |
| NB                        |  |
| Exposure conditions       |   |
| Cross-interference signal |  |

T. Turtiainen, R. Dehganzada, O. Holmgren, S. Georgiev, K. Mitev

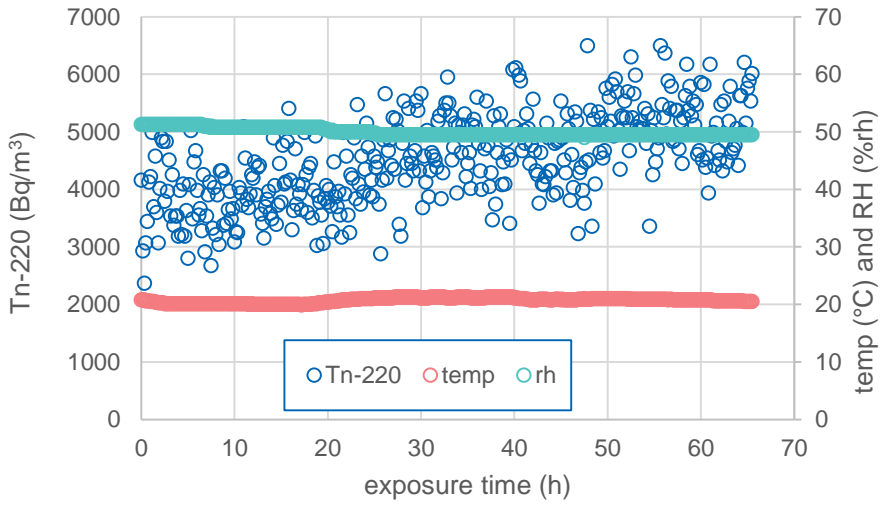
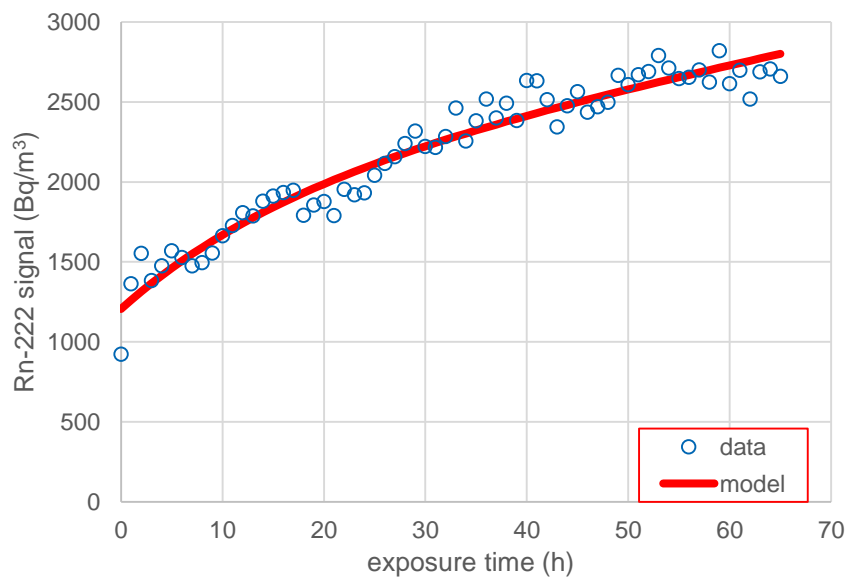
|                                 |  |
|---------------------------------|--|
| Test date                       | 14–17 October 2019   |
| Instrument                      | Alpha E  |
| Instrument s/n                  | AE000499   |
| C(Tn-220) [ Bq/m <sup>3</sup> ] | = 3700 + 25.3*t  |
| CI (initial)                    | 4.5 %  |
| CI (final)                      | 13.7 %   |
| NB                              | The Tn concentration was not constant but increasing with time. It is approximated with a linear function of the exposure time (t) and the modified model was used to estimate CI. |
| Exposure conditions             |   |
| Cross-interference signal       |    |

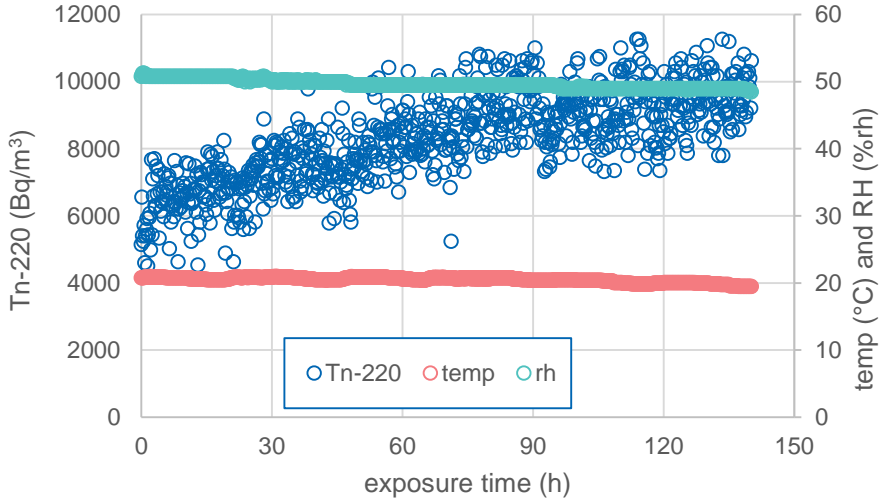
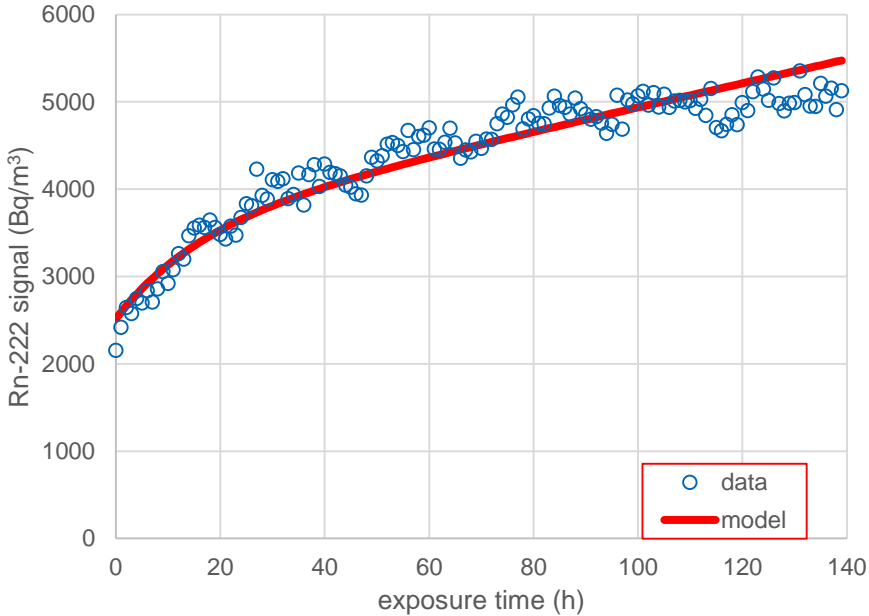
T. Turtiainen, R. Dehganzada, O. Holmgren, S. Georgiev, K. Mitev

|                                 |  |
|---------------------------------|--|
| Test date                       | 22–28 October 2019   |
| Instrument                      | Alpha E  |
| Instrument s/n                  | AE000499   |
| C(Tn-220) [ Bq/m <sup>3</sup> ] | = 6500 + 25.1*t  |
| CI (initial)                    | 11.5%  |
| CI (final)                      | 17%  |
| NB                              | The Tn concentration was not constant but increasing with time. It is approximated with a linear function of the exposure time (t) and the modified model was used to estimate CI. |
| Exposure conditions             |   |
| Cross-interference signal       |    |

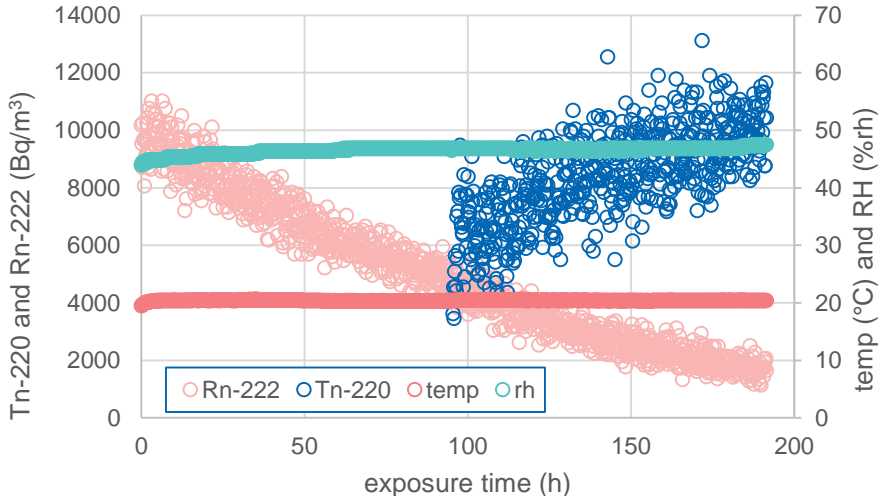
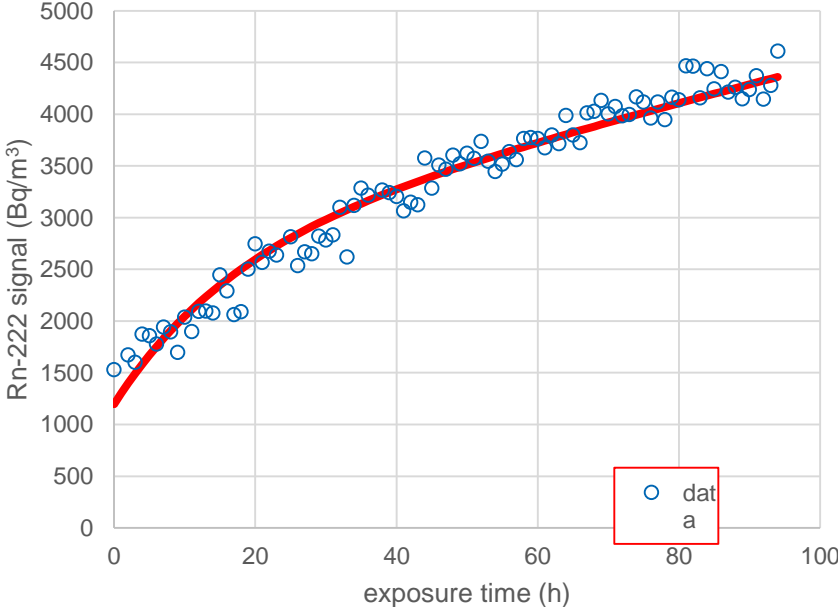


### IV.3 Tests of RadonEye 2+, RadonFTLab

|                                 |  |
|---------------------------------|--|
| Test date                       | 14–17 October 2019   |
| Instrument                      | RadonEye 2+  |
| Instrument s/n                  | PE21904100016  |
| C(Tn-220) [ Bq/m <sup>3</sup> ] | = 3700 + 25.3*t  |
| CI (initial)                    | 32.6 %   |
| CI (final)                      | 52.7 %   |
| NB                              | The Tn concentration was not constant, but increasing with time. It is approximated with a linear function of the exposure time (t) and the modified model was used to estimate CI.  |
| Exposure conditions             |  <p>The plot displays three data series over a 70-hour exposure period. The left y-axis represents Tn-220 concentration in Bq/m<sup>3</sup>, ranging from 0 to 7000. The right y-axis represents temperature in °C and relative humidity in %rh, ranging from 0 to 70. The x-axis is exposure time in hours. Blue circles represent Tn-220 data, showing a steady increase from approximately 3000 to 6000 Bq/m<sup>3</sup>. Red circles represent temperature, which stays around 20°C. Green circles represent relative humidity, which stays around 50%rh. A legend at the bottom identifies the series: blue circle for Tn-220, red circle for temp, and green circle for rh.</p> |
| Cross-interference signal       |  <p>The plot shows the Rn-222 signal in Bq/m<sup>3</sup> on the y-axis (0 to 3000) against exposure time in hours on the x-axis (0 to 70). Blue circles represent the measured data points, and a solid red line represents the model fit. The data points show a strong positive linear correlation, starting at approximately 1000 Bq/m<sup>3</sup> at 0 hours and reaching about 2800 Bq/m<sup>3</sup> at 70 hours. A legend at the bottom right identifies the blue circle as 'data' and the red line as 'model'.</p>  |

|                                 |   |
|---------------------------------|---|
| Test date                       | 22–28 October 2019  |
| Instrument                      | RadonEye 2+   |
| Instrument s/n                  | PE21904100016   |
| C(Tn-220) [ Bq/m <sup>3</sup> ] | = 6500 + 25.1*t   |
| CI (initial)                    | 38.7%   |
| CI (final)                      | 54.7%   |
| NB                              | The Tn concentration was not constant, but increasing with time. It is approximated with a linear function of the exposure time (t) and the modified model was used to estimate CI. |
| Exposure conditions             |    |
| Cross-interference signal       |   |

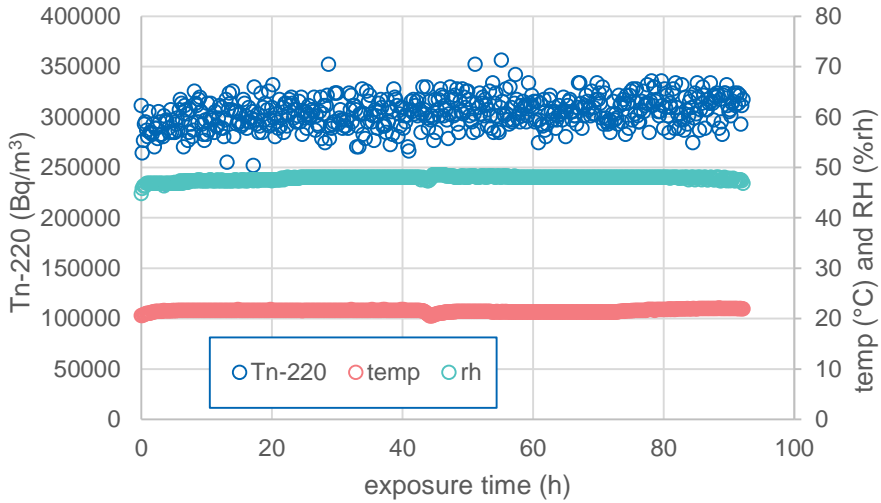
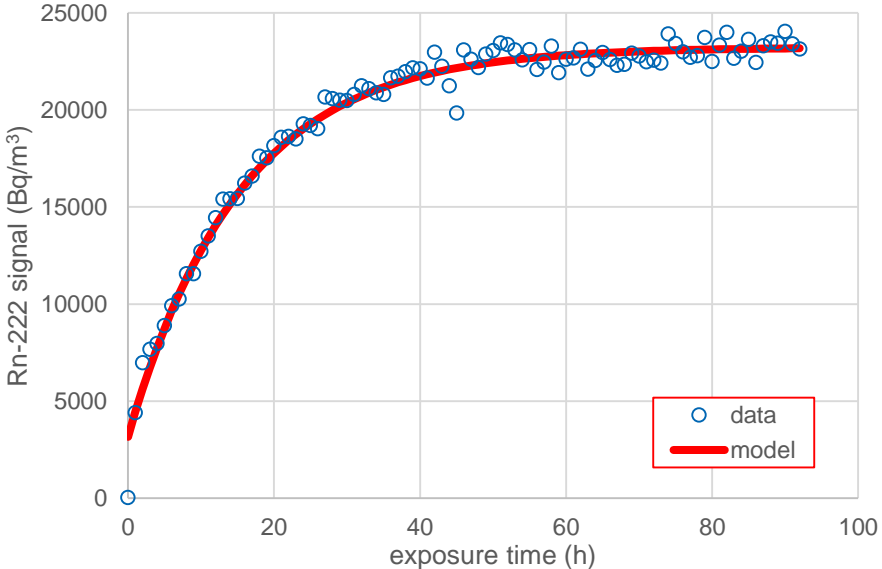
T. Turtiainen, R. Dehganzada, O. Holmgren, S. Georgiev, K. Mitev

|                                |  |
|--------------------------------|--|
| Test date                      | 4–8 October 2019   |
| Instrument                     | RadonEye 2+  |
| Instrument s/n                 | PE21904100016  |
| C(Tn-220) [Bq/m <sup>3</sup> ] | = 6400 + 41.7*t  |
| CI (initial)                   | 19%  |
| CI (final)                     | 43%  |
| NB                             | <b>Mixed Radon and Thoron exposure.</b><br>The Tn concentration was not constant, but increasing with time. It is approximated with linear function of the exposure time (t) and the modified model was used to estimate CI. |
| Exposure conditions            |   |
| Cross-interference signal      |    |

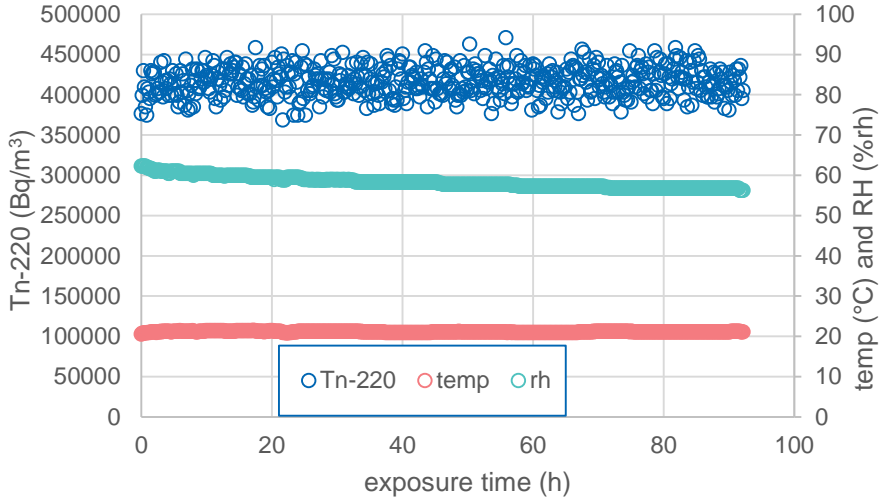
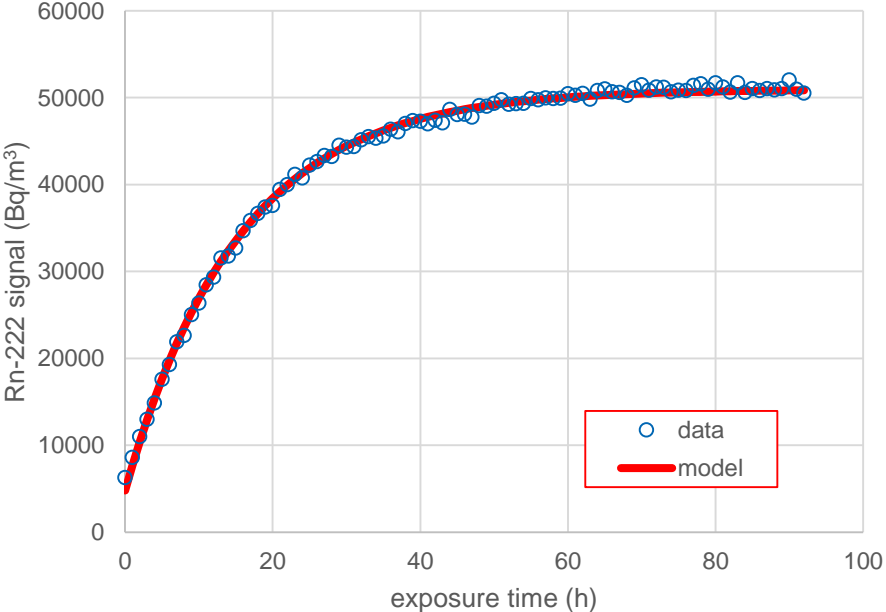
T. Turtiainen, R. Dehganzada, O. Holmgren, S. Georgiev, K. Mitev

#### IV.4 Tests of TSR3

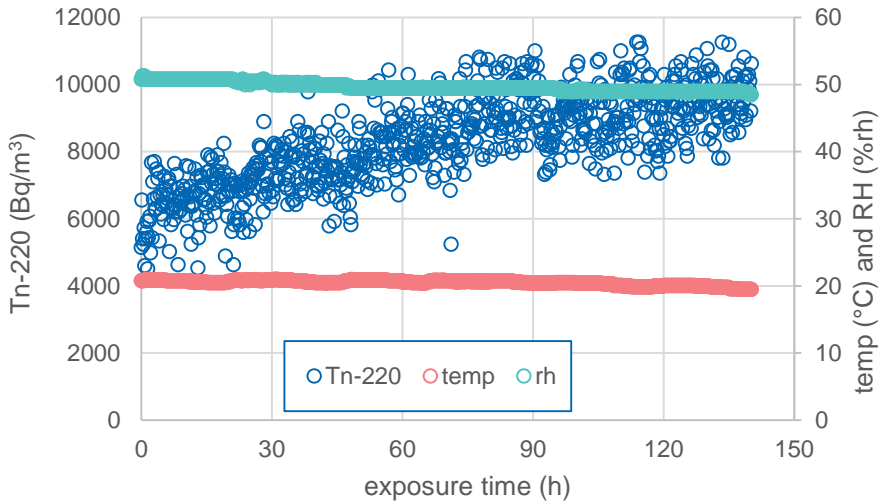
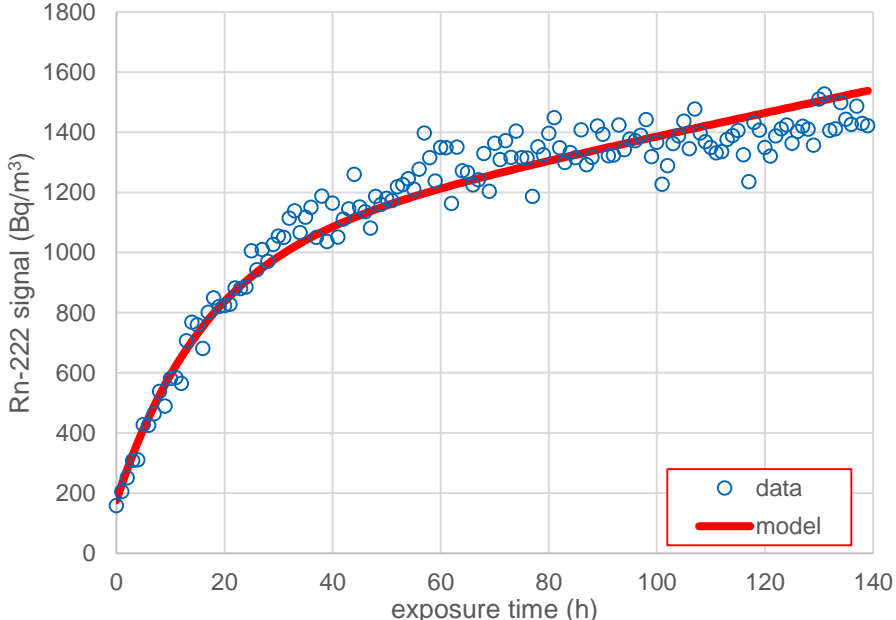
TSR3 is a portable probe designed for continuous measuring of radon concentrations in buildings. The probe basis is a measuring chamber with a semiconductor detector.

|                           |  |
|---------------------------|--|
| Test date                 | 16–20 September 2019   |
| Instrument                | TSR 3  |
| Instrument s/n            | 16014  |
| C(Tn-220) mean            | $(304\,000 \pm 15\,000) \text{ Bq/m}^3$  |
| CI (initial)              | 1.0 %  |
| CI (final)                | 7.7 %  |
| NB                        | Fast mode  |
| Exposure conditions       |   |
| Cross-interference signal |  |

T. Turtiainen, R. Dehganzada, O. Holmgren, S. Georgiev, K. Mitev

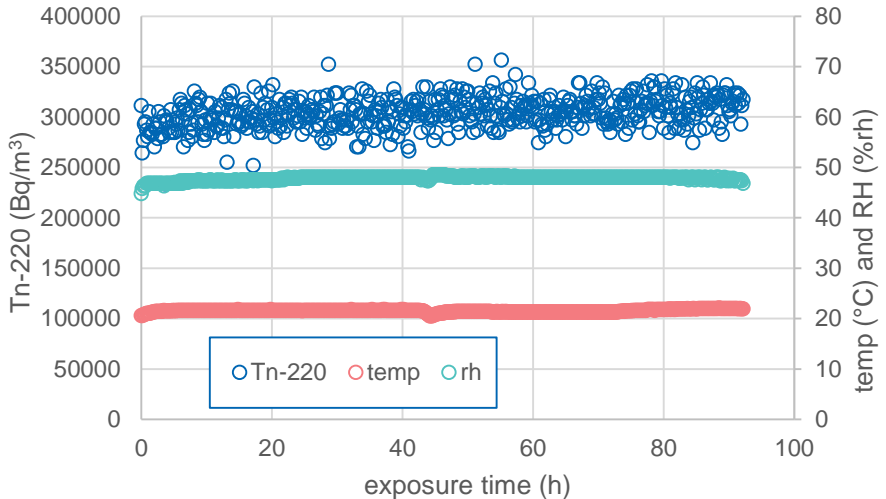
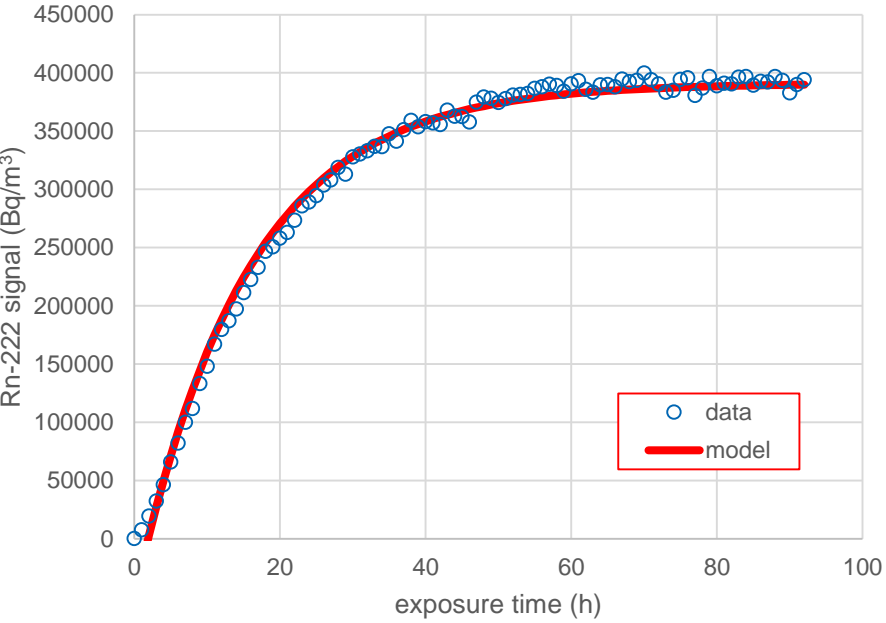
|                           |   |
|---------------------------|---|
| Test date                 | 26–30 September 2019  |
| Instrument                | TSR 3   |
| Instrument s/n            | 16014   |
| C(Tn-220) mean            | (416 000 ± 18 000) Bq/m <sup>3</sup>  |
| CI (initial)              | 1.2%  |
| CI (final)                | 12.3%   |
| NB                        | Fast mode   |
| Exposure conditions       |  <p>The graph displays three data series over a 100-hour exposure period. The left y-axis represents Tn-220 concentration in Bq/m<sup>3</sup>, ranging from 0 to 500,000. The right y-axis represents temperature in °C and relative humidity in %rh, ranging from 0 to 100. The x-axis is exposure time in hours, from 0 to 100. Tn-220 (blue circles) remains stable around 416,000 Bq/m<sup>3</sup>. Temperature (red circles) is constant at approximately 20°C. Relative humidity (green circles) is constant at approximately 60%rh.</p> |
| Cross-interference signal |  <p>The graph shows the Rn-222 signal in Bq/m<sup>3</sup> on the y-axis (0 to 60,000) against exposure time in hours on the x-axis (0 to 100). Blue circles represent the measured data, and a red line represents the model fit. The signal starts at approximately 5,000 Bq/m<sup>3</sup> at 0 hours and rises to about 50,000 Bq/m<sup>3</sup> by 100 hours.</p>   |

T. Turtiainen, R. Dehganzada, O. Holmgren, S. Georgiev, K. Mitev

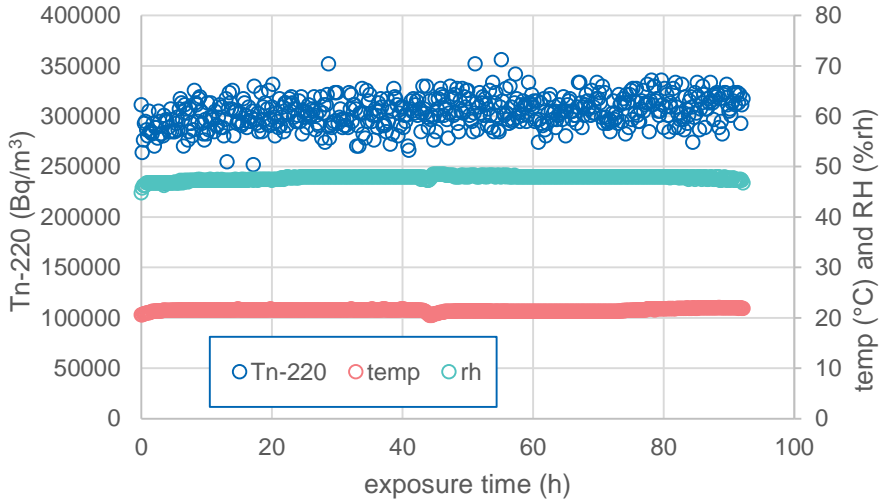
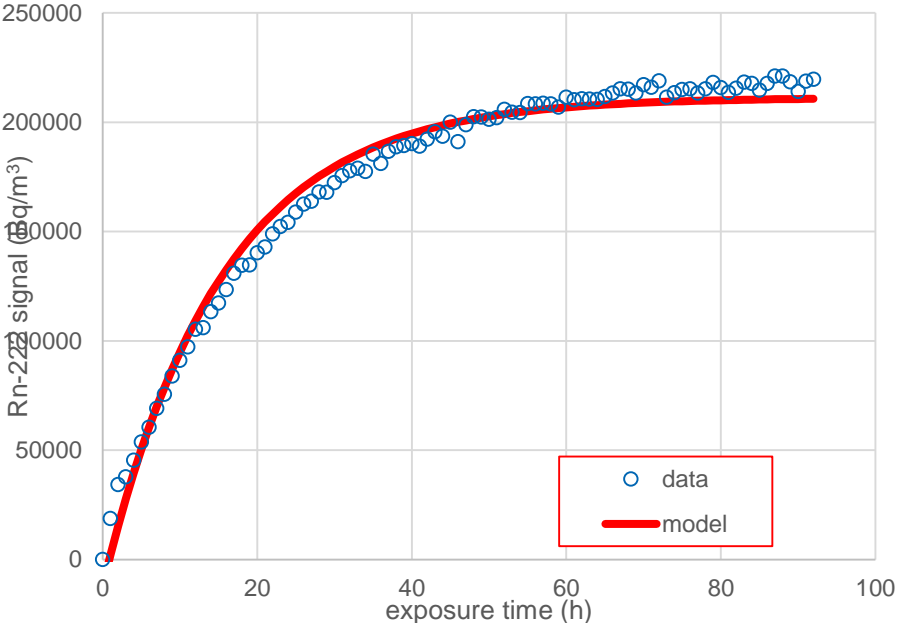
|                                 |   |
|---------------------------------|---|
| Test date                       | 22–28 October 2019  |
| Instrument                      | TSR 3   |
| Instrument s/n                  | 16014   |
| C(Tn-220) [ Bq/m <sup>3</sup> ] | = 6500 + 25.1*t   |
| CI (initial)                    | 2.7%  |
| CI (final)                      | 15.4 %  |
| NB                              | Instrument operated in slow mode.<br>The Thoron concentration was not constant but increasing with time. It is approximated with a linear function of the exposure time (t) and the modified model was used to estimate CI. |
| Exposure conditions             |    |
| Cross-interference signal       |   |

#### IV.5 Tests of TSR4M

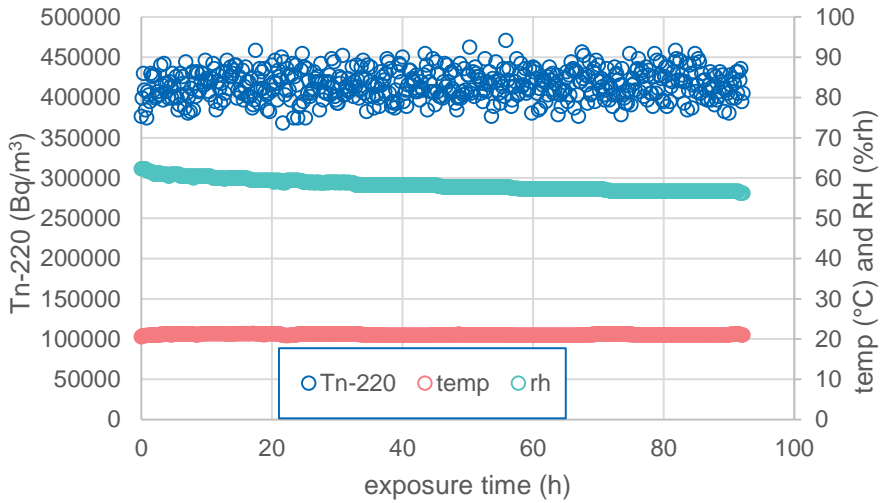
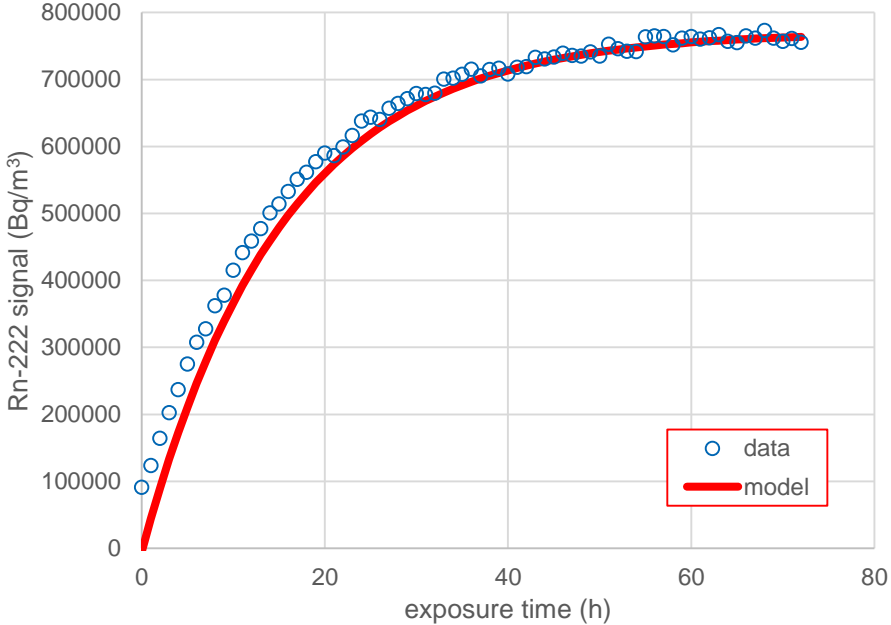
TSR4M is a portable probe with semiconductor photodetector, designed for continuous measuring of radon concentrations in buildings.

|                           |  |
|---------------------------|--|
| Test date                 | 16–20 September 2019   |
| Instrument                | TSR4M  |
| Instrument s/n            | 19015  |
| C(Tn-220) mean            | $(304\ 000 \pm 15\ 000)$ Bq/m <sup>3</sup>   |
| CI (initial)              | N/A  |
| CI (final)                | 127%   |
| NB                        | Fast mode  |
| Exposure conditions       |   |
| Cross-interference signal |  |

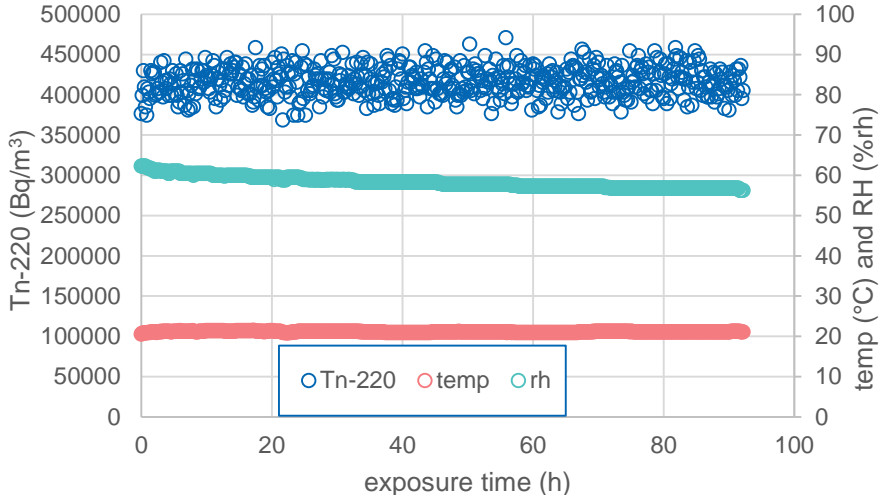
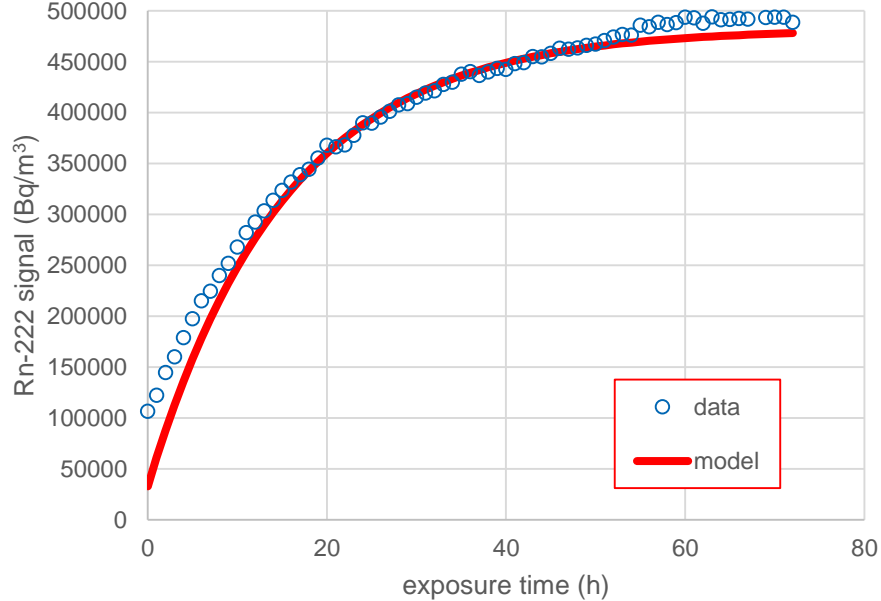
T. Turtiainen, R. Dehganzada, O. Holmgren, S. Georgiev, K. Mitev

|                           |  |
|---------------------------|--|
| Test date                 | 16–20 September 2019   |
| Instrument                | TSR4M  |
| Instrument s/n            | 19015  |
| C(Tn-220) mean            | (304 000 ± 15 000) Bq/m <sup>3</sup>   |
| CI (initial)              | N/A  |
| CI (final)                | 69.5%  |
| NB                        | Slow mode  |
| Exposure conditions       |   |
| Cross-interference signal |  |

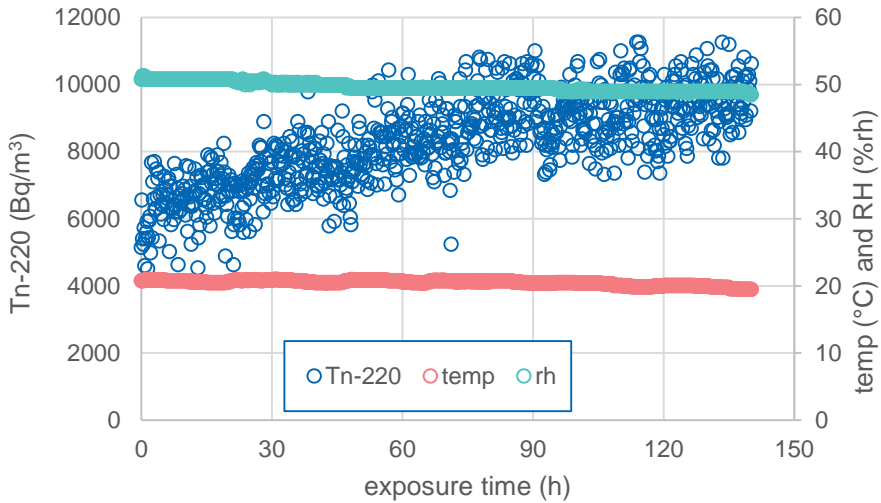
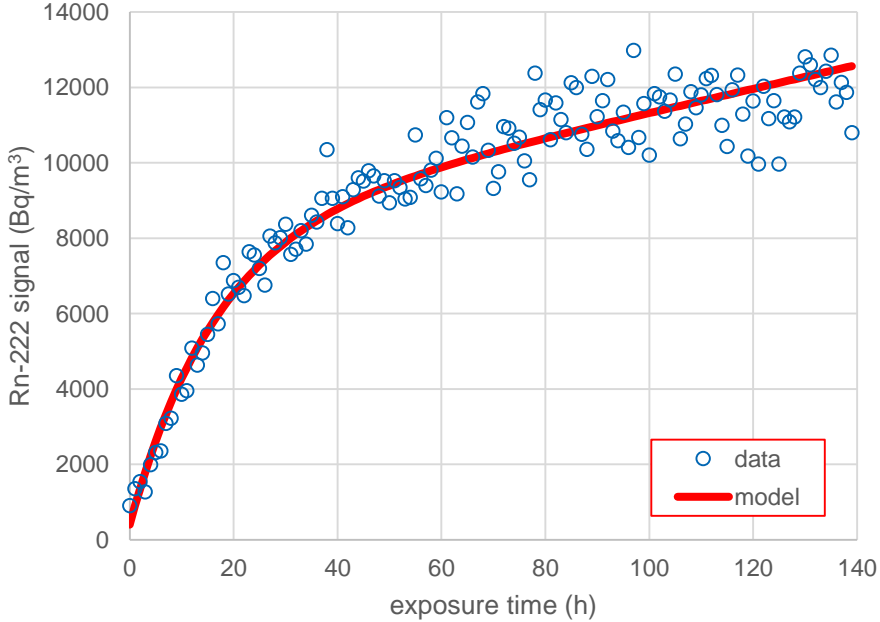
T. Turtiainen, R. Dehganzada, O. Holmgren, S. Georgiev, K. Mitev

|                           |  |
|---------------------------|--|
| Test date                 | 26–30 September 2019   |
| Instrument                | TSR4M  |
| Instrument s/n            | 19015  |
| C(Tn-220) mean            | (416 000 ± 18 000) Bq/m <sup>3</sup>   |
| CI (initial)              | N/A  |
| CI (final)                | 186%   |
| NB                        | Fast mode, bad model fit   |
| Exposure conditions       |   |
| Cross-interference signal |  |

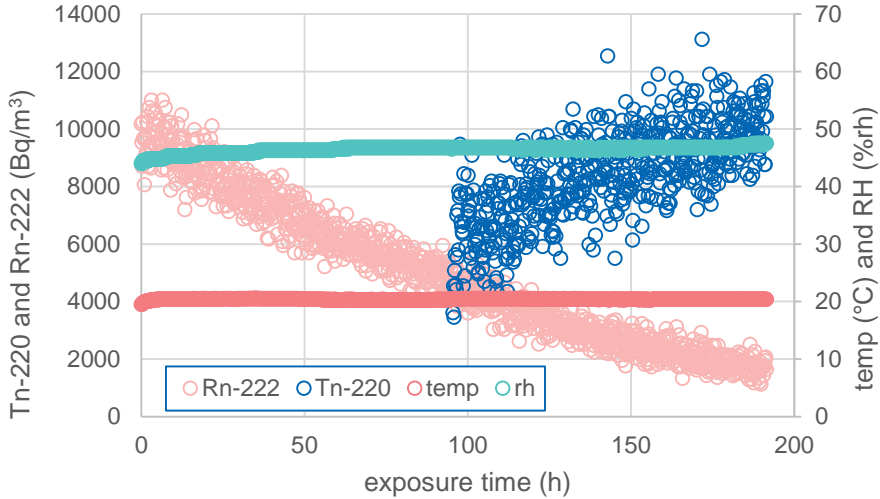
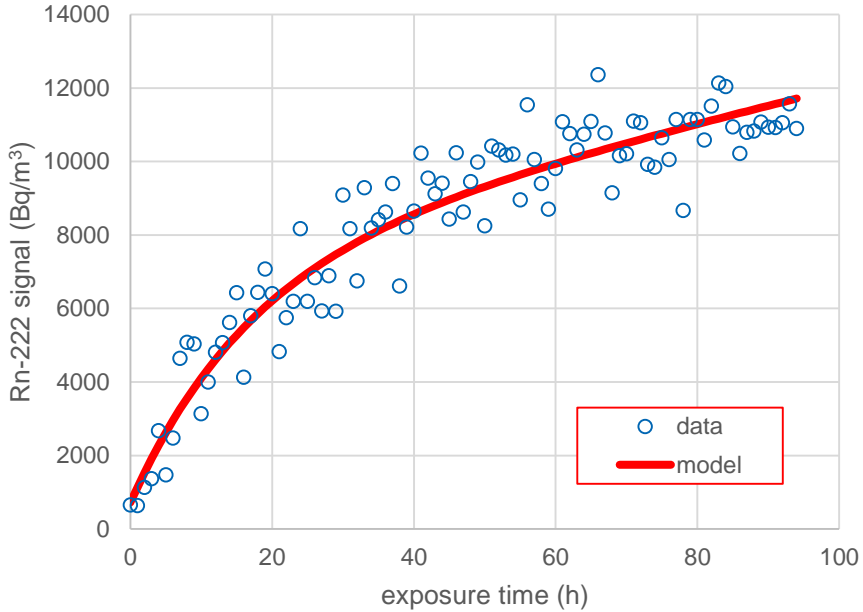
T. Turtiainen, R. Dehganzada, O. Holmgren, S. Georgiev, K. Mitev

|                           |  |
|---------------------------|--|
| Test date                 | 26–30 September 2019   |
| Instrument                | TSR4M  |
| Instrument s/n            | 19015  |
| C(Tn-220) mean            | (416 000 ± 18 000) Bq/m <sup>3</sup>   |
| CI (initial)              | 7.9 %  |
| CI (final)                | 116 %  |
| NB                        | Slow mode, bad model fit   |
| Exposure conditions       |   |
| Cross-interference signal |  |

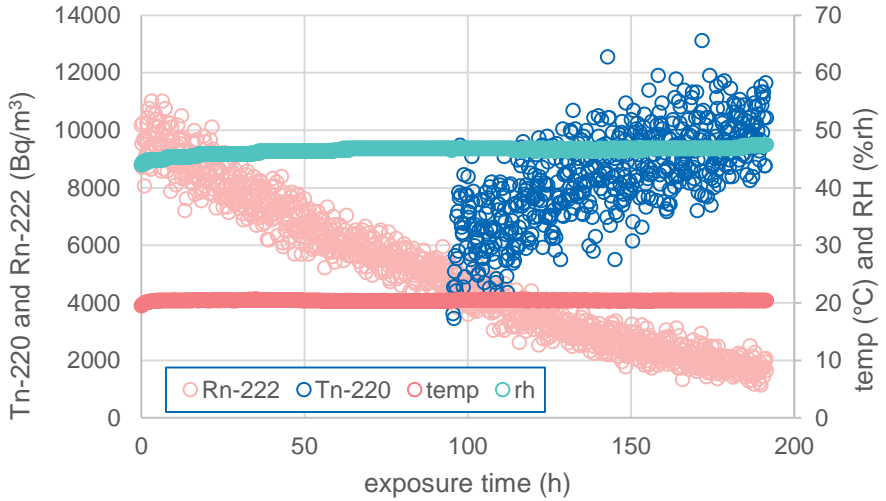
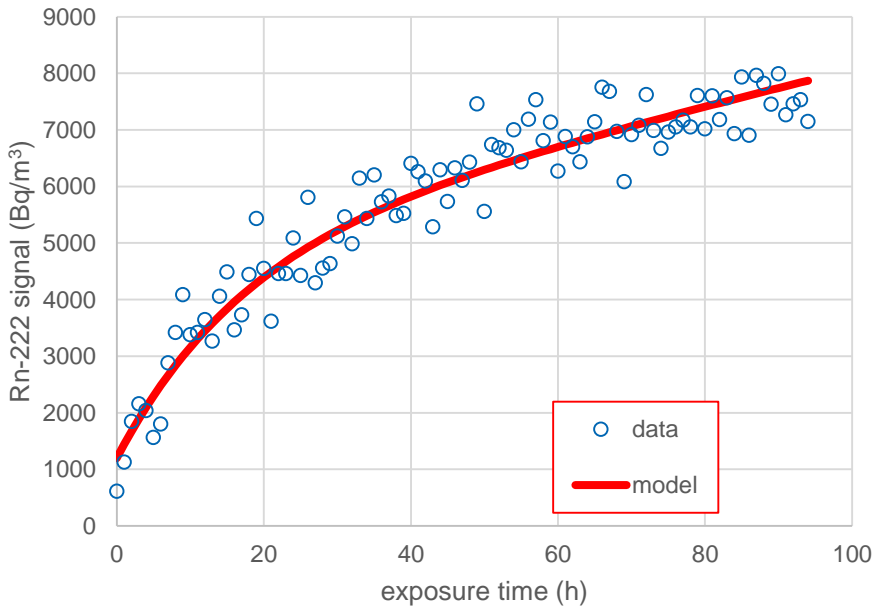
T. Turtiainen, R. Dehganzada, O. Holmgren, S. Georgiev, K. Mitev

|                                 |  |
|---------------------------------|--|
| Test date                       | 22–28 October 2019   |
| Instrument                      | TSR4M  |
| Instrument s/n                  | 19015  |
| C(Tn-220) [ Bq/m <sup>3</sup> ] | = 6500 + 25.1*t  |
| CI (initial)                    | 6.2 %  |
| CI (final)                      | 126%   |
| NB                              | Instrument operated in fast mode.<br>The Tn concentration was not constant, but increasing with time. It is approximated with linear function of the exposure time (t) and the modified model was used to estimate CI. |
| Exposure conditions             |   |
| Cross-interference signal       |    |



|                                |  |
|--------------------------------|--|
| Test date                      | 4–8 October 2019   |
| Instrument                     | TSR4M  |
| Instrument s/n                 | 19015  |
| C(Tn-220) [Bq/m <sup>3</sup> ] | = 6400 + 41.7*t  |
| CI (initial)                   | 11%  |
| CI (final)                     | 114%   |
| NB                             | <p><b>Mixed Radon and Thoron exposure.</b></p> <p>The instrument is operated in fast mode.</p> <p>The Tn concentration was not constant but increasing with time. It is approximated with a linear function of the exposure time (t) and the modified model was used to estimate CI.</p> |
| Exposure conditions            |   |
| Cross-interference signal      |    |

T. Turtiainen, R. Dehganzada, O. Holmgren, S. Georgiev, K. Mitev

|                                |  |
|--------------------------------|--|
| Test date                      | 4–8 October 2019   |
| Instrument                     | TSR4M  |
| Instrument s/n                 | 19015  |
| C(Tn-220) [Bq/m <sup>3</sup> ] | = 6400 + 41.7*t  |
| CI (initial)                   | 18%  |
| CI (final)                     | 76%  |
| NB                             | <p><b>Mixed Radon and Thoron exposure.</b><br/>           The instrument is operated in slow mode.<br/>           The Tn concentration was not constant but increasing with time. It is approximated with a linear function of the exposure time (t) and the modified model was used to estimate CI.</p> |
| Exposure conditions            |   |
| Cross-interference signal      |    |

## V. Intercomparison of cross-interference testing of radon monitors at STUK and SUBG

In order to compare the CI evaluations at STUK and SUBG, the RadonEye and AlphaE monitors of SUBG were sent to STUK for CI evaluation. A comparison of the CI values obtained at SUBG and STUK are shown in Tables A2 and A3.

| CI intercomparison with instrument RadonEye 2+ (s/n PE21904100016) |                   |                                     |              |            |
|--|-------------------|-------------------------------------|--------------|------------|
| Laboratory   | Test date         | Tn concentration, Bq/m <sup>3</sup> | CI (initial) | CI (final) |
| STUK   | 28 Nov–1 Dec 2019 | 6640 (130)                          | 27 %         | 37 %       |
| SUBG   | 14-17 Oct 2019    | 3700 (400)                          | 32.6 %       | 52.7 %     |
|  | 22-28 Oct 2019    | 6500 (700)                          | 38.7 %       | 54.7 %     |
|  | 4-8 Nov 2019      | 6400 (700)                          | 18.7 %       | 42.3 %     |

Table A2. Comparison of RadonEye 2+ CI values obtained at STUK and SUBG.

| CI intercomparison with instrument AlphaE (s/n AE000499) |                |                                      |              |            |
|--|----------------|--------------------------------------|--------------|------------|
| Laboratory   | Test date      | Tn concentration, kBq/m <sup>3</sup> | CI (initial) | CI (final) |
| STUK   | 5-9 Dec 2019   | 70.4 (10)                            | 5.7 %        | 8.6 %      |
| SUBG   | 14–17 Oct 2019 | 3.70(40)                             | 4.5 %        | 13.7 %     |
|  | 22–28 Oct 2019 | 6.50(70)                             | 11.5 %       | 17.0 %     |
|  | 16–20 Sep 2019 | 304(15)                              | 10.0 %       | 17.1 %     |
|  | 26–30 Sep 2019 | 416(18)                              | 12.7 %       | 18.7 %     |
|  | 4-8 Nov 2019   | 6.40(70)                             | 15.5 %       | 20.2 %     |

Table A3. Comparison of AlphaE CI values obtained at STUK and SUBG.

The CI values obtained at STUK and SUBG are similar, but the values obtained at SUBG seem to be higher than those obtained at STUK. We attribute this to the possible higher air velocity near the instruments in the SUBG calibration container compared to that of STUK. As the height of the STUK container is twice the height of the SUBG container, it can be expected that the fan positioned on the top of the container creates air velocity near the instruments, which is higher in the SUBG container compared to that of STUK. The higher air velocity can facilitate the thoron entrance in the instruments active volumes and thus increase the CI.

## VI. On the possible altitude dependence of the AlphaE readings due to sensitivity to radiation produced by cosmic rays

During the transportation from SUBG to STUK and BACK, the AlphaE instrument has been turned on. The readings of the instrument during the transportation SUBG –STUK is shown in Fig. A9. A two-flight transportation is supposed in this case. The readings of the instrument on the way back from STUK to SUBG is shown in Fig. A10. It is supposed that the return of the instrument has been performed by ground transport.



Fig. A9. Readings of the AlphaE instrument during the transportation SUBG-STUK. The instrument left SUBG on 27.11.2019 and was received at STUK on 28.11.2019.

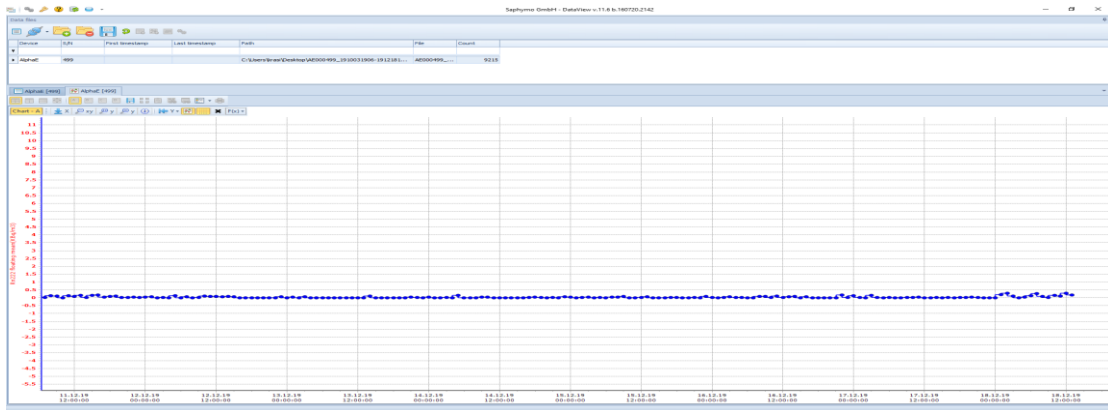


Fig. A10. Readings of the AlphaE instrument during the transportation STUK-SUBG. The instrument left STUK on 11.12.2019 and was received at SUBG on 18.12.2019. Ground transportation is supposed in this case.

The results shown in Fig. A9 suggest that the readings of the AlphaE instrument may depend on the altitude of the measurement point. This could be due to the silicon diode sensitivity to the radiation, produced by the cosmic rays in the upper atmosphere.

### Acknowledgments

The authors from SUBG are grateful to the colleagues from ISS, Italy and AGES, Austria and personally to Gennaro Venoso (ISS) and Gernot Wurm (AGES) for providing us some of the studied monitors and for the collaboration.



# 16ENV10 MetroRADON

## Deliverable D2 Annex VI

Activity A.2.2.1

Study of the influence of thoron on radon activity  
concentration measurement of continuous radon monitors  
at IRSN

Institut de Radioprotection et de Sûreté Nucléaire (IRSN)

N. Michielsen

**EMPIR**



The EMPIR initiative is co-funded by the European Union's Horizon 2020 research and innovation programme and the EMPIR Participating States

## Table of contents

|   |    |
|---|----|
| Object.....                                     | 3  |
| Instruments tested .....                        | 3  |
| Material and method.....                        | 3  |
| Thoron exposures in BACCARA .....               | 5  |
| Influence of thoron on radon measurements ..... | 6  |
| Cross-interference .....                        | 10 |
| Conclusion and recommendations .....            | 13 |
| References .....                                | 14 |

## Object

This work is done in the frame of the EMPIR project 16ENV10 MetroRADON: “Metrology for radon monitoring”, it is a part of the working package 2 (Influence of thoron ( $^{220}\text{Rn}$ ) and its progeny on radon end-user measurements and radon calibrations); and task 2.2 (Investigation of the influence of thoron on radon measurements and calibrations).

The aim of this task is to investigate the influence of thoron on radon measurement devices. This report describes the tests performed at IRSN to study the influence of thoron on radon measurement of radon monitors.

## Instruments tested

Three commercial instruments have been tested, two Doseman (DM 338 and DM357) and one alphaGUARD measuring radon and thoron (EF 2283), identification is given in table 1. One apparatus is equipped with an ionisation chamber used in pulse mode operation with a treatment on the pulses to differentiate the decays, the two others are equipped with a silicon detector (polarised semiconductor) for the measurement of alpha decay and spectrometry.

Table 1 – Instruments identification and characteristics

| Instruments name         | Serial number | Detector system    | Configuration mode |
|--------------------------|---------------|--------------------|--------------------|
| DoseMan                  | 338           | semiconductor      | Fast and slow      |
| DoseMan                  | 357           | semiconductor      | Fast and slow      |
| alphaGUARD 2000 RnTh PRO | EF 2283       | ionisation chamber | Flow through       |

For the Doseman, passive sampling of radon occurs by diffusion through a filter into the detection chamber while for the alphaGUARD, active air sampling with an external pump (1 l/min) is used with an automated sequenced sampling defined by the manufacturer (flow through configuration). The Doseman does not make any corrections of possible influence of thoron on the measurement of radon while the alphaGUARD RnTh make a correction based, at least, on the measurement of the polonium-212.

The DoseMan is equipped with silicon detector, the counts are classified according to the energy of the measured alpha decay, two modes of operation are available: a fast mode taking into account the decay of  $^{222}\text{Rn}$  and  $^{218}\text{Po}$  and a slow mode taking into account, in addition to the two previous radionuclides, the  $^{214}\text{Po}$ .

The pulses or counts are integrated during a predefined period, 10 min for the alphaGUARD and one hour for the DoseMan. The period of one hour was chosen to get a better statistical count.

## Material and method

Experiments were held from the 16<sup>th</sup> to the 29<sup>th</sup> of May 2018 in the BACCARA chamber of IRSN. This chamber consists of a one cubic meter stainless steel cylinder in which instruments to be tested can be placed together (Figure 1). This volume is connected to a  $^{220}\text{Rn}$  flow-through source (Pylon Electronic, Inc.). Clean pressurized air is used to transport the  $^{220}\text{Rn}$  to a mixing pipe for dilution and enters the bottom of the chamber. The

transportation time to the mixing pipe can be adjusted (tube with a longer length) in order to lower the thoron activity. Thoron rich air circulate through the chamber continuously at a flow rate of about  $3 \text{ m}^3/\text{h}$  and a steady thoron activity concentration is obtained after 20 min of the beginning of the injection. A fan is used to ensure homogeneity in the cylinder. Activity concentration of thoron and climatic parameters are measured continuously. Thoron activity concentration was monitored throughout the exposure by the alphaGUARD EF 2283. These monitor was calibrated against the primary thoron system at IRSN in the frames of the calibration exercise organized within Activity 2.1.2 of the project (see Annex III).

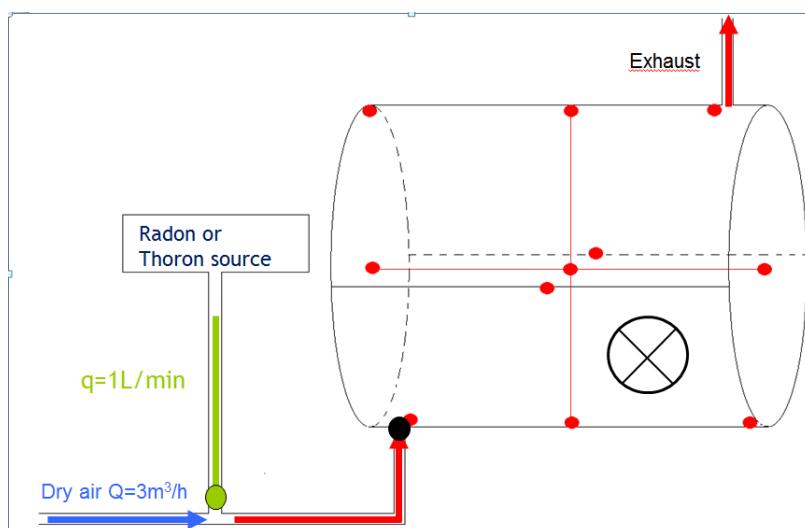


Figure 1 - Schematic diagram of the set-up

The position of the instruments in the chamber are shown in Figure 2. Despite the fact that a lot of instruments were present in this experiments, the results of only three of them were used. The reason was that the first purpose of this experiment was to calibrate thoron measurement instruments so all the instruments configuration were set up on thoron measurement except for the DoseMans which measures only radon. Some instruments recorded both radon and thoron activity concentration, but the radon configuration was not adequate in some apparatus (for example, the Rad7) or the radon results of the instrument were not available.

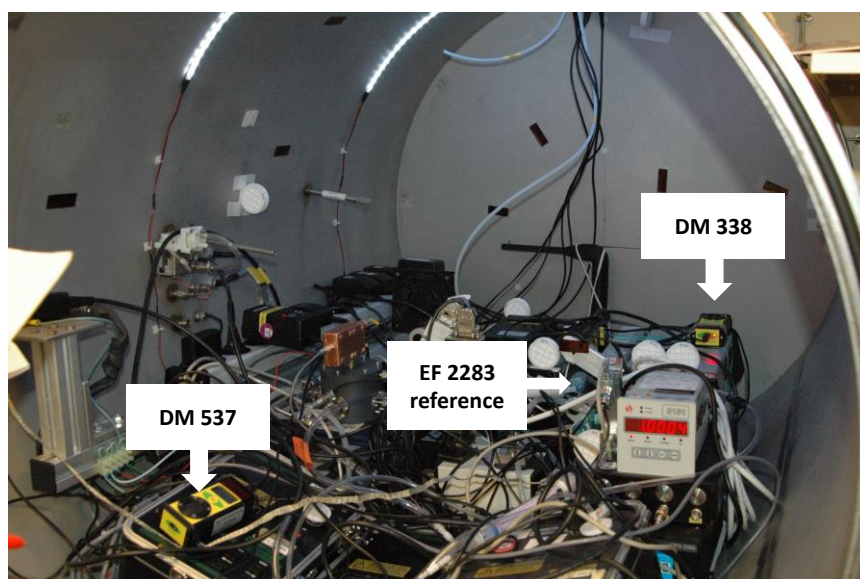


Figure 2 - Instruments in BACCARA  
Activity 2.2.1.

The alphaguard EF2283 is placed in the middle of the chamber while the Dosemans are at both ends. Homogeneity in the chamber was studied experimentally (during this test) and by simulation (A211), both studies concluded to an overexposure at the back of the chamber. In fact the signal on the LR115 (n° 21 and 22), placed on the top of the dosemans, compare to the reference point are 22% above at the end right side and 4% at the entrance on the left side. For this reason the quantification of the influence of thoron on the radon activity concentration measurement by the DM338 will not be taken into account. Nevertheless the raw data of this apparatus are presented in order to check the similarity or the differences on both apparatus DM338 and DM537.

## Thoron exposures in BACCARA

Different constant  $^{220}\text{Rn}$  reference atmospheres were created in BACCARA chamber. The thoron activity concentration over time is presented in figure 3. The exposure start with only compressed air going through the chamber, then thoron is injected and a constant activity concentration of about  $7 \text{ kBq.m}^{-3}$  is obtained followed by another plateau of around  $50 \text{ kBq.m}^{-3}$  of thoron. Then the chamber is open to remove some instruments and the  $50 \text{ kBq.m}^{-3}$  thoron activity concentration is set up again followed by  $10 \text{ kBq.m}^{-3}$  and zero thoron (only air). The reference thoron activity concentration for each plateau are given in table 2.

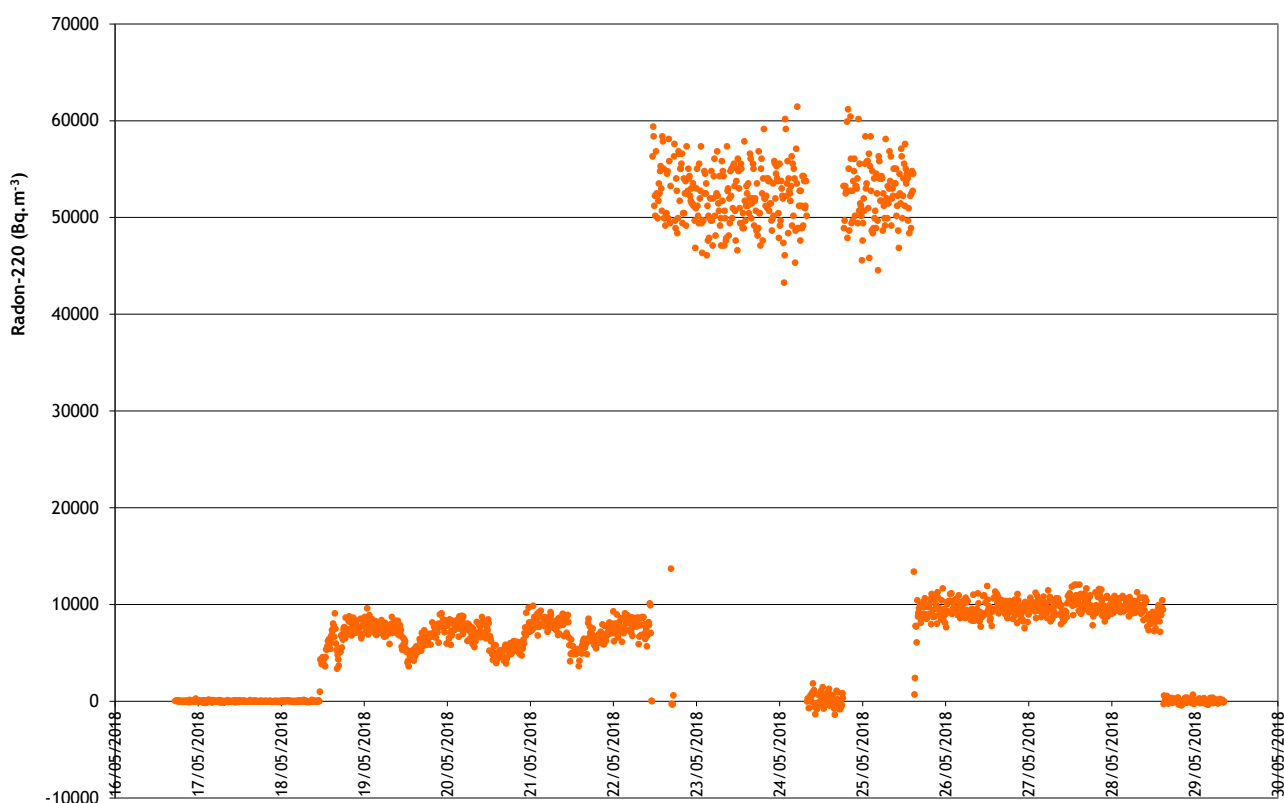


Figure 3 - AlphaGUARD EF2283 thoron raw data

Table 2 - Reference values for thoron activity concentration

| Injection of thoron                 | End of exposure (local hour) | mean thoron (Bq.m <sup>-3</sup> ) | relative uncertainty (Bq.m <sup>-3</sup> ) k=2 |
|-------------------------------------|------------------------------|-----------------------------------|--|
| 17/05/2018 14:50 (background start) | 18/05/2018 10:50             | 0                                 |  |
| 18/05/2018 11:00                    | 22/05/2018 10:50             | 7114                              | 422  |
| 22/05/2018 17:15                    | 24/05/2018 7:40              | 45701                             | 1251   |
| 24/05/2018 18:16                    | 25/05/2018 14:30             | 46169                             | 1200   |
| 25/05/2018 14:56                    | 28/05/2018 14:40             | 9856                              | 503  |

The relative humidity during the exposure were under 5 %. The arithmetic mean of the temperature was 27.6°C with a standard deviation of 0.6°C. For the pressure, the mean was 996 mbar with a standard deviation of 1 mbar.

### Influence of thoron on radon measurements

Figures 4 and 5 show the radon activity concentration measurement results for fast and slow configuration of the two DoseMan (left axis) over time when placed in a thoron atmosphere (right axis).

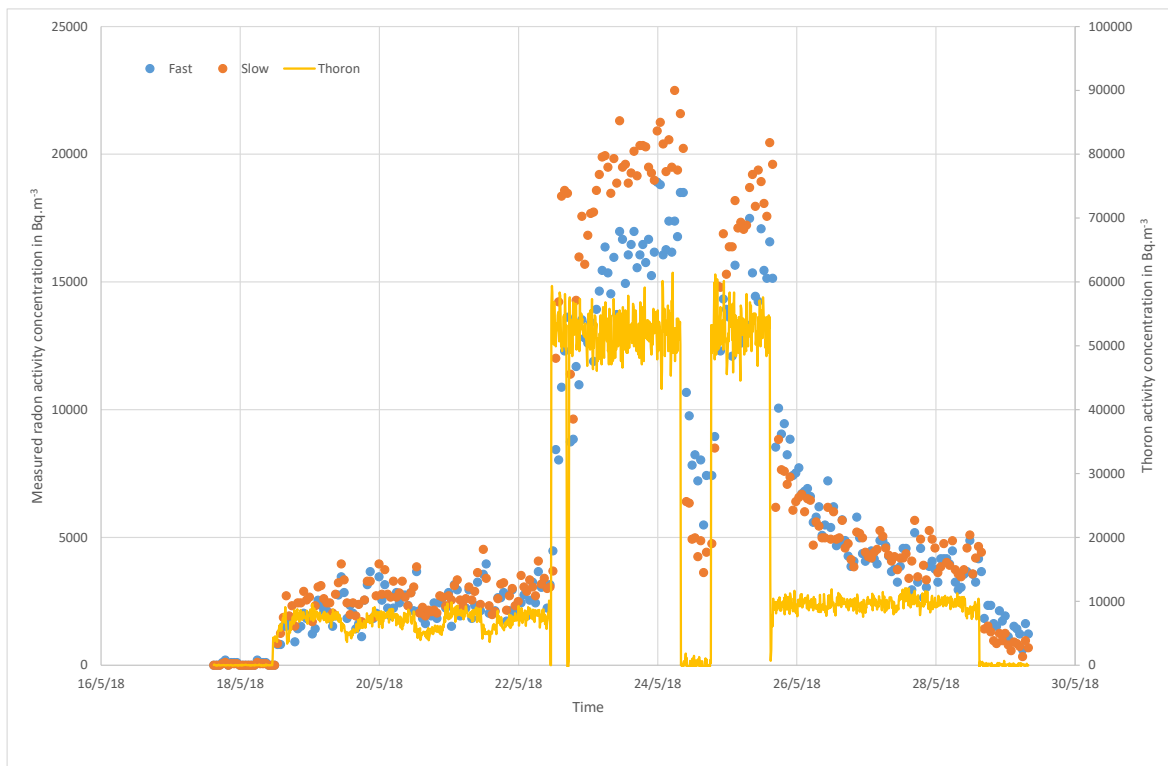


Figure 4 - Radon measurement of the DM357 in a thoron atmosphere

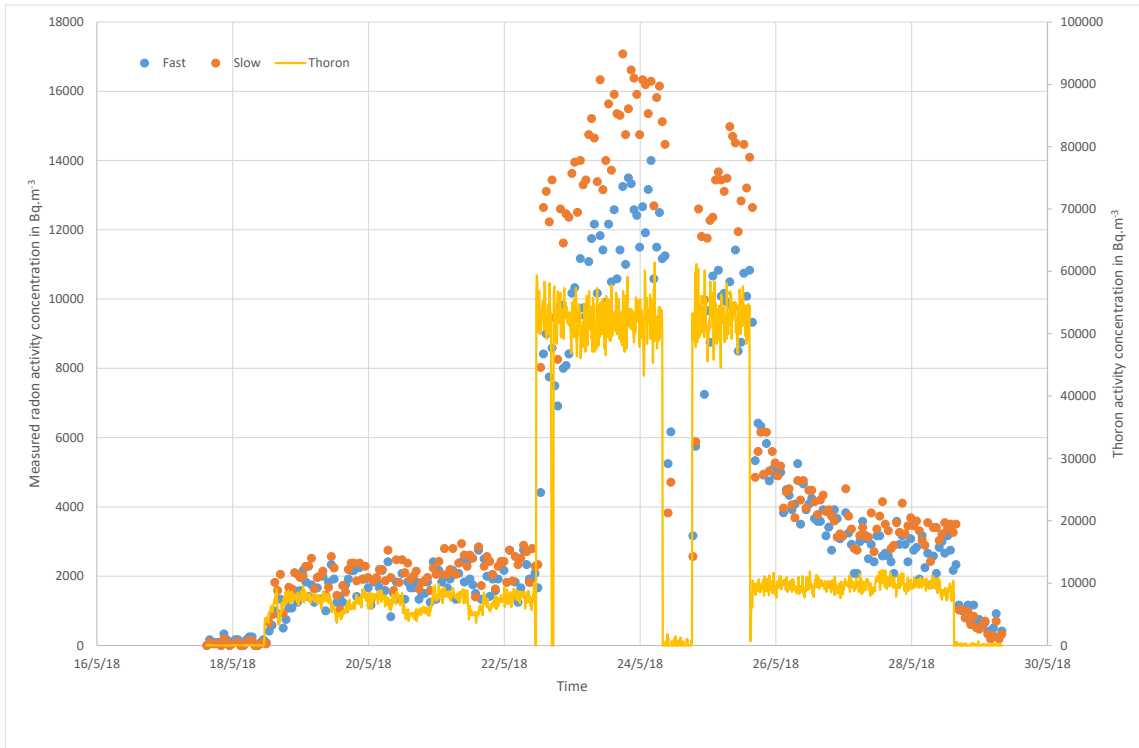


Figure 5 - Radon measurement of the DM338 in a thoron atmosphere

Qualitative response of both apparatus are alike. As soon as the apparatus are exposed to thoron or that the thoron increased suddenly, the recorded radon measurement increased for both apparatus. Then, the response of the instruments still increases and reaches a plateau. Finally, when the injection of thoron dropped or stopped, the recorded values dropped sharply at first and then slowly down to a plateau.

Those responses suggest that, despite its short radioactive half-life, thoron can diffuse in the detection chamber and a certain amount of thoron will decay in the detection chamber. Its first decay (figure 6), the polonium-216, is quickly in equilibrium with the thoron, then other progenies will appear more slowly following the longer half-life of the lead-212. How this can disturb the registration of radon and radon decay products in the Doseman?

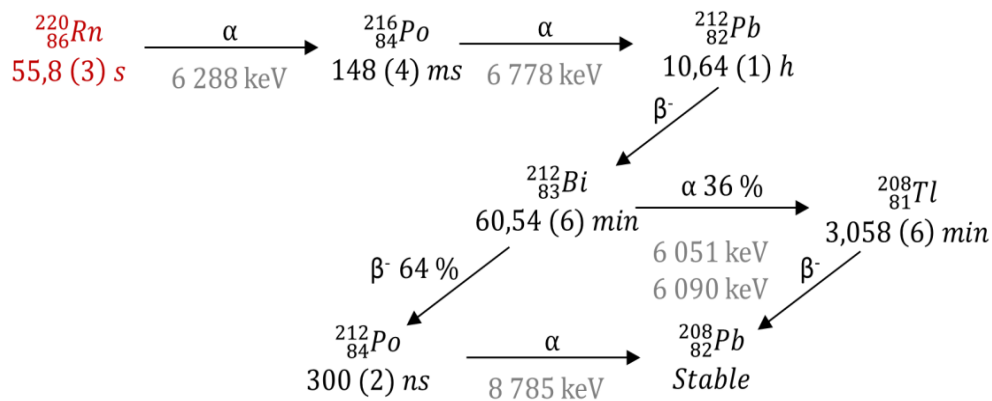


Figure 6 - Thoron disintegration chain

The DoseMan is equipped with silicon detector, the counts are classified according to the energy of the measured alpha decay. Two region of interest (ROI) are taken into account to calculate the radon activity concentration. For the fast mode the ROI (canal 1 to 21) is defined to take into account the decays of  $^{222}\text{Rn}$  and  $^{218}\text{Po}$ . For the slow mode an additional ROI (canal 22 to 37) take into account the decays of  $^{214}\text{Po}$ . The spectrum of one Doseman obtained in one thoron exposure is presented in figure 7.

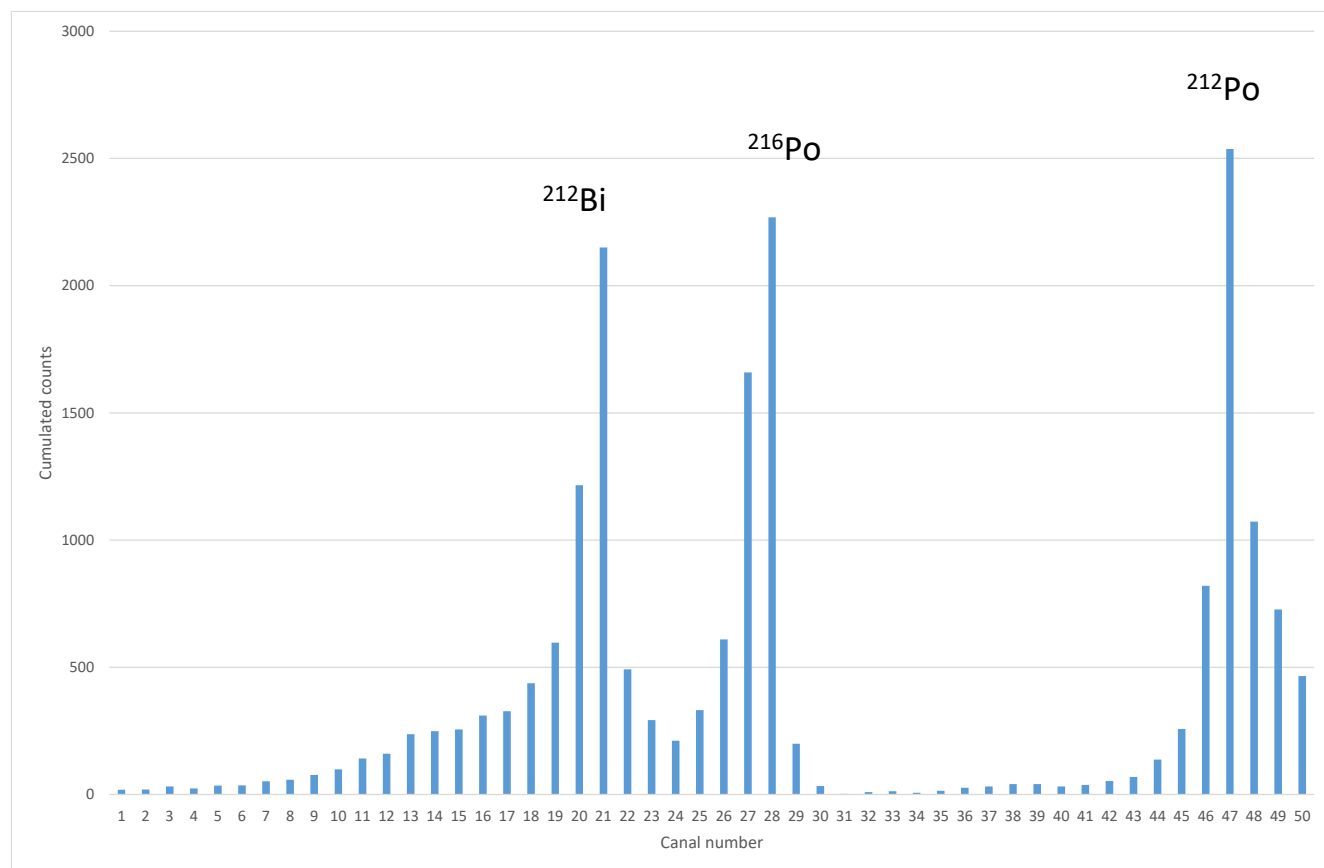


Figure 7 - DoseMan spectrum in a thoron atmosphere

When thoron diffuse into the Doseman detection chamber, it seems that some  $^{220}\text{Rn}$  alpha decays and  $^{212}\text{Bi}$  alpha decays are counted as  $^{222}\text{Rn}$  and  $^{218}\text{Po}$  alpha decays. Also  $^{216}\text{Po}$  alpha decays appear in the ROI where  $^{214}\text{Po}$  alpha decays are usually registered. This can explain the influence of thoron on the radon activity concentration measurement of the Doseman. Also when thoron is not in the air anymore the instrument is still perturbed by  $^{212}\text{Pb}$  and  $^{212}\text{Bi}$  that remains in its detection chamber and continue to slowly decay following an  $\exp(-\lambda(^{212}\text{Pb}) \cdot t)$  function. This was also observed in a previous article (Michielsen and *al.*, 2015).

In conclusion, the influence of thoron on radon measurement of a Doseman is first observed by the registration of  $^{220}\text{Rn}$  and  $^{216}\text{Po}$  alpha decays in the ROI used to registered radon and radon daughters. Response continue to raise with the registration of  $^{212}\text{Bi}$  alpha decays and when thoron is not in the air anymore  $^{212}\text{Bi}$  alpha decays are still disturbing the signal. According to the exponential function that rules the growth and decay of lead-212 progenies, after 3 days the growth of this progenies will reach a 99% equilibrium and so will be the influence on the radon measurement. 99% of the plateau value will be theoretically reached after 3 days and 99% of the signal due to lead-212 progenies will disappear after 3 days without thoron.

Results obtained with the alphaGuard Rn/Th are reported in figures 8 and 9. It should be noted that, on the 29<sup>th</sup> of May an additional exposure to high thoron activity concentration pic (few hours) was held to calibrate the apparatus (action A212). Radon measurement was also recorded during this event.

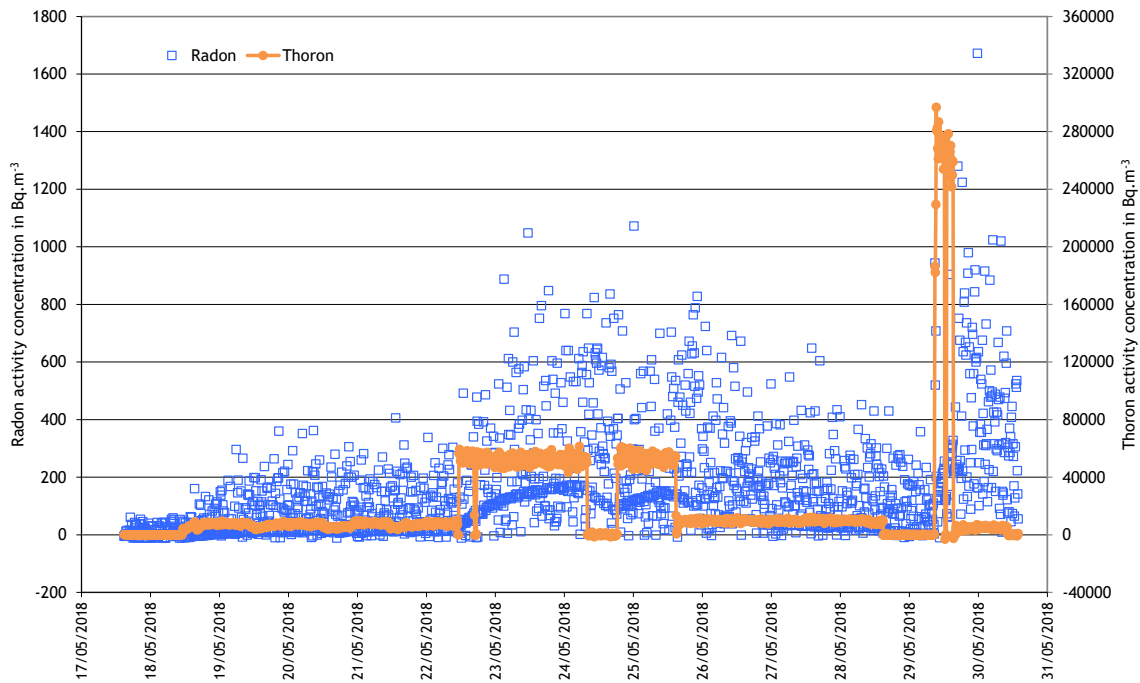


Figure 8 - Radon measurements of the alphaGuard EF2283 in a thoron atmosphere

This instrument makes some corrections to avoid the influence of thoron on the radon measurement. Details of the corrections applied are not known but activity concentration of thoron and of Polonium-212 (figure 9) are a part of it.

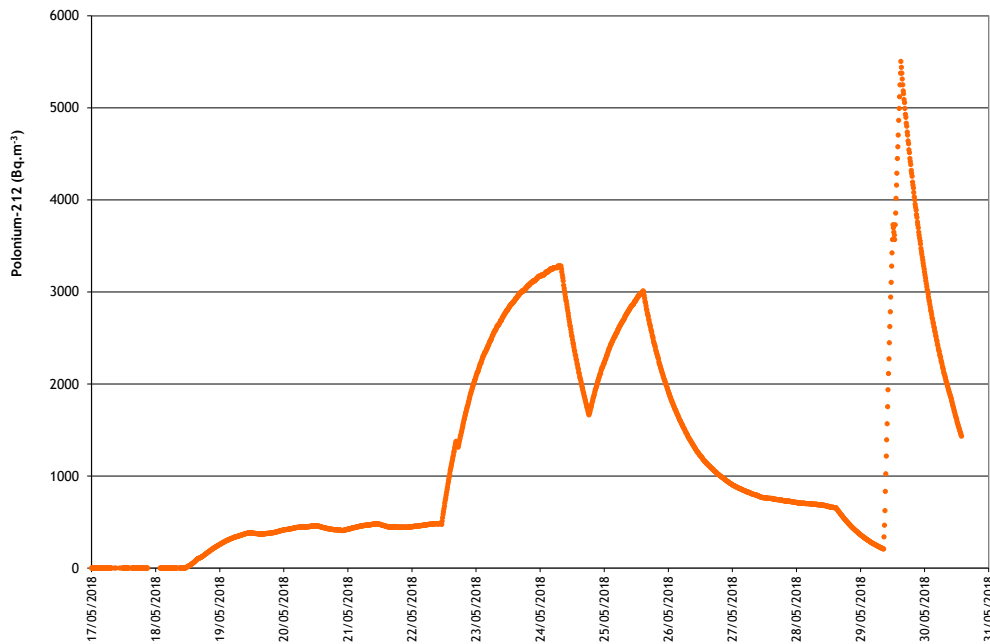


Figure 9 - Polonium-212 measurements of the alphaGUARD EF2283 in a thoron atmosphere

In order to have a better view of the radon measurement, the scattering data due to counting statistic is reduced by taking an hourly mean of the measurements (6 measurements of ten minutes). Data are presented in figure 10.

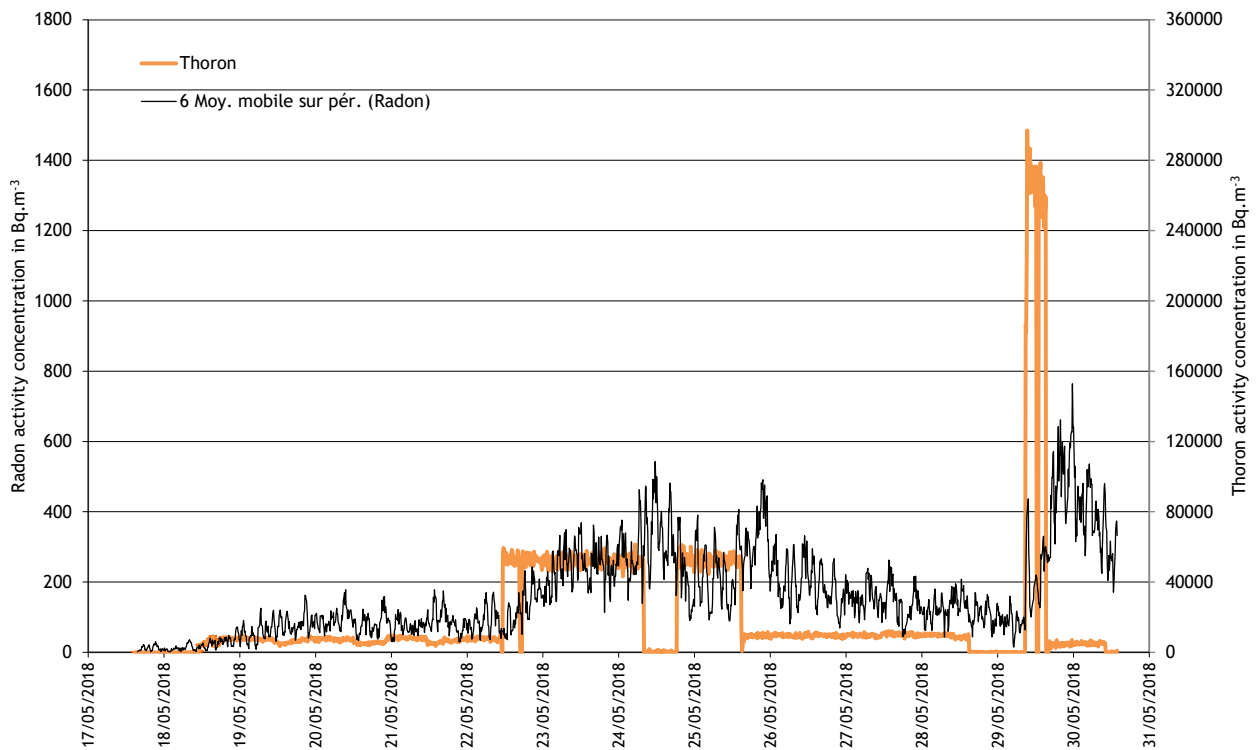


Figure 10 - Hourly radon measurements of the alphaGuard EF2283 in a thoron atmosphere

One can see that the influence of thoron on radon signal is almost 50 times less than for the previous instrument. Indeed this is a far more precise and sophisticated radon monitor where complex signal treatment of the pulses are used and mathematical models are applied to give the best possible estimation of the true value. We do not have hypothesis, as for the doseman, on how the thoron influences the final radon result. We can just observe, despite of a very good correction, similar behavior in growing signal with time and a remaining disturbed radon signal after thoron exposure, noticeable every time that the thoron is switched off, even following a pic of thoron (250 kBq.m<sup>-3</sup> during 5 hours) .

Influence of thoron on radon signal in radon monitors have been described qualitatively, the next paragraph will show means of quantification.

## Cross-interference

The influence of thoron on the radon signal is quantified by the cross-interference  $CI$ :

$$CI = \frac{E_{Rn}}{E_{Tn}} \times 100\%,$$

where  $E_{Rn}$  is the radon activity concentration corrected for background and  $E_{Tn}$  is the reference thoron activity concentration during the exposure to the thoron atmosphere.

As discussed before, while  $E_{Tn}$  is constant during the exposure,  $E_{Rn}$  vary with time. For IEC 61577-2 standard, cross-interference tests shall be carried on for at least four hours at  $1000 \text{ Bq.m}^{-3}$  of thoron. Those testing time and activity concentration seems to be too low in light of our study. We saw in the previous paragraph that the plateau might be reached after 3 days. Therefore we choose to calculate CI either after 3 days of exposure or with the last results of the exposure (called calculation period in table 3). Results of the average and the standard deviation of the cross interference, calculated on the plateau, are given in table 3. Results of the DM338 are not reported here because the instrument was not placed in the homogeneous zone.

Radon background was determined with the measurements made during the period 17-18 May 2018.

For the DM357 the averages are:

$$\text{BCGDM357fast} = 59 \text{ Bq.m}^{-3}$$

$$\text{BCGDM357slow} = 33 \text{ Bq.m}^{-3}$$

And the standard deviation of this average are:

$$\sigma(\text{BCGDM357fast}) = 15 \text{ Bq.m}^{-3}$$

$$\sigma(\text{BCGDM357slow}) = 8 \text{ Bq.m}^{-3}$$

For the EF2283, results are:

$$\text{BCGEF2283} = 12 \text{ Bq.m}^{-3}$$

$$\sigma(\text{BCGDM357}) = 2 \text{ Bq.m}^{-3}$$

Table 3 - CI results

| Exposure dates  | Calculation period                   | Instrument                      | average CI | Standard deviation of the population |
|-----------------|--------------------------------------|---------------------------------|------------|--------------------------------------|
| 18- 22 May 2018 | 21/05/2018 12:50<br>22/05/2018 10:50 | DM357<br>Fast mode<br>Slow mode | 37%<br>41% | 8%<br>7%                             |
| 22- 24 May 2018 | 23/05/2018 23:50<br>24/05/2018 7:40  | DM357<br>Fast mode<br>Slow mode | 38%<br>45% | 2%<br>2%                             |
| 24- 25 May 2018 | 25/05/2018 0:40<br>25/05/2018 14:30  | DM357<br>Fast mode<br>Slow mode | 32%<br>39% | 4%<br>3%                             |
| 25- 28 May 2018 | 28/05/2018 0:40<br>28/05/2018 14:40  | DM357<br>Fast mode<br>Slow mode | 38%<br>42% | 6%<br>5%                             |
| 18- 22 May 2018 | 21/05/2018 11:40<br>22/05/2018 10:50 | EF2283                          | 1.10%      | 1.22%                                |
| 22- 24 May 2018 | 23/05/2018 22:50<br>24/05/2018 7:40  | EF2283                          | 0.59%      | 0.42%                                |
| 24- 25 May 2018 | 25/05/2018 0:00<br>25/05/2018 14:30  | EF2283                          | 0.54%      | 0.41%                                |
| 25- 28 May 2018 | 28/05/2018 0:00<br>28/05/2018 14:40  | EF2283                          | 1.15%      | 1.65%                                |

CI results are very consistent for one experiment to another. Only the radon signal of the DoseMan was influenced by thoron with a CI ranged between 32% and 45%. Those value were comparable to those found by Michielsen and *al.* (2015).

In the Annex V, STUCK propose to approximate the recorded radon signal due to thoron by the function  $\mu$ :

$$\mu(t) = \mu_i + \mu(1 - \exp(-\lambda_{pb-212}t)) ; \quad [1]$$

And calculate two cross-interference factor, Cli and Clf, as follow:

$$Cli = \frac{\mu_i}{E_{Tn}} \times 100\% \text{ and } Clf = \frac{\mu_i + \mu_s}{E_{Tn}} \times 100 \quad [2]$$

Cli is called the initial cross-interference. This cross-interference signal could represents the constant interference in a constant thoron atmosphere, due to thoron and polonium-216. It can also represents a case where there is a short-term, pulse-like thoron concentration around the instrument. If thoron exposure continues, the cross-interference signal increases for the first three days. After this, an equilibrium is attained. This signal is called final cross-interference, Clf.

We have followed this approach and used equations 1 and 2 to calculate Cli and Clf on the Doseman DM357 for the two first exposures. CI results are presented in table 4 and the result of the model (eq. 1) on figures 11 and 12.

Table 4- Cross-interference data in thoron atmosphere

| Instrument | s/n   | Configuration mode | Test dates     | Cli in % | Clf in % |
|------------|-------|--------------------|----------------|----------|----------|
| DoseMan    | DM357 | Fast Mode          | 18-22 Mai 2018 | 11%      | 36%      |
|            |       |                    | 22-24 Mai 2018 | 18%      | 39%      |
| DoseMan    | DM357 | Slow Mode          | 18-22 Mai 2018 | 14%      | 41%      |
|            |       |                    | 22-24 Mai 2018 | 26%      | 48%      |

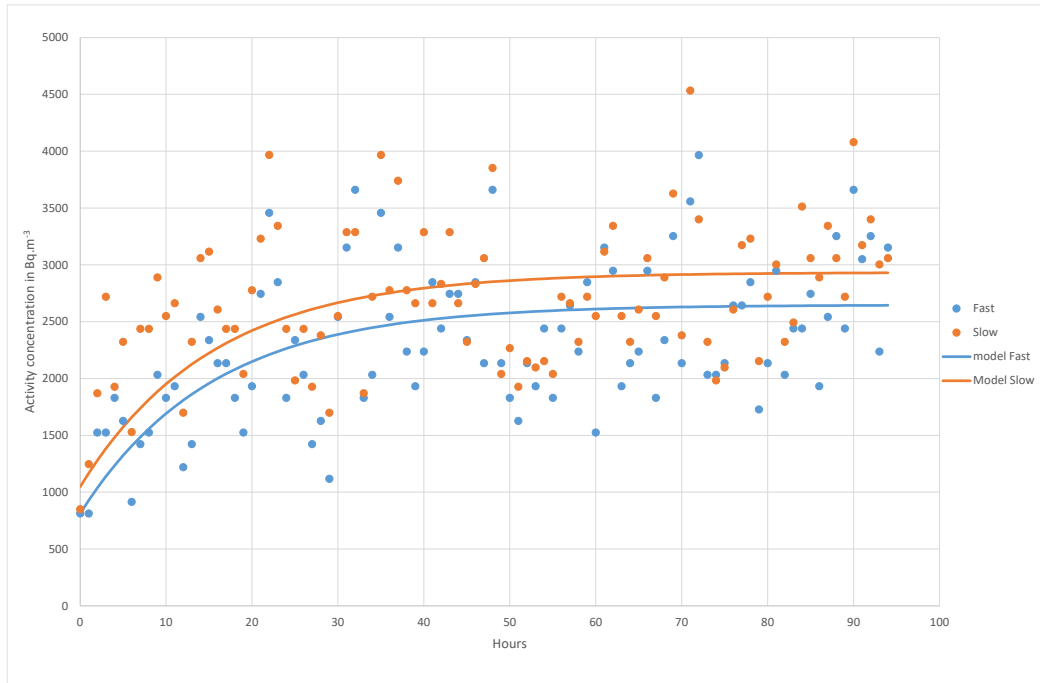


Figure 11 - DM357 radon data during the 18-22 May thoron exposure

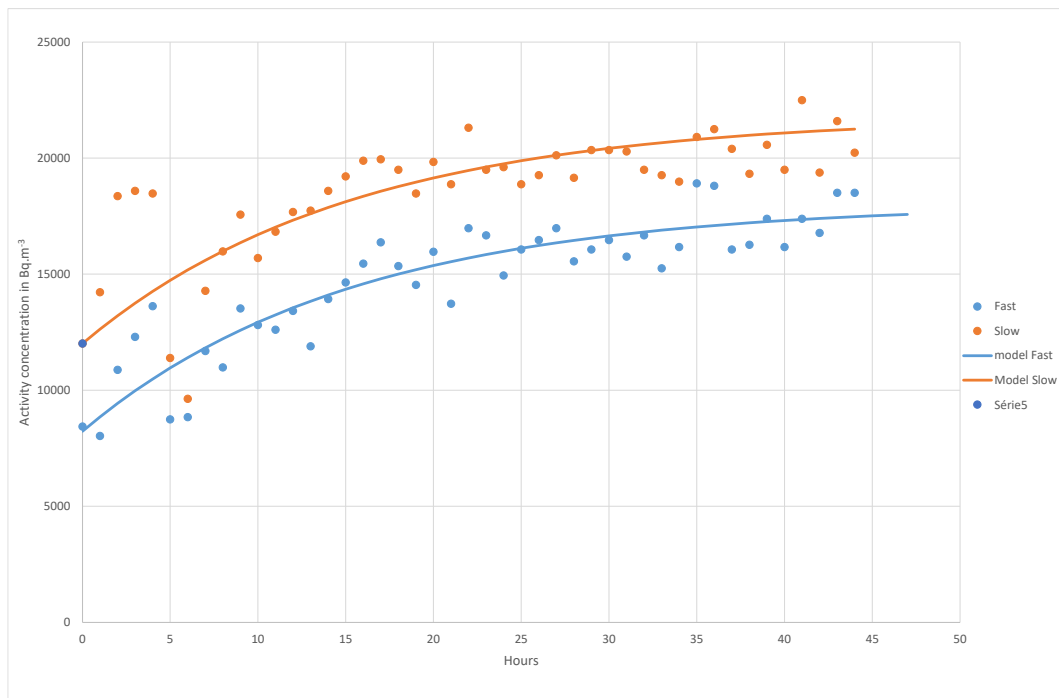


Figure 12 - DM357 radon data during the 22-24 May thoron exposure

## Conclusion and recommendations

The influence of thoron on radon measurement of two type of monitors have been tested in the BACCARA chamber at IRSN. The Doseman is a simple monitor that use, to determine the radon activity concentration in the air, two energy regions (ROI) where alpha radon and radon progenies decays, which are in the detection chamber, are recorded. The results suggest that, despite its short half-life, a certain amount of thoron diffuse

in the detection chamber where thoron progenies can accumulate. Thoron and some alpha progenies can be registered in the same ROI than those used for radon and its progenies and give false signal of a presence of radon. Because of the 10.64 h half-life of the lead-212, the full influence of thoron on a radon signal will be theoretically reached after 3 days. Also, when thoron is not present anymore in the atmosphere, the lead-212 progenies, accumulated in the detection chamber, will take 3 days to disappear. A cross-interference ranged between 32% and 48% has been found for the DoseMan in this study. In contrast, the alphaGUARD 2000 RnTh PRO is a more sophisticated apparatus which corrects for the influence of thoron. This study shows that the applied correction works.

Thoron activity concentration in atmosphere is usually low but, in some cases, cave, air in soil for example, where radon and thoron activity concentrations might be at the same order of magnitude, the interference of thoron on radon measurements cannot be disregarded. Nevertheless the presence or absence of thoron can be easily checked by letting the instrument running in a low (or free) radon and thoron atmosphere. If the measured radon activity concentration of the apparatus does not come down to its background value, in some hours, then a correction might need to be applied. Finally we recommend to determine the cross interference of thoron on radon monitors in a high constant thoron atmosphere for more than 3 days.

## References

IEC 61577-2 standard, RADIATION PROTECTION INSTRUMENTATION – RADON AND RADON DECAY PRODUCT MEASURING INSTRUMENTS – Part 2: Specific requirements for  $^{222}\text{Rn}$  and  $^{220}\text{Rn}$  measuring instruments

N.Michielsen and S.Bondiguel, THE INFLUENCE OF THORON ON INSTRUMENTS MEASURING RADON ACTIVITY CONCENTRATION, Radiation Protection Dosimetry (2015), pp. 1–4



16ENV10 MetroRADON

Deliverable D2

Annex VII

Task A.2.2.2

Cross-interference tests performed on  
track-etch detectors

Tuukka Turtiainen  
STUK

Environmental Radiation Surveillance and  
Emergency Preparedness  
Tuukka Turtiainen

January 15, 2020

### Cross-interference tests performed on track-etch detectors

In this report, thoron cross-interference test performed on track-etch detectors sold in Finland is described. Two separate exposures were carried out and it was concluded that all tested detectors comply with standard IEC 61577-2 requirement.

### Detectors

In Finland, track-etch detectors for radon measurement are available from four manufacturers (Table 1). Fifteen detectors were purchased from each sales agent in Finland and the scope of the tests was not disclosed. 3–4 detectors from each manufacturer were selected for two separate exposures.

Table 1. List of the track-etch detectors. The serial numbers in brackets refer to transit (background) detectors.

| Manufacturer                            | Detector              | Serial numbers exposure 1  | Serial numbers exposure 2  |
|---|-----------------------|--|--|
| <b>STUK</b>                             | Generic               | 429409<br>429410<br>429416   | 429408<br>429415<br>429414<br>(429411)<br>(429412)<br>(429413)                       |
| <b>Radonova</b>                         | RadTrack <sup>2</sup> | 577868-3<br>423531-3<br>541320-8<br>(423507-3)<br>(540811-7)   | 105121-8<br>542925-3<br>579389-8<br>(421817-8)<br>(508230-0)                         |
| <b>AlphaRadon</b>                       | Generic               | 119465-39F<br>119436-328<br>119401-35F<br>119444-38A<br>(120314-6f0)<br>(119133-253)<br>(119041-1f7) | 119347-329<br>119269-2db<br>119270-2dc<br>119345-327<br>(119099-231)<br>(119125-35f) |
| <b>Eurofins Radon Testing Sweden AB</b> | Generic               | 8325892<br>8325814<br>8325891<br>(8325873)<br>(8325874)  | 8325887<br>8325855<br>8325857<br>(8325846)<br>(8325896)                              |

Environmental Radiation Surveillance and  
Emergency Preparedness  
Tuukka Turtiainen

January 15, 2020

## Set-up and instruments

Thoron atmosphere was created in a 101.1-litre Emanation Calibration Container (s/n EV03117, Saphymo GmbH). Air exchange through the container was created with Qdos60 peristaltic pump (Watson Marlow) and monitored from the air outlet with Thermo GFM Pro flow meter (s/n TS561043). The inlet air was first desiccated with Laboratory Drying Unit (DurrIDGE) filled with freshly regenerated Drierite and second, radon was removed with a 1-litre activated carbon unit (Saphymo) before the thoron source. A flow-through thoron source TH-1025 from Pylon Electronics Inc. was used and its certified activity on 14 Sep 2018 is  $(100,83 \pm 0.63)$  kBq (certificate I4751). The thoron-rich air was directed (after a 175 mL transfer volume) in front of a fan situated under the lid of the container (Figure 1).

Homogeneity of thoron gas inside the container has been validated with aerogel samplers before. Reference instrument for thoron concentration measurement was AlphaGuard PQ2000 RnTn (s/n EF2104, Saphymo GmbH) which has been calibrated against the LNHB primary thoron standard at IRSN (May 2018). The instrument was operated with AlphaPump (s/n AP1367), the flow rate of which was checked before and after exposures with Aalborg GFM 17 mass flow meter (calibration certificate M-18D020). Humidity and temperature were measured with HygroClip HC2A-S -probe (Rotronic AG, s/n 0020300479, certificate 9-0366029443). Air velocity measurements were carried with Swema 3000MD (s/n 681989) and SWA31 probe (s/n 421629) calibrated at Pietikko Oy (certificate 201801231).

Relative humidity in air was regulated with supersaturated  $\text{MgCl}_2$  aqueous solution placed inside the container. Temperature was not regulated, and it followed the temperature in the laboratory.

Air flow velocity measurements were performed in the container without instrument detectors placed on the grid. The flow velocity logger was placed next to AlphaGuard on the bottom. The flow rate at the grid level, in the middle was recorded as  $(0.24 \pm 0.03)$  m/s and it was normal to the grid plane. The uncertainty of flow velocity measurements is given with 1 SD.

January 15, 2020

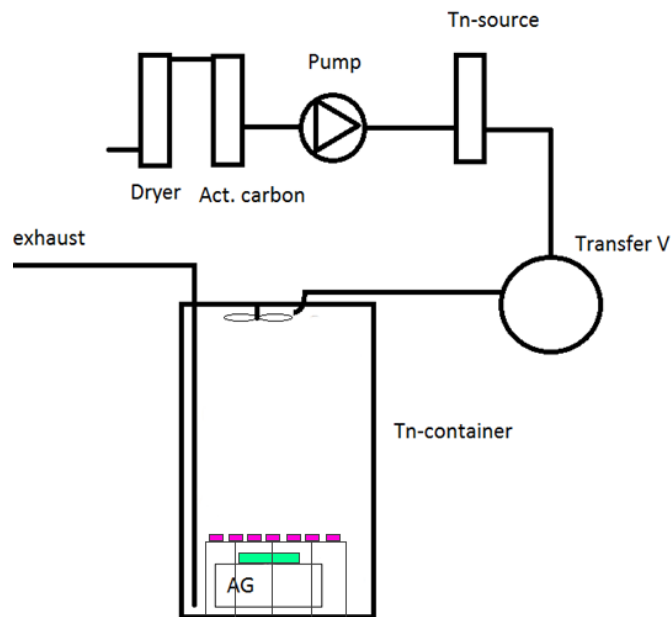


Figure 1. Set-up of the cross-interference test. The tested track-etch detectors were placed on a grid above the reference instrument (AG).

### Exposure 1: Protocol

The seal-bags of the detectors were opened 2–10 minutes before the exposure started. The detectors were sparsely placed on a grid to allow air mixing inside the container (Fig. 3). The flow rate through the chamber was adjusted to 90 mL/min. Considering the transfer volume of 175 mL, there is a 2-minute delay before thoron concentration begins to increase in the chamber and the equilibrium concentration is attained in about 7 minutes.

The exposure lasted for 240.0 hours between 18 and 28 September 2019. The exposure concentration was  $(39.4 \pm 0.7)$  Bq/m<sup>3</sup> and thoron exposure  $(9460 \pm 160)$  kBqh/m<sup>3</sup>.

Temperature and humidity were  $(23.0 \pm 0.1)$  °C and  $(31.5 \pm 0.9)$  %rh, respectively (range given is one SD). Humidity was 39.8 %rh at the beginning of the test (the same as air in the laboratory) until equilibrium humidity was reached. Temperature remained almost constant.

Radon concentration inside the laboratory was  $(20 \pm 6)$  Bq/m<sup>3</sup>. This radon concentration was also sealed into the exposure container. We can hence calculate the radon exposure by solving integral

$$\int_0^{240} C_i(Rn) \times e^{-(q+\lambda_{Rn}) \cdot t} dt$$

Environmental Radiation Surveillance and  
Emergency Preparedness  
Tuukka Turtiainen

January 15, 2020

Where  $C_i$  is the radon concentration in laboratory air ( $20 \text{ Bq/m}^3$ ),  $q$  is the air exchange constant of the container ( $0.054 \text{ h}^{-1}$ ) and  $\lambda_{Rn}$  the decay constant of Rn-222 ( $0.00755 \text{ h}^{-1}$ ). The radon exposure at the beginning of the exposure was hence assessed as  $325 \text{ Bqh/m}^3$  (fig. 2).

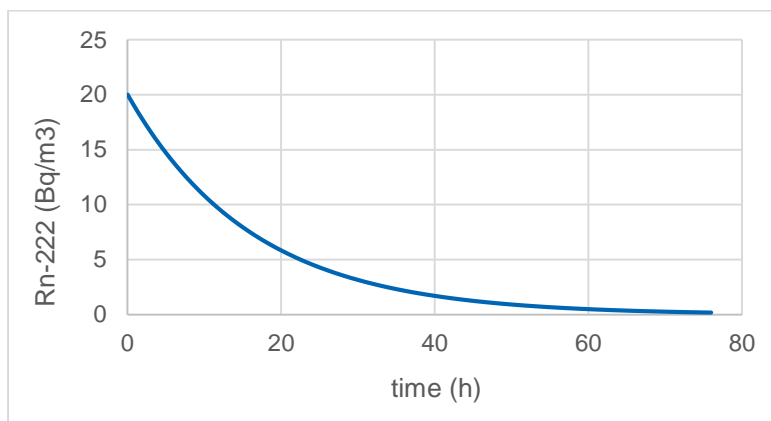


Figure 2. Radon (Rn-222) concentration inside the thoron container at the beginning of the exposure (240 h).

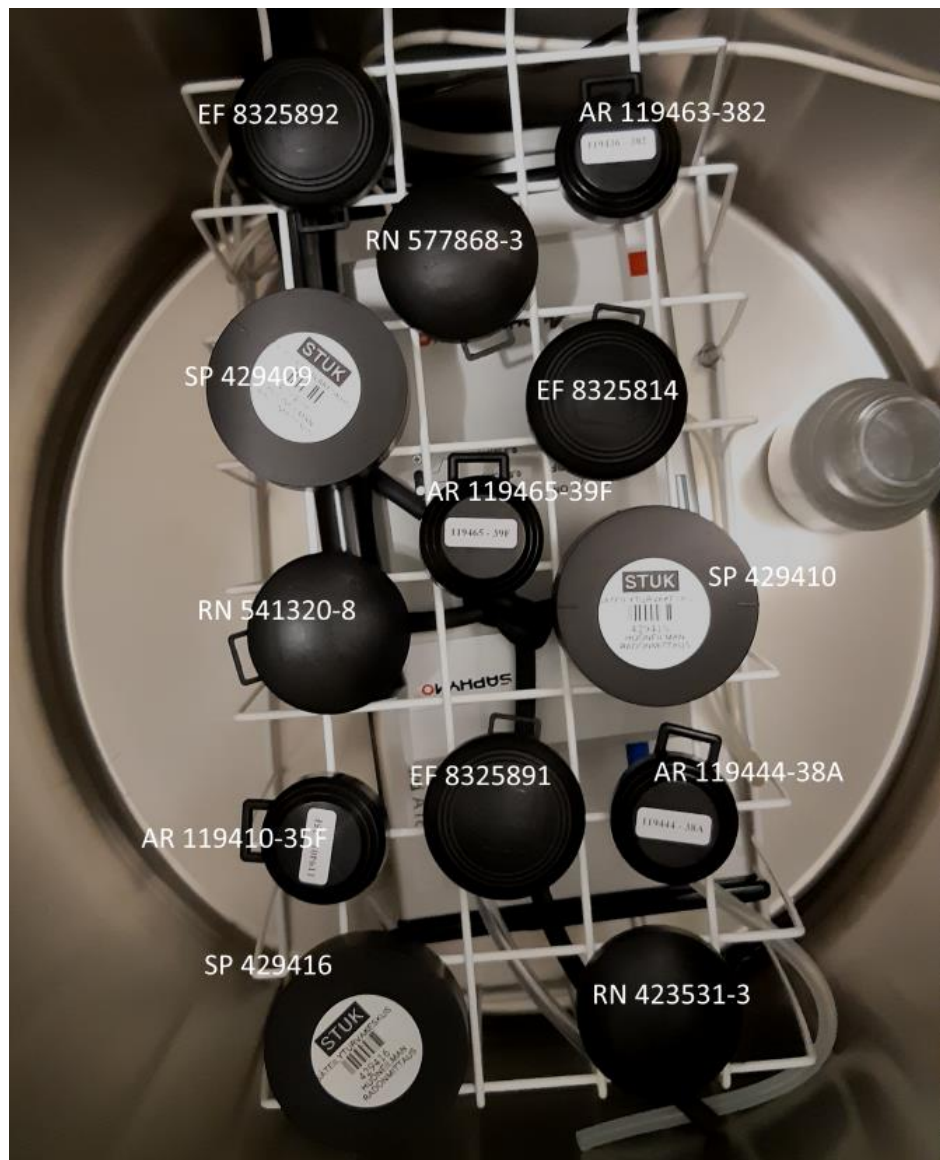


Figure 3. Placement of the detectors during the first exposure. The letter in the figure are as follows: SP = STUK, EF = Eurofins, AR = AlphaRadon Teo and RN = Radonova. The number refers to the serial number of the detector. The reference monitor was on the bottom of the container and its air inlet is situated below SP 429410. The air outlet of the reference instrument is situated on the bottom of the picture. MgCl<sub>2</sub> humidifier is on the right.

After the exposure, the detectors were quickly transferred into a separate container from which radon was removed with activated carbon absorption ( $q=3.5 \text{ h}^{-1}$ ). Radon exposure during this transfer was assessed as  $5 \text{ Bqh/m}^3$ .

The detectors were taken from the radon free atmosphere the next day and packed and posted to the laboratories following their instructions. The sampling period given was as 18.–28.10.2019. Detectors from STUK were

Environmental Radiation Surveillance and  
Emergency Preparedness  
Tuukka Turtiainen

January 15, 2020

delivered to the laboratory for analyses, not posted. Two or three transfer detectors were sent along with the exposed detectors. The seal-bag of the transfer detector was opened when the exposed detectors were taken out of the radon-free atmosphere.

### **Exposure 2: Protocol**

Same procedure was followed as during set-up of exposure 1 except for the exposure time, which was 168.0 hours and the air exchange rate, which was  $0.069 \text{ h}^{-1}$ . Radon concentration inside the laboratory was  $(18 \pm 6) \text{ Bq/m}^3$ . Hence, radon exposure received by the detectors at the beginning of the exposure was assessed as  $235 \text{ Bqh/m}^3$ . The mean exposure concentration was  $(68\,300 \pm 1000) \text{ Bq/m}^3$  and thoron exposure  $(11\,500 \pm 200) \text{ kBqh/m}^3$ . The placement and the serial numbers of the detectors are shown in figure 4.

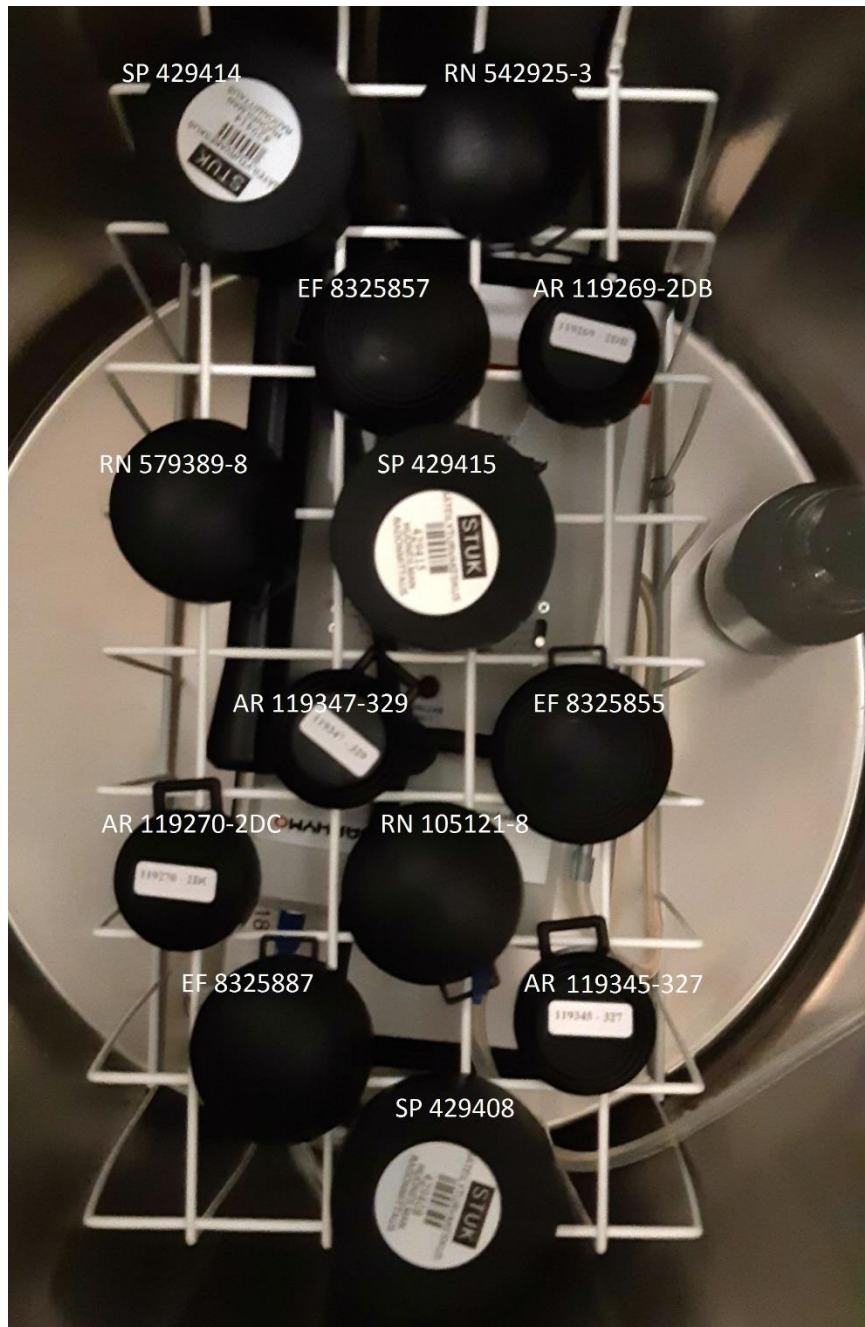


Figure 4. Placement of the detectors during the second exposure. The letter in the figure are as follows: SP = STUK, EF = Eurofins, AR = AlphaRadon Teo and RN = Radonova. The number refers to the serial number of the detector. The reference monitor was on the bottom of the container and its air inlet is situated below EF 8325855. The air outlet of the reference instrument is situated on the bottom right of the picture. MgCl<sub>2</sub> humidifier is on the right.

January 15, 2020

The mean temperature and humidity were  $(21.0 \pm 0.1) ^\circ\text{C}$  and  $(31.0 \pm 1.7) \%$ rh, respectively. The range given is one SD. Humidity was 22 %rh at the beginning of the test (the same as air in the laboratory). It increased to the equilibrium value of 32 %rh in about 30 hours. Temperature remained relatively constant (figure 5).

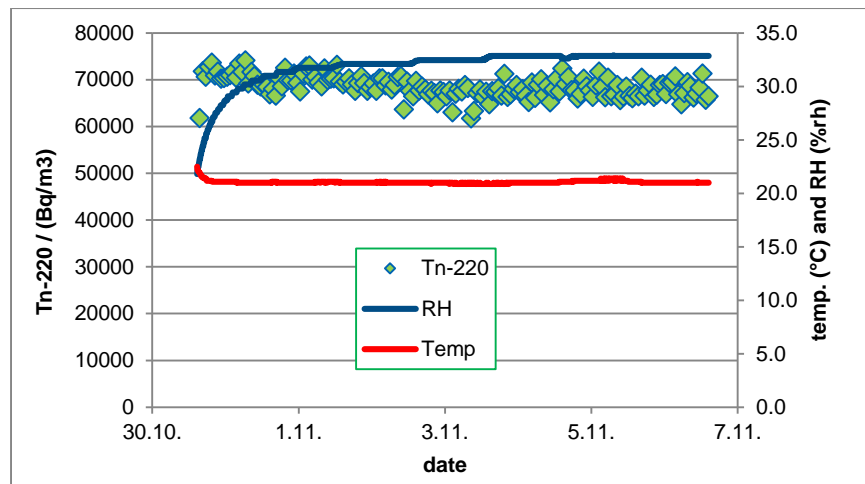


Figure 5. Measured Tn-220 concentration, temperature and relative humidity during exposure 2.

After the exposure, the detectors were quickly transferred into a container from which radon was removed with activated carbon absorption ( $q=3.5 \text{ h}^{-1}$ ). Radon exposure during this transfer was assessed as  $5 \text{ Bqh/m}^3$ .

The detectors were taken from the radon (and thoron) free atmosphere two days later, and they were packed and posted to the laboratories following their instructions. This time also STUK detectors were posted. Two or three transfer detectors were sent along with the exposed detectors. The seal-bag of the transfer detector was opened when the exposed detectors were taken out of the radon-free atmosphere.

## Results

The Cross interference,  $CI$ , was calculated as follows.

$$(1) \quad CI = \frac{E_n}{E_{Tn}} \times 100\%$$

$$(2) \quad E_n = C_{Rn} \times t_e - E_{lab}$$

or

$$(3) \quad E_n = (C_{Rn} - \overline{C_{tr}}) \times t_e - E_{lab}$$

The net exposure,  $E_n$ , was calculated without (2) and with subtraction (3) of the mean concentration by the transfer detectors  $\overline{C_{tr}}$ .  $C_{Rn}$  is the result

January 15, 2020

reported by the detector provider for thoron exposed detectors,  $E_{Tn}$  is the thoron exposure measured with reference instrument,  $E_{lab}$  is radon exposure at the laboratory and  $t_e$  exposure time. If  $\overline{C_{tr}}$  was below detection limit, the value applied was  $0.5 \times$  the mean detection limit with standard uncertainty of  $0.5 \times$  the mean detection limit.

### AlphaRadon

The transit detectors provided by AlphaRadon showed that the postage background subtraction at this laboratory is not optimal (Table 2). All transit detectors resulted in a signal that was above detection limit. Another observation on the results is that many of the reported uncertainties are too small to be realistic,  $\pm 1\%$ . The test report did not specify, which type of uncertainty was reported. Therefore, we assumed standard uncertainty ( $k=1$ ).

Table 2. Results from the AlphaRadon detectors. 'NT' refers to no subtraction of transit detector signal and 'WT' to subtraction of transit detector signal. All uncertainties are reported with coverage factor of  $k=1$ .

| Detector   | Type    | $C_{Rn}$ (Bq/m <sup>3</sup> ) | CI (%) NT     | CI (%) WT     |
|--|---------|-------------------------------|---------------|---------------|
| Exposure 1: (9 460 $\pm$ 160) kBqh/m <sup>3</sup>  |         |                               |               |               |
| 119401   | Tn      | 2567 $\pm$ 24                 | 6.5 $\pm$ 0.1 | 6.3 $\pm$ 0.2 |
| 119436   | Tn      | 2992 $\pm$ 29                 | 7.6 $\pm$ 0.1 | 7.4 $\pm$ 0.2 |
| 119444   | Tn      | 3325 $\pm$ 29                 | 8.4 $\pm$ 0.2 | 6.5 $\pm$ 0.2 |
| 119465   | Tn      | 3304 $\pm$ 31                 | 8.4 $\pm$ 0.2 | 6.5 $\pm$ 0.2 |
| 119041   | Transit | 75 $\pm$ 8                    |               |               |
| 119133   | Transit | 100 $\pm$ 8                   |               |               |
| 120314   | Transit | 29 $\pm$ 6                    |               |               |
| Exposure 2: (11 500 $\pm$ 200) kBqh/m <sup>3</sup> |         |                               |               |               |
| 119347   | Tn      | 5153 $\pm$ 31                 | 7.5 $\pm$ 0.1 | 7.5 $\pm$ 0.2 |
| 119269   | Tn      | 5264 $\pm$ 30                 | 7.7 $\pm$ 0.1 | 7.6 $\pm$ 0.2 |
| 119270   | Tn      | 5340 $\pm$ 29                 | 7.8 $\pm$ 0.1 | 7.7 $\pm$ 0.2 |
| 119345   | Tn      | 6007 $\pm$ 33                 | 8.8 $\pm$ 0.1 | 8.7 $\pm$ 0.3 |
| 119099   | transit | 69 $\pm$ 9                    |               |               |
| 119125   | transit | 63 $\pm$ 8                    |               |               |
|  |         |                               |               |               |

The arithmetic mean of CI without subtracting transit detector signal was 7.8 %. The number of detectors was limited, but it appears that there is only little variance between individual detectors (range 6.5–8.8 %). Difference in CI between detectors is most probably due to the size of the gap in the detector housing.

Environmental Radiation Surveillance and  
Emergency Preparedness  
Tuukka Turtiainen

January 15, 2020

### Eurofins Environment Testing

Eurofins Environment Testing Finland Oy contacted us and explained that the first exposure batch of detectors had spent unexpectedly long time in the post (10 days) and suggested that we cancel the order. The detectors were first sent to Lahti, Finland according to the instructions. The laboratory in Lahti had forwarded the detectors to the laboratory in Sweden. At this time, we disclosed that there were two transit detectors and we would like to receive the results. After this, the lab informed us that no postage background is subtracted from any of the results. Hence, results for CI are calculated only with transit background subtraction.

The envelope containing the detectors after the second exposure was also delayed in the post. Eurofins contacted us 10 days after mailing that the envelope still hadn't arrived. We agreed that the detectors will be analysed without subtracting the generic postage background.

The reported uncertainties appear realistic. The maximum detectable concentration, however, was only 5600 Bq/m<sup>3</sup>. Therefore, results from one detector could not be obtained.

Table 3. Results from the Eurofins Environment Testing Sweden AB detectors. All uncertainties are reported with coverage factor of k=1.

| Detector                                       | Type    | C <sub>Rn</sub> (Bq/m <sup>3</sup> ) | CI (%) WT |
|--|---------|--------------------------------------|-----------|
| Exposure 1: (9 460 ±160) kBq/h/m <sup>3</sup>  |         |                                      |           |
| 8325892  | Tn      | 1180 ± 90                            | 2.6 ± 0.3 |
| 8325814  | Tn      | 1560 ± 110                           | 3.6 ± 0.3 |
| 8325891  | Tn      | 3860 ± 270                           | 9.4 ± 0.7 |
| 8325874  | Transit | 170 ± 30                             |           |
| 8325873  | transit | 110 ± 20                             |           |
| Exposure 2: (11 500 ±200) kBq/h/m <sup>3</sup> |         |                                      |           |
| 8325855  | Tn      | 2300 ± 170                           | 3.1 ± 0.3 |
| 8325857  | Tn      | 2450 ± 180                           | 3.3 ± 0.3 |
| 8325887  | Tn      | >5600                                | >7.9      |
| 8325846  | Transit | 190 ± 30                             |           |
| 8325896  | transit | 210 ± 30                             |           |

The arithmetic mean of CI without subtracting transit detector signal was 4.4 %, when the result from the detector 8325887 was not included. There are obvious differences between individual detectors (range 2.6–9.4 %).

**Radonova**

Radonova did not sent the results from the first exposure because the detectors were exposed for a too short time. After a request, the results of the analyses were sent. The uncertainty relating to the radon concentration was not specified in the test report but was assumed as expanded uncertainty (k=2).

Postal background subtraction was realistic as the results from the transit detectors were below detection limit. The uncertainties were also realistic.

The second batch of detectors spent about one month in the post due to the postal strike. In this batch, the transit detectors resulted a false positive radon signal. Therefore, CI based on transit background subtraction are more realistic.

Table 4. Results from the Radonova detectors. ‘NT’ refers to no subtraction of transit detector signal and ‘WT’ to subtraction of transit detector signal. All uncertainties are reported with coverage factor of k=1.

| Detector                                      | Type    | C <sub>Rn</sub> (Bq/m <sup>3</sup> ) | CI (%) NT | CI (%) WT |
|---|---------|--------------------------------------|-----------|-----------|
| Exposure 1: (9 460 ±160) kBqh/m <sup>3</sup>  |         |                                      |           |           |
| 423531-3                                      | Tn      | 910 ± 80                             | 2.3 ± 0.2 | 2.2 ± 0.2 |
| 541320-8                                      | Tn      | 780 ±80                              | 2.0 ± 0.2 | 1.9 ± 0.2 |
| 577868-3                                      | Tn      | 540 ± 70                             | 1.4 ± 0.2 | 1.3 ± 0.2 |
| 423507-3                                      | Transit | <80                                  |           |           |
| 540811-7                                      | Transit | <50                                  |           |           |
| Exposure 2: (11 500 ±200) kBqh/m <sup>3</sup> |         |                                      |           |           |
| 105121-8                                      | Tn      | 1270 ± 120                           | 1.9 ± 0.2 | 0.8 ± 0.4 |
| 542925-3                                      | Tn      | 1670 ± 140                           | 2.4 ± 0.2 | 1.4 ± 0.4 |
| 579389-8                                      | Tn      | 1520 ± 140                           | 2.2 ± 0.2 | 1.2 ± 0.4 |
| 421817-8                                      | Transit | 580 ± 100                            |           |           |
| 508230-0                                      | Transit | 880 ± 110                            |           |           |

Radonova detectors show only minor CI, the mean value being 1.5 % when transit background subtraction was applied. There is also little variance between detectors.

**STUK**

The first batch of exposed detectors were directly brought to the lab, not sent by post. Therefore, no transit results for transit detectors are reported. The second batch of detectors was sent via post with three transit detectors. The postal strike caused delays: delivery time was 26 days. Nevertheless, normal postal background subtraction was applied to the detectors. One of the transit detectors exhibited a false positive radon signal.

Environmental Radiation Surveillance and  
Emergency Preparedness  
Tuukka Turtiainen

January 15, 2020

Table 5. Results from STUK detectors. 'NT' refers to no subtraction of transit detector signal and 'WT' to subtraction of transit detector signal. All uncertainties are reported with coverage factor of  $k=1$ .

| Detector                                       | Type    | $C_{Rn}$ (Bq/m <sup>3</sup> ) | CI (%) NT | CI (%) WT |
|--|---------|-------------------------------|-----------|-----------|
| Exposure 1: (9 460 ±160) kBq/h/m <sup>3</sup>  |         |                               |           |           |
| 429409   | Tn      | 1490 ± 90                     | 3.8 ± 0.2 | –         |
| 429410   | Tn      | 2460 ± 140                    | 6.2 ± 0.4 | –         |
| 429416   | Tn      | 1490 ± 90                     | 3.8 ± 0.2 | –         |
| Exposure 2: (11 500 ±200) kBq/h/m <sup>3</sup> |         |                               |           |           |
| 429408   | Tn      | 2470 ±190                     | 3.6 ± 0.3 | 3.5 ±0.3  |
| 429414   | Tn      | 3110 ±230                     | 4.6 ± 0.3 | 4.4 ± 0.3 |
| 429415   | Tn      | 2580 ±190                     | 3.8 ± 0.3 | 3.6 ± 0.3 |
| 429411   | Transit | <150                          |           |           |
| 429412   | Transit | <150                          |           |           |
| 4229413  | transit | 157 ±87                       |           |           |

The arithmetic mean of CI without subtracting transit detector signal was 4.3 %. There is some variance between individual detectors (range 3.6–6.2 %).

## Conclusion

All measured cross-interferences by thoron gas on the radon result were below 20 %, which is defined as maximum by standard IEC 61577-2.

Detectors from one manufacturer exhibited larger than average differences between detectors. This is probably due to differences in the detector housing: the gap via which radon enters the detection chamber effects greatly on thoron entry.



16ENV10 MetroRADON

Deliverable D2

Annex VIII

Task A.2.2.2

Study of the influence of thoron on  
passive radon detectors

Ivelina Dimitrova, Strahil Georgiev  
SUBG

## Studied detectors

The studied passive radon devices are based on solid state alpha track detectors, which is currently the most common type of detector used in radon surveys in Europe [1]. The study included the following commercial passive radon monitors (diffusion chambers with CR-39 detector): RSKS and Raduet by Radosys, Radtrak<sup>2</sup>, RapiDOS and Duotrak by Radonova. For most of them no data for the influence of thoron was found in the literature or in the public documentation of the producer. In addition, 3 types of in-house diffusion chambers were tested: 1 designed by SUBG, Sofia (with Kodak-Pathe LR115-II) and 2 designed by ISS, Italy (with CR-39). The thoron protection of these detectors mainly relies on the diffusion of thoron through thin air gaps. Additionally, the thoron influence on the detector track density could be affected by the thoron and thoron progeny distribution inside the chamber and the registration efficiency of the track detector. One type of diffusion chamber (designed by ISS) was studied both bare and packed in low density polyethylene with thickness 35  $\mu\text{m}$ .

Two types detectors based on alpha track detection in DVD were also studied: a DVD etched at a depth greater than 80  $\mu\text{m}$  and a DVD coupled with an external radon absorber.

## Methodology

The influence of thoron on the radon signal was studied by exposure of the detectors to high integrated activity of thoron. The detectors of each type were then processed using the specific protocol for radon measurement and the integrated radon activity concentration was reported.

The influence of thoron on the radon signal was quantified by the cross-interference  $CI$ :

$$CI = \frac{E_n}{E_{Tn}} \times 100\%, \quad (1)$$

where  $E_{Rn}$  is the reported integrated radon activity, corrected for background and  $E_{Tn}$  is the integrated thoron activity concentration during the exposure.

The exposures were carried out at the exposure system at SUBG, Bulgaria [2]. The main components of the system are a flow through  $^{228}\text{Th}$  source (Pylon Electronics Inc., Canada), peristaltic pump, 50 L exposure vessel (AlphaGUARD calibration chamber), active radon and thoron monitor AlphaGUARD PQ2000 PRO RnTn and a thermostatic chamber in which the exposure vessel is placed. The activity concentration of thoron in the system is adjusted by changing the air flow rate through the source. The exposures were carried out in a closed system in which air from the pump consecutively passes through a drier, the flow-through source, a flow-rate meter and then enters the exposure vessel. With the help of a tube, the inlet of the exposure vessel is positioned below a fan mounted on the lid of the vessel. In the conducted exposures the activity concentration in the exposure vessel was monitored continuously by the AlphaGUARD monitor. This monitor was calibrated against the LNHB primary thoron standard at IRSN in the frames of the calibration exercise organized within Activity 2.1.2 of the MetroRADON project.

The integrated thoron activity concentration that was used during the exposures was between 2.5 and 14  $\text{MBq}\cdot\text{h}/\text{m}^3$ . The exposures were carried out under typical indoor conditions. The temperature during each exposure was kept constant at 21°C. More details about the exposure conditions during the exposure of each detector type are provided in the results section.

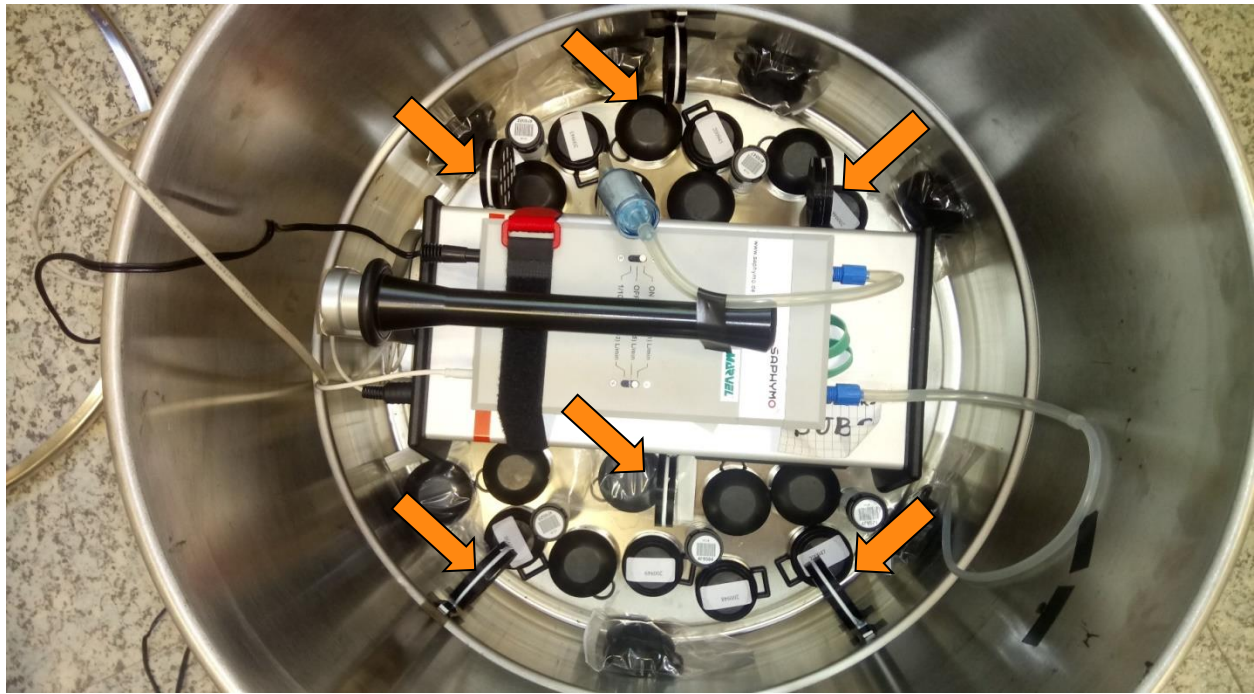


Figure 1 – Positioning of the detectors in the exposure vessel. The detectors of each type are spread at the bottom around the reference monitor. The inlet of the monitor is placed near the detectors. The arrows mark the positions of the aerogel samplers used to verify the homogeneity of the thoron activity concentration.

The homogeneity of thoron in the exposure vessel was ensured in several ways. First, an exposure vessel with a relatively small volume was used (about 50 l). Second, a fan was used to mix the air in the exposure vessel and the inlet of the vessel was positioned right below the fan. During each exposure, the homogeneity of the thoron activity concentration in the chamber was tested by measurements with aerogel samplers (for details see Annex I). At least 6 samplers were positioned between the detectors in each exposure (see Fig. 1). The thoron inhomogeneity was estimated to be within 4 % (values for the separate exposures are given in the results section).

In order to reduce the effect of differences in the air circulation in the exposure vessel, more than one detector of each type was exposed in each exposure session (between 2 and 8 identical detectors depending on the detector type). All detectors were positioned at the bottom of the exposure vessel (see Fig. 1) and the identical detectors of each type were spread evenly. Most types of detectors were exposed in 2 independent exposure sessions at different activity concentrations.

For each type of detector one or more transit detector was provided. The packaging of the transit detectors was removed right at the end of the exposure of the other detectors in the set. The exposed detectors were taken out of the vessel and were stored and shipped together with the transit detectors. The detectors were analysed by the laboratory that provided them. In all cases the reported signal of the transit detectors of a given type was the same within the uncertainties. The background signal for each detector type was estimated as an average of the transit detectors' signal. A critical level was estimated based on the approach of Currie [3]:

$$L_c = ku_b \sqrt{\left(1 + \frac{S_b}{S}\right)}, \quad (2)$$

where  $k$  is the coefficient for one-sided confidence interval ( $k = 1.65$  for 95 % confidence level was used),  $u_b$  is the uncertainty of the background track density,  $S_b$  is the area of the etched surface of the background detectors and  $S$  of the exposed detectors.

In cases in which the detector signal did not exceed the critical level the less-than level was estimated:

$$L_t = \text{"net"} + \sqrt{k^2 \text{"net"} + L_c^2}, \quad (3)$$

where "net" is the observed net signal (the formula is valid when the same confidence level is used for both  $L_c$  and  $L_t$ ). If "net" is negative, then  $L_t = L_c$  is assumed.

The level  $L_t$  was then used to estimate the minimum detectable integral of the activity concentration (MDAC):

$$MDAC = \frac{L_t}{CF} \text{ [kBq. h/m}^3\text{]}. \quad (4)$$

where  $CF$  is the relevant calibration factor for radon measurement.

## Results

### RSKS detector

The RSKS detector is a diffusion chamber with a CR-39 alpha track detector produced by Radosys, Ltd. The detectors for the current study were provided and analysed by LaRUC, Spain. A photo and a scheme of the detector are presented in Fig.2. The results for the individual  $CI$  of the exposed detectors and the integrated activity concentration in the two exposures are shown in Fig. 3. The average value (and the standard deviation) of the  $CI$  is 4.80(0.65) %.



Figure 2 – RSKS passive radon detector. The indicated dimensions are in mm. (source: <http://www.radosys.com/rsks.htm>)

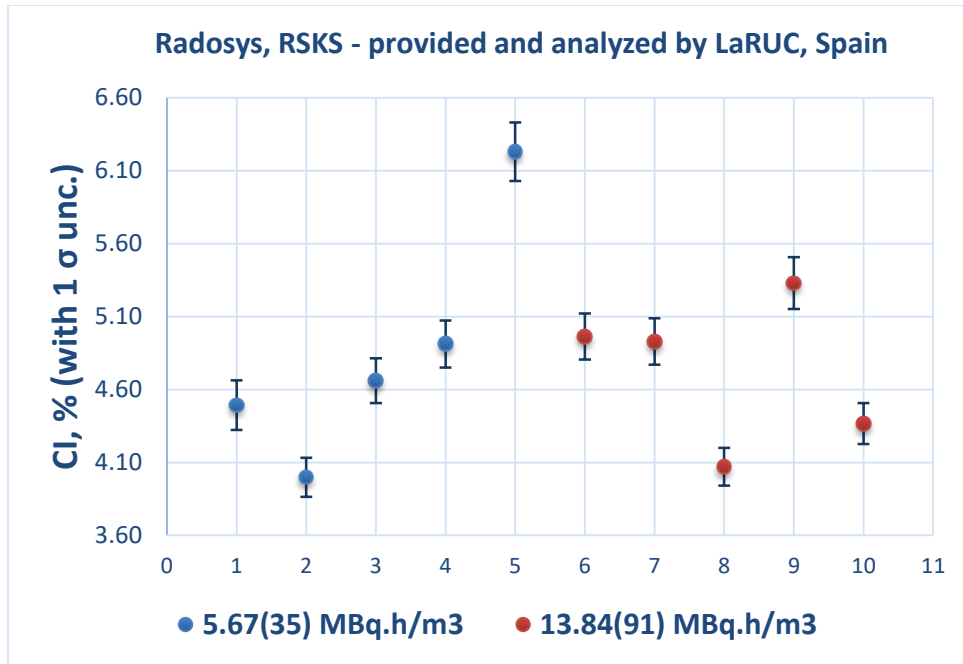


Figure 3 – Cross interference of thoron in RSKS passive radon detectors. The bars represent the absolute uncertainties at the level of 1  $\sigma$ . The first exposure (blue points) was at temperature 21°C, pressure 952 mbar and relative humidity 53%. The estimated thoron inhomogeneity during the exposure was 2.2 %. The second exposure (red points) was at temperature 21°C, pressure 947 mbar and relative humidity 43%. The estimated thoron inhomogeneity during the exposure was 3.6 %. The integrated activity concentration is given in the legend.

*In-house detector by ISS, Italy (CR-39 by Intercast Spa in TASL holder)*

The detector is a diffusion chamber with a CR-39 alpha track detector produced by Intercast Spa, Italy in a holder produced by TASL. The chamber has the shape of a spherical cap with a diameter of about 5 cm and a height of about 2 cm. The detectors for the current study were provided and analysed by ISS (the Italian National Institute of Health). The results for the individual *CI* of the exposed detectors and the integrated activity concentration in the two exposures are shown in Fig. 4. The average value (and the standard deviation) of the *CI* is 9.35(0.93) %.

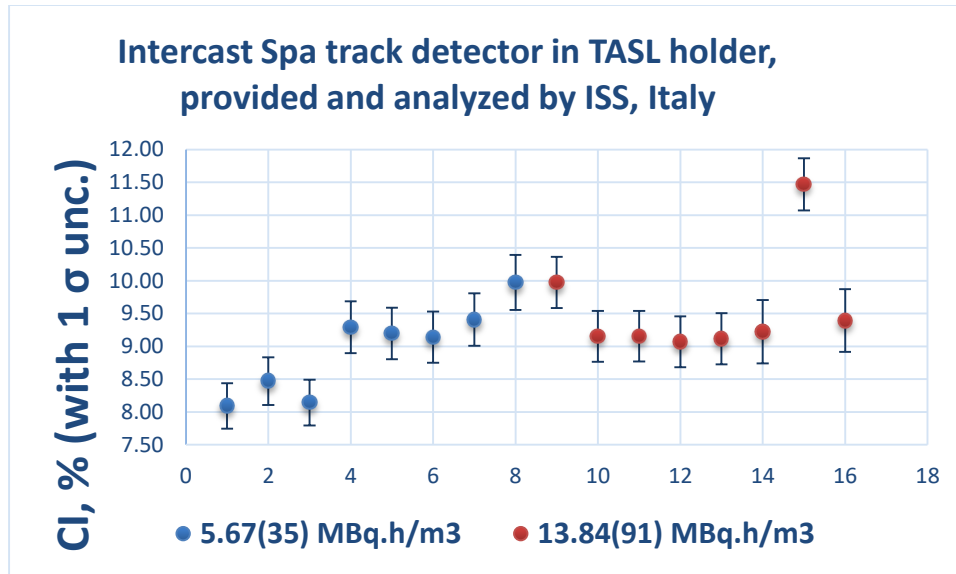


Figure 4 – Cross interference of thoron in the ISS in-house detector based on CR-39 in TASL holder. The bars represent the absolute uncertainties at the level of 1  $\sigma$ . The first exposure (blue points) was at temperature 21°C, pressure 952 mbar and relative humidity 53%. The estimated thoron inhomogeneity during the exposure was 2.2 %. The second exposure (red points) was at temperature 21.0°C, pressure 947 mbar and relative humidity 43%. The estimated thoron inhomogeneity during the exposure was 3.6 %. The integrated activity concentration during the exposures is given in the legend.

*In-house detector by ISS, Italy (CR-39 by Intercast Spa in Radout holder)*

The detector is a diffusion chamber with a CR-39 alpha track detector produced by Intercast Spa, Italy in a Radout holder by Mi.am, Italy. The chamber has the shape of a spherical cap with a diameter of 5 cm and a height of 2 cm. The detectors for the current study were provided and analysed by ISS (the Italian National Institute of Health). The results for the individual *CI* of the exposed detectors and the integrated activity concentration in the two exposures are shown in Fig. 5. The average value (and the standard deviation) of the *CI* is 4.48(0.55)%.

Another set of the same detector was exposed packed in 35-micron-thick low-density polyethylene. It has been previously shown that this approach greatly reduces the sensitivity to thoron [4]. Recent studies of the transport of radon gas through polyethylene also show that at a temperature of 21°C the diffusion length of radon in polyethylene is about 16  $\mu\text{m}$  [5]. The results for the individual *CI* of the packed detectors and the integrated activity concentration in the two exposures are shown in Fig. 6. The signal of five of the 16 exposed detectors exceeded the detection limit. The average value (and the standard deviation) of the *CI* of these five detectors is 0.23(0.14) %.

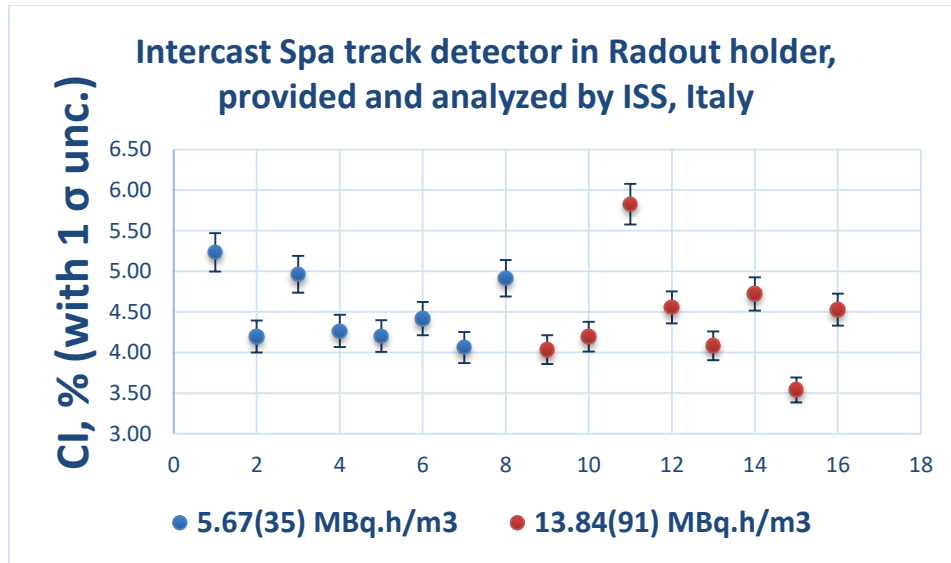


Figure 5 – Cross interference of thoron in the ISS in-house detector based on CR-39 in Radout holder. The bars represent the absolute uncertainties at the level of 1  $\sigma$ . The first exposure (blue points) was at temperature 21°C, pressure 952 mbar and relative humidity 53%. The estimated thoron inhomogeneity during the exposure was 2.2 %. The second exposure (red points) was at temperature 21°C, pressure 947 mbar and relative humidity 43%. The estimated thoron inhomogeneity during the exposure was 3.6 %. The integrated activity concentration during the exposures is given in the legend.

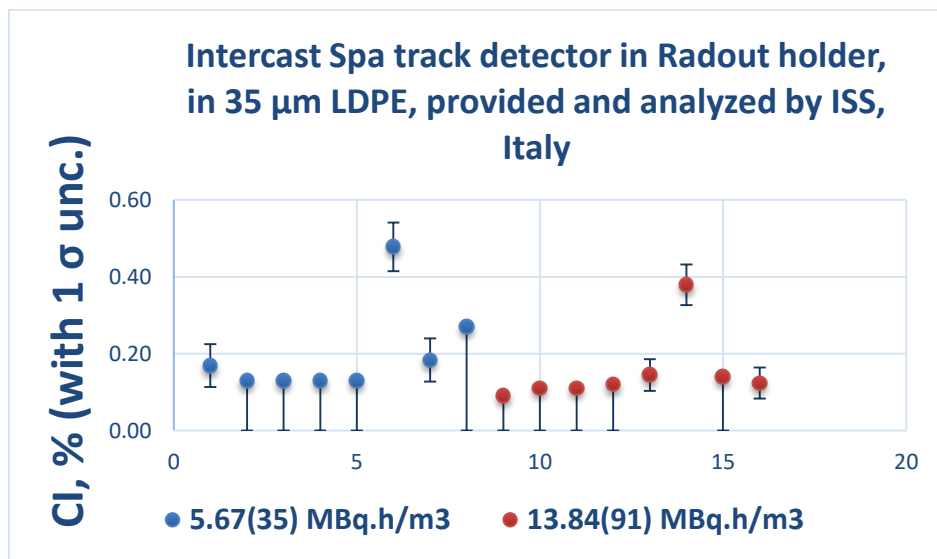


Figure 6 – Cross interference of thoron in the ISS in-house detector based on CR-39 in Radout holder packed in LDPE. The bars represent the absolute uncertainties at the level of 1  $\sigma$ . Where the signal does not exceed the detection limit the maximum value of the *CI* is given (numbers 2 to 5, 8 to 12 and 15). The first exposure (blue points) was at temperature 21°C, pressure 952 mbar and relative humidity 53%. The estimated thoron inhomogeneity during the exposure was 2.2 %. The second exposure (red points) was at temperature 21.°C, pressure 947 mbar and relative humidity 43%. The estimated thoron inhomogeneity during the exposure was 3.6 %. The integrated activity concentration during the exposures is given in the legend.

### Radtrak<sup>2</sup> detector

The Radtrak<sup>2</sup> detector is a diffusion chamber with a CR-39 alpha track detector produced by Radonova Laboratories AB. The chamber has the shape of a spherical cap with a diameter of 5.4 cm and a volume of 25 cm<sup>3</sup>. The chamber has an inner compartment limiting the volume from which alpha-particles reach the detector (Fig.7). The detectors for the current study were provided and analysed by Radonova Laboratories AB. The results for the individual *CI* of the exposed detectors and the integrated activity concentration in the two exposures are presented in Fig. 8. The average value (and the standard deviation) of the *CI* is 1.93(0.39)%.



Figure 7 – An open Radtrak<sup>2</sup> detector.

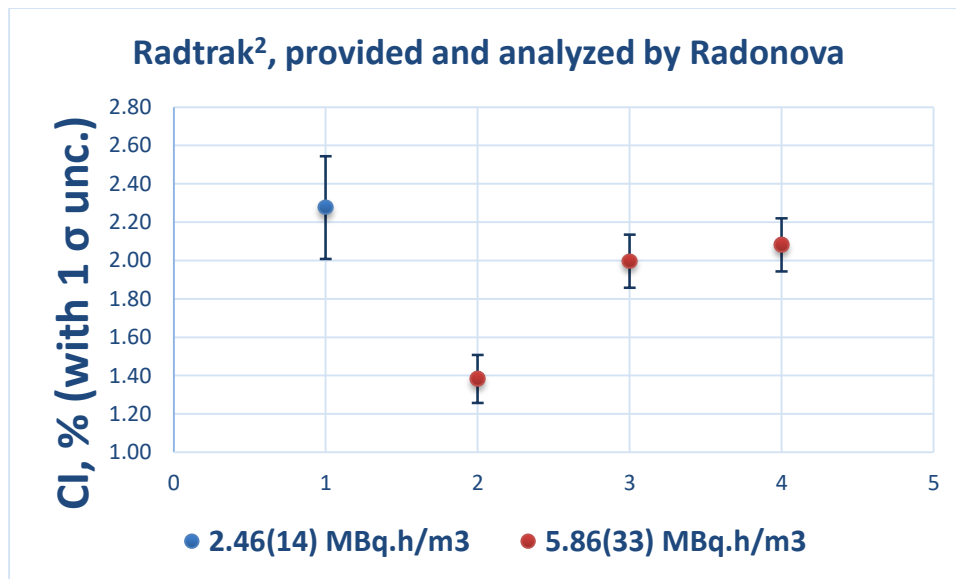


Figure 8 – Cross interference of thoron in Radtrak<sup>2</sup> passive radon detectors. The bars represent the absolute uncertainties at the level of 1  $\sigma$ . The first exposure (blue points) was at temperature 21°C, pressure 947 mbar and relative humidity 32%. The estimated thoron inhomogeneity during the exposure was 2.4 %. The second exposure (red points) was at temperature 21°C, pressure 945 mbar and relative humidity 31%. The estimated thoron inhomogeneity during the exposure was 2.4 %.

### Rapidos detector

The Rapidos detector is a diffusion chamber with a CR-39 alpha track detector produced by Radonova Laboratories AB. The chamber has the shape of a spherical cap with a diameter of 5.4 cm and a volume of 65 cm<sup>3</sup>. The chamber has inner partitions (Fig.9). The detectors for the current study were provided and analysed by Radonova Laboratories AB. The results for the reported integrated radon activity concentration were below the detection limit (see Table 1). The upper limit for the *CI* was estimated at 0.57 % based on the MDAC (Eq. (4)).



Figure 9 – An open Rapidos detector.

Table 1. Results for Rapidos detectors exposed at 2460 (140) kBq.h/m<sup>3</sup> integrated thoron activity concentration at temperature 21 °C, pressure 947 mbar and relative humidity 32%. The estimated thoron inhomogeneity during the exposure was 2.4 %.

| Rapidos                     | Reported radon exposure             |  | MDAC                                   | Cross interference |             |
|-----------------------------|-------------------------------------|--|--|--------------------|-------------|
|                             | $E_{Rn}$<br>(kBq.h/m <sup>3</sup> ) | $u(E_{Rn})$<br>(kBq.h/m <sup>3</sup> )<br>(k =1) | $Enet_{Rn}$<br>(kBq.h/m <sup>3</sup> ) | <i>CI</i> , %      | $u(CI)$ , % |
| <b>134832-5<br/>(blank)</b> | 66                                  | 6  | -                                      |                    |             |
| <b>126927-1</b>             | 55                                  | 6  | < 14                                   | <b>&lt; 0.57</b>   | -           |
| <b>135752-4</b>             | 73                                  | 7  | < 14                                   | <b>&lt; 0.57</b>   | -           |
| <b>130957-4</b>             | 63                                  | 6  | < 14                                   | <b>&lt; 0.57</b>   | -           |

### Duotrak detector

The Duotrak detector is a diffusion chamber with two CR-39 alpha track detectors produced by Radonova Laboratories AB. The chamber has an ON and an OFF position and can be rotated between the two. At each position only one of the detectors faces the interior of the chamber, while the other is

positioned below a cover. The chamber has the shape of a spherical cap with a diameter of 5.4 cm and a volume of 60 cm<sup>3</sup>. Visually the air gap of this chamber is wider than these in the Radtrak<sup>2</sup> and the RapiDOS detectors, possibly because of the rotating mechanism. The detectors for the current study were provided and analysed by Radonova Laboratories AB. The results for the individual *CI* of the exposed are presented in Table. 2. The average value (and the standard deviation) of the *CI* for the detector in the OFF position is 1.75(0.06) %. The two detectors in the ON position gave different results for the *CI*: 11.5(1.3) % and 4.07(0.64) %.

Table 2. Detectors exposed at 2460 (140) kBq.h/m<sup>3</sup> integrated thoron activity concentration at temperature 20.8 °C, pressure 947 mbar and relative humidity 32%. The estimated thoron inhomogeneity during the exposure was 2.4 %. Absolute uncertainties at the level of 1  $\sigma$  are reported.

| Duotrak ON                            | Reported radon exposure                  |   |  |   | Cross interference |             |
|---------------------------------------|--|---|--|---|--------------------|-------------|
|                                       | $E_{Rn}$<br>(k Bq h<br>m <sup>-3</sup> ) | $u(E_{Rn})$<br>(k Bq h<br>m <sup>-3</sup> )           | $E_{net_{Rn}}$<br>(k Bq h<br>m <sup>-3</sup> ) | $u(E_{net_{Rn}})$<br>(k Bq h<br>m <sup>-3</sup> ) | <i>CI</i> , %      | $u(CI)$ , % |
| <b>539771-6<br/>(blank)</b>           | 70                                       | 7   | -  | -   |                    |             |
| <b>539310-3</b>                       | 352                                      | 26  | 282  | 26.9  | <b>11.5</b>        | <b>1.3</b>  |
| <b>539770-8</b>                       | 170                                      | 13  | 100  | 14.8  | <b>4.07</b>        | <b>0.64</b> |
|                                       |  |   |  |   |                    |             |
| Duotrak OFF                           | Reported radon exposure                  |   |  |   | Cross interference |             |
|                                       | $E_{Rn}$<br>(k Bq h<br>m <sup>-3</sup> ) | $u(E_{Rn})$<br>(k Bq h<br>m <sup>-3</sup> )<br>(k =1) | $E_{net_{Rn}}$<br>(k Bq h<br>m <sup>-3</sup> ) | $u(E_{net_{Rn}})$<br>(k Bq h<br>m <sup>-3</sup> ) | <i>CI</i> , %      | $u(CI)$ , % |
| <b>539771-6<br/>(blank)</b>           | 11                                       | 4   | -  | -   |                    |             |
| <b>539310-3</b>                       | 55                                       | 6   | 44   | 7.2   | <b>1.79</b>        | <b>0.31</b> |
| <b>539770-8</b>                       | 53                                       | 6   | 42   | 7.2   | <b>1.71</b>        | <b>0.31</b> |
| <b>Average and standard deviation</b> |  |   |  |   | <b>1.75</b>        | <b>0.06</b> |

#### Raduet detector

The Raduet detector consists of two separate diffusion chambers each with a CR-39 alpha track detector produced by Radosys, Ltd. The chambers have the shape of spherical caps with a diameter of about 5 cm and a volume of 25 cm<sup>3</sup>. One of the chambers is closed tightly and the air enters through a thin gap. This chamber has low-air exchange rate and has low sensitivity to thoron [6]. The other chamber has holes on its side which are covered by electro-conductive sponge. This chamber has high air exchange rate and both thoron and radon contribute to the signal of its detector. The electro-conductive sponge acts as a filter for the radon and thoron progenies in the air. The detectors are mounted in the same holder and are intended to be used as a pair. When the results of the Raduet detectors exposed in the current study were analysed as a pair, the result for the radon activity concentration was below the detection

limit. When the results of the low air exchange chamber were analysed separately, the thoron cross interference for this chamber was estimated at 1.76(30) %. This value is in a good agreement with the value of 1.75 that could be estimated from Ref. [7] as a ratio of the calibration factors for thoron and radon of this chamber. The results for the individual *CI* of the low air exchange rate of the Raduet detector are presented in Fig. 10.

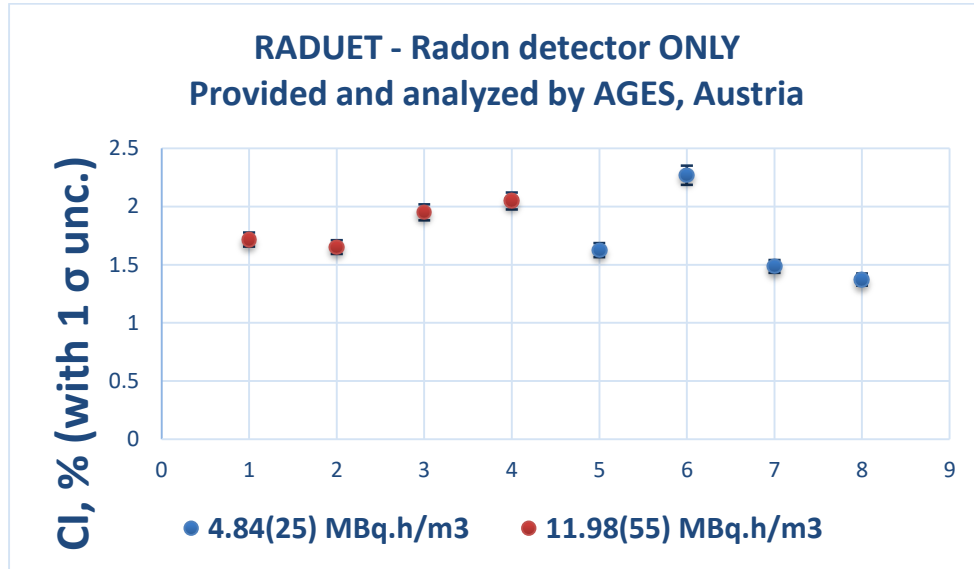


Figure 10 – Cross interference of thoron of Raduet passive radon detectors when only the signal of the low air exchange chamber of the pair is analysed. The bars represent the absolute uncertainties at the level of 1  $\sigma$ . The first exposure (blue points) was at temperature 21°C, pressure 938 mbar and relative humidity 54%. The second exposure (red points) was at temperature 21°C, pressure 948 mbar and relative humidity 48%.

#### *SUBG diffusion chamber*

The in-house diffusion chamber of SUBG is a metal chamber with an alpha track detector Kodak-Pathe LR115/II. The chamber has the shape of a cylinder with a volume of about 290 cm<sup>3</sup>. The chamber is tightly closed with a lid that leaves a very thin air gap. Two exposures of a total of 8 detectors were carried out. The first exposure was at 4840 (250) kBq.h/m<sup>3</sup> integrated thoron activity concentration at temperature 21 °C, pressure 938 mbar and relative humidity 54%. The second exposure was at 11980 (550) kBq.h/m<sup>3</sup> integrated thoron activity concentration at temperature 21 °C, pressure 945 mbar and relative humidity 49%. The track detectors were analysed at SUBG. The results for the reported integrated radon activity concentration were below the detection limit. The upper limit for the *CI* was estimated at 0.29 % based on the MDAC (Eq. (4)).

#### *DVD detector*

The DVD (or CD) is a detector in which radon is absorbed and the tracks developed at a depth greater than 80  $\mu\text{m}$  are only due to the absorbed radon and its progeny. Due to its short half-life, thoron stays within the first 1 $\mu\text{m}$  below the disk surface and the alpha-particles of thoron and its progeny do not form tracks below 79  $\mu\text{m}$  (see Table 3). Previous studies have not detected thoron influence on the radon signal [8].

Two exposures of a total of 7 detectors were made. The disks were electrochemically etched and analysed at SUBG. The first exposure was at 4840 (250) kBq.h/m<sup>3</sup> integrated thoron activity concentration at temperature 21 °C, pressure 938 mbar and relative humidity 54%. The second exposure was at 11980 (550) kBq.h/m<sup>3</sup> integrated thoron activity concentration at temperature 21 °C, pressure 945 mbar and relative humidity 49%. The track detectors were analysed at SUBG. The results for the reported integrated radon activity concentration were below the detection limit. The upper limit for the *CI* was estimated at 1.6 % based on the MDAC (Eq. (4)).

Table 3. Estimated thickness of polycarbonate that reduces the alpha-particle energies to the registration energy range of the Makrofol DE track detector (0.3 – 1.7 MeV) at an incident angle below 50°. The ranges in the polycarbonate are calculated with the ASTAR program (<http://physics.nist.gov/PhysRefData/Star/Text/ASTAR.html>).

| Nuclide                                     | <sup>222</sup> Rn | <sup>218</sup> Po | <sup>214</sup> Po | <sup>220</sup> Rn | <sup>216</sup> Po | <sup>212</sup> Bi | <sup>212</sup> Po |
|---|-------------------|-------------------|-------------------|-------------------|-------------------|-------------------|-------------------|
| Initial energy, MeV                         | 5.49              | 6.00              | 7.69              | 6.29              | 6.78              | 6.1               | 8.79              |
| Interval of length in which is detected, μm | 18.9<br>35.2      | 22.4<br>40.7      | 35.7<br>61.4      | 24.6<br>44.0      | 28.3<br>49.8      | 22.8<br>41.3      | 45.6<br>76.8      |

#### *DVD detector with an external absorber*

More recently, a new more sensitive version of the CD/DVD method was developed in which external radon absorber is used [9]. The absorber is made of two thin Makrofol N foils (with thickness of about 40 μm) which are characterized with high radon partition coefficient. The alpha-particles of radon and its progeny absorbed in the foils are registered at the surface of the disk. The disks are exposed in thin DVD cases, so that the air gaps between the disk and the foils are very small. The holes through which air enters in the DVD cases are relatively large (with thickness of about 1 mm and width of about 1 cm) compared to the gaps in the studied diffusion chambers. The influence of thoron on the signal of the disks is reduced by the diffusion of thoron inside the case (see Fig.11) and the energy dependence of the registration efficiency of the DVD (close to zero outside the range 0.3 – 1.7 MeV). In order to lower their energy sufficiently, the alpha particles of thoron and its progeny should travel a certain distance in the foils (see Table 3).

Two exposures of a total of 8 detectors were made. The disks were electrochemically etched and analysed at SUBG. The results for the individual *CI* of the exposed DVD detectors and the integrated activity concentration in the two exposures are presented in Fig. 12. The observed values of the *CI* ranged from 3.3 to 10.5 %. This large variance can be attributed to the large gaps in the DVD case which allow the air circulation in the exposure vessel to influence the transport of thoron. This hypothesis is supported by the visible inhomogeneity of the track density on the DVD surface.

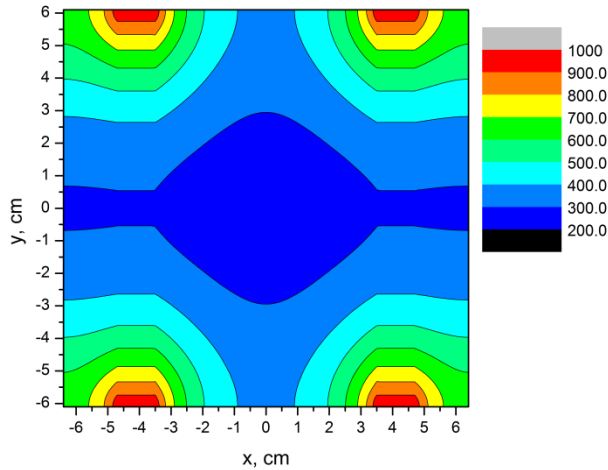


Figure 11 – Thoron distribution in a DVD case due to diffusion (relative scale in which 1000 is the outside activity concentration). The air enters through 4 holes on the sides. The disk inside the case has a radius of 5 cm. The surface in which the tracks are usually developed has the shape of a ring with inner radius of about 2 cm and outer radius of about 4 cm. The assumed diffusion coefficient of radon/thoron at room temperature is  $D = 0.13 \text{ cm}^2/\text{s}$  corresponding to thoron diffusion length  $L_D = 3.2 \text{ cm}$ .

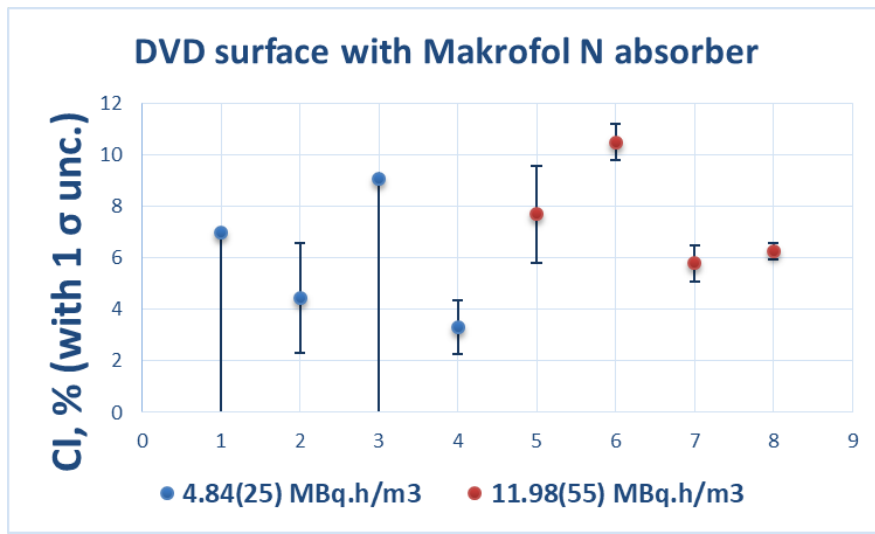


Figure 12 – Cross interference of thoron in DVD + absorber of 2 Makrofol N foils with thickness of about  $40 \mu\text{m}$ . The bars represent the absolute uncertainties at the level of  $1 \sigma$ . Where the signal does not exceed the detection limit the maximum value of the  $CI$  is given (numbers 1 and 3). The first exposure (blue points) was at temperature  $21^\circ\text{C}$ , pressure 938 mbar and relative humidity 54%. The second exposure (red points) was at temperature  $21^\circ\text{C}$ , pressure 945 mbar and relative humidity 49%. The integrated activity concentration during the exposures is given in the legend.

### Comparison with a simple model

The studied diffusion chambers rely mainly on the slow entry of air through thin gaps to reduce the influence of thoron on the radon measurement. A simple model can be used to estimate the transmission factor of thoron  $R$  (defined as the ratio of the activity concentration outside and inside the

chamber) through a thin air gap. The model proposed in Ref. [10] for diffusion through a pin hole leads to the following equation for the transmission factor:

$$R = \left(1 + \frac{AD}{Vh}\right)^{-1}, \quad (5)$$

where  $A$  is the effective area of the pin hole,  $D$  is the diffusion coefficient or the permeability constant,  $V$  is the volume of the detector and  $h$  is the length of the pin hole.

It is clear that the cross interference of thoron ( $CI$ ) on the radon signal could not be predicted solely by the transmission factor. The  $CI$  is also influenced by the thoron and thoron progeny distribution inside the chamber and the energy dependence of the registration efficiency of the track detector. Since thoron diffusion length in air at room temperature is about 3 cm, the distribution of thoron inside the studied diffusion chambers is not homogenous. The thoron progenies also would not be homogeneously deposited on the inner walls. The activity will be higher near the air gap of the chamber which in all studied diffusion chambers was around the side at which the track detector is placed. The activity distribution will affect the energies with which the emitted alpha particles reach the track detector. Table 4 shows the initial energies of the alpha particles of radon, thoron and its progeny and the travel distance in air after which their energy is reduced below 5 MeV. For energies higher than 5 MeV the CR-39 registration efficiency is reduced (the actual value depends on the etching regime) and the LR115/II registration efficiency is close to zero. On average the alpha particles of thoron and its progeny will reach the detector with higher energies than these of radon and its progeny, since they have higher initial energies and on average pass through a thinner layer of air. This should result in lower sensitivity to thoron than to radon. However, due to the complex geometry of the inner volume of the diffusion chambers, it is hard to carry out a precise calculation of the cross interference of thoron.

In Table 5 the thoron cross interference  $CI$  and the transmission factor of thoron  $R$  are compared for some of the chambers for which a rough estimate of  $R$  could be made by measurement of the parameters in Eq.(5). As it could be seen, there is some correlation between the values of  $CI$  and  $R$ . However, the  $CI$  cannot be predicted by such a simple model. It is recommended that the thoron cross interference for each type of detector is studied experimentally.

Table 4. The thickness of air that reduces the energies of the alpha-particles of radon, thoron and their progenies to energy below 5 MeV (calculated with the ASTAR program - <http://physics.nist.gov/PhysRefData/Star/Text/ASTAR.html>).

| Nuclide                                       | <sup>222</sup> Rn | <sup>218</sup> Po | <sup>214</sup> Po | <sup>220</sup> Rn | <sup>216</sup> Po | <sup>212</sup> Bi | <sup>212</sup> Po |
|---|-------------------|-------------------|-------------------|-------------------|-------------------|-------------------|-------------------|
| Initial energy , MeV                          | 5.49              | 6                 | 7.69              | 6.29              | 6.78              | 6.1               | 8.79              |
| Travel distance in air for energy < 5 MeV, cm | 0.55              | 1.2               | 3.5               | 1.5               | 2.2               | 1.3               | 5.2               |

Table 5. The transmission factor of thoron  $R$  at room temperature (rough estimate with Eq.(5)) and the measured thoron cross interference  $CI$  for several radon diffusion chambers. The Radtrak<sup>2</sup> and Rapidos detectors have the same air gap, but Rapidos has a bigger volume. The Duotrak detector has a wider air gap than the rest. For all detectors the transmission factor of radon at room temperature was close to 100 %.

| Detector   | $R$ , % | $CI$ , %     |
|--|---------|--------------|
| <b>RSKS (29 cm<sup>3</sup>)</b>                  | 10      | 4.8          |
| <b>Radtrak<sup>2</sup> (25 cm<sup>3</sup>)</b>   | 17      | 1.9          |
| <b>Rapidos (65 cm<sup>3</sup>)</b>               | 7       | < 0.57 (MDA) |
| <b>Duotrak - ON position (60 cm<sup>3</sup>)</b> | 20      | 4 - 12       |
| <b>SUBG metal chambers (290 cm<sup>3</sup>)</b>  | 2.0     | < 0.29 (MDA) |

### Summary of results

The results for the thoron cross interference ( $CI$ ) on the signal of the passive radon detectors studied at SUBG are summarized in Table 6 and Table 7. For all types of studied passive radon detectors the cross interference of thoron on the radon signal was below 20 %, which is the maximum defined by the standard IEC 61577-2.

A low cross interference could be achieved with diffusion chambers with different constructions (in terms of volume, dimensions and inner compartments). The cross interference cannot be predicted with the simple model of thoron penetration through an air gap.

When DVDs (or CDs) are used as radon detectors the radon signal is not influenced by thoron. This is due to the fact that alpha tracks are analysed at a depth greater than 80  $\mu\text{m}$  at which no alpha-particles of thoron and its progeny could reach. When the DVD surface is used as a track detector that faces an external radon absorber (Makrofol N foils) some sensitivity to thoron is observed.

The ISS diffusion chamber packed in low-density polyethylene with a thickness of 35  $\mu\text{m}$  showed very low thoron cross interference. A study of the transport of radon/thoron through polymer membranes [5] confirmed that low-density polyethylene has suitable properties for anti-thoron packaging.

For all types of detectors a very good agreement between the average values of the  $CI$  obtained in the different exposures was observed. However, the standard deviation of the values of the  $CI$  of individual detectors was higher than the estimated individual uncertainties. This could be due to the local differences in the air circulation at different points in the exposure chamber which might influence the rate of thoron entrance in the detector volume. Another possible explanation lies in the difference in the dimensions of the housing of the individual detectors. Such differences can be incurred in the production process. A small difference in the air gap of the housing could lead to a different thoron entrance rate. The general tendency was that the passive monitors with larger air gaps showed larger variance in the  $CI$ . It could be speculated that the air circulation in the exposure chamber leads to values for the  $CI$  that are higher than the  $CI$  when thoron enters the detector by diffusion.

There is a very good agreement between the results for the *CI* of the Raduet low air exchange rate chamber and the corresponding value that could be estimated from the literature.

There is a very good agreement between the results for the *CI* of the Radtrak<sup>2</sup> radon detector obtained at STUK and SUBG. This shows that the methodologies applied by the two laboratories are comparable.

## **Recommendations**

The recommendations on the procedures for studying thoron sensitivity of passive radon detectors are:

- The homogeneity of thoron activity concentration inside the exposure vessel should be tested during the exposure or with a similar exposure set-up (with the same positioning of the detectors, fans, reference monitors, etc.)
- More than one detector of each type should be exposed in each session, in order to reduce the influence of differences in the housing and in the air circulation. Detectors of the same type should be placed apart from each other. Correspondingly, it is better to conduct more than one independent exposure of each type of detector.

In addition, the following general recommendations could be made:

- No single construction of the studied radon diffusion chambers could be recommended over the others. In general, the chambers with smaller width of the air gaps (of the order of tenths of a millimetre) show lower thoron sensitivity.
- The thoron sensitivity should be studied experimentally for each specific detector type. It could not be predicted by the detector dimensions or simple modelling of the thoron transport.
- The results of such studies (including those presented in this report) should be viewed as an estimate for the thoron *CI* and not as a correction factor to be applied for measurements under diffusion mode.
- In places where significant thoron levels might be expected, polymer membranes can be used to reduce the thoron sensitivity of the detectors.

Table 6 – Cross interference (*CI*) of thoron on the radon signal for the diffusion chambers studied at SUBG. The average *CI*, the standard deviation and the *CI* range are given. Where the signal is below the detection limit an upper limit for the *CI* is given, based on the minimal detectable integrated activity concentration (MDAC) of radon. The *CI* for the Raduet detector was estimated only for the low air exchange rate chamber (not taking into account the result from the high air exchange rate chamber in the pair).

| Manufacturer and detector type   | Detector description   | Number of detectors and exposures | Cross interference , % |                   |                 |
|--|--|-----------------------------------|------------------------|-------------------|-----------------|
|  |  |                                   | av. <i>CI</i>          | <i>CI</i> st. dev | <i>CI</i> range |
| Radosys, RSKS Risk   | CR-39 in diffusion chamber, volume 29 cm <sup>3</sup> , height 5.5 cm                    | 8 detectors, 2 exposures          | 4.80                   | 0.65              | 4.00 – 6.23     |
| „In-house“ by ISS, Italy (CR-39 by Intercast Spa, Italy in TASL holder)            | PADC in diffusion chamber, diameter ≈ 5 cm, height ≈ 2 cm                                | 16 detectors, 2 exposures         | 9.35                   | 0.93              | 8.09 – 9.97     |
| „In-house“ by ISS, Italy (CR-39 by Intercast Spa, Italy in Radout holder)          | CR-39 in diffusion chamber, diameter 5 cm, height 2 cm                                   | 16 detectors, 2 exposures         | 4.48                   | 0.55              | 4.06 – 5.24     |
| „In-house“ by ISS, Italy (CR-39 by Intercast Spa, Italy in Radout holder) - packed | CR-39 in diffusion chamber packed in 35-micron-thick LDPE, diameter 5 cm, height 2 cm    | 16 detectors, 2 exposures         | 0.23                   | 0.14              | <0.13 – 0.48    |
| Radonova, Radtrak <sup>2</sup>   | CR-39 in diffusion chamber, volume 25 cm <sup>3</sup> , diameter 5.4 cm                  | 4 detectors, 2 exposures          | 1.93                   | 0.39              | 1.38 – 2.08     |
| Radonova, Rapidos  | CR-39 in diffusion chamber, volume 65 cm <sup>3</sup> , diameter 5.4 cm                  | 3 detectors, 1 exposure           | <0.57 (MDAC)           |                   |                 |
| Radonova, Duotrak (ON)   | CR-39 in diffusion chamber, volume 60 cm <sup>3</sup> , diameter 5.4 cm                  | 2 detectors, 1 exposure           | 7.8                    | 5.2               | 4.1 - 11.5      |
| Radonova, Duotrak (OFF)  | CR-39 in diffusion chamber, volume 60 cm <sup>3</sup> , diameter 5.4 cm                  | 2 detectors, 1 exposure           | 1.75                   | 0.32              | 1.71 – 1.79     |
| Radosys, Raduet – low air exchange rate chamber only                               | CR-39 in diffusion chamber, volume 25 cm <sup>3</sup> , diameter ≈ 5 cm, height ≈ 2.5 cm | 8 detectors, 2 exposures          | 1.76                   | 0.30              | 1.37 – 2.27     |
| SUBG metal chambers  | Kodak LR-115/II in diffusion chamber, volume 290 cm <sup>3</sup>                         | 8 detectors, 2 exposures          | <0.29 (MDAC)           |                   |                 |

Table 7 – Cross interference (*CI*) of thoron on the radon signal for the DVD-based detectors studied at SUBG. The average *CI*, the standard deviation and the *CI* range are given. Where the signal is below the detection limit an upper limit for the *CI* is given, based on the minimal detectable integrated activity concentration (MDAC) of radon.

| Manufacturer and detector type | Detector description  | Number of detectors and exposures | Cross interference ( <i>CI</i> ), % |                   |                 |
|--------------------------------|---|-----------------------------------|-------------------------------------|-------------------|-----------------|
|                                |   |                                   | av. <i>CI</i>                       | <i>CI</i> st. dev | <i>CI</i> range |
| DVDs at depth > 80 µm          | DVD used as alpha track detector and radon absorber   | 7 detectors, 2 exposures          | <1.6 (MDAC)                         |                   |                 |
| DVDs + radon absorbers         | DVD used as alpha track detector facing 2 foils of radon absorbing material (Markofol N), in a DVD case | 8 detectors, 2 exposures          | 6.3                                 | 2.5               | 3.3 - 10.5      |

**Acknowledgements:** The detectors used in the current study were kindly provided and analysed by Radonova Laboratories AB, LaRUC, Spain; ISS, Italy and AGES, Austria. We are very grateful to Tryggve Rönngqvist, Daniel Rabago, Gennaro Venoso and Gernot Wurm and their colleagues for their collaboration.

## References

- [1] G Pantelic et al, Literature review of Indoor radon surveys in Europe, Publications Office of the European Union, Luxembourg, 2018, ISBN 978-92-79-97643-8(online), doi 10.2760/977726 (online), JRC114370, JRC Technical Report
- [2] D. Pressyanov, K. Mitev, S. Georgiev, I. Dimitrova, J. Kolev., 2017. Laboratory facility to create reference radon þ thoron atmosphere under dynamic exposure conditions. J. Environ. Radioact. 166: p.181.
- [3] L. A. Currie, 1968. Limits for qualitative detection and quantitative determination: application to radiochemistry. Anal. Chem. 40: p.586.
- [4] F. Bochicchio, M. Ampollini, L. Tommasino, A. Sorimachi, S. Tokonami, 2009. Sensitivity to thoron of an SSNTD-based passive radon measuring device: Experimental evaluation and implications for radon concentration measurements and risk assessment. Radiat. Meas. 44: p. 1024.
- [5] S. Georgiev, K. Mitev, Ch. Dutsov, T. Boshkova, I. Dimitrova, 2019. Partition coefficients and diffusion lengths of <sup>222</sup>Rn in some polymers at different temperatures. Int J Environ Res Public Health 16(22): p.4523.
- [6] A. Sorimachi, S. Tokonami, Y. Omori, T. Ishikawa, 2012. Performance test of passive radon/thoron discriminative detectors on environmental parameters. Radiat. Meas. 47: p.438.

[7] Saïdou, S. Tokonami, M. Janik, B. G. Samuel, Abdourahimi, N. N. J. Emmanuel, 2015. Radon-thoron discriminative measurements in the high natural radiation areas of southwestern Cameroon. J. Environ. Radioact. 150: p.242

[8] D. Pressyanov, J. Buysseb, A. Poffijn, A. Van Deynse, G. Meesen, 2004. Integrated measurements of  $^{222}\text{Rn}$  by absorption in Makrofol. Nucl. Instrum. Meth. Phys. Res. A 516: p.203.

[9] D. Pressyanov, 2019. Highly sensitive passive detectors for short-term pre- and post- mitigation measurements. Conference: 33rd Annual International Radon Symposium, Denver, Colorado.

[10] B. K. Sahoo, B. K. Sapra, S. D. Kanse, J. J. Gaware, Y. S . Mayya, 2013. A new pin-hole discriminated  $^{222}\text{Rn}/^{220}\text{Rn}$  passive measurement device with single entry face. Radiat. Meas. 58: p.52.



# 16ENV10 MetroRADON

## Deliverable D2

### Annex IX

#### Activity A.2.2.2

Investigation of the influence of thoron on passive  
integrated radon detectors

Institut de Radioprotection et de Sûreté Nucléaire (IRSN)

N. MICHIELSEN

**EMPIR**



The EMPIR initiative is co-funded by the European Union's Horizon 2020 research and innovation programme and the EMPIR Participating States

## Table of contents

|                                  |   |
|----------------------------------|---|
| Object.....                      | 3 |
| Detectors .....                  | 3 |
| Material and method.....         | 3 |
| Exposure protocol.....           | 5 |
| Results.....                     | 5 |
| Cross-interference .....         | 7 |
| Conclusion.....                  | 8 |
| Annex 1: detectors position..... | 9 |

## Object

This report describes the tests performed at IRSN to study the influence of thoron on radon measurement of track-etch detectors sold in France. Two exposures were carried out, the first one was an exposure to only thoron (and no radon), the second a mixed of thoron and radon.

## Detectors

120 track-etch detectors were used, 6 different instruments from three manufacturers were involved in this tests (Table 1). In each exposure and type of instrument, 10 devices were used.

Table 1 - List of SNTD and characteristics

| Instrument name | manufacturer      | Detector type | configuration |
|-----------------|-------------------|---------------|---------------|
| DPR2            | ALGADE            | LR115         | closed        |
| DRF             | DOSIRAD/ALGADE    | LR115         | closed        |
| EASYRAD         | PEARL             | CR39          | closed        |
| KODALPHA        | DOSIRAD/ALGADE    | LR115         | open          |
| RADTRAK2        | LANDAUER/RADONOVA | CR39          | closed        |
| RAPIDOS         | LANDAUER/RADONOVA | CR39          | closed        |

## Material and method

Thoron and thoron plus radon atmosphere were created in the IRSN reference radon chamber called BACCARA. It consists of a one cubic meter stainless steel cylinder in which instruments to be tested can be placed together (Figure 1 and 2). This volume is connected to a  $^{222}\text{Rn}$  flow-through source and/or a  $^{220}\text{Rn}$  flow-through source (Pylon Electronic, Inc.). Clean pressurized air is used to transport the  $^{220}\text{Rn}$  and /or  $^{222}\text{Rn}$  to a mixing pipe for dilution and enters the bottom of the chamber. Thoron or thoron plus radon rich air circulate through the chamber continuously at a flow rate of about  $6 \text{ m}^3/\text{h}$  and a steady activity concentration is obtained after 10 min of the beginning of the injection. Detectors are placed on two shelves as shown in figure 2, positions of the detectors on the shelves are given in annex 1. Calibrated Rad7 517 and RAD7 2644 instruments are used to measure the activity concentration of thoron continuously. For the mixed thoron plus radon exposure, a calibrated alphaGUARD EF0831 is added to measure the activity concentration of  $^{222}\text{Rn}$ . It should be noted that interference of thoron on the radon activity concentration measured by the alphaGUARD might occur.

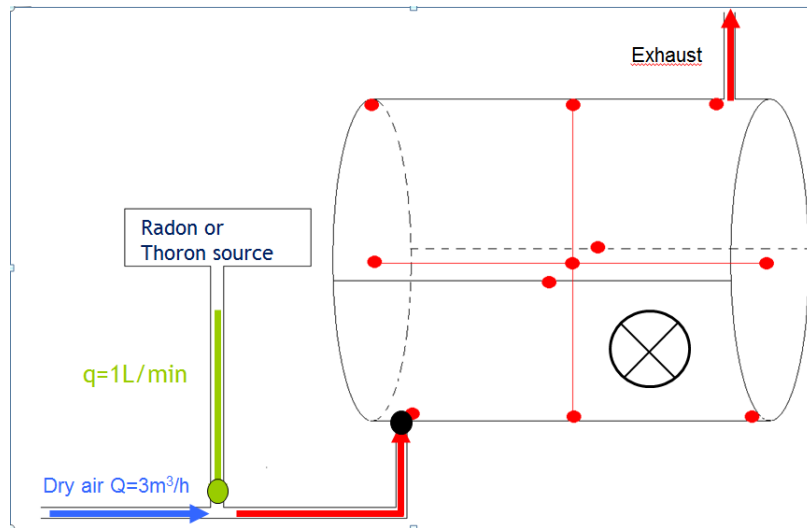


Figure 1 - Schematic diagram of the set-up



Figure 2 - Instruments in BACCARA

The homogeneity in the chamber was tested in A211 and instruments were placed in the homogeneous zone. Moreover, thoron activity concentration was measured on the middle of each shelves by placing the sample probe inlet of the two RAD7 (Figure 2) between the detectors.

## Exposure protocol

Only commercial detectors available in France were tested. Blind tests were performed, that means that the manufacturers did not know that the detectors were tested and even what kind of test was performed. Exposure protocol was as follow:

- prior exposure, detectors are kept in a low radon atmosphere (less than  $20 \text{ Bq.m}^{-3}$ ) ;
- for each type of detectors, 10 devices are prepared. That means that they are switched on exposed position: by opening the seal bags or opening the device (for Kodalpha) or switching the on button for DPR2 ;
- ten devices of each type of detectors are exposed together in BACCARA for 95 hours ;
- BACCARA is flushed with clean air for one hour;
- detectors are removed from the chamber, "switched" to closed configuration and kept in a low radon atmosphere before sending back to the laboratories.

It should be noted that the detectors were kept in a low radon atmosphere for about 6 month in switched off position (closed in sealed bag). The average radon activity concentration during this period was estimated to be  $15 \pm 11 \text{ Bq.m}^{-3}$ .

## Results

Table 2 shows the assigned values for thoron and radon exposure or integrated activity concentration measured by the two Rad7 and the alphaGUARD. Radon activity concentration during the exposure with only thoron is assumed to be negligible.

Table 2 - Reference values for thoron and radon

|                        | Exposure duration (h) | thoron exposure ( $\text{kBq.m}^{-3}.\text{h}$ ) | radon exposure ( $\text{kBq.m}^{-3}.\text{h}$ ) |
|------------------------|-----------------------|--|---|
| Thoron                 | 95                    | top $167 \pm 13$<br>low $161 \pm 13$             | /   |
| Mixed radon and thoron | 95                    | top $165 \pm 13$<br>low $170 \pm 13$             | $421 \pm 84$                                    |

Temperature during the exposure was  $22 \pm 1^\circ\text{C}$ , pressure was  $980 \pm 10 \text{ hPa}$  and the relative humidity was below 5%.

Figure 3 gives the radon measurement results of each device obtained during the thoron exposure, data are reported in annex 2. The error bars are those reported by the laboratories for an extended combined uncertainty of  $k=2$ . The vertical plain bars show that the result was reported as under the apparatus limit of detection.

One can observe that all Kodalpha devices report a high radon integrated activity concentration compared to the other instruments. Indeed, because of its bare LR115 directly exposed to the atmosphere (bare detector) this detector records alpha energy coming from the decay of radon, thoron and their decay products.

The other LR115 detectors, placed in a closed capsule, DPR2 and DRF, did not detect radon or thoron.

The systems using CR39 detectors, EasyRad, RapiDOS and Radtrak2 reported a small amount of radon with spread results for the EasyRad ( $\sigma=21 \text{ kBq}\cdot\text{m}^{-3}\cdot\text{h}$ ).

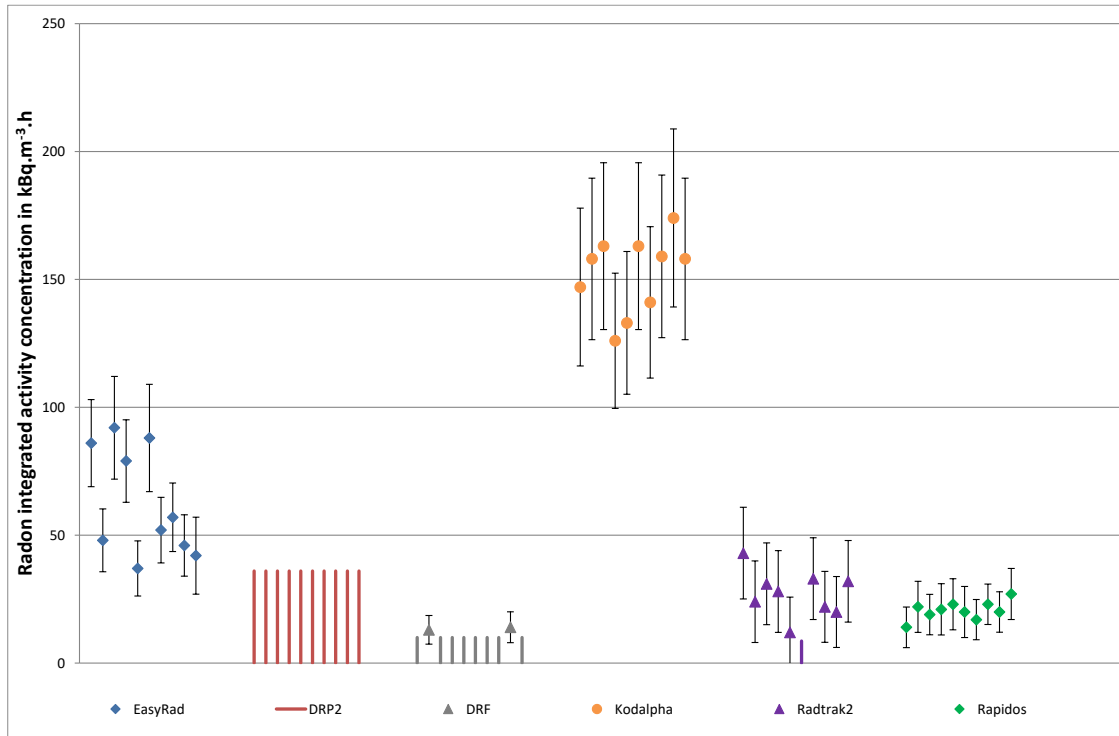


Figure 3 - Radon data measured by each device during the thoron exposure

Figure 4 gives the results for the exposure to a mixed radon and thoron atmosphere; data are reported in annex 3.

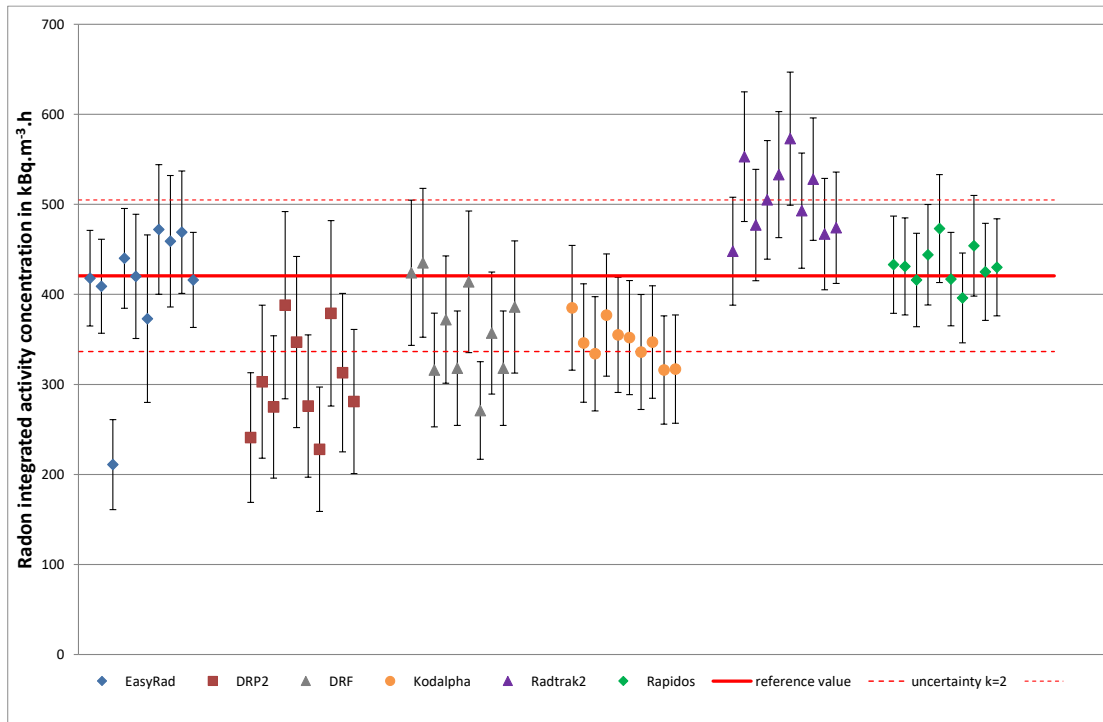


Figure 4 - Radon data measured by each device during the thoron+radon exposure

The influence of the thoron atmosphere on the radon exposure measurement cannot be seen in this exposure. In fact, taking into account the uncertainty of measurements, the device results are comparable to the reference value.

The thoron activity concentration was not high enough compared to the radon concentration and if thoron had an influence on the radon measurement, it might be hidden in the radon measurement uncertainties. Also, the Kodalpha was used outside of its application domain concerning the equilibrium factor. Manufacturer advises to use the Kodalpha in an environment where the equilibrium factor is around 0.4. In both exposure the equilibrium factor, F, is close to 0.006 where the response is about 1.7 times lower than for an F=0.4 (report IRSN PSN-RES/SCA/2017-00033). This correction factor (1.7) was not taken into account in figure 4. Therefore the results of this exposure will not be used to determine a quantitative value of the thoron interference on the radon measurement, also called cross-interference.

For further test with mixed thoron/radon atmosphere, in the aim of determining a cross-interference coefficient, we recommend to use the same level or higher concentration of thoron than radon.

## **Cross-interference**

The influence of thoron on the radon signal was quantified by the cross-interference  $CI$ :

$$CI = \frac{E_{Rn}}{E_{Tn}} \times 100\%,$$

where  $E_{Rn}$  is the reported integrated radon activity concentration corrected for background and  $E_{Tn}$  is the integrated thoron activity concentration during the exposure to the thoron atmosphere.

The background is estimated to be equal to  $20 \times 95 = 1.9 \text{ kBq.m}^{-3} \cdot \text{h}$

The arithmetic mean, the standard deviation and the min and max of  $CI$ , obtained in the thoron exposure, are given in table 3.

Table 3- Cross-interference data in thoron atmosphere

| Detector type /<br>Manufacturer | Detector description  | Number of<br>detectors and<br>exposures | Cross interference (CI) , % |         |          |
|---------------------------------|---|---|-----------------------------|---------|----------|
|                                 |   |   | av. CI                      | st. dev | CI range |
| <b>DPR2 / ALGADE</b>            | LR-115 in diffusion chamber (dome shape)                                | 10 detectors, 1 exposure                | /                           | /       | /        |
| <b>DRF / ALGADE</b>             | LR-115 in diffusion chamber (dome shape)                                | 10 detectors, 1 exposure                | /                           | /       | 7 - 7    |
| <b>EASYRAD / PEARL</b>          | CR-39 in diffusion chamber  | 10 detectors, 1 exposure                | 36                          | 13      | 21 - 54  |
| <b>KODALPHA / ALGADE</b>        | LR-115 (open detector)  | 10 detectors, 1 exposure                | 90                          | 9       | 74 - 103 |
| <b>RADTRAK2 / Radonova</b>      | CR-39 in diffusion chamber, volume 25 cm <sup>3</sup> , diameter 5.4 cm | 10 detectors, 1 exposure                | 14                          | 6       | 4 - 25   |
| <b>RAPIDOS / Radonova</b>       | CR-39 in diffusion chamber, volume 65 cm <sup>3</sup> , diameter 5.4 cm | 10 detectors, 1 exposure                | 11                          | 2       | 7 - 15   |

/ below detection limit

## Conclusion

A blind test has been performed on 6 commercial radon integrated measurement systems available in France in order to test the influence of thoron on reported radon integrated activity concentration. As expected by its measurement principal (open detector) the Kodalpha shows that thoron is well registered by the detector as a radon signal. For exposure in a thoron atmosphere (167 kBq.m<sup>-3</sup>.h) with almost no radon (less than 2 kBq.m<sup>-3</sup>.h), the DPR2 and DRF results are below the detection limit, a cross-interference of around 10% was found for the Radtrack2 and the Rapidos while this value was 36% for the EasyRad. No influence of the thoron on the radon measurement could be seen in the mixed exposure of 170 kBq.m<sup>-3</sup>.h of thoron plus 421 kBq.m<sup>-3</sup>.h of radon.

# Annex 1: detectors position

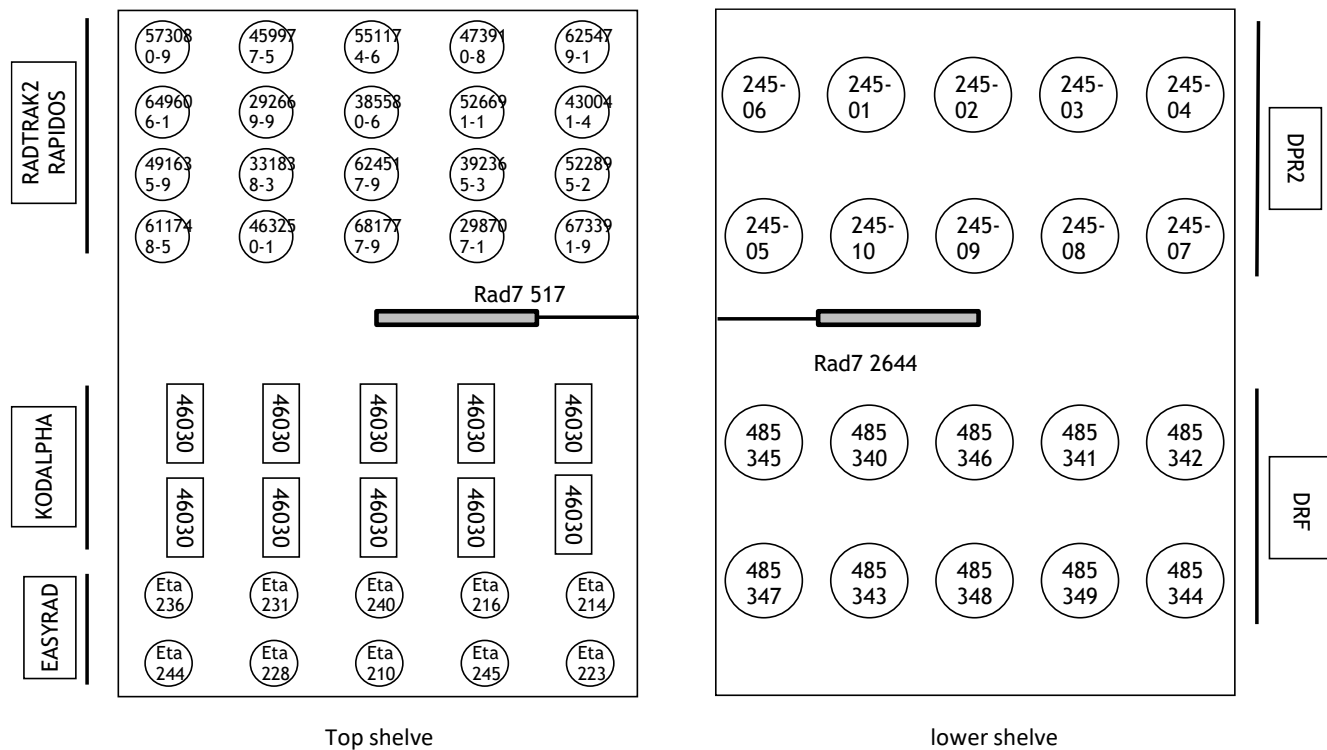


Figure 5 - Detectors position for the thoron exposure

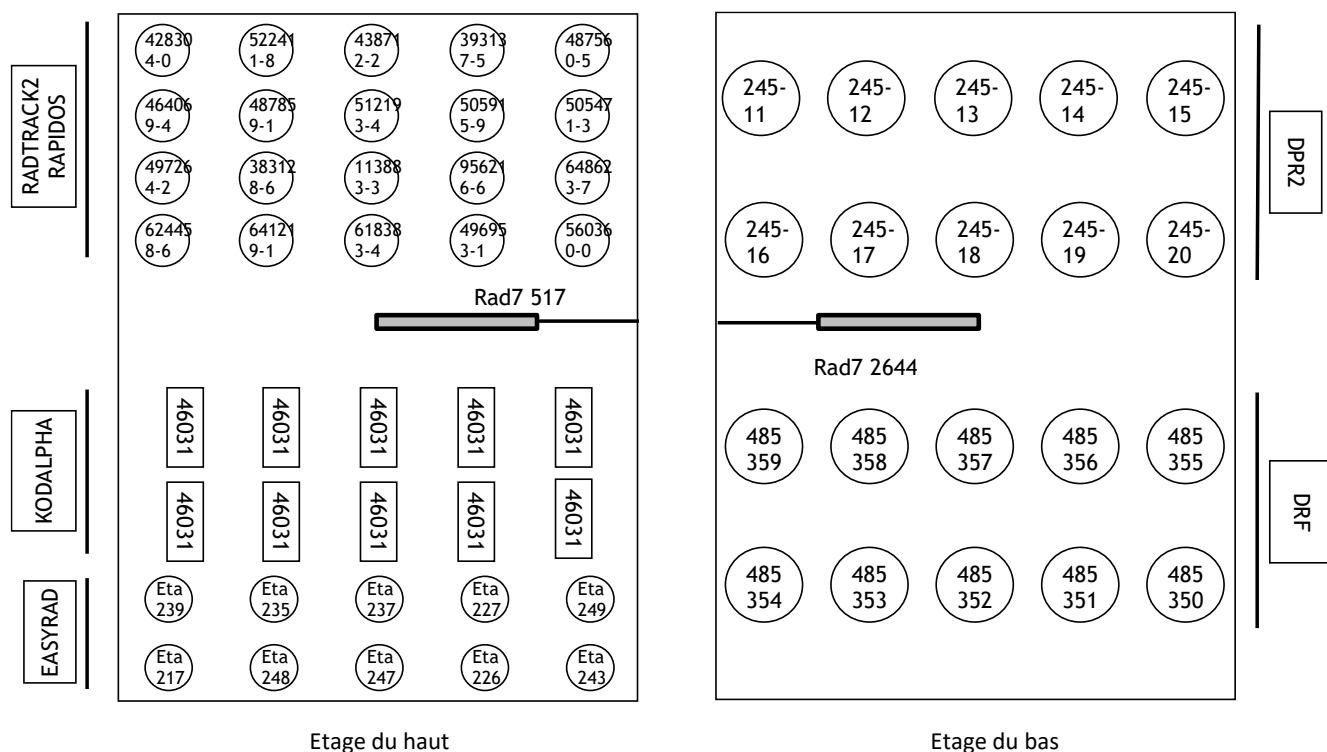


Figure 6 - Detectors position for the mixed thoron/radon exposure

Annex 2 - Results of each device in a thoron atmosphere

| EasyRad<br>(kBq.m <sup>-3</sup> .h) |       | DPR2<br>(kBq.m <sup>-3</sup> .h) |       | DRF<br>(kBq.m <sup>-3</sup> .h) |       | KodAlpha<br>(kBq.m <sup>-3</sup> .h) |       | Radtrak2<br>(kBq.m <sup>-3</sup> .h) |       | Rapidos<br>(kBq.m <sup>-3</sup> .h) |       |
|-------------------------------------|-------|----------------------------------|-------|---------------------------------|-------|--------------------------------------|-------|--------------------------------------|-------|-------------------------------------|-------|
| Av                                  | U(Av) | Av                               | U(Av) | Av                              | U(Av) | Av                                   | U(Av) | Av                                   | U(Av) | Av                                  | U(Av) |
| 86                                  | 17    | <36                              | /     | <10                             | /     | 147                                  | 31    | 43                                   | 18    | 14                                  | 8     |
| 48                                  | 12    | <36                              | /     | 13                              | 6     | 158                                  | 32    | 24                                   | 16    | 22                                  | 10    |
| 92                                  | 20    | <36                              | /     | <10                             | /     | 163                                  | 33    | 31                                   | 16    | 19                                  | 8     |
| 79                                  | 16    | <36                              | /     | <10                             | /     | 126                                  | 26    | 28                                   | 16    | 21                                  | 10    |
| 37                                  | 11    | <36                              | /     | <10                             | /     | 133                                  | 28    | 12                                   | 14    | 23                                  | 10    |
| 88                                  | 21    | <36                              | /     | <10                             | /     | 163                                  | 33    | <8,64                                | /     | 20                                  | 10    |
| 52                                  | 13    | <36                              | /     | <10                             | /     | 141                                  | 30    | 33                                   | 16    | 17                                  | 8     |
| 57                                  | 13    | <36                              | /     | <10                             | /     | 159                                  | 32    | 22                                   | 14    | 23                                  | 8     |
| 46                                  | 12    | <36                              | /     | 14                              | 6     | 174                                  | 35    | 20                                   | 14    | 20                                  | 8     |
| 42                                  | 15    | <36                              | /     | <10                             | /     | 158                                  | 32    | 32                                   | 16    | 27                                  | 10    |

Annex 3 - Results of each device in a mixed thoron-radon atmosphere

| EasyRad<br>(kBq.m <sup>-3</sup> .h) |       | DPR2<br>(kBq.m <sup>-3</sup> .h) |       | DRF<br>(kBq.m <sup>-3</sup> .h) |       | KodAlpha<br>(kBq.m <sup>-3</sup> .h) |       | Radtrak2<br>(kBq.m <sup>-3</sup> .h) |       | Rapidos<br>(kBq.m <sup>-3</sup> .h) |       |
|-------------------------------------|-------|----------------------------------|-------|---------------------------------|-------|--------------------------------------|-------|--------------------------------------|-------|-------------------------------------|-------|
| Av                                  | U(Av) | Av                               | U(Av) | Av                              | U(Av) | Av                                   | U(Av) | Av                                   | U(Av) | Av                                  | U(Av) |
| 418                                 | 53    | 241                              | 72    | 424                             | 81    | 385                                  | 69    | 448                                  | 60    | 433                                 | 54    |
| 409                                 | 52    | 303                              | 85    | 435                             | 83    | 346                                  | 66    | 553                                  | 72    | 431                                 | 54    |
| 211                                 | 50    | 275                              | 79    | 316                             | 63    | 334                                  | 63    | 477                                  | 62    | 416                                 | 52    |
| 440                                 | 55    | 388                              | 104   | 372                             | 71    | 377                                  | 68    | 505                                  | 66    | 444                                 | 56    |
| 420                                 | 69    | 347                              | 95    | 318                             | 64    | 355                                  | 64    | 533                                  | 70    | 473                                 | 60    |
| 373                                 | 93    | 276                              | 79    | 414                             | 79    | 352                                  | 63    | 573                                  | 74    | 417                                 | 52    |
| 472                                 | 72    | 228                              | 69    | 271                             | 54    | 336                                  | 64    | 493                                  | 64    | 396                                 | 50    |
| 459                                 | 73    | 379                              | 103   | 357                             | 68    | 347                                  | 62    | 528                                  | 68    | 454                                 | 56    |
| 469                                 | 68    | 313                              | 88    | 318                             | 64    | 316                                  | 60    | 467                                  | 62    | 425                                 | 54    |
| 416                                 | 53    | 281                              | 80    | 386                             | 73    | 317                                  | 60    | 474                                  | 62    | 430                                 | 54    |



**16ENV10 MetroRADON**

**16ENV10 MetroRADON**

**Deliverable D2**

**Annex X**

**Investigation of the response of radon/thoron  
measurement instruments at different  
temperatures**

**Michael Stietka, Dobromir Pressyanov**

**BEV-PTP, SUBG**

## Contents

|  |    |
|--|----|
| Investigation of the response of radon/thoron measurement instruments..... | 3  |
| Introduction .....   | 3  |
| Materials and methods.....   | 4  |
| Results and discussion .....   | 5  |
| Conclusion.....  | 11 |

# Investigation of the response of radon/thoron measurement instruments

## Introduction

The aim of this work is to investigate the influence of  $^{220}\text{Rn}$  (thoron) and its progeny on  $^{222}\text{Rn}$  (radon) end-user measurements and radon calibrations.

The influence of  $^{220}\text{Rn}$  on  $^{222}\text{Rn}$  activity concentration measurements has already been explored with some radon monitors. This influence, if not properly corrected, can introduce bias in the radon risk estimates or can generate false alarms if the detectors are used to identify dwellings with radon concentrations that exceed reference/action levels. Both thoron and its progeny ( $^{212}\text{Pb}$ ,  $^{212}\text{Bi}+^{212}\text{Po}/^{208}\text{Tl}$ ) need to be taken into account, as the generated thoron progeny can remain within the detector volume long after the decay of the parent thoron nuclides. In experimental studies of the thoron influence on radon monitors reference thoron concentrations should be created and controlled by reference monitors for thoron. In BEV-PTP and SUBG such reference monitors are radon/thoron monitors of AlphaGUARD PQ2000 PRO RnTn.

Reference thoron atmospheres have been established and evaluated in Task 2.1. Within Task 2.1, the secondary  $^{220}\text{Rn}$  reference instruments of BEV-PTP and SUBG, used in this experimental research have been calibrated using the primary thoron standard at IRSN. The instrument used by BEV-PTP is also the traceable calibrated Austrian national standard for  $^{222}\text{Rn}$  activity concentration in air. The reference monitors used in experiments with thoron at different temperatures are usually placed inside the exposure box where different temperatures are created. As these monitors are used to determine the reference thoron exposure in these experiments it is important to check whether the results for thoron concentration they provide are dependent on the temperature. Therefore, their response was studied experimentally at fixed thoron concentration within a temperature range 5-45 °C. According the producer of the thoron source, this temperature range is within the range of temperatures at which the characteristics of the source are stable (-10 to +45 °C). As the possible thoron influence should be taken into account in the calibrations of detectors/apparatus, the influence of thoron on the radon results of the reference monitors was also investigated in this work. This influence was studied experimentally under pure thoron and mixed radon + thoron concentrations and at different temperatures.

## Materials and methods

The investigation of the response of radon/thoron measurement instruments was carried out at the radon laboratory of Sofia University "St. Kliment Ohridski". The tests were made in  $^{220}\text{Rn}$  and  $^{222}\text{Rn}$  atmospheres established in an airtight 50 l calibration container, which is commercially available from Saphymo GmbH. For the measurements, the Austrian national standard for radon activity concentration in air – a traceable calibrated radon/thoron monitor with ionisation chamber AlphaGUARD PQ2000 PRO RnTn, with external pump and accessories – was placed in the calibration container and the corresponding reduction of the chamber volume was estimated. The same was done with the reference instrument of SUBG used – also AlphaGUARD PQ2000 PRO RnTn with external pump and accessories.

With the exposure facility used, (see: D. Pressyanov, K. Mitev, S. Georgiev, I. Dimitrova, J. Kolev. *Laboratory facility to create reference radon + thoron atmosphere under dynamic exposure conditions. J. Envir. Radioact. 166 (2017) 181-187*), two exposure scenarios were set up, one with a pure  $^{220}\text{Rn}$  atmosphere and one with a mixed  $^{222}\text{Rn}$  and  $^{220}\text{Rn}$  atmosphere. The instruments response was studied under different environmental temperatures (between +5 °C and +45 °C) in both scenarios. The  $^{222}\text{Rn}$  atmosphere was generated by a certified emanating  $^{226}\text{Ra}$  source (Czech Metrological Institute, Czech Republic) and the  $^{220}\text{Rn}$  atmosphere by a certified emanating  $^{228}\text{Th}$  source (Pylon Electronics Inc., Canada). The sources were equipped with a dryer at the inlet and a filter at the outlet, so the progeny atoms were trapped. The thermostat containing the calibration container has a working volume of 55 L. The flow-rate of the closed loop setup (Figure 1) was regulated by a finger pump and monitored by a flow rate meter. The working temperature was measured with the internal sensor of the AlphaGUARD monitor. The integration time for all measurements was 10 min in flow mode. It should be noted, that the sources are at room temperature - outside the thermostatic exposure box. The air flow-rate through the source during thoron exposure experiments was about 1 L/min, kept constant within  $\pm 3\%$ . Albeit the circulated air was taken from the exposure box and was of the temperature inside, it passes consecutively through pump, flow-rate meter, drier and the source, which were at the room temperature (20-23 °C). Therefore, with this flow-rate the air-stream cannot change substantially the temperature of the source, which differs much less from the room temperature than the temperature in the exposure box.

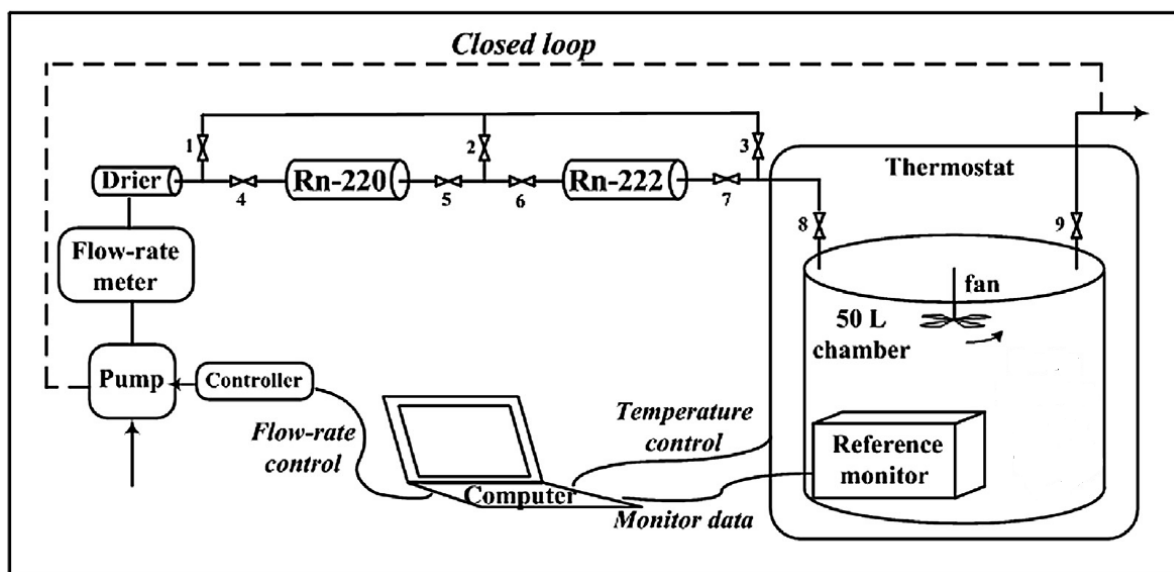


Figure 1 – Scheme of the test setup. The system operated in closed loop. By the valves the air flow can be directed in different ways so that atmospheres containing pure  $^{222}\text{Rn}$ ,  $^{220}\text{Rn}$  or their mixture can be created, as described in D. Pressyanov et al. *J. Envir. Radioact. 166 (2017) 181-187*.

## Results and discussion

To study the possible temperature influence on the results for thoron concentration given by the reference instruments, experiments at constant thoron levels were made over the temperature interval 5 – 45 °C. During exposure the thoron concentrations were kept constant by keeping constant (within  $\pm 3\%$ ) flow-rate of 59 L/h through the source (see fig.1 and the reference quoted there). The correlation between the temperature and the thoron concentrations reported by the instruments was studied.

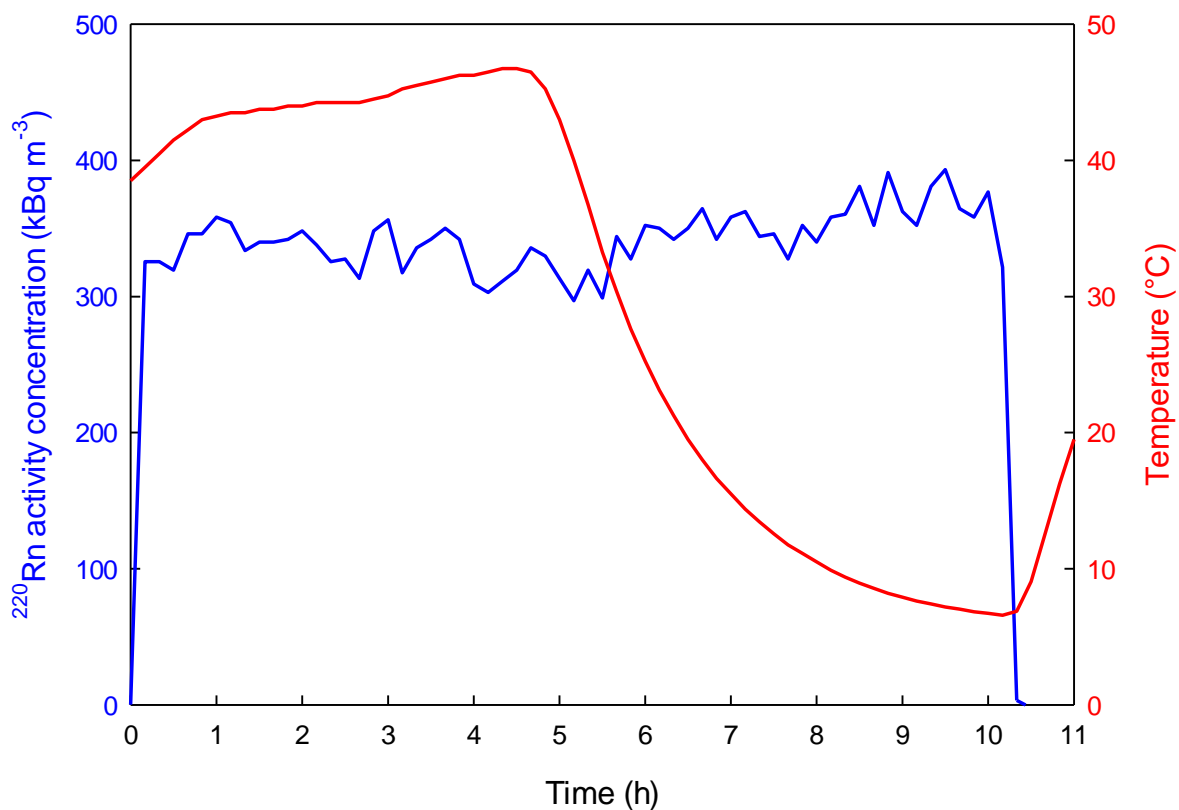


Figure 2 –  $^{220}\text{Rn}$  activity concentration and temperature during the first exposure scenario (10 min measurement intervals).

For the first exposure series, a constant pure  $^{220}\text{Rn}$  atmosphere was setup to test of the influence of temperature on the  $^{220}\text{Rn}$  activity concentration. The relative measurement uncertainty of the  $^{220}\text{Rn}$  activity concentration (10 min measurement intervals) given by AlphaGuard ranges from 5-6 %.The results in figure 2 (based on the BEV-PTP instrument) show no obvious relationship between these two parameters.

Regarding the correlation between the temperature and thoron results, the results of SUBG and BEV-instruments were slightly different:

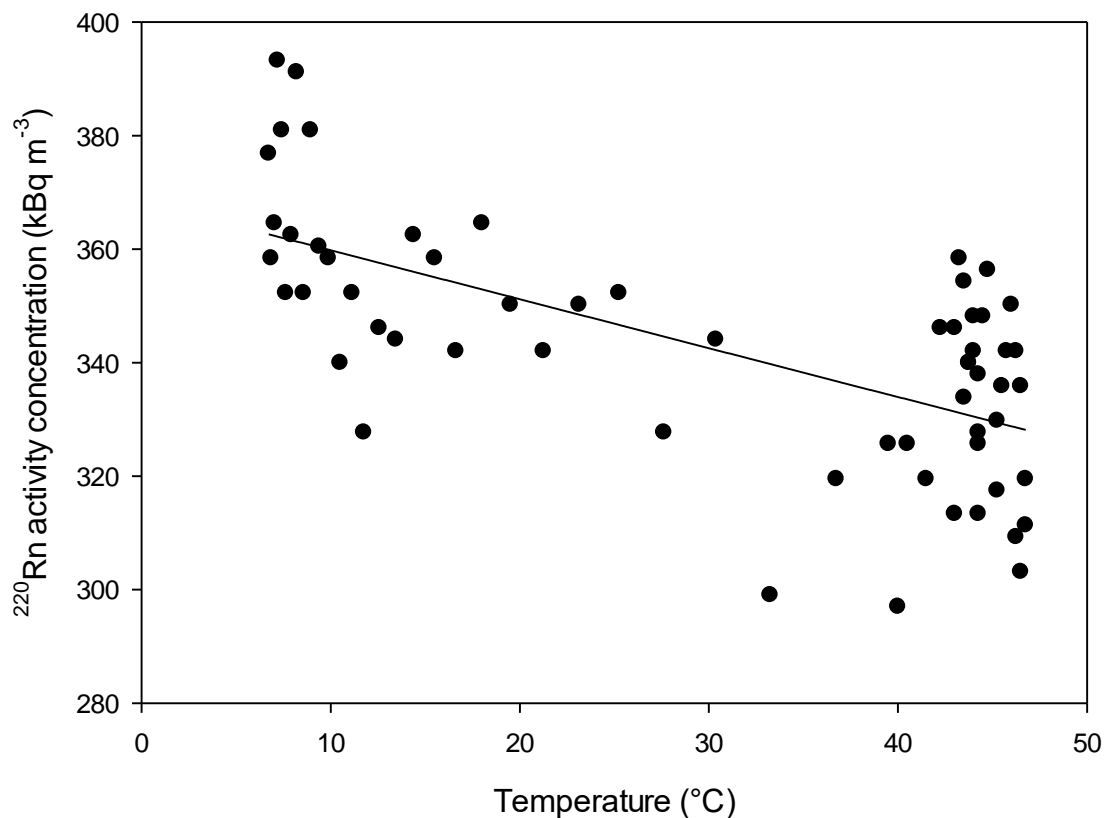


Figure 3 – Linear regression analysis of  $^{220}\text{Rn}$  activity concentration and temperature during the first exposure scenario.

The linear regression analysis in figure 3 is based on the results obtained by BEV-PTP instrument. It shows a slight correlation between the  $^{220}\text{Rn}$  activity concentration and the temperature in the calibration container with a coefficient of determination  $R^2$  of 0.42.

In spite of the slight correlation over the ranges of temperature between 5-45 °C, the calculated relative error (relative deviation) remains within the  $\pm 10\%$  limit for the testing of the influence of the ambient temperature specified by standard IEC 61577-2. The mean value of the measured by the AlphaGUARD  $^{220}\text{Rn}$  concentration is  $369 \text{ kBq m}^{-3} \pm 4 \text{ kBq m}^{-3}$  ( $k=1$ ) between 5-10 °C and  $332 \text{ kBq m}^{-3} \pm 3 \text{ kBq m}^{-3}$  between 40-45 °C. The measured mean  $^{220}\text{Rn}$  activity concentration was  $343 \text{ kBq m}^{-3} \pm 3 \text{ kBq m}^{-3}$  and the measured mean  $^{222}\text{Rn}$  activity concentration was  $289 \text{ Bq m}^{-3} \pm 20 \text{ Bq m}^{-3}$  during the first exposure. The calculated cross-interference of  $^{222}\text{Rn}$  measurements to  $^{220}\text{Rn}$  is about 0.1 % and therefore is well below the maximum of 20 % specified by standard IEC 61577-2.

The results from a similar exposure experiment, carried-out with SUBG instrument are shown in figure 4. Here, in contrast, a slight positive correlation ( $R^2 = 0.08$ ) was observed, but the deviation remains well within the  $\pm 10\%$  limit for the testing of the influence of the ambient temperature specified by standard IEC 61577-2.

At this stage there is no basis to speculate and analyze eventual temperature influence on thoron results given by the reference instruments used for thoron. Conservatively, extra 10% of relative uncertainty can be included in the uncertainty budget of thoron measurements if they are made over the temperature interval 5-45 °C, but the real temperature bias, if any, is probably smaller.

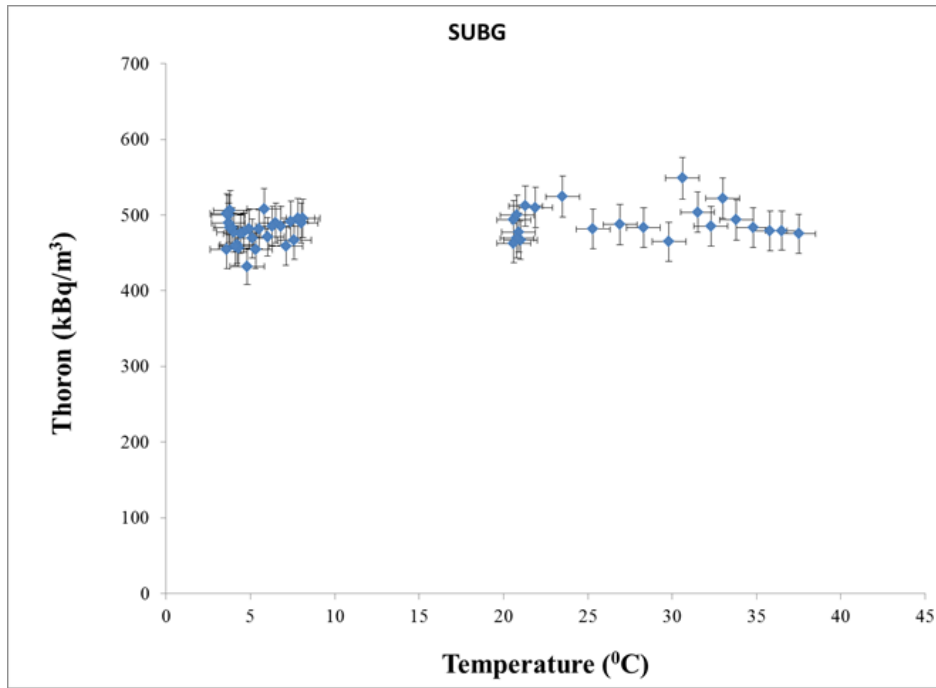


Figure 4 - Results for thoron concentrations obtained by SUBG instrument at different temperatures in another exposure experiment. The somewhat higher thoron levels than those in fig.3 are due to the reduced exposure volume, as other instruments were also placed in the exposure box during this exposure.

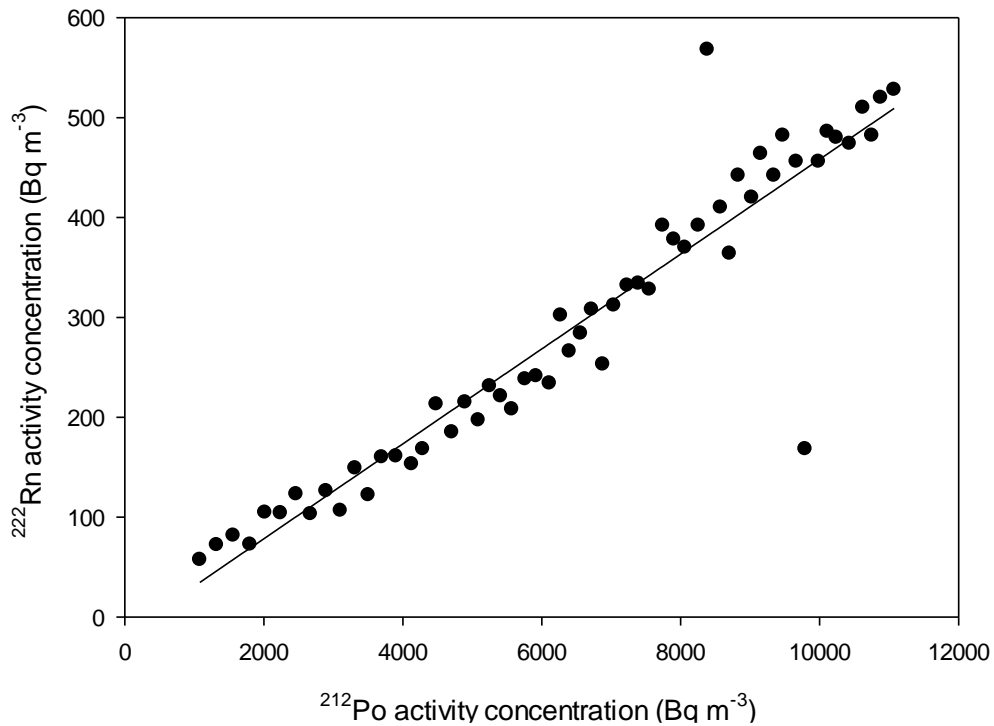


Figure 5 – Linear regression analysis of  $^{220}\text{Rn}$  activity concentration and  $^{212}\text{Po}$  activity concentration during the first exposure scenario.

AlphaGUARD PQ2000 PRO RnTn also measures the activity concentration of the  $^{220}\text{Rn}$  progeny  $^{212}\text{Po}$ . The increasing measured  $^{212}\text{Po}$  activity concentration is generated by the accumulation of  $^{212}\text{Pb}$  in the ionization chamber during longer  $^{220}\text{Rn}$  measurements. As figure 5 clearly shows, the calculated cross-interference of the measured  $^{222}\text{Rn}$  activity concentration to  $^{220}\text{Rn}$  is caused by the accumulation of  $^{212}\text{Pb}$  in the ionization chamber. With a coefficient of correlation  $R^2$  of 0.88, the linear regression analysis underlines the correlation between  $^{220}\text{Rn}$  activity concentration and  $^{212}\text{Po}$  activity concentration during the first exposure scenario.

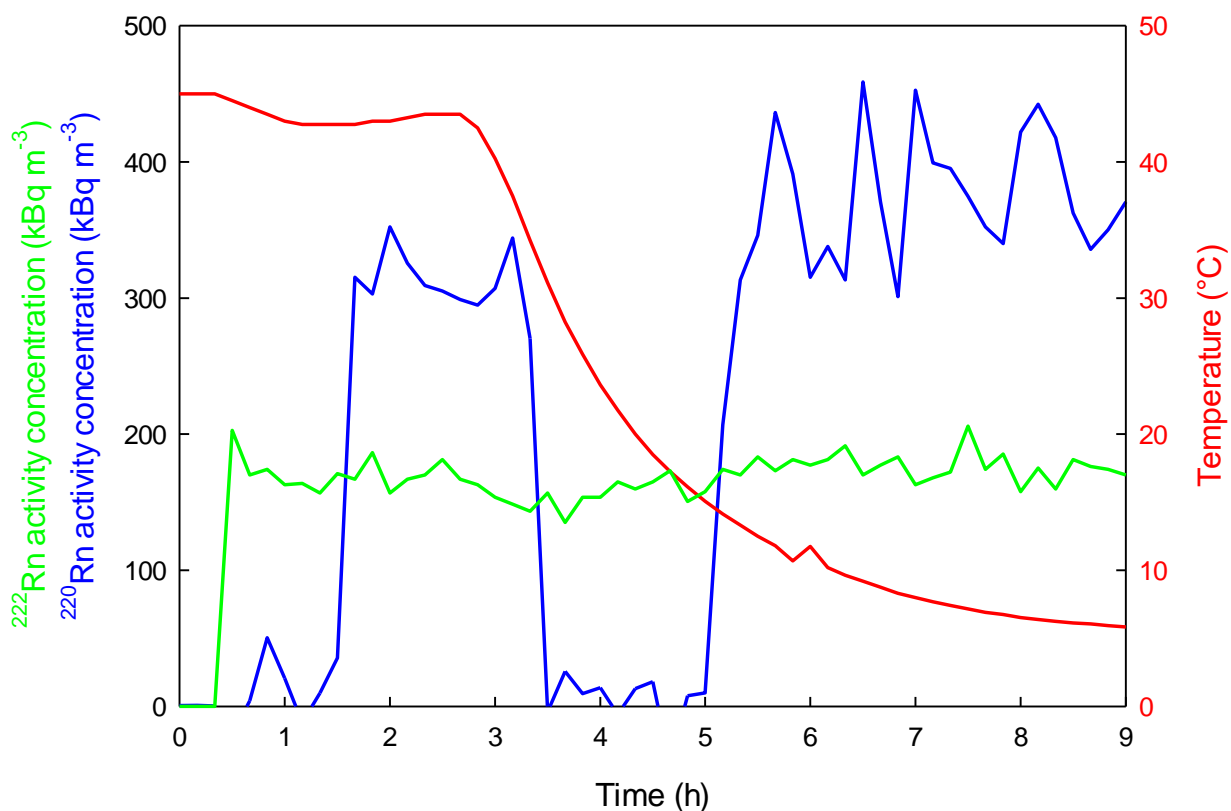


Figure 6 –  $^{222}\text{Rn}$ ,  $^{220}\text{Rn}$  activity concentration and temperature during the second exposure scenario.

In the beginning of the second exposure series, the  $^{222}\text{Rn}$  atmosphere was setup by flushing the  $^{226}\text{Ra}$  source once, (see figure 6). For the rest of the exposure the  $^{222}\text{Rn}$  atmosphere was unsupported. The  $^{222}\text{Rn}$  values of the tested BEV-PTP AlphaGUARD were checked with the AlphaGUARD of SUBG, which was placed outside the exposure box and used to sample air periodically from the box.

To test of the influence of  $^{220}\text{Rn}$  on the  $^{222}\text{Rn}$  measurements, a mixed  $^{222}\text{Rn}/^{220}\text{Rn}$  atmosphere was set up by flushing through the thoron source at a flow rate of 58 L/h. During the exposure, the flushing was stopped for two hours and setup again afterwards. As  $^{220}\text{Rn}$  decays rapidly within few minutes after the flushing is stopped, the atmosphere in the two-hours interval without flushing contains only  $^{222}\text{Rn}$ . The relative measurement uncertainty of the  $^{222}\text{Rn}$  activity concentration (10 min measurement intervals) given by AlphaGuard ranges within 4-5 %. The relative measurement uncertainty of the  $^{220}\text{Rn}$  activity concentration (10 min measurement intervals) given by AlphaGuard while flushing with  $^{220}\text{Rn}$  ranges within 4-10 %.

In the first three hours of the exposure, a constant temperature of 45 °C was setup. To perform measurements under dynamic conditions, the temperature was slowly decreased to 5 °C. For the statistical data analyses, the  $^{222}\text{Rn}$  values were corrected for the decay during the exposure.

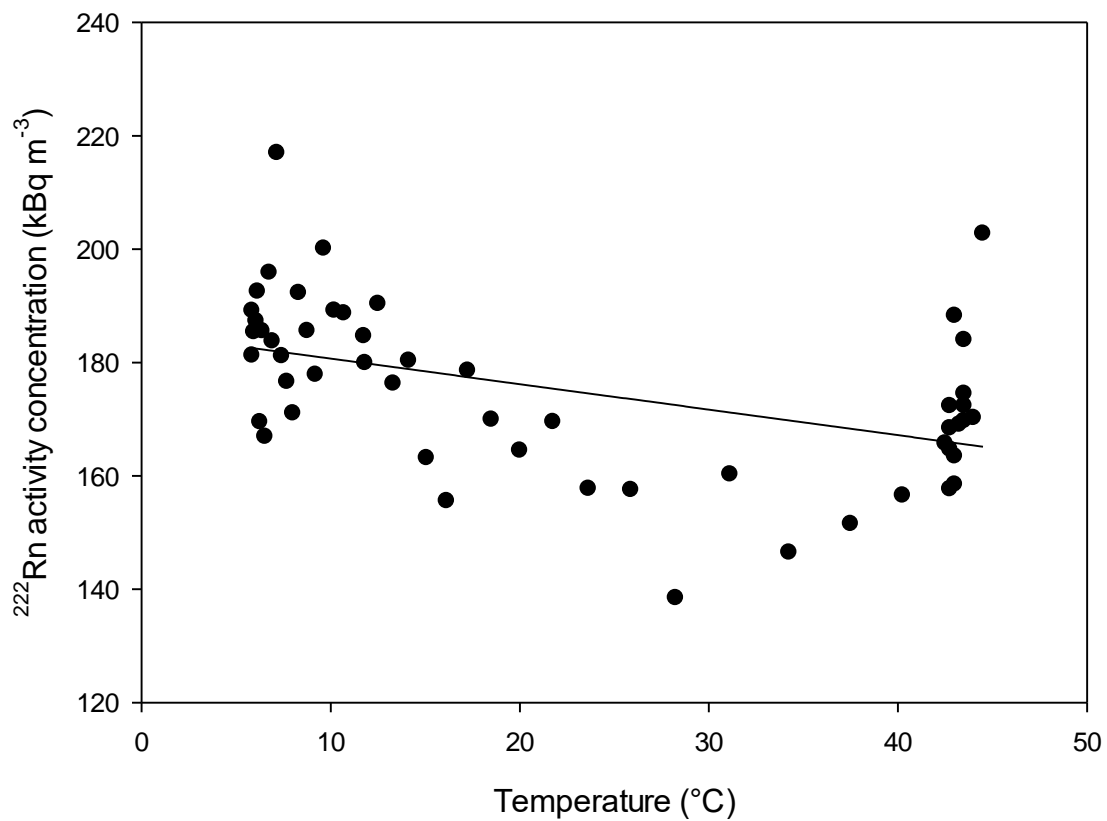


Figure 7 – Linear regression analysis of  $^{222}\text{Rn}$  activity concentration and temperature during the second exposure scenario.

The linear regression analysis in figure 7 shows no clear correlation between the  $^{222}\text{Rn}$  activity concentration and the temperature in the calibration container during the second exposure ( $R^2=0.21$ ). The calculated relative error (relative deviation) remains within the  $\pm 10\%$  limit for the testing of the influence of the ambient temperature specified by standard IEC 61577-2.

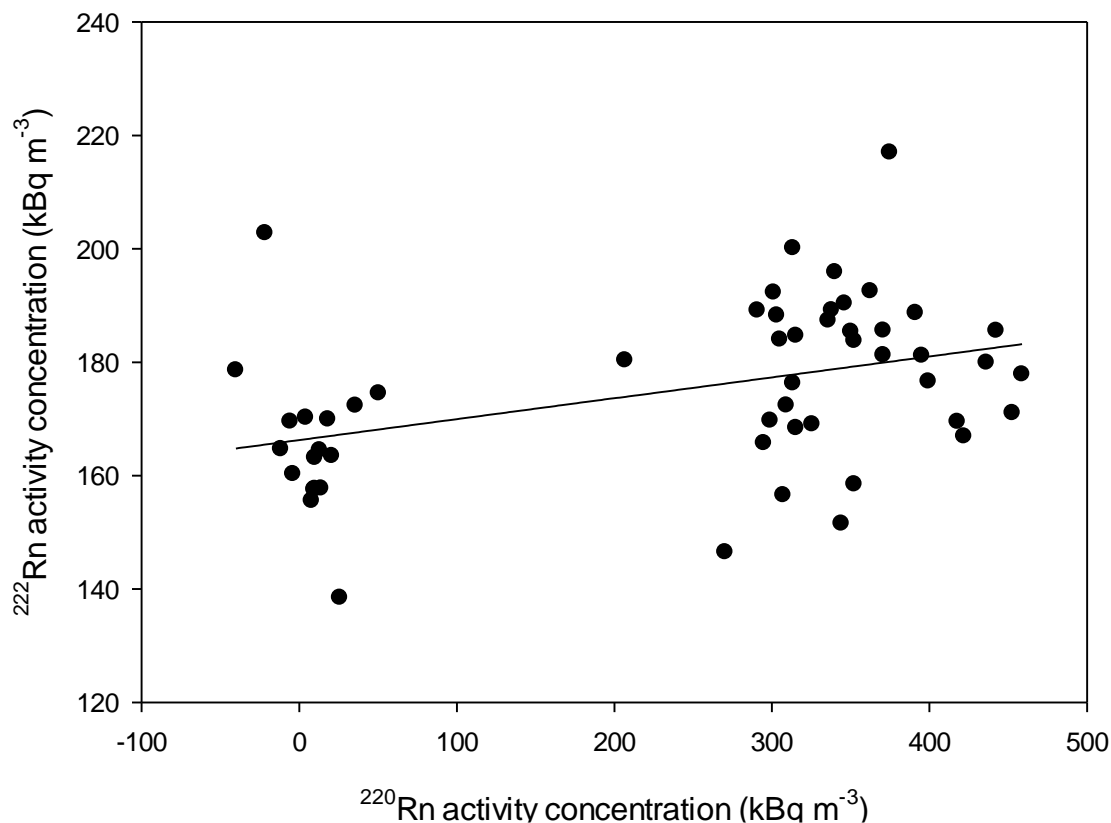


Figure 8 – Linear regression analysis of  $^{222}\text{Rn}$  activity concentration and  $^{220}\text{Rn}$  activity concentration during the second exposure scenario.

The linear regression analysis in figure 8 shows slightly but no significant correlation between the  $^{222}\text{Rn}$  and  $^{220}\text{Rn}$  activity concentration activity during the second exposure ( $R^2=0.21$ )

The measured mean  $^{220}\text{Rn}$  activity concentration, while  $^{220}\text{Rn}$  support was turned off, was  $6 \text{ kBq m}^{-3} \pm 5 \text{ kBq m}^{-3}$  and the measured mean  $^{222}\text{Rn}$  activity concentration, while  $^{220}\text{Rn}$  support was turned off, was  $166 \text{ kBq m}^{-3} \pm 3 \text{ kBq m}^{-3}$ . The calculated cross-interference of  $^{220}\text{Rn}$  measurements to  $^{222}\text{Rn}$  is  $4 \% \pm 3 \%$  and therefore is well below the maximum of 20 % specified by standard IEC 61577-2. The high uncertainty of the cross interference is caused by the high relative uncertainty of the measured  $^{220}\text{Rn}$  activity concentration, while  $^{220}\text{Rn}$  support was turned off.

## Conclusion

The results of the BEV-PTP reference instrument showed a slight negative correlation between the measured  $^{220}\text{Rn}$  activity concentration and the temperature in the exposure box, while the SUBG reference instrument showed a slight positive correlation. At this stage the results have no sufficient statistical power to state that such correlations really exist. In spite of the slight correlation over the ranges of temperature between 5-45 °C, the calculated relative error (relative deviation) remains within the  $\pm 10\%$  limit for the testing of the influence of the ambient temperature specified by standard IEC 61577-2.

Though the calculated cross-interference of  $^{222}\text{Rn}$  measurements to  $^{220}\text{Rn}$  is about 0.1 %, it could be clearly shown that  $^{220}\text{Rn}$  decay products, which accumulate in the ionization chamber, mainly cause this cross-interference. The content of  $^{212}\text{Pb}$  and  $^{212}\text{Bi}+^{212}\text{Po}/^{208}\text{Tl}$  ( $^{212}\text{Po}$  is always in equilibrium with  $^{212}\text{Bi}$ ) in the ionisation chamber is increasing during longer measurements. With an alpha energy of 6.1 MeV,  $^{212}\text{Bi}$  is supposed to cause this slight interference for the detection of the alpha energy of  $^{222}\text{Rn}$  at 5.6 MeV. Though this observation is very clear, it is metrologically irrelevant because of the overall very low cross-interference. The calculated cross-interference is well below the maximum of 20 % specified by standard IEC 61577-2.

On basis of the statistical analysis of the results, no significant correlation between the  $^{222}\text{Rn}$  activity concentration and the temperature in the calibration container could be shown. Furthermore, no clear correlation between the  $^{222}\text{Rn}$  and  $^{220}\text{Rn}$  activity concentration activity was observed. The calculated cross-interference of  $^{220}\text{Rn}$  measurements to  $^{222}\text{Rn}$  is  $4\% \pm 3\%$  and therefore well below the maximum of 20 % specified by standard IEC 61577-2.



# 16ENV10 MetroRADON

## Deliverable D2

### Annex XI

#### Task A.2.2.3

The problem with temperature dependence of radon diffusion chambers with anti-thoron barrier

(Rom. J. Phys. 65 (2020) 801)

D. Pressyanov, D. Dimitrov  
SUBG

# THE PROBLEM WITH TEMPERATURE DEPENDENCE OF RADON DIFFUSION CHAMBERS WITH ANTI-THORON BARRIER

DOBROMIR PRESSYANOV<sup>1</sup>, DIMITAR DIMITROV<sup>2</sup>

<sup>1</sup> Faculty of Physics, Sofia University “St. Kliment Ohridski”, Sofia, Bulgaria

<sup>2</sup> Mining and Geology University “St. Ivan Rilski”, Sofia, Bulgaria

*E-mail:* pressyan@phys.uni-sofia.bg

*Received July 18, 2019*

*Abstract.* The response of radon diffusion chambers that use polymer membranes or small gaps/holes as anti-thoron barriers at different temperatures is studied. A theoretical model of radon diffusion through polymer foils is presented. Experiments were made at 2°C, 21.5°C and 45°C. Results show that polymer foils introduce significant temperature dependence in radon response. The chambers with small gaps/holes do not show significant temperature dependence but their response may be affected by humidity and air turbulence. A novel approach to overcome these problems and design chambers with efficient anti-thoron and anti-humidity barrier as well as compensated temperature dependence is discussed.

*Key words:* radon, diffusion chambers, radon permeability, compensated temperature bias.

## 1. INTRODUCTION

The implementation of the EC directive 2013/59/EURATOM [1] needs metrological/quality assurance of  $^{222}\text{Rn}$  measurements at low concentrations. One problem addressed in the ongoing European MetroRADON project is to investigate and reduce the influence of thoron ( $^{220}\text{Rn}$ ) on radon end-user measurements [2]. Widely used anti-thoron barrier for radon detectors is thin polymer foil that stops  $^{220}\text{Rn}$  while allowing  $^{222}\text{Rn}$  to diffuse through it in the detector volume [3–5]. As noted elsewhere [6, 7], albeit effective against thoron and humidity, such barrier may introduce significant temperature bias in the radon response due to the temperature dependence of the diffusion properties of polymer foils. Other anti-thoron barriers are based on small gaps/pin-holes, usually around the chamber cap, through which radon diffuses in their volume [8]. If sufficiently small, the gaps/holes can serve as diffusion barriers against thoron, but their performance at high humidity or under turbulent air conditions might be problematic [8, 9].

In this report we present an experimental and theoretical study of the influence of the temperature on the response of two kinds of diffusion chambers with track detectors for  $^{222}\text{Rn}$  measurement. Both kind of chambers were metallic cylinders. In the first kind of chambers radon diffused through polyethylene foils into the volume. The second kind of diffusion chambers were where radon penetrated into the volume

by diffusion through small gaps/holes around the chamber cap. The alpha track detectors used in both kind of chambers were Kodak-Pathe LR-115 type II. Exposures to controlled  $^{222}\text{Rn}$  concentrations were made at temperatures of  $2^\circ\text{C}$ ,  $21.5^\circ\text{C}$  and  $45^\circ\text{C}$  using a dedicated laboratory facility [10]. A generalized theoretical model of radon diffusion through polymer foils was developed and applied to model radon and thoron penetration through polymer foils into the chamber volume. A novel concept to minimize the thoron influence on the passive radon detectors, not introducing in the same time strong temperature bias in the radon response is proposed and pilot experimental results that demonstrate its feasibility are shown.

## 2. THEORETICAL MODEL

Consider a closed volume  $V$ , where at least one of the sides is a foil of material through which radon can penetrate by diffusion, while the other sides are not permeable for radon. The total area of all permeable sides is  $S$ , the thickness of the polymer foil  $h$ , the diffusion coefficient of radon in the polymer material is  $D$ . Assume that radon can penetrate into the volume  $V$  only by diffusion through the permeable sides. The radon diffusion through the foil is described by the diffusion equation:

$$\frac{\partial c}{\partial t} = D \frac{\partial^2 c}{\partial x^2} - \lambda c, \quad (1)$$

where  $c$  is radon concentration in the foil material and  $\lambda$  is the decay constant of the isotope of interest ( $^{222}\text{Rn}$  or  $^{220}\text{Rn}$ ). Equation (1) is considered with the initial condition  $c(t=0, x) = 0$  and border conditions  $c(t, x=0) = Kc_{out}(t)$  and  $c(t, x=h) = Kc_{in}(t)$ , where  $x=h$  is the coordinate of the internal surface of the foil,  $x=0$  is that of its external surface. The quantities  $c_{out}(t)$  and  $c_{in}(t)$  are the ambient concentration outside the chamber and the concentration inside the chamber volume, respectively, and  $K$  is the partition coefficient of the foil material (the partition coefficient is the dimensionless solubility of the material that is the ratio on the border of the concentration in the material to that in air). The time evolution of the concentration inside the chamber volume is described by the equation:

$$\frac{dc_{in}}{dt} = \frac{SD}{V} \left. \frac{\partial c}{\partial x} \right|_{x=h} - \lambda c_{in}. \quad (2)$$

The first term in the right-side of equation (2) describes the flux by diffusion (Fick's law) from the internal surface of the foil, while the second term is for the radioactive decay. Further passive (integrated) mode of measurement is modeled, in which the determined quantity is the time-integrated radon concentration for exposure time  $t_{exp}$ . The integrated quantities will be denoted by capital symbols, e.g.:

$$C = \int_0^T c(t) dt, \quad (3)$$

where the integration time  $T$  is the time for which the detector in the chamber gathers signal. In our experiments, after exposure to radon the chamber is left at radon-free air (or at concentration that is of lower orders of magnitude than that during the exposure) until all  $^{222}\text{Rn}$  (or  $^{220}\text{Rn}$ ) and its progeny atoms degas or decay, before analyzing the detectors. Under such circumstances the upper limit of integration can be replaced by  $\infty$ . Let's transform the equations (1,2) by integrating both sides:

$$\int_0^\infty \frac{\partial c}{\partial t} dt = D \frac{\partial^2}{\partial x^2} \int_0^\infty c(x,t) dt - \lambda \int_0^\infty c(x,t) dt \quad (4)$$

$$\int_0^\infty \frac{dc_{in}}{dt} dt = -\frac{SD}{V} \frac{\partial}{\partial x} \int_0^\infty c(x,t) dt \Big|_{x=h} - \lambda \int_0^\infty c_{in}(t) dt. \quad (5)$$

The left side of equations (4) and (5) is zero, as  $c(t=0) = c(t=\infty) = 0$  and the same goes for  $c_{in}$ :  $c_{in}(t=0) = c_{in}(t=\infty) = 0$ . Then, the equations for the integrated quantities become:

$$D \frac{d^2 C}{dx^2} - \lambda C = 0, \quad (6)$$

$$-SD \frac{dC}{dx} \Big|_{x=h} - \lambda C_{in} V = 0, \quad (7)$$

considered with border conditions:

$$C(0) = KC_{out}; \quad (8)$$

$$C(h) = KC_{in}, \quad (9)$$

where  $C_{out}$  is the integrated for the exposure time ambient  $^{222}\text{Rn}$  concentration outside the chamber. By combining (7) and (9) one obtains:

$$C(h) = -\frac{KSD}{\lambda V} \frac{dC}{dx} \Big|_{x=h}. \quad (10)$$

It will be convenient to introduce the diffusion length of the particular isotope ( $^{222}\text{Rn}$  or  $^{220}\text{Rn}$ ) in the material:  $L_D = \sqrt{D/\lambda}$ . By standard methods the solution of (6) is obtained in the form:

$$C(x) = Ae^{x/L_D} + Be^{-x/L_D} \quad (11)$$

At the given border conditions the expressions for the constants A and B are:

$$A = \frac{KC_{out}e^{-2h/L_D}}{1 + e^{-2h/L_D} \left( \frac{SP - \lambda VL_D}{SP + \lambda VL_D} \right)} \left( \frac{SP - \lambda VL_D}{SP + \lambda VL_D} \right); \quad (12)$$

$$B = \frac{KC_{out}}{1 + e^{-2h/L_D} \left( \frac{SP - \lambda VL_D}{SP + \lambda VL_D} \right)}, \quad (13)$$

where  $P = KD$  is the “permeability” of the material through which radon diffuses.

This way, using also eqn. (7), for the integrated concentration in the volume one obtains:

$$C_{in} = C_{out} \frac{2SP}{SP + \lambda VL_D + (SP - \lambda VL_D)e^{-2h/L_D}} e^{-\frac{h}{L_D}}. \quad (14)$$

Actually, the signal of the detector is proportional to  $C_{in}$ , while “the calibration factor of the chamber” is the ratio “signal/ $C_{out}$ ”. To distinguish between the temperature dependence of radon penetration through the membrane, from eventual temperature dependence of the detector response, we will describe the first one by the “penetration ratio”  $R$ , which is the ratio of the integrated concentrations inside and outside the volume:

$$R = \frac{C_{in}}{C_{out}} = e^{-\frac{h}{L_D}} \frac{2SP}{SP + \lambda VL_D + (SP - \lambda VL_D)e^{-2h/L_D}}. \quad (15)$$

For thin foils, when  $h \ll L_D$  the expression for  $R$  simplifies to:

$$R \xrightarrow{h \ll L_D} R = \frac{1}{1 + \lambda \frac{hV}{PS}}. \quad (16)$$

The last term of eqn. (16) is what one usually finds in the literature for the penetration ratio  $R$  [3, 4]. Notably, this expression is valid for thin membranes – whose thickness is less than the diffusion length of the considered radon isotope.

Because of the short half-life of  $^{220}\text{Rn}$  its  $L_D$  is way smaller than that of  $^{222}\text{Rn}$ . One membrane that is thin regarding  $^{222}\text{Rn}$  can be thick regarding  $^{220}\text{Rn}$ . For instance,

in the described experiments foils of *low density polyethylene* (LDPE) of thickness 75  $\mu\text{m}$  and *high density polyethylene* (HDPE) of thickness 120  $\mu\text{m}$  were used. At room temperature the diffusion length of  $^{222}\text{Rn}$  in LDPE is about 1500  $\mu\text{m}$  and 700  $\mu\text{m}$  for HDPE [11]. In the same materials the diffusion length of  $^{220}\text{Rn}$  in these materials are about 19  $\mu\text{m}$  and 9  $\mu\text{m}$ , correspondingly. Therefore, the used foils can be considered as “thin” regarding  $^{222}\text{Rn}$  and “thick”, regarding  $^{220}\text{Rn}$ .

The difference between the diffusion length and half-life of radon and thoron makes it possible to use diffusion barriers, like polymer membranes, to discriminate between these isotopes. For instance, the penetration ratio in chambers of  $V/S = 7.5 \text{ cm}$  (the same used in our experiments), and covered with 10  $\mu\text{m}$  thick LDPE will be  $R(^{222}\text{Rn}) = 0.86$  and  $R(^{220}\text{Rn}) = 0.001$ , *i.e.* the thoron influence on the signal of the detector placed inside the chamber in this case will be reduced by three orders of magnitude. With 75  $\mu\text{m}$  thick LDPE the reduction will be almost five orders of magnitude. Such close to the absolute anti-thoron protection can hardly be achieved by other anti-thoron barriers. Another benefit of the use of polymer foils as a barrier is that they also provide an effective protection of the chamber volume against moisture/humidity.

The major problem in the use of membrane-based anti-thoron barriers arises from the temperature dependence of the penetration ratio  $R$  which makes their response to radon temperature dependent. Actually, the temperature dependence of  $R$  is due to the temperature dependence of the foil permeability  $P$ .

### 3. EXPERIMENTAL

Experiments at different temperatures were carried-out at the Laboratory of Dosimetry and Radiation Protection at the Sofia University “St. Kliment Ohridski”. Diffusion chambers covered by foils were cylinders of diameter 80 mm and height 75 mm. At the bottom of the chamber a piece of detector Kodak-Pathe LR-115 type II was fixed. Chambers’ openings were covered by different materials: filter paper, LDPE of thickness 75  $\mu\text{m}$  or HDPE of thickness 120  $\mu\text{m}$ . Special care was taken to check that the fixing of the foils (by hot and cold silicone, applied consecutively) was hermetic. For that purpose other chambers were covered by metal foil, not permeable for radon, which was fixed in the same manner as plastic foils. A set of chambers that contain at least one chamber of any kind (covered by filter paper, metal foil, foil of LDPE, foil of HDPE) were loaded for exposure in a 50 L exposure vessel. In the same vessel a second set of diffusion chambers of “gaps/holes” type were also loaded. Those chambers were of size  $\varnothing 75 \times 75 \text{ mm}$  with SSNTDs of Kodak-Pathe LR-115/II and were traditionally used for radon monitoring at the Laboratory of Dosimetry and Radiation Protection (see the photo Fig. 1 in [12]). Details about their calibration and traceability are provided elsewhere [13]. Three different exposure to reference  $^{222}\text{Rn}$  concentrations at three different temperatures: 2°C, 21.5°C and 45°C were made, using the dedicated calibration

facility [10]. During exposure the  $^{222}\text{Rn}$  concentration was followed by a reference radon monitor AlphaGUARD PQ2000 Pro (Bertin/Saphymo GmbH). After exposure the set of chambers was left at the same temperature but at low radon levels ( $\sim 20 \text{ Bq m}^{-3}$ ) for two weeks to allow practically full  $^{222}\text{Rn}$  decay and out-gazing (from the materials where it can be absorbed – *e.g.* the polymers). After that the detectors were etched with 10% NaOH at  $60^\circ\text{C}$  for 100 min, followed by 30 min washing in agitating water and 2 min wash in still solution of 50% ethanol. After the detectors dried the tracks were counted visually, by a microscope.

As the track-density of the chambers covered by metal foils was equal to the background track density ( $21 \pm 4 \text{ cm}^{-2}$ ), we consider the technique used to fix hermetically the foil to the chamber to be efficient and to guarantee that radon penetrates in the chamber volume only by diffusion through the polymer membrane. For the cans covered with filter paper  $R = 1$  was assumed. This way, the penetration ratio for the other chambers was determined as the ratio of the detector signal (net track density) of the detector placed in foil-covered chamber to that from a chamber covered with a filter paper.

#### 4. RESULTS AND DISCUSSION

Experimentally determined values of  $R$  at the three different exposure temperatures are shown in Fig. 1. Clearly, the response of the diffusion chambers with polymer foil strongly depends on the temperature. The results for the calibration factor ( $CF = \text{net track density}/\text{integrated } ^{222}\text{Rn concentration } (C_{out})$ ) of the “pin-hole” diffusion chambers are shown in Fig. 2. For these chambers there is no statistically significant indication for temperature dependence of their response.

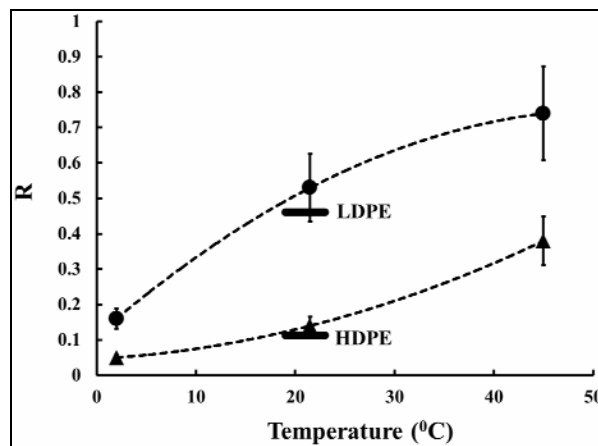


Fig. 1 – The penetration ratio at different temperatures of the chambers covered by LDPE (●) and HDPE (▲) with interpolation curves shown. The horizontal section-lines represent the estimates based on LDPE and HDPE data reported in [11]. As experiments [11] were made at a room temperature, that is typically within  $19\text{--}23^\circ\text{C}$ , the section-lines cover this temperature range.

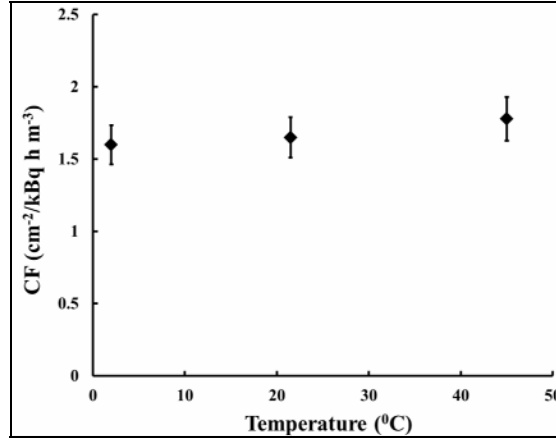


Fig. 2 – The CF of diffusion chambers in which radon diffuses through small gaps/holes. No significant difference between the results at different temperatures are visible.

Despite the temperature bias, the polymer foils can provide an efficient anti-thoron and anti-humidity barrier. Therefore, we focused efforts on whether this dependence can be reduced or even eliminated. Using the expression for  $R$  for a specified material and the experimental value  $R_0$  at given  $h_0$ ,  $V_0$ ,  $S_0$  one can model  $R$  for the same material at the same temperature for different  $h$ ,  $V$ ,  $S$  using the expression that can be derived from eqn. (16):

$$R = \frac{1}{1 + \left( \frac{1 - R_0}{R_0} \right) \frac{hVS_0}{h_0V_0S}}. \quad (17)$$

The modeling of  $R$  for temperature different from 2°C, 21.5°C and 45°C were made by polynomial interpolation between the experimental points at 2°C, 21.5°C and 45°C.

By varying parameters of the foil-coverage and  $V/S$  ratio, the temperature dependence can be somewhat reduced, but not eliminated, as seen in Fig. 3. In addition when using thin polymers (*e.g.*  $h \leq 10 \mu\text{m}$ ) care about their integrity during exposure may be needed. It appears that measurements with foil-covered diffusion chambers over wide range of ambient temperatures need to account for the temperature bias that can be substantial.

However, the identified problem of temperature dependence of radon permeability through polymer foils offers a surprising opportunity to compensate the temperature dependence of many kinds of radon detectors. There are many radon detectors whose sensitivity decreases with increasing the temperature. Those include *e.g.* detectors based on activated charcoal [14], detectors that use radon absorbers/adsorbers [15], the most widely used alpha track detectors of CR-39

which show fading that is greater at higher temperature [16]. The key concept is to combine the increase of the penetration ratio with the reciprocal decrease of the sensitivity of the radon detectors placed in the chamber.

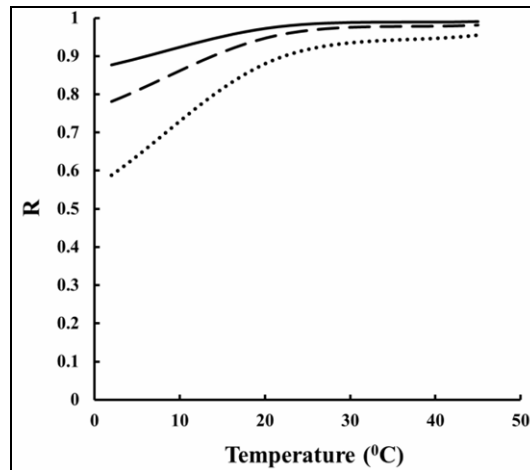


Fig. 3 – Modeled dependence of the penetration ratio ( $R$ ) on the temperature for thin foils of LDPE and different volume to surface ratios. The solid line is for  $h = 10 \mu\text{m}$  and  $V/S = 1.5 \text{ cm}$ , the dashed line is for  $h = 10 \mu\text{m}$  and  $V/S = 3.0 \text{ cm}$  and the dotted line is for  $h = 50 \mu\text{m}$  and  $V/S = 1.5 \text{ cm}$ .

The technical approach is to construct modules in which the increased permeability of radon inside with increasing temperature compensates the decreasing sensitivity to radon of detectors placed inside. The design of such “compensating modules” is described in the patent application [17]. Its potential can be demonstrated by a dedicated experiment carried out by the authors. One kind of detectors for which our experience indicated significant temperature dependence is those based on Kodak Pathe LR-115/II detectors covered with solid absorbers as radiators [15]. The best response with such detectors is obtained when the foil is of Makrofol N. This foil is of uniquely high radon absorption ability ( $K = 112 \pm 12$  at  $20^\circ\text{C}$ ) [18]. In present experiments detector of Kodak-Pathe LR-115/II covered with 2 foils of  $43 \mu\text{m}$  Makrofol N was used. However, when the foils of Makrofol N are used a strong temperature dependence of the response is observed, the signal decreases about 2.7 times when the temperature increases from  $5$  to  $35^\circ\text{C}$ . By technical concept described in [17] and modeling, using the present experimental data and equations (16, 17) it was found that if a module is designed with a covering foil of  $120 \mu\text{m}$  thick HDPE and  $V/S = 1.5 \text{ cm}$ , and the detector is placed inside, the temperature dependence should be compensated. The experimental results are shown in Fig. 4. As seen, such construction provides very good temperature compensation. Notably, we are at the very beginning of studies and the practical application of this approach for different kind of detectors is a matter for the future. However, the pilot experimental results suggest for its promising potential.

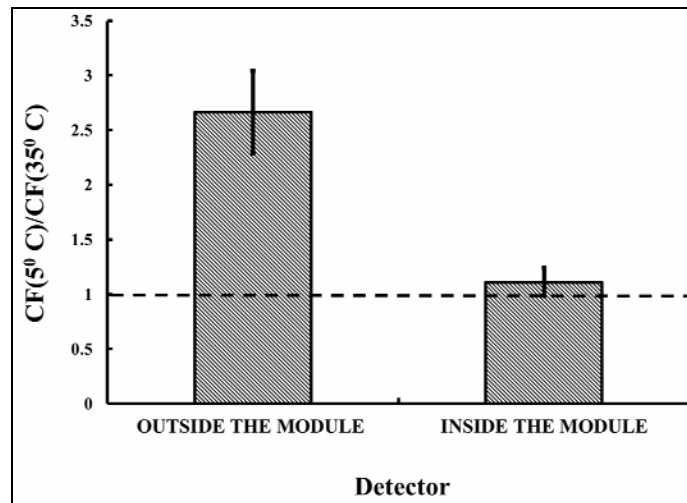


Fig. 4 – The CF ratio of 5°C to 35°C for detectors of Kodak Pathe LR-115/II covered with Makrofol N. Outside the compensation module the temperature bias is about 270% while inside it is within about 10%.

## 5. CONCLUSION

This work was focused on the temperature dependence of the response of radon diffusion chambers with anti-thoron barrier. One kind of such chambers was with polymer foils used to cover their volume. The foils used were of low density polyethylene with thickness 75  $\mu\text{m}$  or high density polyethylene of thickness 120  $\mu\text{m}$ . The second kind was “gap/ holes” kind of chambers. The experimental results revealed strong temperature dependence of the chambers with polymer foils. The temperature influence on the response of the other kind of chambers was not significant. A theoretical model of radon penetration through polymer foils was developed and used the radon penetration by diffusion through foils. The modeling and the experimental data suggest that the temperature influence on the penetration ratio of  $^{222}\text{Rn}$  in chambers covered by polymer membranes can hardly be eliminated.

However, a surprising opportunity was found and explored. By combining the temperature dependence of radon penetration ratio through polymer membranes with the reciprocal temperature dependence of some widely used radon sensors/detectors, a novel design of radon monitors with highly efficient anti-thoron/anti-humidity barriers and compensated temperature dependence becomes possible. The key-concept is to place the detector with decreasing with the temperature response in a module in which the radon penetration ratio increases reciprocally thus the temperature bias being compensated. The pilot experimental results with detectors of Kodak-Pathe LR-115/II covered by absorber of Makrofol N showed that the temperature bias between 5°C and 35°C is reduced from about 270% to within 10%.

*Acknowledgement.* This work is supported by the *European Metrology Programme for Innovation and Research* (EMPIR), JRP-Contract 16ENV10 MetroRADON (<http://www.euramet.org>). The EMPIR initiative is co-funded by the European Union's Horizon 2020 Research and Innovation Programme and the EMPIR Participating States.

## REFERENCES

1. Council Directive 2013/59/EURATOM of 5 December 2013. *Official Journal of the European Union* L 13/17.1.2014.
2. Metrology for radon monitoring. 16ENV10 MetroRADON project, <http://metroradon.eu>
3. W. J. Ward III, R. L. Fleischer and A. Mogro-Campero, *Rev. Sci. Instrum.* **48**, 1440–1441 (1977).
4. R. L. Fleischer, *Health Phys.* **62**, 91–95 (1992).
5. F. Bochicchio, M. Ampollini, L. Tommasino, A. Sorimachi, S. Tokonami, *Radiat. Meas.* **44**, 1024–1027 (2009).
6. R.L. Fleischer, W.R. Giard, and L.G. Turner, *Radiat. Meas.* **32**, 325–328 (2000).
7. Tommasino L. (2016). Concealed errors in radon measurements and strategies to eliminate them. Presented at the 8th Int. Conf. on Protection against Radon at Home and Work, Prague, 12–16 September 2016.
8. B.K. Sahoo, B.K. Sapra, S.D. Kanse, J.J. Gaware, Y.S. Mayya, *Radiat. Meas.* **58** 52–60 (2013).
9. L. Tommasino, D. Pressyanov, *A better understanding of the morphology and the structure of the plastics versus the temperature, conducive to correct radon measurements and to advanced radon monitors*, Workshop within MetroRADON project, Sofia 21–22 March 2019 (head organizer K. Mitev).
10. D. Pressyanov, K. Mitev, S. Georgiev, I. Dimitrova, J. Kolev, *J. Env. Radioact.* **166**, 181–187 (2017).
11. D. Pressyanov, S. Georgiev, I. Dimitrova, K. Mitev and T. Boshkova, *Radiat. Prot. Dosim.* **145**, 123–126 (2011).
12. D. Pressyanov, *Rom. Journ. Phys.* **58**, S221–S229 (2013).
13. S. Georgiev, D. Pressyanov, K. Mitev, Dimitrova I. *BgNS Trans.* **12(1)**, 3–6 (2008).
14. A. Cooper, T. N. Le, T. Iimoto, T. Kosako, *J. Env. Radioact.* **102**, 60–63 (2011).
15. L. Tommasino, M.C. Tommasino, P. Viola, *Radiat. Meas.* **44**, 719–723 (2009).
16. M. Caresana et al., *Radiat. Meas.* **45**, 183–189 (2010).
17. D. Pressyanov, Bulg. Pat. Appl. Reg. Nr. 112897, priority: 19.03.2019 (assignee: Sofia University “St. Kliment Ohridski”).
18. K. Mitev, P. Cassette, S. Georgiev, I. Dimitrova, B. Sabot, T. Boshkova, I. Tartès, D. Pressyanov, *Appl. Radiat. Isot.* **109**, 270–275 (2016).



# 16ENV10 MetroRADON

## Deliverable D2 Annex XII

### Task A.2.3.1

Review of potential techniques and materials to reduce the influence of thoron on radon measurements and calibrations

O. Holmgren<sup>1</sup>, T. Turtiainen<sup>1</sup>, K. Mitev<sup>2</sup>, D. Pressyanov<sup>2</sup>

<sup>1</sup>) STUK

<sup>2</sup>) SUBG



# **Review of potential techniques and materials to reduce the influence of thoron on radon measurements and calibrations**

Olli Holmgren<sup>1</sup>, Tuukka Turtiainen<sup>1</sup>, Krasimir Mitev<sup>2</sup> and Dobromir Pressyanov<sup>2</sup>

<sup>1</sup>STUK, <sup>2</sup>SUBG

## **MetroRadon WP 2, Report on the activity A2.3.1**

### **Contents**

|  |    |
|--|----|
| Background .....                                 | 2  |
| Introduction .....                               | 3  |
| Discriminative radon and thoron detectors .....  | 3  |
| Diffusion through an air gap or a pin hole ..... | 5  |
| Foil materials used as diffusion barriers. ....  | 5  |
| Diffusion through polymer foils.....             | 8  |
| Diffusion through pin hole .....                 | 10 |
| Delay due to air flow in a pipe .....            | 12 |
| Discussion and future tasks/activities .....     | 13 |
| References .....                                 | 16 |

## **Background**

This work is a part of MetroRadon project (Metrology for radon monitoring) supported by the European Metrology Programme for Innovation and Research (EMPIR), JRP-Contract 16ENV10 MetroRADON ([www.euramet.org](http://www.euramet.org)). The EMPIR initiative is co-funded by the European Union's Horizon 2020 research and innovation program and the EMPIR Participating States.

This work is a part of the Activity A2.3.1 at WP 2: “STUK and SUBG will undertake a literature review of potential techniques and materials to reduce the influence of thoron on radon measurements and calibrations. Based on these findings, STUK and SUBG will perform an analytical analysis of the different techniques/materials and will identify the most promising ones, based on the effectiveness of the relative differentiation between thoron and radon.”

“In Task 2.3 the properties of different filters/foils/membranes that might potentially serve as efficient barriers for thoron, whilst not reducing radon permeability significantly, will be investigated in order to propose methods for reducing the influence of thoron on the radon measurements.”

## **Introduction**

Radon ( $^{222}\text{Rn}$ ) in indoor air is a well known problem. In most cases, the most important source of indoor radon is the soil below the building. Thoron ( $^{220}\text{Rn}$ ) has a short half life of 55.6 sec and therefore the transport distance of thoron in the soil is short. Hence, the indoor thoron concentration due to transport from the soil is in most cases negligible. However, in some cases, building materials emit radon and/or thoron increasing the indoor concentrations significantly (Wiegand et al. 2000, Reddy et al. 2004, Shang et al. 2005, Gierl et al. 2014).

It is known that some radon detectors are sensitive to thoron. Number of thoron interference tests has been conducted (Tokonami et al. 2001, Ishikawa 2004, Bochicchio et al. 2009, Chen et al. 2009, Chen and Moir 2012, Sumesh et al. 2012, Michielsen and Bondiguel 2015). Thoron interference varies typically in the range 0.4 % - 74 % for alpha track detectors and in the range 4 % - 66 % for radon monitors based on ionization chamber or semiconductor detector.

In many cases, the error caused by interference is smaller than the measurement uncertainty. On the other hand, the error would be systematic and hence it would cause bias increasing the measurement result.

In this document, we present a literature review of potential techniques and materials to reduce the influence of thoron on radon measurements and calibrations. More than 70 scientific articles were reviewed, but only a part was included in this document. First discriminative radon-thoron detectors are discussed shortly. After that diffusion through membranes, air gaps and pin holes as well as different membrane materials are discussed. Problems that need more detailed research within the MetroRADON project are identified.

## **Discriminative radon and thoron detectors**

Both radon and thoron can be measured using discriminating radon-thoron detectors. Many measurement techniques have been developed. McLaughlin (2010) has divided them in to two categories. The first category includes techniques using two passive alpha track detectors, i.e., solid state nuclear track detectors (SSNTD). The two detectors have essentially identical geometry, but some differences exist. One of the detectors is designed to have low diffusion barrier, and therefore, it measures both radon and thoron gas concentrations. The other

detector has higher diffusion barrier that eliminates the entry of thoron into the detector but allows the entry of radon. The difference is due to the different half-lives of radon and thoron. Based on the difference between the signals in the two detectors, both radon and thoron gas concentrations can be determined. Several authors have reported such radon-thoron detectors (Guo et al. 1995, Zhou et al. 2002, Tokonami et al. 2005, Eappen and Mayya 2004, Calamosca and Penzo 2009, Sciocchetti et al. 2010, Sahoo et al. 2013, Griel et al. 2014).

The second category includes continuous and active techniques. These can be based on the analysis of the time sequence of the alpha signals recoded in the devices such as Lucas scintillation cells (Tokonami et al. 2002, Eappen et al. 2008, Zhang et al. 2010 and Sumesh et al. 2014) and ionization chambers (Tripathi et al. 2013), such as AlphaGuard (Saphymo GmbH). Time sequence differences arise due to the different half-lives of the alpha emitters in the radon and thoron chains. Some commercially available instruments utilize alpha spectroscopy to discriminate the radon and thoron-related signal, such as RAD 7 (Durrige Company Inc.). The discrimination is based on the measurement of alpha energies emitted by the radon and thoron progeny, that has been collected onto the surface barrier detector by an electric field.

A delayed coincidence technique has also been used for thoron measurements (Falk et al. 1992, Bochicchio et al. 1996). The method consists of a multiple time analysis of the pulse events detected by a flow-through scintillation cell and a phototube. It takes advantage of the relatively short time delay between the alpha particles emitted by  $^{220}\text{Rn}$  and  $^{216}\text{Po}$  (0.145 s half time).

A method utilizing a thin walled plastic tube has been reported by Falk et al. (2008). The technique is similar with the double-filter method based on the collection of decay products of thoron (Knutson et al.). The setup consists of a plastic tube, an entrance filter and an exit filter. The air is sucked through the filters and tube with a constant flowrate. Inside the tube, thoron decays and its progeny is attached to the inner walls of the tube as well as on the exit filter. After the sampling period (typically 8 h), the exit filter and the inner plastic tube are folded and compressed into a standard vial for gamma counting.

## Diffusion through an air gap or a pin hole

Many discriminative radon-thoron alpha track detectors are designed to possess optimal diffusion properties, Table 1. Different designs have been published. Guo et al. (1995) used an opening of 5 mm in diameter for radon detectors and four openings of 20 mm in diameter for the thoron detectors. The openings were covered with filter to allow entry only of the radon and thoron gases, but not of their progenies.

Tokonami et al. (2005) and Gierl et al. (2014) used a small gap between the lid and bottom of the detector for radon detection and several holes for radon and thoron detection. Diffusion through pin holes were used by Sahoo et al. (2013). They have calculated theoretically and verified experimentally the diffusion of radon and thoron into the detectors.

Table 1. Different designs for discriminative radon-thoron detectors.

| Publication          | Low diffusion rate                                       | High diffusion rate                   |
|----------------------|--|---------------------------------------|
| Guo et al. 1995      | Opening of 5 mm in diameter                              | Four openings of 20 mm in diameter    |
| Tokonami et al. 2005 | Small air gap between the lid and bottom of the detector | Six holes of 6 mm in diameter         |
| Sahoo et al. 2013    | Four small pin holes, e.g. diameter of 2 mm              | -                                     |
| Gierl et al. 2014    | Small air gap between the lid and bottom of the detector | Several holes, diameter not specified |

## Foil materials used as diffusion barriers.

Possibly, the first attempt to eliminate thoron in radon detectors was done by using membrane foils as diffusion barriers (Ward et al., 1977). Several types of plastic foils (Table 2) have been studied by Hafez and Somogyi (1986). Considerable differences in radon diffusion coefficient was found due to different chemical structures. They concluded that the polyethylene proved to have the highest gas diffusion coefficient. Arafa (2002) has defined permeability constants  $P$  for 16 different materials and compared them to values found in the literature. The permeability constant was defined as  $P=KD$ , where  $D$  is the radon diffusion coefficient in the material and  $K$  is its “partition coefficient” (this is the dimensionless solubility of radon in the material, equal to the ratio of the radon concentration in the material to that in the ambient air). Thoron separation was not reported.

Table 2. Characteristics of foils according to Hafez and Somogyi (1986).

| Short name | Chemical name              | Mean foil thickness ( $\mu\text{m}$ ) | Radon permeability $P_{exp}$ ( $10^{-12} \text{ m}^2/\text{s}$ ) | Radon attenuation $R$ (%) | Thoron separation = $C(\text{Thoron}) / C(\text{Radon})$ |
|------------|----------------------------|---------------------------------------|--|---------------------------|--|
| PE         | polyethylene               | 70                                    | $7.8 \pm 1.5$  | 96.6                      | 0.53   |
| PC-G       | polycarbonate              | 15                                    | $2.4 \pm 0.1$  | 89.5                      | 0.12   |
| HC         | hydrate cellulose          | 25                                    | $0.97 \pm 0.06$  | 77.7                      | 0.15   |
| CA         | cellulose acetate          | 25                                    | $0.75 \pm 0.1$   | 72.9                      | 0.055  |
| PVC1       | polyvinyle chloride        | 10                                    | $0.58 \pm 0.13$  | 67.6                      | 0.044  |
| PVC2       | polyvinyle chloride        | 10                                    | $0.61 \pm 0.1$   | 68.7                      | 0.058  |
| PC-KG      | polycarbonate              | 15                                    | $0.55 \pm 0.15$  | 66.4                      | 0.045  |
| PET        | polyethylene-terephthalate | 12                                    | $0.30 \pm 0.05$  | 51.9                      | 0.038  |

Table 3 and Table 4 summarizes the reported values of the radon permeability constant. Some variation may be observed. A review of different measurement methods has been published by Rovenska and Jiranek (2012). They concluded that differences in results can mainly be attributed to insufficient duration of the tests, insufficient radon concentration to which the samples are exposed and the use of steady state calculation procedures for data measured under non-steady state conditions. The results in Table 4 show that the differences in the values of  $D$ ,  $K$  and  $P$  in different materials could be orders of magnitude. They can differ even when the chemical composition of the materials is the same (e.g Makrofol DE and Makrofol N polycarbonate). Moreover, the publication of Minelli and Doghieri (2017) of a study with stable gases indicate that, for a given polymer, the polymer pre-treatment and its prior history have an effect on the resulting gas solubility. The publication of Laot et. al. (2003) discusses the effects of the cooling rate and physical aging on the gas transport properties of bisphenol A polycarbonates.

Table 3. Radon permeability constants ( $10^{-12} \text{ m}^2/\text{s}$ ) reported by different authors.

| Short name | Chemical name              | Hafez and Somogyi 1986 | Giridhar et al. 1982 | Abdel-Fattah et al. 1987 | Ramachandran et al. 1987 | Wojcik 1991 | Arafa 2002  |
|------------|----------------------------|------------------------|----------------------|--------------------------|--------------------------|-------------|-------------|
|            | aluminized polycarbonate   |                        |                      |                          |                          |             | 0.4         |
|            | aluminized mylar           |                        |                      |                          |                          |             | 0.02        |
| CA         | cellulose acetate          | 0.75                   | 0.38                 | 0.55                     | 0.38                     |             | 2.1         |
| CN         | cellulose nitrate          |                        | 12.4                 |                          | 12.5                     |             | 1.6         |
| HC         | hydrate cellulose          | 0.97                   |                      |                          |                          |             | 3.6         |
| PC         | polycarbonate/ macrofol    | 0.55 - 2.4             |                      |                          |                          |             | 0.03 - 0.06 |
| PE         | polyethylene               | 7.8                    |                      | 7.8                      | 0.3                      |             | 0.2 - 3.6   |
| PET        | polyethylene-terephthalate | 0.30                   | 0.08                 | 0.3                      | 0.08                     |             | 3.0         |
|            | polyester                  |                        | 0.2                  |                          | 0.2                      |             | 4.3         |
| PVC        | polyvinyle chloride        | 0.58 - 0.61            | 5                    | 0.6                      | 5                        | 42          | 0.5         |
|            |                            |                        |                      |                          |                          |             |             |

Table 4. Radon diffusion coefficient  $D$ , partition coefficient  $K$  and permeability  $P$  values for Nylon 6, Makrofol DE and Makrofol N polycarbonates.

| Material   |                   | Partition coefficient | Diffusion coefficient                   | Permeability constant , calculated             | Reference              | Comments        |
|------------|-------------------|-----------------------|---|--|------------------------|-----------------|
| Short name | Chemical name     | $K$                   | $D$ ( $10^{-12} \text{ m}^2/\text{s}$ ) | $P = KD$ , ( $10^{-12} \text{ m}^2/\text{s}$ ) |                        |                 |
| N6         | Nylon 6           | 5                     | 0.0001                                  | 0.0005   | Wojcik et. al 2000     | T= 17.3 °C      |
| K4079      | Karlez comp. 4079 | 12.1                  | 0.00012                                 | 0.0015   | Wojcik et. al 2000     | T not specified |
| MAK_DE     | Makrofol DE       | 25.4                  | 0.0072                                  | 0.18   | Pressyanov et. al 2011 | T= 25 °C        |
| MAK_DE     | Makrofol DE       | 26.2                  | 0.0057                                  | 0.15   | Mitev et. al 2016      | T= 20 °C        |
| MAK_N      | Makrofol N        | 112                   | 0.0032                                  | 0.36   | Mitev et. al 2016      | T= 20 °C        |

Radon detectors have been enclosed in plastic (LDPE) bags to prevent the entry of radon and thoron progeny and to reduce entry of thoron in the detector. The sensitivity of these detectors to thoron was 0.4 % of their sensitivity to radon (Bochicchio et al. 2009).

A semi-permeable membrane filter has also been used as a diffusion barrier (e.g. latex or cellulose nitrate (SN)) in radon measurement techniques. Thickness of the membrane was 25  $\mu\text{m}$  and diffusion coefficient in the range of  $10^{-8}$  -  $10^{-7}$   $\text{cm}^2/\text{s}$  (Eappen and Mayya 2004). It allows the build-up of about 90 % of the radon gas and suppress the thoron gas concentration by more than 99 %. The mean time for radon to reach the steady-state concentration inside the detector is about 4.5 h.

Furthermore, aluminized mylar film with thickness of 76  $\mu\text{m}$  (Harley et al. 2005) and polyethylene film with thickness of 40  $\mu\text{m}$  (Leung et al. 2007) have been used to separate radon and thoron. Tyvek membrane can also be used to separate radon and thoron (Kotrappa et al. 2014). A 1-mm-thick and a 4-mm-thick Tyvek membrane is reported to attenuate thoron approximately by 50 % and 95 % respectively.

### **Diffusion through polymer foils.**

The penetration of radon through solids has been considered by many authors (e.g. Beckman, 1981; Durcik and Havlik, 1996). A useful approach to describe the radon/thoron penetration through membrane in a volume in which the detector is placed (e.g. the internal volume of a diffusion chamber with alpha track detector inside) has been described by Fleischer and Likes (1979). According to the theory described the growth of radon/thoron concentration in a volume V can be described by the expression:

$$C_{in} = C_{out} \frac{1}{1+\lambda\tau} (1 - \exp(-\lambda_{eff}t)), \quad (1)$$

where  $C_{in}$  and  $C_{out}$  are the concentrations in the volume and outside,  $\lambda$  is the decay constant,  $t$  is the time after the start of exposure,  $\lambda_{eff} = \lambda + \tau^{-1}$  and  $\tau$  is the “mean permeation time” (Tommasino 2016) which is given by the expression:

$$\tau = \frac{hV}{PS}, \quad (2)$$

where  $h$  is the thickness of the membrane,  $V$  is the internal volume that is “protected” by the membrane,  $S$  is the area of the membrane and  $P$  is the radon permeability in the membrane material. It follows that the equilibrium “radon/thoron transmission factor (attenuation)”  $R$  is expressed as:

$$R = \frac{C_{in}}{C_{out}} = \frac{1}{1 + \lambda\tau}. \quad (3)$$

Ideally, the membrane foil that stops thoron but not radon should be chosen so that  $R$  (for radon) is close to one, while  $R$  (for thoron) is close to zero. Notably, this depends not only on the permeability and thickness of the foil, but also on its area and the volume that is “protected” by this foil. For instance at 20<sup>0</sup> C the NRPB monitor has  $R$  (for radon) of 0.80, while the ENEA monitor it is 0.96. However, there is another problem that we aim to address within the MetroRADON project. This is the large temperature dependence of the diffusion coefficient of many polymer materials which results to large variation of their radon permeability with the temperature, as first demonstrated by Fleischer et al. (2000). Table 5 (Tommasino, 2016) shows the temperature dependence of the permeability of polyethylene foils used in three passive radon monitors and its effect on  $R$  (for radon).

Table 5. Permeability and radon transmission factor ( $R$ ) of polyethylene at different temperatures (Tommasino, 2016).

| TEMPERATURE<br>(°C) | PERMEABILITY<br>( $\times 10^{-7} \text{cm}^2/\text{s}$ ) | $R$<br>Cup | $R$<br>NRPB | $R$<br>ENEA |
|---------------------|---|------------|-------------|-------------|
| 0                   | $0.15 \pm 0.04$   | 0.32       | 0.33        | 0.73        |
| 20                  | $1.20 \pm 0.04$   | 0.80       | 0.80        | 0.96        |
| 40                  | $3.60 \pm 0.50$   | 0.92       | 0.92        | 0.99        |

As seen in Table 5  $R$  (for radon) can vary by a factor of three within the temperature interval 0-40<sup>0</sup> C. This is a challenge, since to avoid complicated calibration adjusted to the temperature during exposure, it should be ensured that both  $R$  (for thoron)  $\ll 1$  and  $R$  (for radon)  $\approx 1$  and their values do not vary substantially with the temperature. In order to study this problem and to be able to find practical solutions at different situations, the permeability of different polymer foils at different temperatures will be studied within the MetroRADON project.

### Diffusion through pin hole

Diffusion through a pin hole has been calculated by Sahoo et al. (2013). If the exposure time is long enough, the transmission factor (or ratio)  $R$  can be approximated by the following equation:

$$R = \frac{C_{in}}{C_{out}} \cong \frac{1}{1 + \frac{\lambda}{x}}, \quad (4)$$

where  $C_{in}$  and  $C_{out}$  is the radon or thoron concentration inside and outside of the detector, respectively,  $\lambda$  is the decay constant and

$$x = \frac{AD}{Vd}, \quad (5)$$

where  $A$  is the effective area of the pin hole or membrane,  $D$  is the diffusion coefficient,  $V$  is the volume of the detector and  $d$  is length of the pin hole. Hence, radon and thoron concentrations will be different due to their different half-lives. If the partition coefficient  $K =$

1, equations (2) and (5) are the same, i.e.  $x = \tau^{-1}$ .

Sahoo et al. (2013) also calculated the transmission time  $T_{95}$  for which radon/thoron reach 95 % of its final steady state concentration in the detector:

$$T_{95} = \frac{3}{\lambda+x}. \quad (6)$$

Table 6 presents some values of the transmission factor and time. If thoron is eliminated almost completely, i.e., if diffusion is slow, the sensitivity of the detector to radon is also reduced and the response time of the detector increases. For example, for  $x = 0,02 \text{ ms}^{-1}$ , the transmission factor for radon and thoron is 90.5 % and 0.2 %, respectively, but the transmission time  $T_{95}$  for radon is 38 hours.

Table 6. Transmission factors  $R$  and transmission time  $T_{95}$  for diffusion of radon and thoron through a membrane or a pin hole.

| $x$ (ms <sup>-1</sup> ) | $T_{95}$ (Radon) |       | $T_{95}$ (Thoron) |       |
|-------------------------|------------------|-------|-------------------|-------|
|                         | $R$ (Radon)      | (min) | $R$ (Thoron)      | (min) |
| 0.01                    | 0.826            | 4128  | 0.001             | 4.0   |
| 0.02                    | 0.905            | 2261  | 0.002             | 4.0   |
| 0.04                    | 0.950            | 1187  | 0.003             | 4.0   |
| 0.08                    | 0.974            | 609   | 0.006             | 4.0   |
| 0.16                    | 0.987            | 308   | 0.013             | 4.0   |
| 0.32                    | 0.993            | 155   | 0.025             | 3.9   |
| 0.64                    | 0.997            | 78    | 0.049             | 3.8   |
| 1.3                     | 0.998            | 39    | 0.093             | 3.6   |
| 2.6                     | 0.999            | 20    | 0.170             | 3.3   |
| 5.1                     | 1.000            | 10    | 0.291             | 2.8   |
| 10                      | 1.000            | 4.9   | 0.451             | 2.2   |
| 20                      | 1.000            | 2.4   | 0.622             | 1.5   |
| 41                      | 1.000            | 1.2   | 0.767             | 0.9   |

### Delay due to air flow in a pipe

In active detectors thoron can be eliminated using a long pipe or hose. Thoron or radon concentration  $C(t)$  at the end of the pipe at time  $t$  is

$$C(t) = C_0 e^{-\lambda t}, \quad (7)$$

where  $C_0$  is the concentration at the beginning of the pipe. Assuming a flow rate  $Q$  in a pipe with length  $L$  and diameter  $\Phi$ , the delay time can be expressed as:

$$t = \frac{V}{Q} = \frac{\pi L \Phi^2}{4Q}, \quad (8)$$

where  $V$  is the inner volume of the pipe. Solving  $L$  from this equation gives:

$$L = \frac{4tQ}{\pi \Phi^2}. \quad (9)$$

Table 7 shows the relative radon and thoron concentration  $C(t)/C_0$  at the end of the pipe for some values of the delay time  $t$ . After 8 minutes of flow in the pipe, the thoron concentration is reduced to 0.3 % of the original concentration  $C_0$ . The influence of this delay on the radon concentration is negligible. Flow time of 8 minutes can be achieved by varying the different parameters as shown in Table 8. Doubling of the length of the pipe or flow rate, doubles the delay time.

Radon concentration at the beginning of the pipe can be calculated, when the dimension of the pipe, the flow rate and the radon concentration at the end of the pipe are known.

Table 7. Relative radon and thoron concentration at the end of the pipe as a function of the delay time  $t$ .

| $t$ (min) | $C(t)/C_0$ |          |
|-----------|------------|----------|
|           | Radon      | Thoron   |
| 1         | 1,000      | 0,473    |
| 2         | 1,000      | 0,224    |
| 4         | 0,999      | 0,050    |
| 8         | 0,999      | 0,003    |
| 16        | 0,998      | 6,34E-06 |

Table 8. Length of the pipe necessary to achieve delay time of 8 minutes at air-flow rate 0.5 l/min for different pipe diameters.

| Diameter<br>(mm) | Length<br>(m) |
|------------------|---------------|
| 10               | 50,9          |
| 20               | 12,7          |
| 30               | 5,7           |

### Discussion and future tasks/activities

The influence of thoron on radon detectors can be significantly reduced with the discussed techniques, but a philosophical question remains: shouldn't both radon and thoron be measured, if it is known that thoron is present. If thoron concentration is small, only radon

can be measured and in some cases radon detectors sensitive to thoron could be used. If radon detectors sensitive to thoron are used where thoron is present, this leads to a systematic error, which is a confounding factor in epidemiological studies. The epidemiological studies are only one area in which the application of thoron discrimination techniques is important. Other areas are radon surveys and mapping. Another important application is for the aims of radon measurements in dwellings and work places that indicate if radon remediation is needed or not. Buildings with high thoron but low radon concentrations have been observed (Pressyanov et al., 2013). If radon identification or diagnostics in such buildings is made by a detectors sensitive to thoron wrong conclusions will be drawn and resources can be wasted. However, keeping in mind the optimization principle, the possible bias due to thoron interference can be accepted in some cases. For example, a bias of  $\pm 20 \text{ Bq/m}^3$  causes only minor error in the estimation of health risk and decisions about radon remediation.

The diffusion properties of radon detectors or thoron barrier membranes may be optimized to minimize the transport of thoron. However, if the diffusion is too slow, the response time of the detector increases and the sensitivity of the detector to radon is reduced. In some cases, it is important to have a fast time response (Tommasino and Pressyanov, 2018). For example, a work place could have a mechanical supply and exhaust ventilation system, which operates only at daytime and is shut down at nights and weekends to save heating energy. This leads to a situation, where radon concentration is higher during the nights and weekends than during the workdays. In this case, a significant error could be induced when measuring the daytime radon concentration, if the response time of the radon monitor is too slow.

Regarding calibration exposures, the influence of thoron can be eliminated using pure radon sources. If this is not possible and natural materials are used instead, the above mentioned techniques can be used to eliminate thoron from the calibration chamber. The natural sources can be placed in a plastic bag or connected to the exposure chamber through a pipe or hose that is long enough.

With respect to the usage of polymer foils as thoron barriers, the major challenge identified is the temperature dependence of the radon permeability of the polymer materials. This can change not only their properties as thoron barriers, but also the sensitivity to radon of monitors, the volume of which is “protected” by such membranes. Dedicated experimental and modeling research is planned to select materials and membrane design, so that this effect is sufficiently minimized.

In the planned tasks of the MetroRadon projects:

- The influence of thoron on active radon monitors that implement some of the reviewed techniques for thoron discrimination will be studied (A2.2.1);
- The influence of thoron on passive integrating radon detectors that implement some of the reviewed techniques for thoron reduction will be studied (Task 2.2.2);
- The properties of the above discussed filters/foils/ membranes as selective thoron barriers will be studied (Task 2.3.2 and Task 2.3.3);

Based on the results from these studies recommendations on the construction of radon detectors will be developed (Taks 2.3.4.).

## References

Arafa, W. (2002). Permeability of radon-222 through some materials. *Radiation measurements*, 35(3), 207-211.

Beckman, I. N. (1981). Experimental studying methods of radioactive gases diffusion in solid. *Radiochimia* 23, 281-287 /in Russian/.

Bohicchio, F., Ampollini, M., Tommasino, L., Sorimachi, A., & Tokonami, S. (2009). Sensitivity to thoron of an SSNTD-based passive radon measuring device: Experimental evaluation and implications for radon concentration measurements and risk assessment. *Radiation Measurements*, 44(9-10), 1024-1027.

Bohicchio, F., Venuti, G. C., Nuccetelli, C., Risica, S., & Tancredi, F. (1996). Indoor measurements of  $^{220}\text{Rn}$  and  $^{222}\text{Rn}$  and their decay products in a Mediterranean climate area. *Environment International*, 22, 633-639.

Calamosca, M., & Penzo, S. (2009). A new CR-39 nuclear track passive thoron measuring device. *Radiation Measurements*, 44(9-10), 1013-1018.

Chen, J., Walker, B., Sorimachi, A., Takahashi, H., & Tokonami, S. (2009). An investigation on radon and thoron response of alpha-track detectors used in the Winnipeg case-control study. *Radiation protection dosimetry*, 138(1), 83-86.

Chen, J., & Moir, D. (2012). A study on the thoron sensitivity of radon detectors available to Canadians. *Journal of Radiological Protection*, 32(4), 419.

Durcik M. and Havlik H. (1996). Experimental study of radon and thoron diffusion through barriers. *Journal of Radioanalytical and Nuclear Chemistry* 209/2, 307-313.

Eappen, K. P., & Mayya, Y. S. (2004). Calibration factors for LR-115 (type-II) based radon thoron discriminating dosimeter. *Radiation measurements*, 38(1), 5-17.

Eappen, K. P., Sapra, B. K., & Mayya, Y. S. (2007). A novel methodology for online measurement of thoron using Lucas scintillation cell. *Nuclear Instruments and Methods in Physics Research Section A: Accelerators, Spectrometers, Detectors and Associated Equipment*, 572(2), 922-925.

Eappen, K. P., Nair, R. N., & Mayya, Y. S. (2008). Simultaneous measurement of radon and thoron using Lucas scintillation cell. *Radiation Measurements*, 43(1), 91-97.

Falk, R. Möre, H., Nyblom, L. (1992). Measurements of  $^{220}\text{Rn}$  in Air Using a Flow-Through Lucas Cell and Multiple Time Analysis of Recorded Pulse Events. *Radiation Protection Dosimetry*, Volume 45, Issue 1-4, 1, Pages 111–113.

Falk, R., Åkerblom, G., & Nyblom, L. (2008). A method for the determination of thoron and thoron progeny concentration at workplaces and thoron concentration in calibration chambers. *Radiation protection dosimetry*, 131(4), 444-448.

Fleischer, R.L. and Likes, R.S. (1979). Integrated radon monitoring by the diffusional barrier technique. *Geophysics* 44, 1863-1873.

Fleischer, R.L., Giard, W.R., and Turner L.G. (2000). Membrane-based thermal effects in  $^{222}\text{Rn}$  dosimetry. *Radiation Measurements* 32, 325-328.

Giridhar, J.H.A., Raghavayya, M., Padmanabhan, N. (1982). Radon permeability of some membranes. *Health Phys.*, 42, pp. 723-725.

Gierl, S., Meisenberg, O., Feistenauer, P., & Tschiersch, J. (2014). Thoron and thoron progeny measurements in German clay houses. *Radiation protection dosimetry*, 160(1-3), 160-163.

Guo, Q., Iida, T., Okamoto, K., & Yamasaki, T. (1995). Measurements of Thoron Concentration by Passive Cup Method and Its Application to Dose, Assessment. *Journal of nuclear science and technology*, 32(8), 794-803.

Hafez, A. F., & Somogyi, G. (1986). Determination of radon and thoron permeability through some plastics by track technique. *International Journal of Radiation Applications and Instrumentation. Part D. Nuclear Tracks and Radiation Measurements*, 12(1-6), 697-700.

Harley, N. H., Chittaporn, P., Heikkinen, M., Merrill, R., & Medora, R. (2005). Outdoor radon and thoron in the USA, Canada, Finland and Thailand. In *Radioactivity in the Environment* (Vol. 7, pp. 670-677). Elsevier.

Ishikawa, T. (2004). Effects of thoron on a radon detector of pulse-ionization chamber type. *Radiation protection dosimetry*, 108(4), 327-330.

Knutson, E. O., George, A. C., Shebell, P., & Gogolak, C. V. (1994). EML thoron gas measurements. *Radiation Protection Dosimetry*, 56(1-4), 263-266.

Kotrappa, P., Stieff, L., & Stieff, F. ATTENUATION OF THORON (Rn 220) IN TYVEK (®) MEMBRANES. In *Proceedings of the 2014 International Radon Symposium Accepted for publication*.

Laot. M. Marand. E., Schmittmann. B., Zia. R.K.P. (2003). Effects of Cooling rate and Physical Aging on the Gas Transport Properties in Polycarbonate, *Macromolecules*, 36, 8673-8684.

Leung, S. Y. Y., Nikezic, D., Leung, J. K. C., & Yu, K. N. (2007). A study of the polyethylene membrane used in diffusion chambers for radon gas concentration measurements. *Nuclear Instruments and Methods in Physics Research Section B: Beam Interactions with Materials and Atoms*, 263(1), 311-316.

McLaughlin, J. (2010). An overview of thoron and its progeny in the indoor environment. *Radiation protection dosimetry*, 141(4), 316-321.

Michielsen, N., & Bondiguel, S. (2015). The influence of thoron on instruments measuring radon activity concentration. *Radiation protection dosimetry*, 167(1-3), 289-292.

Minelli, M., Doghieri. F. (2017). Predictive model for gas and vapor sorption and swelling in glassy polymers: II. Effect of sample previous history, *Fluid Phase Equilibria*, 444, 47-55.

Mitev, K., Cassette, P., Georgiev, S., Dimitrova, I., Sabot, B., Boshkova, T., Tartès, I., Pressyanov, D. (2016) “Determination of <sup>222</sup>Rn absorption properties of polycarbonate foils by liquid scintillation counting. Application to <sup>222</sup>Rn measurements”, *Applied Radiation and Isotopes*, 109, 270 - 275.

Pressyanov, D., Mitev, K., Dimitrova, I., Georgiev, S. (2011) “Solubility of krypton, xenon and radon in polycarbonates. Application for measurement of their radioactive isotopes”, *Nuclear Instruments and Methods in Physics Research, section A*, 629, 323-328.

Ramachandran, T.V., Lalit, B.Y., Mishra, U.C. (1987). Measurement of radon permeability through some membranes. *Nucl. Tracks Radiat. Meas.*, 13, pp. 81-84.

Reddy, M. S., Reddy, P. Y., Reddy, K. R., Eappen, K. P., Ramachandran, T. V., & Mayya, Y. S. (2004). Thoron levels in the dwellings of Hyderabad city, Andhra Pradesh, India. *Journal of environmental radioactivity*, 73(1), 21-28.

Rovenská, K., & Jiránek, M. (2012). Radon diffusion coefficient measurement in waterproofings—A review of methods and an analysis of differences in results. *Applied Radiation and Isotopes*, 70(4), 802-807.

Sahoo, B. K., Sapra, B. K., Kanse, S. D., Gaware, J. J., & Mayya, Y. S. (2013). A new pin-hole discriminated  $^{222}\text{Rn}/^{220}\text{Rn}$  passive measurement device with single entry face. *Radiation Measurements*, 58, 52-60.

Sciocchetti, G., Sciocchetti, A., Giovannoli, P., DeFelice, P., Cardellini, F., Cotellessa, G., & Pagliari, M. (2010). A new passive radon–thoron discriminative measurement system.

Shang, B., Chen, B., Gao, Y., Wang, Y., Cui, H., & Li, Z. (2005). Thoron levels in traditional Chinese residential dwellings. *Radiation and environmental biophysics*, 44(3), 193-199.

Shweikani, R., Al-Bataina, B., & Durrani, S. A. (1997). Thoron and radon diffusion through different types of filter. *Radiation measurements*, 28(1-6), 641-646.

Sumesh, C. G., Kumar, A. V., Tripathi, R. M., & Puranik, V. D. (2013). Comparison study and thoron interference test of different radon monitors. *Radiation protection dosimetry*, 153(3), 309-315. *Radiation protection dosimetry*, 141(4), 462-467.

Sumesh, C. G., Ashokkumar, P., Kumar, A. V., Ratheesh, M. P., Ravi, P. M., Tripathi, R. M., & Mitra, A. K. (2014). Continuous thoron gas measurement using single scintillation cell—Correction for  $^{212}\text{Pb}$  deposition. *Radiation Measurements*, 67, 1-4.

Tokonami, S., Yang, M., Yonehara, H., & Yamada, Y. (2002). Simple, discriminative measurement technique for radon and thoron concentrations with a single scintillation cell. *Review of scientific instruments*, 73(1), 69-72.

Tokonami, S., Yang, M., & Sanada, T. (2001). Contribution from thoron on the response of passive radon detectors. *Health physics*, 80(6), 612-615.

Tokonami, S., Takahashi, H., Kobayashi, Y., Zhuo, W., & Hulber, E. (2005). Up-to-date radon-thoron discriminative detector for a large scale survey. *Review of scientific instruments*, 76(11), 113505.

Tommasino L. (2016). Concealed errors in radon measurements and strategies to eliminate them. Presented at the 8<sup>th</sup> Int. Conf. on Protection against Radon at Home and Work, Prague, 12-16 September 2016.

Tommasino L., Pressyanov D. (2018). A new generation of passive radon monitors: the film-badges for occupation exposures. *Radiation Protection Dosimetry* (in press) DOI: 10.1093.

Tripathi, R. M., Sumesh, C. G., Vinod Kumar, A., & Puranik, V. D. (2013). Application of thoron interference as a tool for simultaneous measurement of radon and thoron with a pulse ionisation chamber. *Radiation protection dosimetry*, 155(2), 155-160.

Ward, W.J., Fleischer, R.L. and Mogro-Campero, A., 1997. Barrier techniques for separate measurement of radon isotopes. *Rev. Sci. Instrum.* 48, 1440-1441.

Wiegand, J., Feige, S., Quingling, X., Schreiber, U., Wieditz, K., Wittmann, C., & Xiarong, L. (2000). Radon and thoron in cave dwellings (Yan'an, China). *Health physics*, 78(4), 438-444.

Wojcik, M. (1991). Measurement of radon diffusion and solubility constant in membranes. *Nucl. Instrum. Methods*, B 61, pp. 8-11.

Wojcik, M., Wlazlo, W., Zuzel, G., Heusser, G., (2000). Radon diffusion through polymer membranes used in the solar neutrino experiment Borexino. *Nucl. Instrum. Methods*, B 449, pp. 158-171.

Zhuo, W., Tokonami, S., Yonehara, H., & Yamada, Y. (2002). A simple passive monitor for integrating measurements of indoor thoron concentrations. *Review of scientific instruments*, 73(8), 2877-2881.

Zhang, L., Wu, J., Guo, Q., & Zhuo, W. (2010). Measurement of thoron gas in the environment using a Lucas scintillation cell. *Journal of Radiological Protection*, 30(3), 597.



16ENV10 MetroRADON

Deliverable D2  
Annex XIII

Task A.2.3.2

Partition Coefficients and Diffusion  
Lengths of  $^{222}\text{Rn}$  in Some Polymers at  
Different Temperatures

S. Georgiev, K. Mitev, Ch. Dutsov,  
T. Boshkova, I. Dimitrova

SUBG

(Article published in: International Journal of Environmental Research  
and Public Health, 16 (2019) 4523, doi:10.3390/ijerph16224523 )



Article

# Partition Coefficients and Diffusion Lengths of $^{222}\text{Rn}$ in Some Polymers at Different Temperatures

Strahil Georgiev , Krasimir Mitev \* , Chavdar Dutsov, Tatiana Boshkova and Ivelina Dimitrova

Faculty of Physics, Sofia University “St Kliment Ohridski”, 5 James Bourchier Blvd, 1164 Sofia, Bulgaria; strahilg@phys.uni-sofia.bg (S.G.); ch.dutsov@phys.uni-sofia.bg (C.D.); boshkova@phys.uni-sofia.bg (T.B.); divelina@phys.uni-sofia.bg (I.D.)

\* Correspondence: kmitev@phys.uni-sofia.bg

Received: 20 September 2019; Accepted: 11 November 2019; Published: 15 November 2019



**Abstract:** In this work, the partition coefficients  $K$  and diffusion lengths  $L_D$  of radon in some polymers are experimentally determined for several temperatures in the range  $T = 5\text{--}31\text{ }^\circ\text{C}$ . Some of the obtained values are compared to published data available for the given temperatures. It is shown that the temperature dependencies of the partition coefficients  $K(T)$ , the diffusion lengths  $L_D(T)$ , and the permeabilities  $P(T)$  could be described analytically for the studied temperature range  $5\text{--}31\text{ }^\circ\text{C}$ . This allows estimation of these quantities in the given temperature range and quantitative description of the transport of radon in the studied polymers.

**Keywords:** radon; diffusion; absorption; polymers; polycarbonates

## 1. Introduction

Indoor radon ( $^{222}\text{Rn}$ , half-life 3.8232 d) is recognized as a severe health-risk factor, being the leading cause for lung-cancer after smoking [1]. Due to its short half-life, thoron ( $^{220}\text{Rn}$ , half-life 55.8 s) appears indoors in significant concentrations only under specific circumstances. However, in such cases, thoron could be a health-hazard too [2–4]. Therefore, a wide range of methods for radon and thoron measurements are developed dealing with different aspects of the problem—metrological assurance, risk assessment, dose estimation, average activity concentration measurement, mitigation, etc.

Most of the devices used for radon and thoron measurement (either passive or active) are sensitive to both isotopes and some of them are also sensitive to their short-lived progenies (SLPs) [2–9]. The devices able to discriminate between radon, thoron, and SLPs typically use diffusion barrier (incl. polymer membranes) and some are even packed in polymer bags [6–8,10,11]. The SLPs are effectively stopped by any diffusion barrier as their atoms are chemically active. On the other hand, radon and thoron are inert gases, and the discrimination between them is based on their different half-lives and the decay during the diffusion through the barrier. The polymer membranes are preferred as they are easy to handle, hydrophobic, flexible, and durable, produced in various thicknesses, and their diffusion properties at room temperature allow good discrimination between radon and thoron. However, the diffusion properties of Rn isotopes in the polymers are temperature dependent. Thus, at a given temperature, the membrane could be almost fully permeable to radon while fully stopping thoron, while, at another temperature, it could be partially permeable to both radon and thoron, which could lead to systematic error in the measurements. The diffusion properties of some polymers are studied in the literature and are quantified by the diffusion coefficient, the permeability, etc. [12–15]; however, their temperature dependence is rarely mentioned and the obtained values of these parameters vary a lot. A possible reason for these variations could be the different temperatures during the parameters'

estimation. Other reasons that could lead to such variations are related to the production process. It is known that factors such as melting and extrusion temperatures and pressure, cooling speed, presence of some solvents or catalysts have influence on the gas transport properties of the polymers [16]. Additionally, the polymer membranes, depending on their purpose of use, could be compounds of various polymers or polymer layers of different properties and could contain various additives such as fillers, softening agents, UV stabilizers, reinforcements, etc. that could influence their gas transport properties. Therefore, it is important to study the properties of the membranes when the production process (or the producer/supplier) is changed or when they are used under extreme conditions.

Moreover, in the last two decades, it was shown that some polycarbonates such as the Makrofol N and Makrofol DE (Makrofol® family are polycarbonate-based products by Bayer AG, Leverkusen, Germany) have a remarkably high absorption ability to Rn (and other noble gases) [17,18]. Based on that property of the polycarbonates, several methods for radon and other radioactive noble gases (RNGs) measurement were developed. These methods use the polycarbonate as a passive sampler that absorbs and concentrates the RNG from the ambient media. Some of these methods measure the cumulative activity of the absorbed radon relying on the track-etched properties of the Makrofol DE or another (external) track detector [19–21], while others register the alpha-, beta- or gamma-particles of the absorbed radon and its SLP (or other RNG) by active detectors—Liquid Scintillation (LS) counters, gross alpha/beta counters, HPGe gamma-spectrometers and others (see [22–25] and the references there). To apply these methods, the temperature dependence of the diffusion properties of the polycarbonates should be known. This dependence is studied for Makrofol DE [26,27], but, for Makrofol N, the diffusion properties are known only for a single temperature value [23,28].

In [29], it is shown that the transport of RNGs in polymers could be described by two physical parameters: the diffusion length  $L_D$  of the RNG in the polymer and the partition coefficient  $K$  of the RNG at the border between the polymer and the ambient media. The purpose of the present work is to estimate experimentally these parameters for radon in some polymers (Makrofol DE, Makrofol N, polypropylene, high-density polyethylene, and low-density polyethylene) at different temperatures and to study their temperature dependence. In the course of the studies, a new approach for precise measurement of the activity of radon in polymers was developed and utilized.

## 2. Materials and Methods

In this work, several polymer foils are studied: Makrofol DE, Makrofol N, polypropylene (PP), high-density polyethylene (HDPE), and two types of low-density polyethylene—plain and anti-slip covered (resp. LDPE and LDPE-A) (The polymer foils PP, HDPE, LDPE, and LDPE-A are supplied from Extrapack OOD, Sofia, Bulgaria.). The choice of the first two is determined by their high absorption ability to RNGs [23,29] and their application for radon measurements. The last four materials are chosen since membranes are made of similar polymers. Such membranes are used for radon/thoron discrimination in some detectors and for radon prevention and mitigation [12].

### 2.1. Transport of RNGs in Polymers

The theoretical model presented and validated in [29] describes the transport of RNG in polymers in two steps/assumptions:

1. The atoms of the RNG are caught in the polymer matrix at the border ambient media/polymer and, in any moment, the ratio of the RNG concentrations at the surface of the polymer  $c_{in}$  and, in the ambient media,  $c_{out}$  is given by the partition coefficient  $K = \frac{c_{in}}{c_{out}}$ . It must be noted that the partition coefficient of some polymers could be greater than one (For example,  $K \approx 100$  for  $^{222}\text{Rn}$  at the border Makrofol N/air at room temperature, which makes it very appropriate for a radon sampler). One possible explanation of this phenomenon could be the presence of free-volume traps in the polymer matrix (see [28] and the references there). In the free-volume trap models, it is considered that there are small voids in the polymer matrix with sizes close to the dimensions

of the RNG atoms. The RNG atoms are trapped in these voids, and the concentration of the RNG in the polymer appears to be higher than in the ambient media;

2. Once the RNG atoms are caught in the polymer matrix, their transport in the polymer is described by the diffusion equation (Fick's second law) with an additional term that accounts for the radioactive decay:

$$\frac{\partial c}{\partial t} = D \left( \frac{\partial^2 c}{\partial x^2} + \frac{\partial^2 c}{\partial y^2} + \frac{\partial^2 c}{\partial z^2} \right) - \lambda c, \quad (1)$$

where  $c(x, y, z, t)$  [ $\text{m}^{-3}$ ] is the RNG concentration in the polymer sample as a function of the space  $x, y, z$  [m] and time  $t$  [s] coordinates (Hereafter, the units of the quantities according to the International System of Units (SI) are given in square brackets "[ ]", when the quantity is introduced for the first time in the text),  $D$  [ $\text{m}^2/\text{s}$ ] is the diffusion coefficient of the atoms of the noble gas in the polymer, and  $\lambda$  [ $\text{s}^{-1}$ ] is the decay constant of the RNG. In [29], Equation (1) is solved for some given shapes of the polymer samples, immersed in RNG-containing media. Once the polymer sample is exposed, it absorbs the RNG, and the dynamics of the absorption depends on the exposure conditions, polymer geometry, and on the parameters  $K$  [dimensionless] and  $D$ . In the present work, plate-shaped specimens are considered exposed to radon in air for time  $t_s$  [s] and left to desorb in infinite radon-free media for time  $t_d$  [s]. In the considered exposure, radon is promptly introduced in the exposure volume and then the activity concentration of radon decreases exponentially (due to radioactive decay) with the decay constant of radon. For plate-shape specimens (specimens for which one of the dimensions is orders of magnitude smaller than the others), the process is considered one-dimensional, and the solution for the RNG activity  $A(t_s, t_d)$  [Bq] absorbed in the specimen is [29]:

$$A(t_s, t_d) = \frac{8\lambda L_D^2 V K C_A}{L^2} \sum_{k=0}^{\infty} \frac{e^{-\lambda t_s} - e^{-\lambda_k t_s}}{\lambda_k - \lambda} e^{-\lambda_k t_d}, \quad (2)$$

with

$$\lambda_k = \lambda \left( 1 + \left( \frac{(2k+1)\pi L_D}{L} \right)^2 \right), \quad (3)$$

where  $L$  [m] and  $V$  [ $\text{m}^3$ ] are the thickness and the volume of the specimen,  $C_A$  [ $\text{Bq}/\text{m}^3$ ] is the initial activity concentration of the RNG in the media, and  $L_D$  [m] is the diffusion length of the RNG in the polymer. In this model, the only two parameters are the partition coefficient  $K$  and the diffusion length  $L_D$ . The latter is by definition related to the diffusion coefficient  $D$ :  $L_D = \sqrt{D/\lambda}$ . Thus, if the two parameters  $K$  and  $L_D$  (or  $D$ ) are known, the transport of the RNG in/through a polymer membrane could be quantitatively described. It must be noted that Equation (2) is derived for the more general case of transient radon distribution in the sample and is valid for arbitrary sorption and desorption times. The only restrictions to Equation (2) are the plate shape of the specimens and the exponentially decreasing ambient activity concentration (In [29], Equation (1) is also solved for constant ambient activity concentration and for cylindrical specimens).

## 2.2. Method for Estimation of $K$ and $L_D$

Based on the above-described model, a method for estimation of  $K$  and  $L_D$  is developed [30] and later modified [23]. In the modified method, several identical plate-shaped polymer specimens are exposed in RNG-containing media under controlled conditions. The specimens are then left to desorb in RNG-free media, and each one is submerged in an LS cocktail and measured by LS counting at a different moment after the exposure, in order to study the decrease of the absorbed activity due to decay and desorption. The obtained time-dependence  $A(t_d)$  is fitted with the theoretical function

given by Equation (2). For that purpose, it is more convenient to combine Equations (2) and (3) in the following way:

$$A(t_d; K, L_D) = 8VC_A K \sum_{n=1}^{\infty} \frac{e^{-\lambda t_s} - e^{-\lambda(1+(n\pi)^2(\frac{L_D}{L})^2)t_s}}{(n\pi)^2} e^{-\lambda(1+(n\pi)^2(\frac{L_D}{L})^2)t_d}, \quad (4)$$

where  $n = 2k + 1$  is an odd number. Since the exposure conditions and the specimen dimensions are known, the only unknown (free) parameters in Equation (4) are  $K$  and  $L_D$ . The infinite sum in Equation (4) is convergent and it converges faster with the increase of  $t_d$  and the ratio  $L_D/L$ . Thus, after a certain time of desorption  $t_d$  (depending on the ratio  $L_D/L$ ), the sum could be restricted to a reasonable number of terms  $n$  and  $K$  and  $L_D$  could be estimated by fitting the experimental data for  $A_i(t_{d,i})$  with the model curve  $A(t_d; K, L_D)$  from Equation (4). An important advantage of the method is that it is applicable in transient (non steady-state) conditions. The only restrictions to it are: (1) The specimens have to be plate-shaped and the ambient activity has to decrease exponentially (see Section 2.1) and (2)  $L_D/L > 0.2$ , preferably  $L_D/L > 1$ , so that the convergence of the series in Equation (4) is faster. In all experiments presented in this manuscript, these restrictions are obeyed.

### 2.3. Measurement of the Absorbed Activity

For the activity follow up, two approaches are considered. The first is direct LS measurement of the absorbed activity. In [23], it is shown that Makrofol N is soluble in a toluene-based LS cocktail. In the present work, the same toluene-LS cocktail is used for the Makrofol N measurements: high performance glass vials with a foil-line cap by PerkinElmer (Waltham, MA, USA) are fully filled with the toluene-LS cocktail and the Makrofol N foils are periodically immersed in it. Once the foils are closed in the vials, they are dissolved in the LS cocktail—the activity is fully transferred in the cocktail and, when equilibrium is reached between radon and its SLP (after 4h), the activity in the vials decreases with the half-life of radon. Makrofol N fully dissolves in a toluene-based cocktail, which allows the absorbed activity to be measured with a common LS counter or via absolute measurement with a TDCR-counter [23] (TDCR — Triple to Double Coincidence Ratio).

On the other hand, the Makrofol DE foil is only partially soluble in toluene-based cocktail (some fine particles remain) while the other four polymers are insoluble in toluene. This could lead to variations in the measurement efficiency, since the RNG partially desorbs from the specimen to the LS cocktail during the measurement. The change in efficiency due to the different distribution of activity in the specimen and the cocktail could be significant especially for alpha-particles: an alpha-particle emitted in the scintillator is detected with 100% detection efficiency [31] while one emitted in the volume of the polymer will be detected only if it reaches the scintillator. Some other organic solvents—Gasoline, Bensol (Benzene), 1,2Dichloroethane (ethylene dichloride) were also tested and they did not dissolve PP, HDPE, and LDPE—despite the fact that the storage of some of these solvents in PE bottles is not allowed, suggesting they should react with PE. Further discussions with chemists confirmed that PE is somewhat resistive to lots of chemical solvents. Therefore, the second approach chosen in the current work is Cherenkov-counting of the polymer by LS-counter. A similar approach for direct Cherenkov-counting of RNGs absorbed in Makrofol DE grains is presented in [32]. The basic idea is to place the Makrofol DE grains in LS-vial and to register the Cherenkov light (e.g., with a common LS-counter) emitted by the beta-particles (of the SLP of  $^{222}\text{Rn}$ ) passing through the Makrofol DE. However, the polymer foils used in the present work are thin, which leads to very fast desorption of radon from the specimen to the air in the empty LS-vial. This could lead to a change in the counting efficiency and a loss of radon from the vial that could not be followed and corrected for. This is why the approach was modified: the LS-vials are fully filled with distilled water, and the polymer specimen is immersed in it. When the polymer foil is immersed in the water, some of the radon absorbed in the foil is released in the water until equilibrium between the radon concentration in the two media is reached. The equilibrium is determined by the partition coefficient at the border water–polymer. During the

process of redistribution of the activity, the Cherenkov counting efficiency changes as the Cherenkov effect depends on the refraction index of the media. Once equilibrium is reached, the efficiency is constant (as it is shown further in this work), and it could be used to determine the activity in the sample.

The two approaches (LS and Cherenkov counting) were chosen due to several advantages they offer, compared to gamma-spectrometry or external gross beta-counting:

- These approaches allow precise timing—when the foil is closed in the vial, the activity is “trapped” in the vial, thus it could be attributed to the exact moment of desorption within 1–2 s.
- There is a small (for the Cherenkov) or even no (for the LS) activity leakage from the vials (see further in Section 3.1). Thus, if the samples have to be measured later or for a longer time, the activity will be sufficient for a longer time and precise long measurements can be performed.
- As the activity is “trapped” in the vial, there is no need for temperature control during the measurement. In the case of gamma-spectrometry and external gross counting, the samples have to be kept at the studied temperature; otherwise, the desorption will be compromised. This is inconvenient or even unachievable in the case of a temperature that differs with more than 5–10 °C from the normal room temperature.

### 3. Experiments

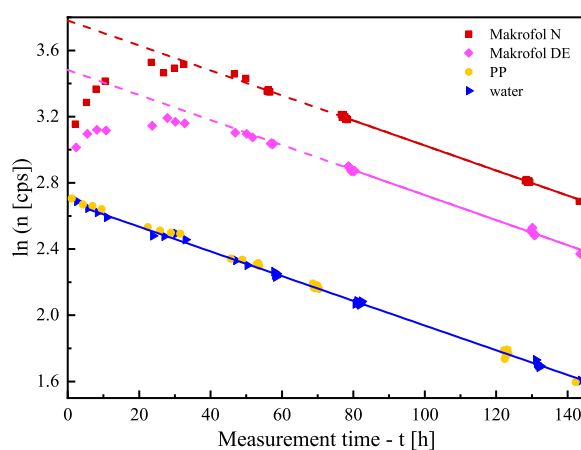
Two series of experiments were carried out. In all experiments high-performance glass vials with foil-lined caps (Perkin Elmer, Waltham, MA, USA) were used. All polymer foils were cut in the same rectangular shape 1.60(5) cm × 5.70(5) cm (The uncertainties of the quantities reported hereafter are given in parenthesis according to [33]) in order to fit reproducibly in the glass vials. The thicknesses of the foils were measured with micrometer with 1 µm instrumental uncertainty. For the measurements of the activity in the foils, three detectors were used: a TDCR-counter [34], a HPGe detector with relative efficiency 24.9 %, and resolution 1.9 keV for the gamma-line 1332 keV of <sup>60</sup>Co (ORTEC, Oak Ridge, TN, USA) and an LS-analyzer RackBeta 1219 (Wallac, Turku, Finland). For the measurements of the activity concentration of radon in air during the exposure a reference monitor AlphaGUARD RnTn Pro (Saphymo, Frankfurt, Germany) was used.

#### 3.1. Estimation of the Counting Efficiencies

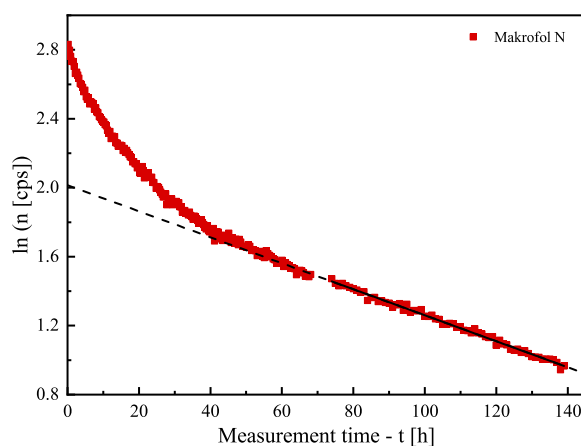
The first series of experiments was dedicated to the estimation of the counting efficiency  $\epsilon_c$  of the RackBeta 1219 LS-counter for LS-counting of Makrofol N in the toluene LS-cocktail and for Cherenkov counting of polymer foils in water. In the case of Makrofol N in LS-cocktail, a foil was exposed to radon; then, it was dissolved in the toluene cocktail and measured on the LS-counter and on the TDCR-detector. The TDCR allows absolute measurement of the activity in the vial [23], and the efficiency was estimated as the ratio of the counting rate of the LS-counter and the activity in the vial. The obtained value was  $\epsilon_c = 4.946(29)$ . Note that this is the efficiency for radon in equilibrium with its SLP, i.e., 5 particles (the 3 alphas of <sup>222</sup>Rn, <sup>218</sup>Po, <sup>214</sup>Po and the 2 betas of <sup>214</sup>Pb, <sup>214</sup>Bi) are emitted per one decay of radon.

For the estimation of the counting efficiency of the polymer foils in water, spring water from the town of Momin Prohod, Bulgaria with high radon concentration (about 2 MBq/m<sup>3</sup>) was used. Glass vials were fully filled with this water, unexposed foils were placed in the vials, and the vials were closed tightly. Two vials with water without foils were also prepared for comparison. Then, all the vials were periodically measured on the LS counter in order to follow the signal change in time. The duration of a single measurement was 10 minutes, and the whole follow-up experiment continued for about one week. The vials were also measured at the HPGe detector (2–3 measurements of each vial with a few hours duration) in order to estimate the activity in the vials, thus to estimate the counting efficiency of the LS counter. For the gamma-spectrometry analysis, the 295 keV and 352 keV gamma-lines of <sup>214</sup>Pb were used. The experiment was carried-out contrariwise—unexposed foil in

water with activity, instead of exposed foil in distilled water, in order to ensure better counting statistics, thus, to be more sensitive to slight changes in the signal due to the redistribution of radon between the water and the foils. The follow-up measurements at the LS-counter show that the signal of all samples, except those with Makrofol foils, decreases purely exponentially with the same (statistically) effective half-life as the signal of the distilled water samples (see, for example, Figure 1a). The average value of the effective half-life is 3.728(36) d, which is slightly lower than the radon half-life of 3.8232(8) d [35]. It was also observed that, in the first 60–70 h of the follow-up, the signal from the samples with the two types of Makrofol foils increases, reaches a maximum and then starts to decrease and, after 60–70 h, the decrease becomes exponential with the same above-mentioned effective half-life (see Figure 1a). The initial increase of the signal could be explained by the absorption of radon in the Makrofol foils—these foils absorb a significant part of the radon from the water. Due to their higher refraction index  $\sim 1.6$  [36] (compared to that of the water 1.33), they have higher efficiency for Cherenkov light emission (the higher the refraction index is, the lower is the threshold energy for the beta-particles to produce Cherenkov effect). Additionally, the Makrofol material possesses some (poor) scintillation properties [36], which also might lead to increasing the counting efficiency.



(a)



(b)

**Figure 1.** Signal follow-up (in semi-logarithmic scale) of several samples measured at the liquid scintillation counter in Cherenkov-counting mode: (a) unexposed polymer foils immersed in water with radon activity and (b) a Makrofol N foil exposed to radon immersed in distilled water. The points are the experimental data (the uncertainties—not shown, are within the size of the symbols), the solid line is a linear fit of the data, and the dashed line is extrapolation of the fit for better visualization. The signals decrease linearly in semi-log. scale (i.e., exponentially) and the slopes are very close.

The activity measurements with the HPGe show that the signals of all samples decrease with the same (statistically) effective half-lives that coincide with the average half-life obtained for the LS-counting. This leads to a few conclusions: the samples are almost hermetic to radon with a small leakage of radon that could be accounted for; the effect of the redistribution of radon between the water and the polymer is significant only for the two types of Makrofol; for all samples, the counting efficiency becomes constant, after a certain period of time—for PP, LDPE, LDPE-A, and HDPE, this period is 3–5 h (the time needed for reaching secular equilibrium between radon and its SLP) and, for Makrofol N and Makrofol DE, this period is about 60–70 h (the time needed for radon redistribution and reaching equilibrium in the two phases—polymer–water).

In this series, one more experiment was carried out: a Makrofol N foil was exposed to radon and then immersed in an LS glass vial full with distilled water—in the same way, the further experiments on  $K$  and  $L_D$  estimation are made. The purpose was to check if it matters for the counting efficiency in which direction the activity redistribution between water–polymer goes. In this experiment, only Makrofol N foil was used for two reasons: first, Makrofol N has the highest absorption ability, so it is the best for the counting statistics and, second, the change of the signal due to the redistribution is most pronounced for Makrofol N. Again, the signal from the foil was followed by the LS-counter (see Figure 1b) and measured several times at the HPGe detector. In this case, the LS-counting shows a faster decrease of the Cherenkov signal (due to desorption of the activity from the Makrofol N foil in the water, thus the Cherenkov efficiency decreases) in the first 60–70 h and, then, after equilibrium is reached between the radon in the two phases polymer–water, the signal decrease becomes exponential as in the previous experiment. Again, the gamma–spectrometry shows a single exponential decrease for the entire time of the follow-up. Additionally, the Cherenkov counting efficiencies as a function of time  $\epsilon_c(t)$  [dimensionless] were estimated for all foils in the two experiments using the net LS-counting rate  $n_0(t)$  [ $s^{-1}$ ] and the gamma-spectroscopically measured activity in the sample  $A(t)$ :

$$\epsilon_c(t) = \frac{n_0(t)}{A(t)}. \quad (5)$$

For the PP, LDPE, LDPE-A, and HDPE, no time-dependence of  $\epsilon_c(t)$  was observed. The obtained dependence of  $\epsilon_c(t)$  for the Makrofol DE and Makrofol N (both experiments) is shown in Figure 2. It is seen that, after 60–70 h, the counting efficiencies become constant and, for the Makrofol N foils from the two “Cherenkov-counting” experiments, the counting efficiencies are in excellent agreement. These observations lead to the conclusion that the Cherenkov-counting efficiency does not depend on the initial distribution of radon in the two phases. The counting efficiencies obtained in these series of experiments are given in Table 1. It should be noted that the Cherenkov-counting efficiencies of PP, LDPE, LDPE-A, and HDPE are very close to each other and to that of the pure water, while those of the Makrofol foils are significantly higher. This could be due to the much lower partition coefficients of the first four polymers compared to the partition coefficients of the Makrofol foils (see below) or due to the weak scintillation properties of the polycarbonate. Rough estimates show that, when equilibrium of radon between the two phases is reached, the activity of radon in the first four polymer foils used in this work is less than 1% of the total activity in the vial, while, in the Makrofol DE, it is about 15% and in Makrofol N—about 30%.

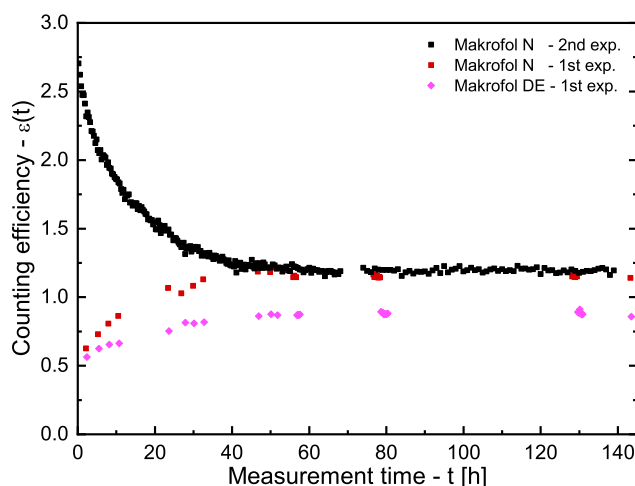


**Figure 2.** Cherenkov-counting efficiencies as a function of time for the two types Makrofol foils immersed in water. The uncertainties (not shown) at the level of  $1\sigma$  are about 5% for the points from the first experiment and about 3% for the points from the second experiment.

**Table 1.** Counting efficiencies for: polymer foils in distilled water counted in Cherenkov mode (1–6), distilled water counted in Cherenkov mode (7) and Makrofol N foil dissolved in toluene based liquid scintillation cocktail (LSC) (8). The counting efficiencies are given after reaching equilibrium distribution between radon concentration in the two phases (polymer–water) and/or equilibrium of radon and its short-lived progeny, i.e., these are steady-state counting efficiencies. For (1–4, 7,8), equilibrium is reached after 3–5 h and for (5,6) equilibrium is reached after 60–70 h.

| No | Sample               | Counting Efficiency |
|----|----------------------|---------------------|
| 1  | PP in water          | 0.380(12)           |
| 2  | LDPE in water        | 0.371(12)           |
| 3  | LDPE-A in water      | 0.400(14)           |
| 4  | HDPE in water        | 0.407(13)           |
| 5  | Makrofol N in water  | 1.168(36)           |
| 6  | Makrofol DE in water | 0.883(29)           |
| 7  | distilled water      | 0.376(12)           |
| 8  | Makrofol N in LSC    | 4.946(29)           |

PP – Polypropylene, LDPE – Low-Density Polyethylene, LDPE-A – Low-Density Polyethylene with Anti-slip coating, HDPE – High-Density Polyethylene.

### 3.2. Estimation of $K$ and $L_D$

The second series of experiments was dedicated to estimation of the partition coefficient and the diffusion length of radon in the studied polymers at different temperatures. Four experiments were carried out at four different temperatures. In these experiments, the foils were exposed to known radon concentration in air. In the first three experiments, six rectangular pieces of each type of foil (36 pieces in total) with dimensions  $1.6 \text{ cm} \times 5.6 \text{ cm} \times L$  (the thickness of the foils  $L$  is measured by a digital micrometer with  $1 \mu\text{m}$  resolution) were stacked in a holder and placed in a hermetic “exposure” drexel. The “exposure” drexel (700 mL) was connected in a closed loop with  $^{222}\text{Rn}$  source ( $\approx 100 \text{ kBq}$ ,  $\approx 200 \text{ mL}$ ), a peristaltic pump, and another “control” drexel (700 mL) (see Figure 3). The radon activity was promptly introduced in the system by opening all valves and turning on the pump at  $2 \text{ L/min}$  flow-rate for 5 min. After that, all valves were closed and the foils were exposed for 2–3 days. Thus, the exposure activity concentration in these three experiments was of the order of tens of  $\text{MBq/m}^3$ . Such high activity concentration was needed to ensure good counting statistics for the follow-up of the foils. During the exposure, each drexel was placed in a bigger hermetic vessel, and the radon concentration in the bigger vessels was measured by the AlphaGUARD. This was done in order

to check for radon leakage from the drexels. In all experiments, the leakage from the drexels was found to be less than 1% of the radon activity in the drexel. During the exposure, the bigger vessel (with the “exposure” drexel inside) was placed in a thermostat [37] and the exposure temperature was kept stable within 1 °C. The “control” drexel was used for estimation of the activity concentration during the exposure: Because the exposure activity concentration was above the measurement range of the AlphaGUARD, the activity from the “control” drexel was diluted in a larger vessel with a well-known volume. Thus, the activity concentration in the larger vessel was lowered to the measurement range of the AlphaGUARD—it was measured, and the initial (exposure) activity concentration was calculated based on this measurement and the volume ratio of the drexel and the larger vessel. The exposure data are summarized in Table 2.

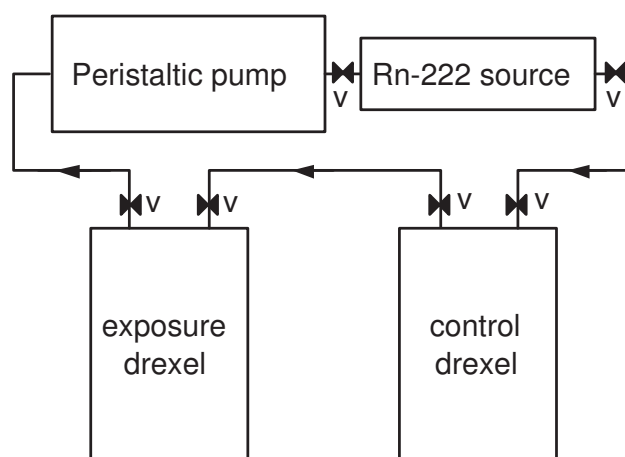


**Figure 3.** A scheme of the exposure system. In the beginning of the exposure, the activity of the radon source was promptly introduced in the system by the pump. Then, the valves “V” were closed, and the system was disconnected.

**Table 2.** Exposure conditions of the four experiments for estimation of the partition coefficients and diffusion lengths of radon in polymer foils: initial activity concentration of radon  $C_A$  [MBq/m<sup>3</sup>], exposure duration (sorption time)  $t_s$  [h], temperature  $T$  [°C], and the average thickness  $L$  [μm] of the stack of polymer foils of the given type. The uncertainties are at the level of  $1\sigma$ . The uncertainties of the thickness include the instrumental uncertainty of the micrometer and the standard deviation of the thickness of the stack of the polymers. “N/A” means that polymers of that type are not used in the given experiment.

| $C_A$ [MBq/m <sup>3</sup> ] | $t_s$ [h] | $T$ [°C] | $L$ [μm] |          |          |           |            |             |  |
|-----------------------------|-----------|----------|----------|----------|----------|-----------|------------|-------------|--|
|                             |           |          | PP       | LDPE     | LDPE-A   | HDPE      | Makrofol N | Makrofol DE |  |
| 52.4(36)                    | 46.23     | 21(1)    | 31.4(11) | 74.0(28) | 97.0(37) | 123.8(18) | 42.1(11)   | 50.6(12)    |  |
| 49.5 (31)                   | 52.03     | 5(1)     | 31.1(10) | 74.1(24) | 92.0(24) | 123.8(30) | 41.9(11)   | 50.0(10)    |  |
| 31.4 (20)                   | 48.17     | 31(1)    | 29.7(11) | 76.7(39) | 89.6(11) | 120.3(12) | 42.0(11)   | 50.2(11)    |  |
| 1.442(75)                   | 69.43     | 10(1)    | N/A      | N/A      | N/A      | N/A       | 41.6(11)   | 50.7(11)    |  |

PP – Polypropylene, LDPE – Low-Density Polyethylene, LDPE-A – Low-Density Polyethylene with Anti-slip coating, HDPE – High-Density Polyethylene.

The fourth experiment was carried out in a 50 L calibration container, which is a part of the AlphaGUARD set. In this experiment, the activity concentration was lower (not enough to obtain measurable signal from all polymers) and therefore only Makrofol foils were exposed. In this experiment, seven pieces of Makrofol DE and twelve pieces of Makrofol N with the same dimensions as in the previous experiments were used. The activity concentrations during the exposure were measured by the AlphaGUARD monitor. The exposure vessel was placed in the hermostat [37], and the exposure temperature was kept stable within 1 °C. The exposure data are shown in Table 2.

After the exposure, the desorption of the radon absorbed in the foils was followed according to the procedures described in Section 2.3. Then, the method described in Section 2.2 was applied on the obtained time dependences in order to estimate  $K$  and  $L_D$ .

#### 4. Results

At the end of the exposure, for all experiments in the second series ( $K$  and  $L_D$  estimation series), the foils were removed from the exposure vessel and left to desorb in radon-free air. The temperature of the air was kept the same as the one during the corresponding exposure. Periodically, a foil of each type was immersed in an LS vial filled with distilled water or toluene LS cocktail (in the case of Makrofol N). The time intervals between the immersion of the foils of each type were optimized according to the desorption speed and varied from one minute to 10–15 hours. This optimization aimed to balance between the following two factors:

1. The uncertainties of the individual points of the desorption follow-up. We aim to achieve relative uncertainty of the net counting rate comparable to or better than that of the counting efficiency (see Table 1), i.e., a few percent;
2. The change (decrease) of the absorbed activity due to the desorption. The model curve (see Equation (4)) is a sum of several exponents in which the quantities  $K$  and  $L_D$  are parameters. In order to achieve a better estimate of the parameters, it is important to observe greater differences in the activity in the sample, i.e., to follow the desorption for a longer time. However, this leads to a decrease in the counting rate and an increase in its statistical uncertainty.

When the foils were placed in the LS vials, they were measured consecutively on the LS-counter. After the time needed to reach equilibrium (see Section 3.1), the obtained LS-signal was plotted in a semi-logarithmic scale (similarly to the data shown in Figure 1), and the data after the equilibrium were used to estimate the net counting rate at the moment the foil was placed in the vial. The obtained net counting rate and the counting efficiencies were used to estimate the activity in the foil at the moment of its placement in the LS-vial. In this way, the combination of the individual activities of the foils of given material constructs a very precise follow-up curve of the desorption of radon from the different materials. The obtained desorption data were fitted with the model curve (For the nonlinear curve fitting, the Levenberg–Marquardt optimization algorithm [38] is used. The uncertainties of the experimental points were used as weights for the fitting.) following Equation (4) and the partition coefficient and the diffusion length were estimated from the fit (see Table 3). An example of the fitting is shown in Figure 4.

Additionally, in the fourth experiment in which twelve Makrofol N were exposed, six of them were measured in water and six—in toluene LS cocktail. This was done in order to compare the two measurement approaches. The results obtained for both  $K$  and  $L_D$  are in very good agreement within the uncertainties.

For comparison, the values of  $K$  and  $L_D$  for some of the materials obtained in previous studies are also shown in Table 3. It is seen that all of them except Makrofol N show significant differences. The differences are even more pronounced when comparing  $K$  and  $L_D$  for Makrofol DE at different temperatures. It should be noted that only Makrofol N is physically the same foil—all Makrofol N foils used in the current and the previous study are cut from a single (larger) sheet. All other foils are different (including from different producers), even though the materials (chemical compound) are the same. A very probable reason for that could be the differences in the process of production of the foils e.g., melting and extrusion temperatures and pressure, the presence of some solvents or catalysts, cooling speed, etc. This implies that the production process has an effect on the diffusion properties of the polymers [16].

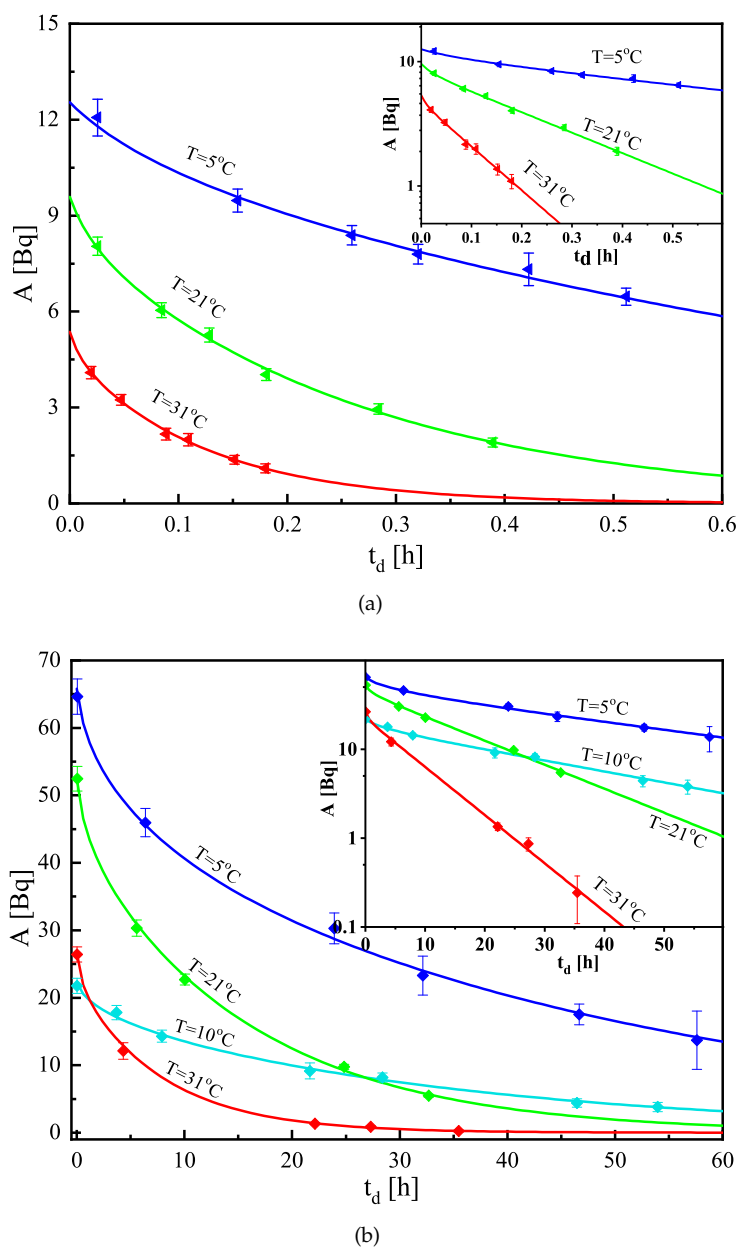


**Figure 4.** Experimental data (points) and theoretical curve fits (solid lines) of the desorption follow-up of radon from (a) High-density polyethylene and (b) Makrofol DE foils for the estimation of the partition coefficient and diffusion length at different temperatures. To fit the same scale, the activity data of Makrofol DE at 10 °C are multiplied by 10, as the radon activity concentration in this experiment was one order of magnitude lower than in the other three. The uncertainties are at the level of  $1\sigma$ . The embedded smaller graph presents the same data in semi-log scale—it is seen that, in the early desorption the dependences are nonlinear in semi-log scale, i.e., they are sums of several exponents rather than single exponents.

**Table 3.** Partition coefficients polymer–air, diffusion lengths, diffusion coefficients and permeabilities of radon for the studied polymers at different temperatures. The temperature was kept constant within 1 °C. All uncertainties are at the level of  $1\sigma$ . For comparison, values obtained in previous studies are given.

|   | PP       | LDPE   | LDPE-A   | HDPE                  | Makrofol N            | Makrofol DE | CD/Makrofol <sup>a</sup> |
|---|----------|--|----------|-----------------------|-----------------------|-------------|--------------------------|
| Partition Coefficient $K$                                 |          |  |          |                       |                       |             |                          |
| $T$ [°C]  |          |  |          |                       |                       |             |                          |
| 5   | 6.13(55) | 4.18(39)                                       | 4.05(42) | 3.63(33)              | 211(16)               | 77.5(67)    | 21.5(43)                 |
| 10  | –        | –  | –        | –                     | 183(12)               | 72.8(58)    | 24.3(36)                 |
| 21  | 3.69(38) | 3.66(38)                                       | 3.13(41) | 2.51(22)              | 103.3(79)             | 34.6(30)    | 26.2(19)                 |
| 31  | 3.25(43) | 3.70(43)                                       | 2.96(30) | 2.44(21)              | 70.2(51)              | 27.8(24)    | 22.9(10)                 |
| 20  |          | 2.17(14) <sup>b</sup><br>2.40(22) <sup>b</sup> |          | 2.21(13) <sup>b</sup> | 112(12) <sup>c</sup>  |             | 27.6(16) <sup>b</sup>    |
| Diffusion Length $L_D$ [μm]                               |          |  |          |                       |                       |             |                          |
| $T$ [°C]  |          |  |          |                       |                       |             |                          |
| 5   | 67.6(51) | 605(30)  | 646(36)  | 460(19)               | 18.0(10)              | 20.8(10)    | 42.2(16)                 |
| 10  | –        | –  | –        | –                     | 23.9(10)              | 26.8(10)    | 42.8(11)                 |
| 21  | 198(10)  | 1210(64)                                       | 1204(85) | 880(22)               | 36.2(10)              | 43.3(13)    | 53.8(5)                  |
| 31  | 300(15)  | 1880(140)                                      | 1722(54) | 1252(23)              | 52.1(15)              | 62.9(16)    | 75.5(8)                  |
| 20  |          | 1463(33) <sup>b</sup><br>1437(94) <sup>b</sup> |          | 721(9) <sup>b</sup>   | 38.9(13) <sup>c</sup> |             | 50.8(10) <sup>b</sup>    |
| Diffusion Coefficient $D$ [ $10^{-14}$ m <sup>2</sup> /s] |          |  |          |                       |                       |             |                          |
| $T$ [°C]  |          |  |          |                       |                       |             |                          |
| 5   | 0.96(14) | 76.9(77)                                       | 87.4(97) | 44.3(37)              | 0.0677(79)            | 0.0911(84)  |                          |
| 10  | –        | –  | –        | –                     | 0.120(10)             | 0.151(11)   |                          |
| 21  | 8.20(85) | 307(33)  | 304(43)  | 162(8)                | 0.275(15)             | 0.394(25)   |                          |
| 31  | 18.9(19) | 739(111)                                       | 623(39)  | 329(12)               | 0.570(32)             | 0.831(43)   |                          |
| Permeability $P$ [ $10^{-13}$ m <sup>2</sup> /s]          |          |  |          |                       |                       |             |                          |
| $T$ [°C]  |          |  |          |                       |                       |             |                          |
| 5   | 0.59(10) | 32.1(44)                                       | 35.4(54) | 16.1(20)              | 1.43(20)              | 0.706(89)   |                          |
| 10  | –        | –  | –        | –                     | 2.20(24)              | 1.10(12)    |                          |
| 21  | 3.03(44) | 113(17)  | 95.1(18) | 40.7(41)              | 2.84(27)              | 1.36(15)    |                          |
| 31  | 6.1(10)  | 273(52)  | 184(22)  | 80.4(75)              | 4.00(37)              | 2.31(23)    |                          |

<sup>a</sup> Values for Compact Discs (CD) and Makrofol foils reported in [26] (should be compared to Makrofol DE).

<sup>b</sup> Values for LDPE, HDPE and Makrofol foil (same as <sup>(a)</sup>) reported in [30]. <sup>c</sup> Values for Makrofol N reported in [23].

PP – Polypropylene, LDPE – Low-Density Polyethylene, LDPE-A – Low-Density Polyethylene with Anti-slip coating, HDPE – High-Density Polyethylene.

The estimated values of  $K$  and  $L_D$  (shown in Table 3) are used to calculate the other two quantities, often used to describe the transport of radon through polymer membranes—the diffusion coefficient  $D = \lambda L_D^2$  and the permeability  $P = KD$  [m<sup>2</sup>/s] (also shown in Table 3). The diffusion coefficients, the partition coefficients, and the permeabilities versus temperature are also shown in Figures 5–7 (the diffusion lengths are not shown as  $L_D = \sqrt{D/\lambda}$ ). It is seen that their temperature dependences could be described analytically for the studied temperature interval (5–31 °C). The parameters of the linear fits shown in Figures 5–7 are summarized in Table 4. That allows for estimating the values of the quantities for a given temperature in that interval and thus to model the absorption and transport of radon in the polymers.

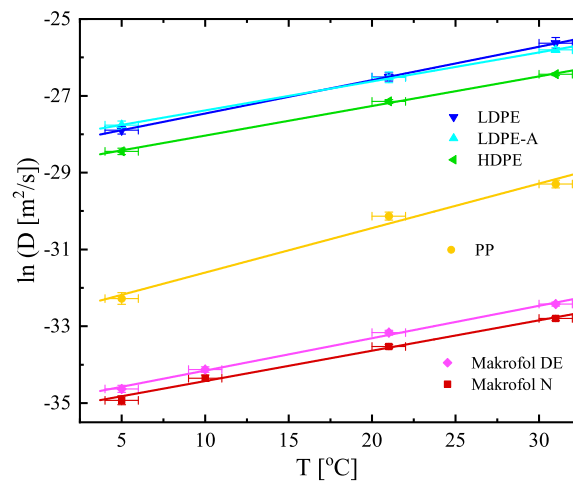


**Figure 5.** Temperature dependence of the diffusion coefficients of the studied materials. Note that the dependence is  $\ln(D)$  vs.  $T$ . The points are the experimental data and the solid lines are linear fits of the data. The uncertainties are at the level of  $1\sigma$ .

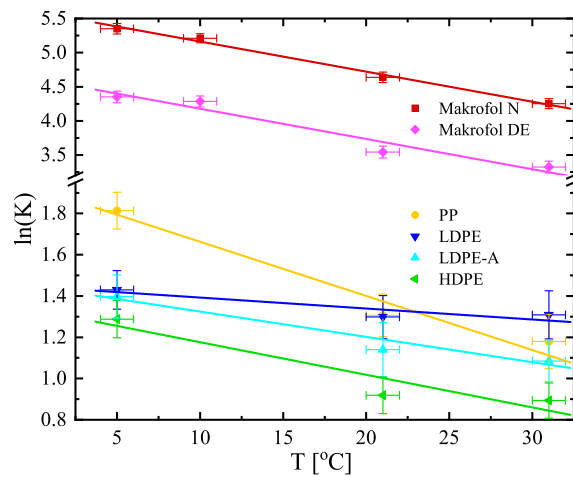


**Figure 6.** Temperature dependence of the partition coefficients of the studied materials. Note that the dependence is  $\ln(K)$  vs.  $T$ . The points are the experimental data and the solid lines are linear fits of the data. The uncertainties are at the level of  $1\sigma$ .

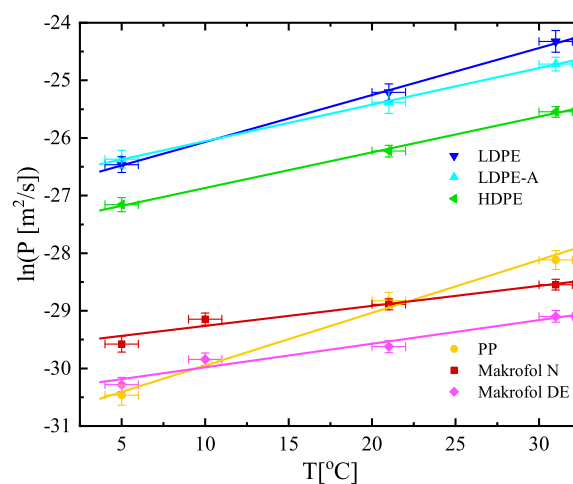


**Figure 7.** Temperature dependence of the permeabilities of the studied materials. Note that the dependence is  $\ln(P)$  vs.  $T$ . The points are the experimental data and the solid lines are linear fits of the data. The uncertainties are at the level of  $1\sigma$ .

**Table 4.** Parameters of the linear fits applied to the experimental data shown in Figures 5–7, respectively.

| Polymer     | $\ln(D) = a_D + b_D T$<br>Figure 5 |            | $\ln(K) = a_K + b_K T$<br>Figure 6 |             | $\ln(P) = a_P + b_P T$<br>Figure 7 |            |
|-------------|------------------------------------|------------|------------------------------------|-------------|------------------------------------|------------|
|             | $a_D$                              | $b_D$      | $a_K$                              | $b_K$       | $a_P$                              | $b_P$      |
| PP          | −32.76(35)                         | 0.1159(51) | 1.93(11)                           | −0.0262(59) | −30.87(23)                         | 0.092(10)  |
| LDPE        | −28.33(16)                         | 0.0869(80) | 1.45(11)                           | −0.0053(56) | −26.88(19)                         | 0.0815(96) |
| LDPE–A      | −28.13(16)                         | 0.0755(64) | 1.45(12)                           | −0.0123(56) | −26.69(19)                         | 0.0635(82) |
| HDPE        | −28.81(13)                         | 0.0771(55) | 1.33(12)                           | −0.0158(56) | −27.49(16)                         | 0.0619(68) |
| Makrofol N  | −35.22(12)                         | 0.0791(57) | 5.603(82)                          | −0.0441(43) | −29.61(13)                         | 0.0347(59) |
| Makrofol DE | −35.00(11)                         | 0.0844(54) | 4.62(14)                           | −0.0443(73) | −30.39(14)                         | 0.0410(69) |

PP – Polypropylene, LDPE – Low-Density Polyethylene, LDPE-A – Low-Density Polyethylene with Anti-slip coating, HDPE – High-Density Polyethylene.

## 5. Conclusions

In the present work, the temperature dependence of the physical parameters (diffusion length, partition coefficient, diffusion coefficient, and permeability) that describe the transport of radon through some polymers are studied. The values of these parameters are determined at several temperatures in the interval 5–31 °C and their temperature dependences are modeled analytically. Significant temperature dependence of the parameters for all polymers is observed. The knowledge of the temperature dependences of the parameters and the possibility to model those dependencies analytically allow for predicting the behavior of the polymers at different temperatures, which would facilitate their various applications (e.g., radon/thoron discrimination, radon mitigation, radon sampling, etc.). The results reported in this work allow for modeling radon transport in polypropylene, low- and high-density polyethylene, Makrofol N and DE polycarbonates in the temperature range 5–31 °C.

The estimated values of the diffusion lengths and the partition coefficients are compared with such from previous studies of materials declared as chemically the same. Significant discrepancies are observed for all of the compared materials except for Makrofol N. Discrepancies are observed even for the two LDPE materials (LDPE and LDPE-A) from the current study (the LDPE-A material is LDPE from the same producer with anti-slip coating). These discrepancies are attributed to differences in the production process of the polymers. Therefore, it is recommended to test the properties of the specific material from the selected producer including at the extreme exploitation temperatures.

In addition, a new method for radon-in-polymer measurement is proposed. In this method, a thin polymer foil that already is exposed to radon is immersed in an LS-vial fully filled with distilled water. The vial is closed and measured by a standard LS-analyser. The beta-particles of the short-lived progeny of radon emit Cherenkov light in the water, which is detected by the LS-analyser. The method is very appropriate for studies of the RNG-transport properties of polymers, especially when the transport process is fast, as it allows precise timing, long duration of the measurements (with decay correction), and it does not require temperature control during the measurement.

**Author Contributions:** Conceptualization, K.M. and S.G.; methodology, K.M. and S.G.; investigation, S.G., K.M., C.D., T.B., and I.D.; formal analysis S.G. and T.B.; data curation S.G.; validation, S.G.; visualization, S.G.; writing—original draft preparation, S.G. and K.M.; writing—review and editing, K.M., I.D., C.D., S.G., and T.B.; funding acquisition K.M.; project administration, S.G. and K.M.; supervision, S.G. and K.M.

**Funding:** This research is funded by the European Metrology Program for Innovation and Research (EMPIR), JRP-Contract 16ENV10 MetroRADON ([www.euramet.org](http://www.euramet.org)). The EMPIR initiative is co-funded by the European Union’s Horizon 2020 research and innovation program and the EMPIR Participating States.

**Acknowledgments:** The authors are in debt to Philippe Cassette and Luigi Tommasino for the fruitful discussions on the polymer properties. The authors are also grateful to Luigi Tommasino for the Makrofol DE and Makrofol N foils provided. The authors thank the unknown Reviewers for the recommendations that led to the improvement of the manuscript.

**Conflicts of Interest:** The authors declare no conflict of interest.

## Abbreviations

The following abbreviations are used in this manuscript:

|          |   |
|----------|---|
| LDPE     | Low-Density Polyethylene  |
| LDPE-A   | Low-Density Polyethylene with Anti-slip coating                                       |
| HDPE     | High-Density Polyethylene   |
| PE       | Polyethylene  |
| PP       | Polypropylene   |
| LS       | Liquid Scintillation  |
| HPGe     | High-Purity Germanium   |
| TDCR     | Triple to Double Coincidence Ratio  |
| RNG      | Radioactive Noble Gas   |
| SLP      | Short-Lived Progeny   |
| CD       | Compact Disc  |
| SI       | International System of Units (from French: <i>Système International</i> (d'unités)); |
| "radon"  | short for the $^{222}\text{Rn}$ isotope   |
| "thoron" | short for the $^{220}\text{Rn}$ isotope   |

## References

- World Health Organization (WHO). WHO Handbook on Indoor Radon—A Public Health Perspective. Available online: [https://www.who.int/ionizing\\_radiation/env/9789241547673/en/](https://www.who.int/ionizing_radiation/env/9789241547673/en/) (accessed on 13 November 2019).
- Tokonami, S.; Yang, M.; Sanada, T. Contribution from thoron on the response of passive radon detectors. *Health Phys.* **2001**, *80*, 612–615. [[CrossRef](#)]
- Chen, J.; Moir, D. A study on the thoron sensitivity of radon detectors available to Canadians. *J. Radiol. Prot.* **2012**, *32*, 419–425. [[CrossRef](#)] [[PubMed](#)]
- Meisenberg, O.; Mishra, R.; Joshi, M.; Gierl, S.; Rout, R.; Guo, L.; Agarwal, T.; Kanse, S.; Irlinger, J.; Sapra, B.K.; et al. Radon and thoron inhalation doses in dwellings with earthen architecture: Comparison of measurement methods. *Sci. Total. Environ.* **2017**, *579*, 1855–1862. [[CrossRef](#)] [[PubMed](#)]
- Csige, I.; Csegzi, S. The Radamon radon detector and an example of application. *Radiat. Meas.* **2001**, *34*, 437–440. [[CrossRef](#)]
- Nikolaev, V.; Ilić, R. Etched track radiometers in radon measurements: A review. *Radiat. Meas.* **1999**, *30*, 1–13. [[CrossRef](#)]
- Dwivedi, K.; Mishra, R.; Tripathy, S.; Kulshreshtha, A.; Sinha, D.; Srivastava, A.; Deka, P.; Bhattacharjee, B.; Ramachandran, T.; Nambi, K. Simultaneous determination of radon, thoron and their progeny in dwellings. *Radiat. Meas.* **2001**, *33*, 7–11. [[CrossRef](#)]
- Nikezic, D.; Stevanovic, N. Behavior of  $^{220}\text{Rn}$  progeny in diffusion chamber. *Nucl. Instruments Methods Phys. Res. Sect. A Accel. Spectrometers, Detect. Assoc. Equip.* **2007**, *570*, 182–186. [[CrossRef](#)]
- Michielsen, N.; Bondiguel, S. The influence of thoron on instruments measuring radon activity concentration. *Radiat. Prot. Dosim.* **2015**, *167*, 289–292. [[CrossRef](#)]
- Leung, S.; Nikezic, D.; Leung, J.; Yu, K. A study of the polyethylene membrane used in diffusion chambers for radon gas concentration measurements. *Nucl. Instruments Methods Phys. Res. Sect. B Beam Interact. Mater. Atoms* **2007**, *263*, 311–316. [[CrossRef](#)]
- Bochicchio, F.; Ampollini, M.; Tommasino, L.; Sorimachi, A.; Tokonami, S. Sensitivity to thoron of an SSNTD-based passive radon measuring device: Experimental evaluation and implications for radon concentration measurements and risk assessment. *Radiat. Meas.* **2009**, *44*, 1024–1027. [[CrossRef](#)]
- Jiránek, M.; Kotrbatá, M. Radon diffusion coefficients in 360 waterproof materials of different chemical composition. *Radiat. Prot. Dosim.* **2011**, *145*, 178–183. [[CrossRef](#)] [[PubMed](#)]
- Rovenská, K.; Jiránek, M. 1st international comparison measurement on assessing the diffusion coefficient of radon. *Radiat. Prot. Dosim.* **2011**, *145*, 127–132. [[CrossRef](#)] [[PubMed](#)]
- Rovenská, K.; Jiránek, M. Radon diffusion coefficient measurement in waterproofings—A review of methods and an analysis of differences in results. *Appl. Radiat. Isot.* **2012**, *70*, 802–807. [[CrossRef](#)] [[PubMed](#)]
- Rau, W. Measurement of radon diffusion in polyethylene based on alpha detection. *Nucl. Instruments Methods Phys. Res. Sect. A Accel. Spectrometers, Detect. Assoc. Equip.* **2012**, *664*, 65–70. [[CrossRef](#)]

16. Laot, C.M.; Marand, E.; Schmittmann, B.; Zia, R.K.P. Effects of Cooling Rate and Physical Aging on the Gas Transport Properties in Polycarbonate. *Macromolecules* **2003**, *36*, 8673–8684. [CrossRef]
17. Möre, H.; Hubbard, L.  $^{222}\text{Rn}$  Absorption in Plastic Holders for Alpha Track Detectors: A Source of Error. *Radiat. Prot. Dosim.* **1997**, *74*, 85–91. [CrossRef]
18. Pressyanov, D.; Mitev, K.; Stefanov, V. Measurement of  $^{85}\text{Kr}$  and  $^{133}\text{Xe}$  in air by absorption in Makrofol. *Nucl. Instruments Methods Phys. Res. Sect. A Accel. Spectrometers, Detect. Assoc. Equip.* **2004**, *527*, 657–659. [CrossRef]
19. Pressyanov, D.; Mitev, K.; Dimitrova, I.; Georgiev, S. Retrospective radon measurements: Techniques and perspectives. In *Handbook on Radon: Properties, Measurements and Health Effects*; Li, Z., Feng, C., Eds.; Nova Science Publishers Inc.: New York, NY, USA, 2012; pp. 101–130.
20. Dimitrova, I.; Mitev, K.; Pressyanov, D.; Georgiev, S.; Boshkova, T. Measurement of  $^{222}\text{Rn}$  and  $^{226}\text{Ra}$  in water by absorption of radon in polycarbonates and etching alpha-tracks. *Radiat. Meas.* **2011**, *46*, 119–126. [CrossRef]
21. Tommasino, L.; Tommasino, M.; Viola, P. Radon-film-badges by solid radiators to complement track detector-based radon monitors. *Radiat. Meas.* **2009**, *44*, 719–723. [CrossRef]
22. Mitev, K. Measurement of  $^{222}\text{Rn}$  by absorption in plastic scintillators and alpha/beta pulse shape discrimination. *Appl. Radiat. Isot.* **2016**, *110*, 236–243. [CrossRef]
23. Mitev, K.; Cassette, P.; Georgiev, S.; Dimitrova, I.; Sabot, B.; Boshkova, T.; Tartès, I.; Pressyanov, D. Determination of  $^{222}\text{Rn}$  absorption properties of polycarbonate foils by liquid scintillation counting. Application to  $^{222}\text{Rn}$  measurements. *Appl. Radiat. Isot.* **2016**, *109*, 270–275. [CrossRef] [PubMed]
24. Mitev, K.; Dutsov, C.; Georgiev, S.; Tsankov, L.; Boshkova, T. Study of  $^{222}\text{Rn}$  Absorption and Detection Properties of EJ-212 and BC-400 Plastic Scintillators. *IEEE Trans. Nucl. Sci.* **2017**, *64*, 1592–1598. [CrossRef]
25. Pelay, E.; Tarancón, A.; Mitev, K.; Dutsov, C.; Georgiev, S.; Tsankov, L.; García, J.F. Synthesis and characterisation of scintillating microspheres made of polystyrene/polycarbonate for  $^{222}\text{Rn}$  measurements. *J. Radioanal. Nucl. Chem.* **2017**, *314*, 637–649. [CrossRef]
26. Pressyanov, D. Modeling a  $^{222}\text{Rn}$  measurement technique based on absorption in polycarbonates and track-etched counting. *Health Phys.* **2009**, *97*, 604–612. [CrossRef] [PubMed]
27. Dimitrova, I.; Georgiev, S.; Mitev, K.; Pressyanov, D. Influence of the water temperature on measurements of Rn-222 in water by liquid scintillation counting of polycarbonates. In Proceedings of the 2012 IEEE Nuclear Science Symposium and Medical Imaging Conference Record (NSS/MIC), Anaheim, CA, USA, 29 October–3 November 2012; pp. 1941–1944. [CrossRef]
28. Mitev, K.; Cassette, P.; Tartès, I.; Georgiev, S.; Dimitrova, I.; Pressyanov, D. Diffusion lengths and partition coefficients of  $^{131m}\text{Xe}$  and  $^{85}\text{Kr}$  in Makrofol N and Makrofol DE polycarbonates. *Appl. Radiat. Isot.* **2018**, *134*, 269–274. [CrossRef] [PubMed]
29. Pressyanov, D.; Mitev, K.; Georgiev, S.; Dimitrova, I. Sorption and desorption of radioactive noble gases in polycarbonates. *Nucl. Instruments Methods Phys. Res. Sect. A Accel. Spectrometers, Detect. Assoc. Equip.* **2009**, *598*, 620–627. [CrossRef]
30. Pressyanov, D.; Georgiev, S.; Dimitrova, I.; Mitev, K.; Boshkova, T. Determination of the diffusion coefficient and solubility of radon in plastics. *Radiat. Prot. Dosim.* **2011**, *145*, 123–126. [CrossRef] [PubMed]
31. Cassette, P.; Sahagia, M.; Grigorescu, L.; Lépy, M.; Picolo, J. Standardization of  $^{222}\text{Rn}$  by LSC and comparison with  $\alpha$ - and  $\gamma$ -spectrometry. *Appl. Radiat. Isot.* **2006**, *64*, 1465–1470. [CrossRef] [PubMed]
32. Mitev, K. On the possibility to detect some radioactive noble gases by Cherenkov counting of polycarbonates. In Proceedings of the 2013 IEEE Nuclear Science Symposium and Medical Imaging Conference (2013 NSS/MIC), Seoul, Korea, 27 October–2 November 2013. [CrossRef]
33. Joint Committee for Guides in Metrology (JCGM). JCGM 100:2008: Evaluation of Measurement Data—Guide to the Expression of Uncertainty in Measurement. Available online: <https://www.bipm.org/en/publications/guides/gum.html> (accessed on 13 November 2019).
34. Mitev, K.; Cassette, P.; Jordanov, V.; Liu, H.R.; Dutsov, C. Design and performance of a miniature TDCR counting system. *J. Radioanal. Nucl. Chem.* **2017**, *314*, 583–589. [CrossRef]
35. Laboratoire National Henri Becquerel (LNHB). LNHB Recommended Data. Available online: [http://www.nucleide.org/DDEP\\_WG/DDEPdata.htm](http://www.nucleide.org/DDEP_WG/DDEPdata.htm) (accessed on 13 November 2019).
36. Nakamura, H.; Shirakawa, Y.; Kitamura, H.; Sato, N.; Takahashi, S. Undoped Polycarbonate for Detection of Environmental Radiation. *Jpn. J. Health Phys.* **2014**, *49*, 98–101. [CrossRef]

37. Pressyanov, D.; Mitev, K.; Georgiev, S.; Dimitrova, I.; Kolev, J. Laboratory facility to create reference radon + thoron atmosphere under dynamic exposure conditions. *J. Environ. Radioact.* **2017**, *166*, 181–187. [[CrossRef](#)] [[PubMed](#)]
38. Press, W.; Teukolsky, S.; Vetterling, W.; Flannery, B. *Numerical Recipes—The Art of Scientific Computing*; Cambridge University Press: New York, NY, USA, 2007.



© 2019 by the authors. Licensee MDPI, Basel, Switzerland. This article is an open access article distributed under the terms and conditions of the Creative Commons Attribution (CC BY) license (<http://creativecommons.org/licenses/by/4.0/>).



16ENV10 MetroRADON

Deliverable D2  
Annex XIV

Task A.2.3.2

Highly sensitive passive detectors for  
short-term pre- and post- mitigation

D. Pressyanov

SUBG

(Article published in: Proc. 33<sup>rd</sup> AARST 2019 Int. Radon Symp.,  
Denver, USA)

# **HIGHLY SENSITIVE PASSIVE DETECTORS FOR SHORT-TERM PRE- AND POST- MITIGATION MEASUREMENTS**

Dobromir Pressyanov  
Sofia University “St. Kliment Ohridski”  
Sofia, Bulgaria  
E-mail: [pressyan@phys.uni-sofia.bg](mailto:pressyan@phys.uni-sofia.bg)

## **Abstract**

It is required to evaluate the achieved radon reduction, preferably shortly after the mitigation system is activated. As instantaneous measurements are affected by short term radon variations, few days pre- and post-mitigation integrated measurements of sufficient sensitivity is preferred. Within the European MetroRADON project novel detectors of sufficient sensitivity and with compensated temperature dependence of the response were developed. They are based on using DVDs of low intrinsic background as track detectors, covered with Makrofol N foils. The absorption of radon by Makrofol N is very high (concentration ratio foil/air is  $> 100$ ). The Makrofol N foil serves as radon absorber/radiator that greatly amplifies the signal (net track-density at etched DVDs). The achievable sensitivity is sufficient to prove quantitatively (within one-week exposure) that the reduction to low radon levels ( $< 100 \text{ Bq m}^{-3}$ ) is achieved after mitigation. The detectors are cheap and usable for measurements at many points in large buildings. A novel technical concept (patent pending) to reduce the temperature dependence of the detectors and to eliminate the influence of thoron and humidity is described. The results of pilot experiments shown demonstrate the feasibility of this concept.

## **Introduction**

The efficient way to reduce the radon risk in buildings with high  $^{222}\text{Rn}$  levels is mitigation. Despite that the radon mitigation industry exists for more than 30 years, still the “mitigation outcome” can hardly be predicted and the achieved mitigation efficiency is case-specific (Kumar et al, 2012; Pressyanov, 2016). The achieved efficiency and post mitigation radon levels have to be assessed in any mitigated building. The World Health Organization (WHO, 2009) recommends the reference levels, above which mitigation should be considered, to be set within the range of  $100\text{-}300 \text{ Bq m}^{-3}$ . Therefore, ideally the mitigation outcome should be radon concentrations reduced to less than  $100 \text{ Bq m}^{-3}$ . Although the  $^{222}\text{Rn}$  concentrations before mitigation are usually above the European Union’s reference level (that shall not be higher than  $300 \text{ Bq m}^{-3}$  in the Member states of the EU, according to the European Council Directive (2014)), those after the mitigation could (and should) be well below  $100 \text{ Bq m}^{-3}$ . Preferably, post mitigation levels should be evaluated by integrated measurements under conditions at which the inhabitants normally live. At the same time the mitigation contract may require verifying the achieved efficiency in a reasonably short time after the mitigation work is completed. In addition, depending on the size of the building, measurements in many points may be needed,

---

*This work is supported by the European Metrology Programme for Innovation and Research (EMPIR), JRP-Contract 16ENV10 MetroRADON (<http://www.euramet.org>). The EMPIR initiative is co-funded by the European Union’s Horizon 2020 research and innovation programme and the EMPIR Participating States.*

which makes the use of, for example, integrating electronic monitors or electret chambers a difficult option for many mitigation contractors. In this work we studied a new design of a passive alpha-track detector in which the tracks can be etched and analyzed from a large detection area and which can provide reliable quantitative measurements at levels below  $100 \text{ Bq m}^{-3}$  within one week exposure time. The increased sensitivity is achieved by using of DVDs of low background as large area track detectors, and use of radon absorbing foils to amplify the signal, as first proposed by Tommasino et al. (2009). Constructively, DVDs consist of two halves stuck together, as shown in Figure (1). The front half is made of polycarbonate material that has radon absorption and track-etch properties (Pressyanov et al., 2001). After mechanical splitting of DVDs the internal surface of the polycarbonate half of the DVDs is used as the detection surface. It is covered by two foils of Makrofol N. Because of the unique radon absorption ability of Makrofol N (the radon concentration in it is 112 times higher than that in the ambient air, at room temperature (Mitev et al., 2016)) it serves as absorber/radiator that sufficiently amplifies the signal (net track density, i. e. the track density after the background is subtracted). The results from experiments and modeling that are presented below demonstrate the ability of the proposed detectors to measure low  $^{222}\text{Rn}$  concentrations within relatively short exposure time (e.g. a week).

One limitation identified of this kind of detectors is the significant dependence of their response on the temperature. In this report we are proposing a novel concept (Pressyanov, 2019) that makes it possible to reduce or even to eliminate the temperature dependence of the detectors. The results of the pilot experiments presented below demonstrate the feasibility of this concept.

## Materials and Methods

Widely preferred methods for integrated  $^{222}\text{Rn}$  measurements employ alpha track detectors. In the commercial monitors small area track detectors are used, usually of area of few  $\text{cm}^2$ , which limits their sensitivity. Following the approach of Currie (1968) the minimum detectable average concentration (*MDAC*) after exposure time  $t$  is:

$$MDAC = \frac{2.71+4.65\sqrt{n_B}}{CF.t.\sqrt{S}}, \quad (1)$$

where  $n_B$  is the background track density,  $CF$  is the calibration factor ( $CF = \text{net track density} / \text{integrated } ^{222}\text{Rn concentration in the ambient air}$ ),  $S$  is the etched detector area from which the tracks are counted and  $t$  is the exposure time. In the present study the *MDAC* is reduced by:

- increasing  $CF$ , by coupling the detector with an external radiator with high radon absorption ability (Makrofol N);
- increasing  $S$ , using DVDs as large area alpha track detectors;
- reducing  $n_B$  by using the internal surface of the DVDS, which has very low background.

In the last years the CD/DVDs method has been widely used for measurements in dwellings, caves and workplaces (Pressyanov et al., 2019; Dimitrov and Pressyanov; 2018, Burgele et al., 2017). The method employs the high radon absorption ability of the polycarbonate material of

which the commercial CDs and DVDs are made and its track-etch properties (Pressyanov et al., 2001). The tracks created by the absorbed radon and its progeny are analyzed at certain depth (usually about 80  $\mu\text{m}$ ) beneath the disk front surface (Pressyanov, 2009). In the present version, which is also suited for short-term prospective measurements, the sensitivity is increased by covering the sensitive surface of the DVDs by two foils of 43  $\mu\text{m}$  thick Makrofol N - a material which radon absorption ability is much higher than that of the CD/DVDs (Mitev et al., 2016), and etching tracks on that surface. As noted elsewhere (Dimitrova et al., 2011), the internal surface of the DVDs has a very low background track density:  $1.1 \pm 0.3 \text{ cm}^{-2}$  (see Figure (1)) and it can be reduced to about  $0.5 \text{ cm}^{-2}$  by thermal annealing at 120  $^{\circ}\text{C}$ . In the same time the DVDs are “track detectors” of large area – up to 100  $\text{cm}^2$  can be etched and the tracks from the etched area counted. The time needed the absorbed  $^{222}\text{Rn}$  to reach 99% of its equilibrium level (with foils of thickness 43  $\mu\text{m}$ ) varies from several hours (at 38  $^{\circ}\text{C}$ ) to about two days (at 5  $^{\circ}\text{C}$ ) (Pressyanov, 2011). Therefore, the present design could be used for exposure times of one week or more and it is a good practice to dismantle and etch detectors at least two days after the end of exposure.

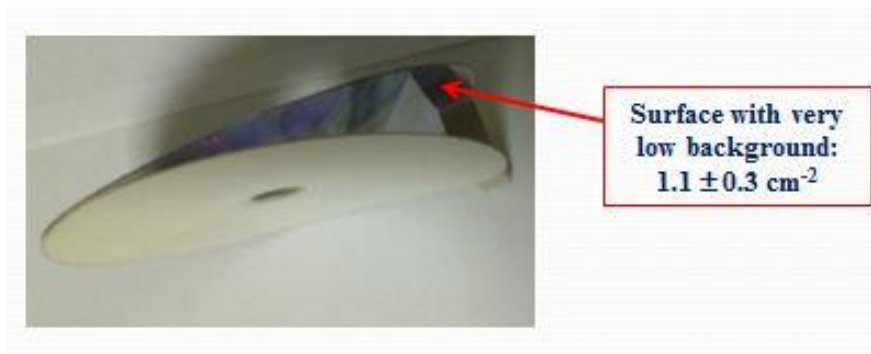


Figure (1): The structure of a DVD: it consists of two halves stuck together. The front half is made of polycarbonate which can be used as alpha-track detector. The background of the internal polycarbonate surface is very low, and can be additionally reduced by thermal annealing.

The design of the described  $^{222}\text{Rn}$  detector is shown in Figure (2). Two DVD polycarbonate halves are stuck together with 2 foils of Makrofol N in between. Each of the detection surfaces look to the absorber/radiator. The disks and foils are not stuck hermetically and radon can diffuse freely between them (Tommasino et al., 2009). Modeling (Pressyanov, 2009, Pressyanov et al., 2018) suggests that more than 80% of the signal is due to the absorbed radon in the foils of Makrofol N and the rest is due to the absorbed radon in the polycarbonate material of the disk. After exposure, the disk surface is etched electrochemically (ECE). The ECE process is performed at effective electric field of 3  $\text{kV/mm}$ . The etching solution is mixture of ethanol with 6M KOH solution with 1:4 volume ratio. The process starts with 30 min pre-etching with the same solution. After pre-etching the electric field is applied for 3 hours. With this ECE regime tracks are enlarged to a diameter of about 100  $\mu\text{m}$  (visible by naked eye) and are usually counted by a computer scanner (Mitev et al., 2010).



Figure (2): (a) Scheme of the detector element; (b) Detector element ready to use.

## Results and Discussion

The proposed detectors were experimentally studied and calibrated using the dedicated exposure facility at the Laboratory of Dosimetry and Radiation Protection, Sofia University “St. Kliment Ohridski” (Pressyanov et al., 2017). With these detectors we had participated successfully in the international 2017 radon intercomparison organized by Public Health England. Assessment of the *MDAC* showed that after one-week exposure the *MDAC* is less than  $20 \text{ Bq m}^{-3}$  when the entire  $200 \text{ cm}^2$  surface of the detector element is etched and the tracks counted. If the background is reduced by thermal annealing the *MDAC* of about  $12 \text{ Bq m}^{-3}$  can be achieved after one-week exposure time. However, a problem with strong dependence of detector’s response on the temperature has been identified.

The type of detectors, described above, employ radon solubility in plastics – a process which is known to depend on the temperature. Therefore we have studied the influence on the detector response of the temperature during exposure. Experiments at three different temperature levels were carried-out. The results revealed that the response of these detectors is highly dependent on the temperature. As seen in Figure (3a) the *CF* drops about 2.6 times when the temperature raises from  $5 \text{ }^{\circ}\text{C}$  to  $35 \text{ }^{\circ}\text{C}$ . This seems to be a significant obstacle to perform precise  $^{222}\text{Rn}$  measurements with these detectors, when the temperature during exposure is not known and/or it may vary. The last is frequently experienced in practice when measurements are performed in different seasons in buildings which are not or are partly heated/air-conditioned.

However, a novel technical concept was proposed (Pressyanov, 2019) with a potential to overcome “the temperature dependence problem” of these, and possibly of many other types of detectors. Consider an alpha-track detector placed in a cup/chamber (“diffusion chambers”) in which radon gas diffuses from outside. To protect the detector from humidity and thoron influence, many such chambers are covered by, or packed with, a polymer foil (Ward et al., 1977). The foil stops radon and thoron progeny, as well as the short-lived thoron ( $^{220}\text{Rn}$ ) and prevents moisture penetration. However,  $^{222}\text{Rn}$  diffuses through the foil and reaches concentration inside the chamber that is proportional to that outside. As shown elsewhere (Ward et al., 1977, Fleischer 1992), the ratio of the  $^{222}\text{Rn}$  concentration inside the chamber ( $C_{in}$ ) to that in the ambient air ( $C_{out}$ ) is given by the expression:

$$\frac{C_{in}}{C_{out}} = \frac{1}{1 + \lambda \frac{hV}{PS}} \quad (2)$$

where  $h$  is the thickness of the polymer foil,  $V$  is the volume of the chamber,  $S$  is the area, covered with the polymer foil,  $\lambda$  is  $^{222}\text{Rn}$  decay constant and  $P$  is the “radon permeability” (Ward et al., 1977) of the material of which the polymer foil is made.

Although polymer foils are effective barriers against humidity and thoron, it has been noted that due to the temperature dependence of the radon permeability, the ratio  $C_{in}/C_{out}$  and therefore the response of these chambers to radon depends on the temperature (Fleischer et al., 2000; Tommasino, 2016). Figure (3b) displays that this dependence seems reciprocal to that of the detectors described in the presented report. This led to a novel, patent pending technical concept (Pressyanov 2019): designing a “compensated module” in which the detector is placed, that facilitates reduction or elimination of the temperature dependence of the detector (Figure (3c)) by selecting the parameters  $h$ ,  $V$ ,  $S$  of the module and the foil material. Pilot modeling showed that this goal is achievable, but detailed data on the radon permeability of polymer foils at different temperatures may be needed.

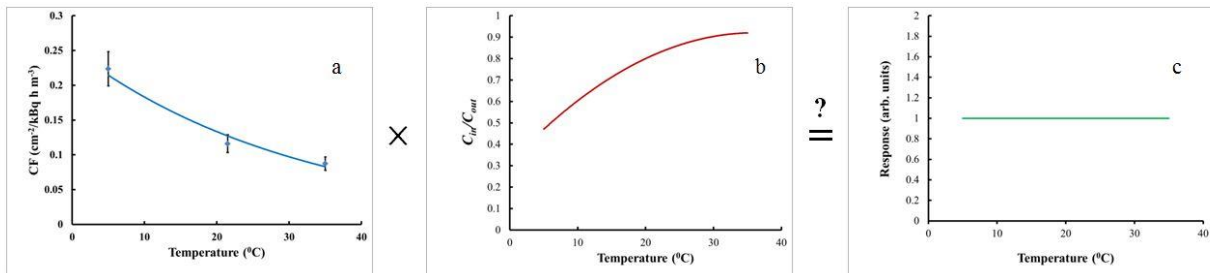


Figure (3): (a) Temperature dependence of the  $CF$  of detectors; (b) Typical dependence on the temperature of the ratio  $C_{in}/C_{out}$  in a volume in which radon penetrates by diffusion through plastic wall(s) (Tommasino, 2016); (c) The concept: would it be possible by placing the detectors (a) in a volume (b) to achieve compensated temperature dependence of the response.

At this stage we made a proof-of-concept study based on rather scarce data available for the permeability of low density polyethylene at different temperatures. Using the experimental results for  $C_{in}/C_{out}$  at three different temperature levels for chambers covered by low density polyethylene and interpolation between the experimental points (Pressyanov, 2019) it was crudely estimated that if the detectors described here are hermetically packed with 75  $\mu\text{m}$  thick low density polyethylene, so that the ratio of the internal pack volume to the polyethylene surface is 3-4 cm, the temperature dependence would be significantly reduced. A photo of the packed detector element is shown in Figure (4).



Figure (4): Detector packed in the “compensated module”.

Experiments were made at temperatures of 5 °C, 21.5 °C and 35 °C with packed and non-packed detectors. During exposure the  $^{222}\text{Rn}$  concentrations were followed by a reference radon monitor AlphaGUARD PQ 2000 Pro (Saphymo/Bertin instruments). The results for the *CFs* of packed and non-packed detectors are shown in Figure (5). As seen the temperature dependence is significantly reduced when the detectors are packed in such package.

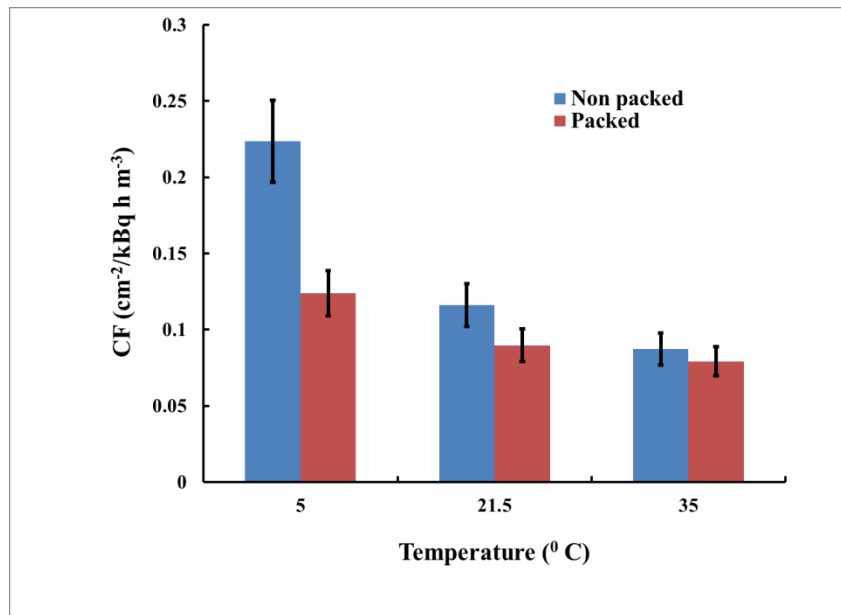


Figure (5): Dependence of the CF on the temperature of packed and not-packed detectors. The temperature dependence of packed detectors is significantly reduced.

In general, such “compensated modules” can be used with many kinds of radon detectors which response decreases with increasing the temperatures. The list of such detectors include those using activated charcoal (Cooper et al., 2011), track detectors, e.g. CR-39 which show fading (fading is greater at higher temperature (Caresana et al., 2010)) etc. At present extensive research work is ongoing both in the direction to determine precisely the permeability of various polymer foils over wide range of temperatures and to design compensated modules suitable for different kinds of radon detectors.

As the ratio  $C_{in}/C_{out}$  -is always less than 1, the  $CF$  and therefore the  $MDAC$  of packed detectors will be somewhat worsen. The most conservative estimate for the reduced sensitivity was for packed detectors that were exposed at  $35^{\circ}C$  where the lowest  $CF$  was obtained (see Figure (5)). The results are illustrated in Figure (6), which is based on application of eqn. (1) using the experimental values obtained for  $n_B$  and  $CF$ . As seen, the  $MDAC$  is still well below  $100 \text{ Bq m}^{-3}$  if more than  $20 \text{ cm}^2$  of the detector's surface is analyzed. When the entire surface of the detector element is etched and the tracks counted, for one-week exposure the minimum detectable  $^{222}\text{Rn}$  concentration can be even less than  $20 \text{ Bq m}^{-3}$  if thermal annealing is applied prior the exposure of the DVDs used. Therefore, the packed detectors still fit the required sensitivity for post-mitigation measurements. In addition, the used compensated package is also an efficient barrier against moisture/humidity and thoron interference.

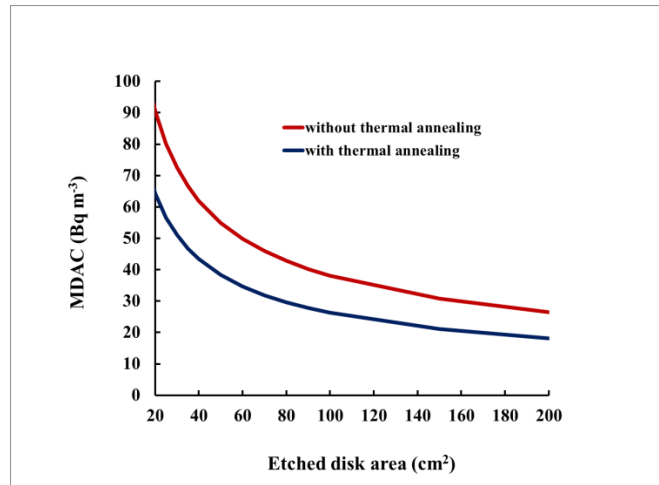


Figure (6): Minimum detectable average  $^{222}\text{Rn}$  concentrations after one week of exposure of “packed detectors” as dependent on the surface which is etched and tracks are counted.

The detectors design described in this report provides new opportunity for application of CD/DVDs in radon industry. That is for using them for  $^{222}\text{Rn}$  diagnostics before mitigation (Pressyanov, 2016) and for post-mitigation measurements to verify the mitigation goal is achieved. With a compensated module/package they can be used over a wide range of environmental temperatures, being protected also from humidity and thoron influence. Further research will be focused at achieving the best possible temperature compensation.

## Conclusion

In this work a passive radon detector of sufficient sensitivity for post-mitigation measurements is described. It is based on DVDs used as alpha track detectors of large area, which detection surface is covered by 2 foils of  $43 \mu\text{m}$  thick Makrofol N. The foil serves as radon absorber/radiator. Due to the uniquely high radon absorption ability of Makrofol N, low background and the large detection area the sensitivity of this detector is significantly increased. As a result the  $MDAC$  below  $20 \text{ Bq m}^{-3}$  is achievable within one week exposure time. With such sensitivity the detectors can be used for pre- and post-mitigation measurements. The detectors are simple, cheap (the cost of one new DVD on the market is usually less than 0.5 USD and

Makrofol N foils can be used many times) and parallel measurements in many points are possible. Although the response of the detector depends on the temperature, a novel technical concept was tested. This concept allows, by placing the detector in a special package/box (“compensated module”) to sufficiently reduce the temperature dependence. In addition to the temperature compensation, the “compensated module” would be an efficient barrier against humidity and thoron influence on the detector’s response. Further research will be focused on improving the design of the compensated modules to achieve the best possible temperature compensation. This would open the possibility to expand the concept of temperature compensation towards many kinds of detectors, response of which depends on the temperature similarly to that of the detectors described in this report.

**Acknowledgement:** The author is grateful to Mr. Dimitar Dimitrov for the laboratory work and to Dr. Luigi Tommasino for providing Makrofol N foil.

## References

- Burghele, B. D., Cucos, A., Papp, B., Dicu, T., Pressyanov, D., Dimitrov, D., Dimitrova, I., Constantin, S., 2017. Comparative study of radon and thoron measurements in four Romanian show caves. *Radiat. Prot. Dosim.* 177, 181-185.
- Caresana, M., Ferrarini, M., Garlati L., Parravicini A., 2010. About ageing and fading of CR-39 PADC track detectors used as air radon concentration measurement devices. *Radiat. Meas.* 45, 183–189.
- Cooper, A., Le, T. N., Iimoto, T., Kosako, T., 2011. Temperature calibration formula for activated charcoal radon collectors. *J. Env. Radioact.* 102, 60-63.
- Council of the European Union, 2014. Council Directive 2013/59/EURATOM. Official Journal of the European Union L13/1-73, 17 Jan 2014.
- Currie, L. A., 1968. Limits for qualitative detection and quantitative determination. *Anal. Chem.* 40, 586-593.
- Dimitrova, I., Mitev, K., Pressyanov, D., Georgiev, S., Boshkova, T., 2011. Measurement of  $^{222}\text{Rn}$  and  $^{226}\text{Ra}$  in water by absorption of radon in polycarbonates and etching alpha-tracks. *Radiat. Meas.* 46, 119-126.
- Dimitrov, D., Pressyanov, D. 2018. The CD/DVD method as a tool for the health physics service and ventilation diagnostics in underground mines. *Radiat. Prot. Dosim.* 181, 30-33.
- Fleischer, R. L., 1992. Permeability of caulking compounds to  $^{222}\text{Rn}$ . *Health Phys.* 62, 91-95.
- Fleischer, R.L., Giard, W.R., Turner, L.G., 2000. Membrane-based thermal effects in  $^{222}\text{Rn}$  dosimetry. *Radiat. Meas.* 32, 325-328.
- Kumar A. et al., 2012. Analysis of indoor radon mitigation systems in Ohio, USA. IN: *Handbook of Radon*. Nova Science Publishers Inc., pp. 447-462.
- Mitev, K., Madzhunkov, Y., Gerganov, G., Dimitrova, I., Georgiev, S., Pressyanov, D., 2010. Automatic counting of electrochemically etched tracks in compact discs. Application to retrospective measurements of Rn-222. *IEEE Trans. Nucl. Sci.* 57, 300-308.
- Mitev, K., Cassette, P., Georgiev, S., Dimitrova, I., Sabot, B., Boshkova, T., Tartès I., Pressyanov D., 2016. Determination of  $^{222}\text{Rn}$  absorption properties of polycarbonate foils by liquid scintillation counting. Application to  $^{222}\text{Rn}$  measurements. *Appl. Radiat. Isotopes* 109, 270–275.
- Pressyanov, D., Buysse, J., Van Deynse, A., Poffijn, A., Meesen, G., 2001. Indoor radon detected by compact discs. *Nucl. Instrum. Methods. Phys. Res. A* 457, 665-666.
- Pressyanov, D., 2009. Modeling a  $^{222}\text{Rn}$  measurement technique based on absorption in polycarbonates and track-etch counting. *Health Phys.* 97, 604-612.

Pressyanov, D., 2011. Modeling response of radon track detectors with solid absorbers as radiators. *Radiat. Meas.* 46, 357-361.

Pressyanov, D., 2016. Long-term average radon levels measured in a few days: implications to risk communication and mitigation strategy. *Proc. AARST 2016 International Radon Symposium, San Diego, CA, 18-21 September 2016.*

Pressyanov, D., Mitev, K., Georgiev, S., Dimitrova, I., Kolev, J., 2017. Laboratory facility to create reference radon + thoron atmosphere under dynamic exposure conditions. *J. Env. Radioact.* 166, 181-187.

Pressyanov, D., Dimitrov, D., Dimitrova, I., 2018. Passive radon monitors with part-time sensitivity to radon. *Radiat. Meas.* 118, 72–76.

Pressyanov, D., Dimitrova, I., Mitev, K., Georgiev, S., Dimitrov D., 2019. Identifying radon priority areas and dwellings with radon exceedances in Bulgaria using stored CD/DVDs. *J. Env. Radioact.* 196, 274–280.

Pressyanov, D., 2019. Bulg. Pat. Appl. Reg. Nr. 112897, priority: 19.03.2019 (assignee: Sofia University “St. Kliment Ohridski”).

Tommasino, L., Tommasino, M.C., Viola, P., 2009. Radon-film-badges by solid radiators to complement track detector-based radon monitors. *Radiat. Meas.* 44, 719-723.

Tommasino, L., 2016. Concealed errors in radon measurements and strategies to eliminate them. Presented at the 8th Int. Conf. on Protection against Radon at Home and Work, Prague, 12-16 September 2016.

Ward III, W. J., Fleischer, R. L., Mogro-Campero, A., 1977. Barrier technique for separate measurements of radon isotopes. *Rev. Sci. Instrum.* 48, 1440-1441.

World Health Organization (WHO), 2009. WHO Handbook on Indoor Radon: A Public Health Perspective. Geneva, WHO publications.



# 16ENV10 MetroRADON

## Deliverable D2

### Annex XV

#### Task A.2.3.3

Characterization of polyethylene as a selective  
barrier for  $^{220}\text{Rn}$

S. Georgiev<sup>1</sup>, B. Sabot<sup>2</sup>, K. Mitev<sup>1</sup>

<sup>1</sup>SUBG, <sup>2</sup>CEA

## Table of contents

|   |   |
|---|---|
| I. Introduction .....   | 3 |
| II. Description, calibration and implementation of the CEA reference $^{220}\text{Rn}$ detector at SUBG ..... | 3 |
| III. Diffusion Model for Radon and Thoron transport through polymers .....                                    | 6 |
| IV. Validation of radon transport parameters in polyethylene. ....  | 8 |

## I. Introduction

The rubbery low density polyethylene was identified in the previous activities as a very suitable material for the development of anti-thoron membranes. The radon diffusion properties of polyethylene were determined in Activity A.2.3.2 and published in [1]. The objective of this activity is to validate the radon diffusion properties through polyethylene with an independent and well established technique and to validate the diffusion model for radon transport and accumulation in volumes, protected by polymer membranes.

## II. Description, calibration and implementation of the CEA reference $^{220}\text{Rn}$ detector at SUBG

In order to have more and independent experimental methods for the characterization of radon and thoron transport through polymer membranes, a modified version of the French reference thoron detector developed at Laboratoire National Henri Becquerel (CEA/LNHB), was installed in SUBG. The primary thoron detector is described in detail in [2,3]. The system is based on a PIPS detector coupled to an electric field in order to catch the decay products of  $^{222}\text{Rn}$  or  $^{220}\text{Rn}$  at the surface of the detector. To allow the precise study (including the dynamics) of the transport of radon and thoron through polymer membranes in a well-defined volume, the CEA/LNHB has modified the device. It possesses now two chambers as shown in Fig. A1:

- The first chamber with circulation of air flow containing  $^{222}\text{Rn}$  and/or  $^{220}\text{Rn}$ ,
- The second chamber, which is separated by a stainless steel grid and with metalized surface in front of the silicon detector, in order to perform direct measurement of the gas and the decay products.

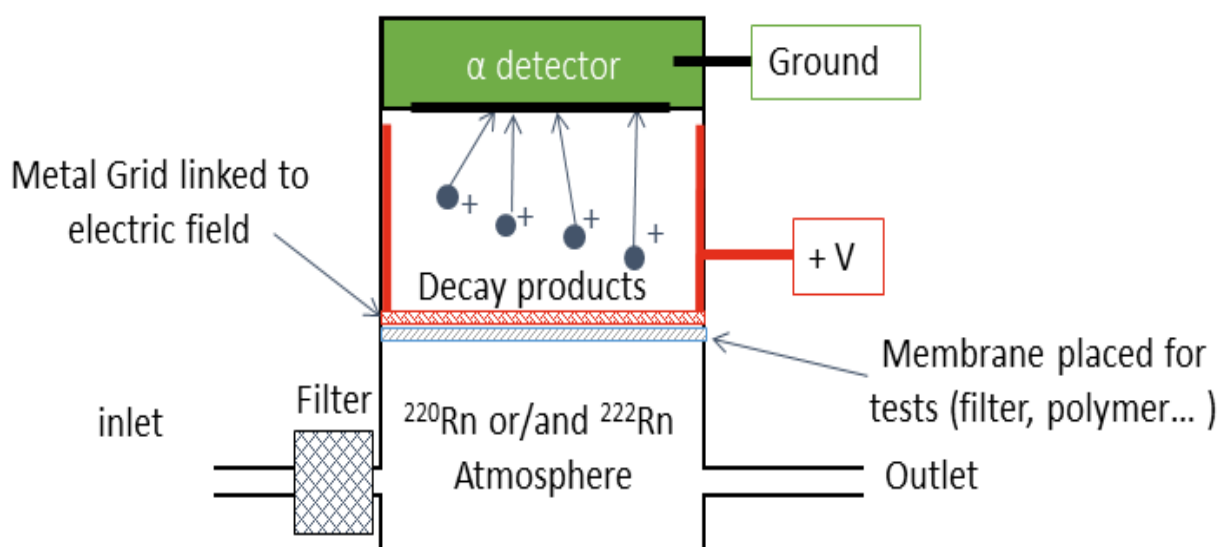


Figure Fig. A1 – Scheme of the device built by CEA/LNHB.

The scheme of this new device is presented in Fig. A1. The grid between the two chambers allows us to place any kind of thin membrane and then perform measurement of the  $^{222}\text{Rn}$  and/or  $^{220}\text{Rn}$  passing through the membrane using any kind of setup which produces atmosphere of  $^{220}\text{Rn}/^{222}\text{Rn}$ .

A scheme of the experimental setup in SUBG with the PIPS system included is shown in Fig. A2. A peristaltic pump (typically operating at about  $1 \text{ L}\cdot\text{min}^{-1}$ ) supplies radon and/or thoron from a reference source to a 50 L radon calibration container (Saphymo GmbH). The reference monitor AlphaGUARD  $^{220}\text{Rn}/^{222}\text{Rn}$  is placed in the box to measure the activity concentration created in the exposure setup. The air goes through an aerosol filter (to filter the decay products of  $^{220}\text{Rn}$  and or  $^{222}\text{Rn}$ ) and enters in the lower chamber of the PIPS system. Further the loop is closed through a 1 L drexel to the pump. The purpose of the 1 L drexel is to cancel the pressure spikes in the PIPS system due to the peristaltic pump. The lower chamber has volume of about  $14 \text{ cm}^3$  and the connecting tubes from the 50 L box to the PIPS system have volume of about  $30 \text{ cm}^3$ . As the flow-rate through the system is about  $1 \text{ L}\cdot\text{min}^{-1}$  it is considered that the activity concentration in the lower chamber is the same as measured by the AlphaGUARD in the 50 L box for both radon and thoron.

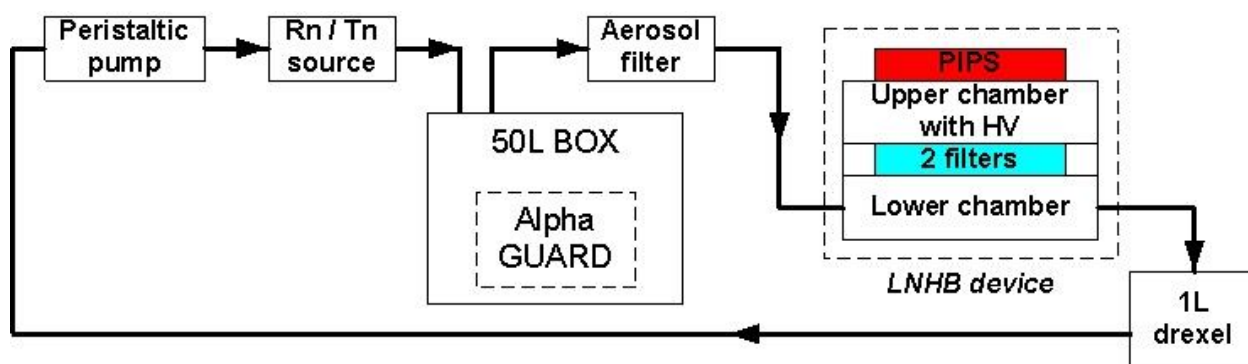


Figure A2 – Scheme of the experimental setup in SUBG with the PIPS system. The setup is built to study the transport of radon and/or thoron through polymer membranes (filters).

Once in the lower chamber  $^{220}\text{Rn}/^{222}\text{Rn}$  diffuses in the upper chamber through the diffusion barrier shown in the figure as “2 filters”. When  $^{220}\text{Rn}/^{222}\text{Rn}$  decays in the upper chamber, the short-lived progenies are electrostatically deposited on the surface of a PIPS detector and their alpha-particles are registered in an alpha spectrum. Examples of radon and thoron alpha-spectra obtained with the system are shown in Figs. A3 and A4. A combined alpha-spectrum of both radon and thoron is illustrated in Fig. A5.

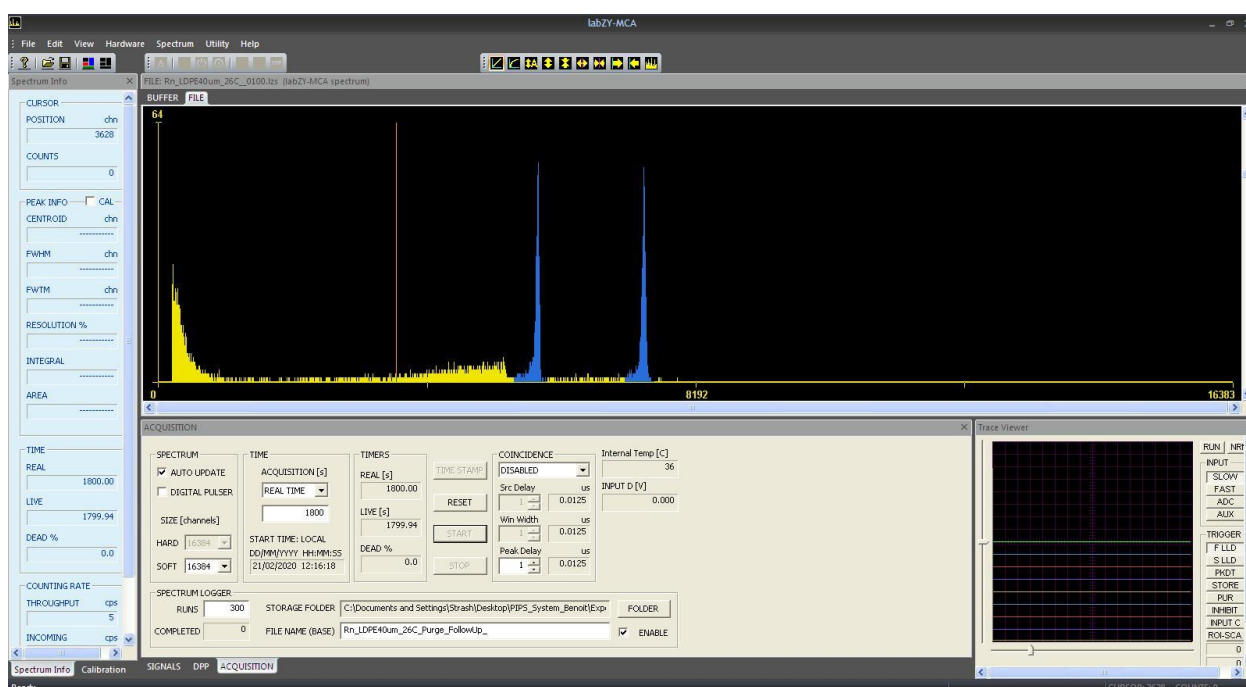


Figure A3 – Radon spectrum obtained with the CEA reference system.

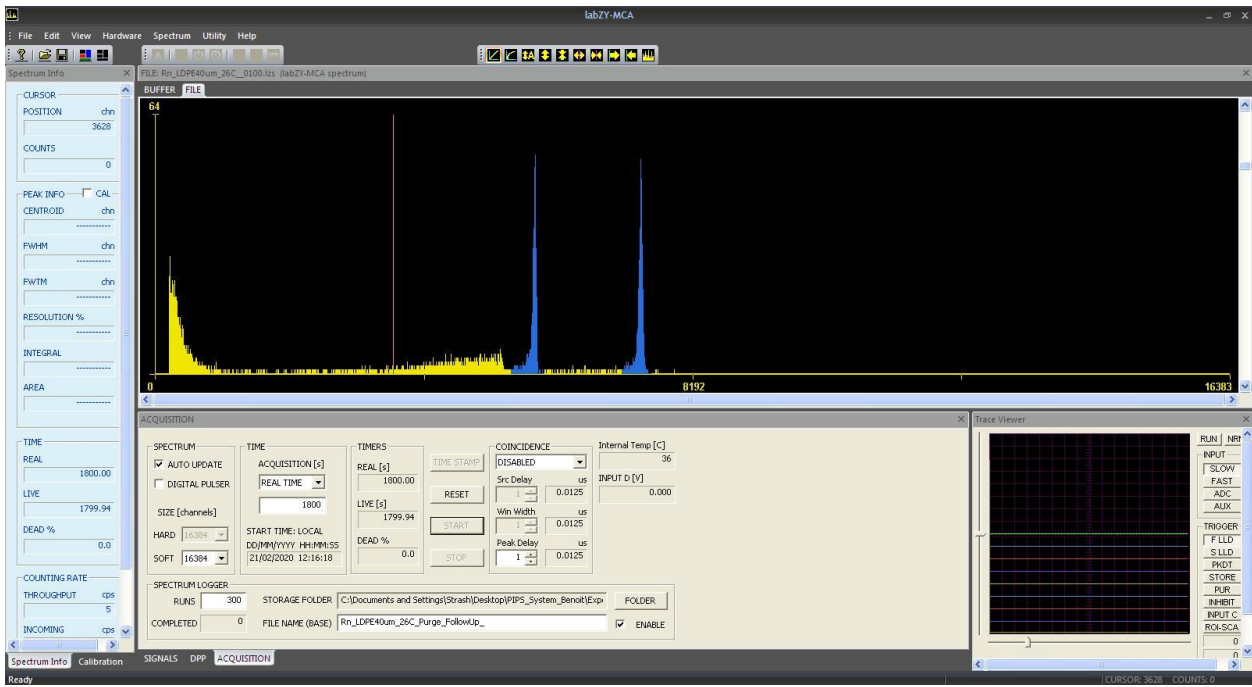


Figure A4 – Thoron spectrum obtained with the CEA reference system.

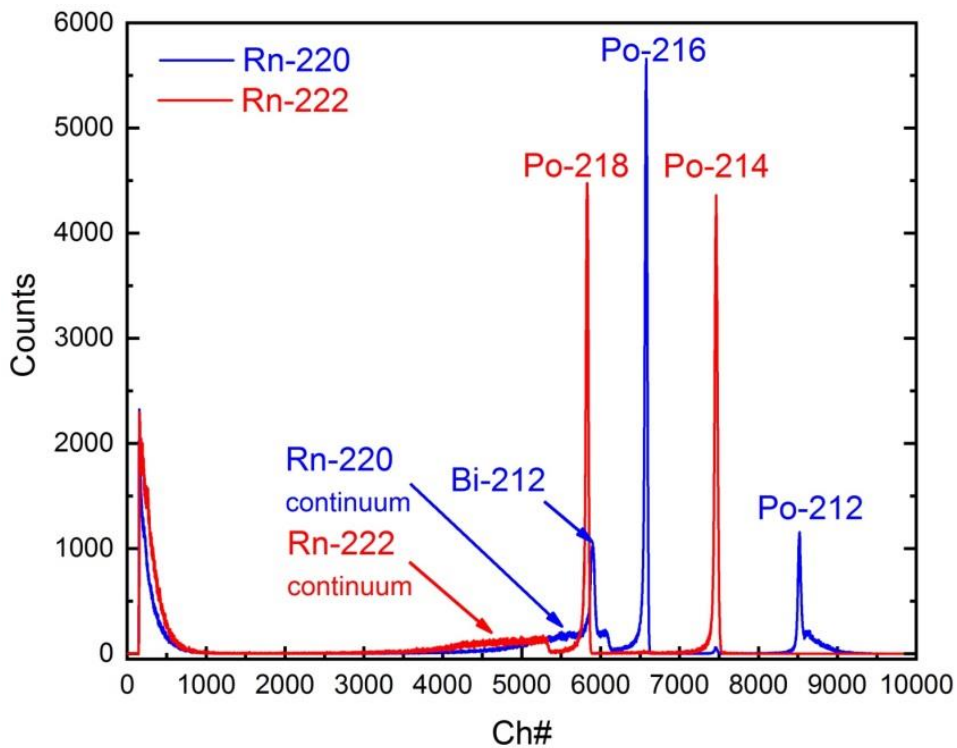


Figure A5 – Radon and Thoron spectra with their alpha-lines and the alpha lines of their short-lived progenies.

In order to make quantitative measurements, the PIPS system was first calibrated. For that purpose, the upper and the lower chamber were separated only by two nitrocellulose membrane filters (Millipore PHWP04700, pore size  $0.3\ \mu\text{m}$ ). Packs of two of these filters were previously tested and proved to be transparent to radon and thoron and to stop their progenies. Thus, the activity concentration of radon or thoron in the upper chamber is equal to that in the lower chamber (measured by the reference instrument AlphaGUARD) and all  $^{220}\text{Rn}/^{222}\text{Rn}$  progenies are generated by  $^{220}\text{Rn}/^{222}\text{Rn}$  in the upper chamber. The alpha-peaks of  $^{218}\text{Po}$  and  $^{214}\text{Po}$  (for  $^{222}\text{Rn}$ ) and  $^{216}\text{Po}$  (for  $^{220}\text{Rn}$ ) were used in the calibration and in the measurements. Therefore, the calibration and the measurements are carried out after secular equilibrium between the

nuclides in the corresponding decay chain is reached. The efficiencies  $\varepsilon_i$  of the detector system for each isotope of polonium were estimated as:

$$\varepsilon = \frac{n_0}{VC_A} \quad (A1)$$

where  $n_0$  is the counting rate in the alpha-peak,  $C_A$  is activity concentration of radon or thoron and  $V = 15.64$  (18)  $\text{cm}^3$  is the volume of the upper chamber. The obtained efficiencies are shown in Table A1.

Table A1 – Counting efficiencies of the PIPS system for the alpha-peaks of  $^{218}\text{Po}$  and  $^{214}\text{Po}$  (for  $^{222}\text{Rn}$ ) and  $^{216}\text{Po}$  (for  $^{220}\text{Rn}$ ).

|             | $\varepsilon$ | $\sigma(\varepsilon)$ | $\delta(\varepsilon)$ |
|-------------|---------------|-----------------------|-----------------------|
| Po-218 (Rn) | 0.435         | 0.023                 | 5.4%                  |
| Po-214 (Rn) | 0.429         | 0.024                 | 5.4%                  |
| Po-216 (Tn) | 0.325         | 0.035                 | 11%                   |

The calibrated reference system is used for experimental determination of the radon permeability of polyethylene foils. For that purpose the polyethylene foil was placed after (closer to the upper chamber) the filters (See Fig. A2) and the pips detector was used to measure the radon (or thoron) which has penetrated in the upper volume through the membrane.

### III. Diffusion Model for Radon and Thoron transport through polymers

The diffusion model which is used hereafter is previously developed and presented in [4]. It was initially developed to study the diffusion properties of thin films. Here the model is slightly modified and adapted. In the model it is assumed that a volume, which could be considered as an infinite source of radon (Rn reservoir, see Fig. A6), is separated from a small volume by a thin film and radon will diffuse in the small volume through the film.

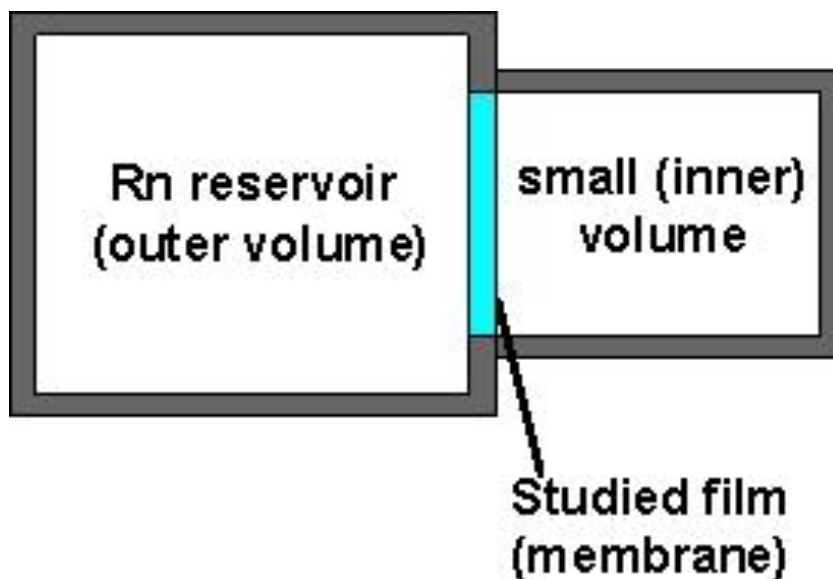


Figure A6 – Scheme of the experimental set-up assumed in the diffusion model.

The diffusion of radon through the thin film is described by the diffusion equation with additional term that accounts for the radioactive decay:

$$\frac{\partial c}{\partial t} = D \frac{\partial^2 c}{\partial x^2} - \lambda c, \quad (\text{A2})$$

where  $c$  is the radon atomic concentration,  $D$  is the diffusion coefficient of radon in the film,  $\lambda$  is the decay constant of radon,  $t$  is a time variable and  $x$  is a space coordinate in direction perpendicular to the surface of the film. The characteristic time for reaching steady state diffusion in the membrane is [4]:

$$\tau_r = (\lambda + \pi^2 D d^{-2})^{-1}, \quad (\text{A3})$$

where  $d$  is the thickness of the film. If that time is much smaller than the mean lifetime  $\tau$  of radon  $\tau_r \ll \tau$ , it can be assumed that the transport of radon through the film is under steady-state condition and Eq. (A2) becomes:

$$\frac{\partial c}{\partial t} = 0 = D \frac{\partial^2 c}{\partial x^2} - \lambda c \quad (\text{A4})$$

It is worth noting here that the condition  $\tau_r \ll \tau$  is equivalent to  $L_D \gg d$  ( $L_D = (D/\lambda)^{1/2}$  is the diffusion length of radon atoms in the polymer). Equation (A4) is solved in [4] for a thin film and the solution is:

$$C_{in}(t) = C_{out} \frac{SD}{VL_D(\lambda + \lambda_d) \sinh(d/L_D)} (1 - e^{-(\lambda + \lambda_d)t}) \quad (\text{A5})$$

where  $C_{in}$  and  $C_{out}$  are the activity concentration in the inner and outer volume (see Fig. A6),  $S$  is the surface of the membrane,  $V$  is the volume of the inner volume and  $\lambda_d$  is given by:

$$\lambda_d = \frac{SD}{VL_D \tanh(d/L_D)} \quad (\text{A6})$$

However, this solution does not account for the partition coefficient of the membrane. Taking into accounting the partition coefficient  $K$  of the membrane, Eqs. (A5) and (A6) take the form:

$$C_{in}(t) = C_{out} \frac{SP}{VL_D(\lambda + \lambda_d) \sinh(d/L_D)} (1 - e^{-(\lambda + \lambda_d)t}) \xrightarrow{L_D \gg d} C_{out} \frac{\lambda_d}{(\lambda + \lambda_d)} (1 - e^{-(\lambda + \lambda_d)t}) \quad (\text{A7})$$

and

$$\lambda_d = \frac{SP}{VL_D \tanh(d/L_D)} \xrightarrow{L_D \gg d} \frac{SP}{Vd} \quad (\text{A8})$$

where  $P = KD$  is the permeability of the membrane.

Finally, after a certain time  $t_{eq} \gg (\lambda + \lambda_d)^{-1}$  an equilibrium is reached and Eq. (A7) simplifies to:

$$C_{in}(t_{eq}) = C_{out} \frac{\lambda_d}{(\lambda + \lambda_d)} = C_{out} \frac{1}{(1 + \frac{\lambda}{\lambda_d})} \quad (\text{A9})$$

It can be seen from Eqs. (A7)-(A9) that, for a well-defined volume which is separated from the ambient air by a diffusion membrane with given surface and thickness, the ratio  $C_{in}/C_{out}$  depends only on the permeability of the membrane. It follows that:

- If the permeability of the membrane is known then the transmission ratio  $C_{in}/C_{out}$  could be estimated, which is essentially the transmission (or attenuation) factor of the membrane for the isotope of interest.
- If the transmission ratio  $C_{in}/C_{out}$  is measured then the permeability of the membrane can be calculated.

It is worth noting here that the experimental system with the CEA/LNHB detector, which was described in the previous chapter, is very convenient for measurement of the permeability of polymer foils. The foil to be studied is placed between the two volumes (see Fig. A7) and the outside concentration ( $C_{out}$ ) is measured with the reference monitor (AlphaGuard) and the inside concentration is measured with the PIPS detector ( $C_{in}$ ).

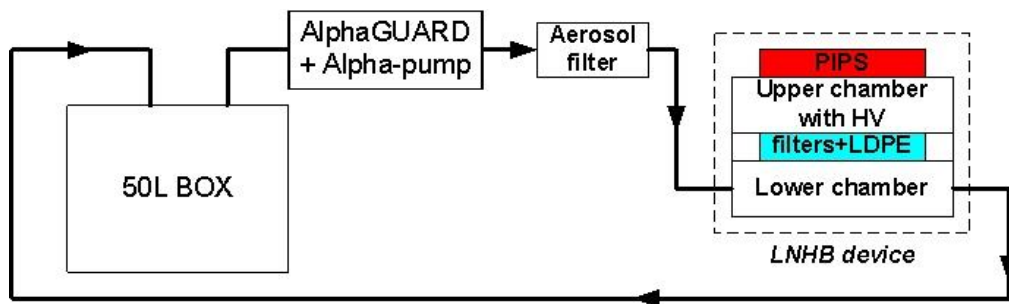


Figure A7 – Scheme of the experimental set-up used for the determination of the permeability of low density polyethylene (LDPE).

**This approach allows direct and accurate determination of the permeability of the membrane.** The approach is different and independent of the approach used in Task A.2.3.2 to determine radon transport properties of the foils [1], and it is therefore interesting and important to compare and validate both techniques.

#### IV. Validation of radon transport parameters in polyethylene.

A series of experiments were carried out at different temperatures in order to cross-check and validate the dependencies  $L_D(T)$  and  $K(T)$ , which were determined previously in Task A.2.3.2 (see also [1]). The experimental setup shown in Fig. A7 was used. A low density polyethylene (LDPE) membrane with thickness  $d = 91 \mu\text{m}$  and with already known diffusion properties (incl. permeability) [1] was used. It was placed after the nitrocellulose filters (closer to the upper chamber) in the PIPS system. Three exposures at three different temperatures were carried out. The activity concentration of radon in the upper chamber of the PIPS system (corresponding to  $C_{in}$ ) was estimated by the already calibrated PIPS system and the activity concentration in the lower chamber of the PIPS system (corresponding to  $C_{out}$ ) was estimated by the AlphaGUARD. In this way the ratio  $C_{in} / C_{out}$  was experimentally estimated. The ratio  $C_{in} / C_{out}$  was also estimated from the theoretical model, using the  $L_D(T)$  and  $K(T)$  dependencies published in [1]. Figure A8 shows the measured  $C_{in} / C_{out}$  ratios as well as the  $C_{in} / C_{out}(T)$  dependence expected from the model.

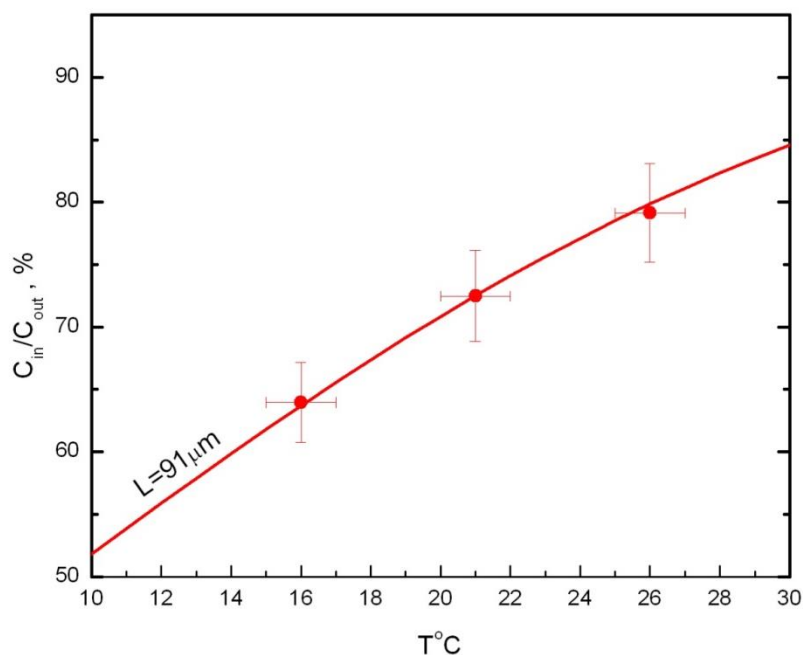


Figure A8. Comparison between experimentally measured  $C_{in} / C_{out}$  ratios with the PIPS system and the diffusion model (solid line), which uses the  $L_D(T)$  and  $K(T)$  data published in [1].

The results in Fig. A8 indicate an excellent agreement between the measurements and the model. This agreement confirms (by a different experimental technique) the validity of the  $L_D(T)$ ,  $K(T)$  and  $P(T)$  data for polyethylene published in [1]. Thus, the radon and thoron transmission factors (or attenuation factors) of a polyethylene membrane can be calculated by Eq. A9 using the permeability data published in [1].

The CEA/LNHB reference system is very useful for the determination of radon or thoron permeability of polymer foils. Due to its high energy resolution, it is also appropriate for permeability measurements in mixed radon and thoron atmospheres. It should be noted that during the experiments in the framework of this activity it was observed that the radon absorption properties of the polyethylene may vary slightly between polyethylene of different batches or producers, probably due to differences in the production process. Thus, it is important to emphasize that a reference system with a PIPS detector, like the one developed at CEA/LNHB, is very convenient for measurement of radon transport properties of polyethylene membranes.

## References

1. Georgiev S., Mitev, K., Dutsov, Ch., Boshkova, T., Dimitrova I., 2019. Partition coefficients and diffusion lengths of  $^{222}\text{Rn}$  in some polymers at different temperatures. Int. J. Env. Res. Publ. Health, 16, 4523.
2. B. Sabot, S. Pierre, N. Michielsen, S. Bondiguel, P. Cassette, A new thoron atmosphere reference measurement system, Applied Radiation and Isotopes, 109, 2016, 205-209
3. B. Sabot, Calibration of thoron activity concentration monitors, PhD Thesis defended on 25th November 2015 in Gif-sur-Yvette, France, NNT2015SACLS122, <https://tel.archives-ouvertes.fr/tel-01253649>
4. Ronald B. Mosley, Description of a Method for Measuring the Diffusion Coefficient of Thin Films to  $^{222}\text{Rn}$  Using a Total Alpha Detector, 1996 International Radon Symposium 29.9-02.10.1996, Haines City, FL, USA



# 16ENV10 MetroRADON

## Deliverable D2

### Annex XVI

#### Task A.2.3.4

Methods for reduction of  
thoron-related bias in the radon signal of  
existing radon monitors

K. Mitev, S. Georgiev

SUBG

## **Table of contents**

|   |          |
|---|----------|
| <b>I. Introduction.....</b>   | <b>3</b> |
| <b>II. Reduction of thoron influence by packing in polyethylene foils. Practical aspects. ....</b>                        | <b>5</b> |
| <b>III. Reduction of thoron influence by packing in polyethylene foils and performing differential measurements. ....</b> | <b>8</b> |

## I. Introduction

It was already shown in activities A2.3.2 (Annex XIII) and A.2.3.3 (Annex XV) that the amorphous (rubbery) polyethylene is a very appropriate material for development of thoron barriers. It is a hydrophobic and bio-inert polymer, which is easy for temperature welding, and has the highest radon permeability among the tested polymers.

The concept of reduction of thoron influence on radon monitors by packing in polyethylene is illustrated in Fig. A1. The Radon-222 atoms from the outside can enter in the packed volume by diffusion through the polyethylene membrane due to its high radon permeability, while most of the  $^{220}\text{Rn}$  atoms will decay before entering in the packed volume, due to the short half-life of  $^{220}\text{Rn}$ .

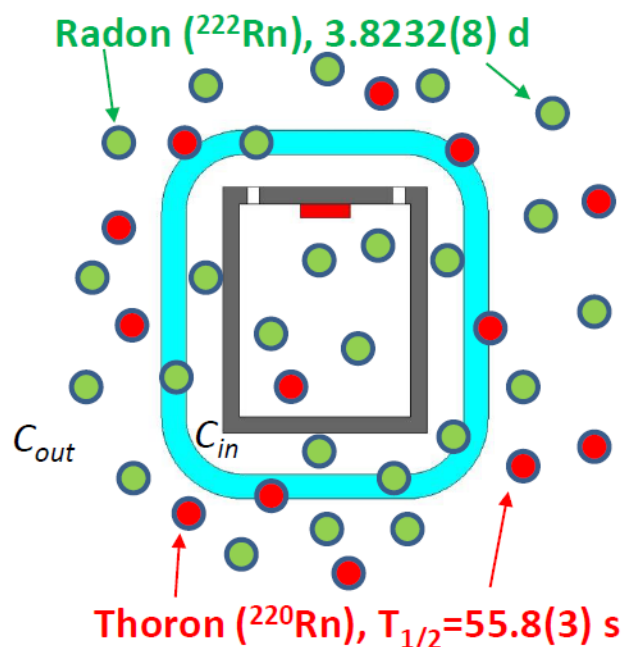


Figure A1. Illustration of the idea for the usage of polymer foils as thoron barriers.

The process of transport of  $^{222}\text{Rn}$  and/or  $^{220}\text{Rn}$  through the polymer is governed by the diffusion equation, taking into account the radioactive decay:

$$\frac{\partial c}{\partial t} = D \frac{\partial^2 c}{\partial x^2} - \lambda c, \quad (\text{A1})$$

where  $c$  is the radon atomic concentration,  $D$  is the diffusion coefficient of radon in the film,  $\lambda$  is the decay constant of radon,  $t$  is a time variable and  $x$  is a space coordinate in direction perpendicular to the surface of the polymer. Under the common assumptions of steady state diffusion and diffusion length of the gas in the material much greater than the thickness of the membrane, the ratio of the radon (or thoron) activity concentration inside the packed volume ( $C_{in}$ ) to that outside ( $C_{out}$ ) is given by:

$$R_{tr} = \frac{C_{in}}{C_{out}} = \frac{1}{\left(1 + \frac{\lambda}{\lambda_d}\right)}, \quad (\text{A2})$$

where  $\lambda_d = \frac{SP}{Vd}$  with  $S$  being the surface through which the gas can diffuse in the volume ( $V$ ) and  $P$  is the permeability of the membrane.  $R_{tr}$  is referred to as “transmission ratio”. The permeability is expressed by the partition coefficient ( $K$ ) and the diffusion

coefficient ( $D$ ) of the gas in the material through the relation  $P=KD$ . The partition coefficient and the diffusion length both depend on the temperature ( $T$ ). In the framework of Task A2.3.2 their dependence on  $T$  is evaluated in the range  $T= 5-31^{\circ}\text{C}$  (for more details see Annex XIII and Annex XV). This allows to quantify the radon diffusion properties of the polymers and to calculate the transmission ratio at different temperatures.

Note that the transmission ratio  $R_{tr}$  depends on the surface-to-volume ratio ( $S/V$ ) and on the thickness of the polymer ( $d$ ) as well as on the temperature  $T$ . In order to illustrate the applicability of polyethylene foils to stop thoron, Table A1 contains the calculated thoron transmission ratios through polyethylene packaging for 3 surface-to-volume ratios, 3 temperatures and 4 polyethylene thicknesses.

Table A1. Thoron transmission ratios through rubbery low-density polyethylene for different surface-to-volume ratios, temperatures and thicknesses of the polyethylene.

| d,<br>μm | C <sub>in</sub> /C <sub>out</sub> ratio for S/V=2 |        |        | C <sub>in</sub> /C <sub>out</sub> ratio for S/V=0.8 |        |        | C <sub>in</sub> /C <sub>out</sub> ratio for S/V=0.2 |        |        |
|----------|---|--------|--------|---|--------|--------|---|--------|--------|
|          | T=10°C  | T=20°C | T=30°C | T=10°C  | T=20°C | T=30°C | T=10°C  | T=20°C | T=30°C |
| 30       | 0.32%   | 0.72%  | 1.62%  | 0.13%   | 0.29%  | 0.65%  | 0.03%   | 0.07%  | 0.16%  |
| 50       | 0.19%   | 0.43%  | 0.97%  | 0.08%   | 0.17%  | 0.39%  | 0.02%   | 0.04%  | 0.10%  |
| 70       | 0.14%   | 0.31%  | 0.69%  | 0.05%   | 0.12%  | 0.28%  | 0.01%   | 0.03%  | 0.07%  |
| 100      | 0.10%   | 0.22%  | 0.49%  | 0.04%   | 0.09%  | 0.19%  | 0.01%   | 0.02%  | 0.05%  |

The thoron transmission factors shown in Table A1 show that polyethylene is a very effective thoron barrier. Even in the extreme scenarios of large surface to volume ratio ( $S/V=2$ ), high temperature ( $30^{\circ}\text{C}$ ) and thin polyethylene ( $30\ \mu\text{m}$ ) the inside thoron concentration is 1.62 % of the outside concentration.

As noted previously, the usage of polymer membranes as thoron diffusion barriers may introduce bias in the radon readings of the instruments, when the temperature during the measurement varies significantly with respect to that during the calibration. **Three technical approaches to cope with this possible bias are proposed hereafter:**

- Reduction of the thoron influence by packing in polyethylene foils and evaluation of the possible bias in the radon readings due to temperature variations;
- Reduction of thoron influence by packing in polyethylene foils and performing differential measurements.
- Reduction of thoron influence by packing in polyethylene foils and performing temperature correction (for active monitors with temperature record).

## II. Reduction of thoron influence by packing in polyethylene foils.

### Practical aspects.

The idea of this approach is to pack the radon detectors in polyethylene foil and use Eq. A2 and the  $K(T)$  and  $D(T)$  data from Annex XIII to estimate the possible bias that can be expected from temperature variations.

It is worth noting here that:

- The transmission ratio  $R_{tr}$  depends on the surface-to-volume ratio  $S/V$  of the packaging. The higher the  $S/V$  is, the smaller the deviation due to the temperature and the temperature sensitivity of  $R_{tr}$  are;
- The radon detectors that are packed in polyethylene foil for reduction of thoron-related bias must be calibrated **packed** in their packaging and at known and controlled temperature.

In order to illustrate the temperature dependence of  $R_{tr}$ , Tables A2-A4 show the radon and thoron transmission factors for different surface-to-volume ratios, temperatures and polyethylene thicknesses.

Table A2. Transmission factors of  $^{222}\text{Rn}$  and  $^{220}\text{Rn}$  through polyethylene packages with different  $S/V$  and  $d$  at  $T=20\text{ }^{\circ}\text{C}$ .

| T=20°C |                  |                  |                  |                  |                  |                  |
|--------|------------------|------------------|------------------|------------------|------------------|------------------|
| d, um  | S/V =2           |                  | S/V =0.8         |                  | S/V =0.2         |                  |
|        | Rn               | Tn               | Rn               | Tn               | Rn               | Tn               |
|        | $C_{in}/C_{out}$ | $C_{in}/C_{out}$ | $C_{in}/C_{out}$ | $C_{in}/C_{out}$ | $C_{in}/C_{out}$ | $C_{in}/C_{out}$ |
| 30     | 97%              | 0.72%            | 93%              | 0.29%            | 77%              | 0.07%            |
| 50     | 95%              | 0.43%            | 89%              | 0.17%            | 67%              | 0.04%            |
| 70     | 93%              | 0.31%            | 85%              | 0.12%            | 59%              | 0.03%            |
| 100    | 91%              | 0.22%            | 80%              | 0.09%            | 50%              | 0.02%            |

Table A3. Transmission factors of  $^{222}\text{Rn}$  and  $^{220}\text{Rn}$  through polyethylene packages with different  $S/V$  and  $d$  at  $T=10\text{ }^{\circ}\text{C}$ .

| T=10°C |                  |                  |                  |                  |                  |                  |
|--------|------------------|------------------|------------------|------------------|------------------|------------------|
| d, um  | S/V =2           |                  | S/V =0.8         |                  | S/V =0.2         |                  |
|        | Rn               | Tn               | Rn               | Tn               | Rn               | Tn               |
|        | $C_{in}/C_{out}$ | $C_{in}/C_{out}$ | $C_{in}/C_{out}$ | $C_{in}/C_{out}$ | $C_{in}/C_{out}$ | $C_{in}/C_{out}$ |
| 30     | 94%              | 0.32%            | 86%              | 0.13%            | 60%              | 0.03%            |
| 50     | 90%              | 0.19%            | 78%              | 0.08%            | 48%              | 0.02%            |
| 70     | 86%              | 0.14%            | 72%              | 0.05%            | 39%              | 0.01%            |
| 100    | 81%              | 0.10%            | 64%              | 0.04%            | 31%              | 0.01%            |

Table A4. Transmission factors of  $^{222}\text{Rn}$  and  $^{220}\text{Rn}$  through polyethylene packages with different  $S/V$  and  $d$  at  $T=30\text{ }^{\circ}\text{C}$ .

| T=30°C |                  |                  |                  |                  |                  |                  |
|--------|------------------|------------------|------------------|------------------|------------------|------------------|
|        | S/V =2           |                  | S/V =0.8         |                  | S/V =0.2         |                  |
| d, um  | Rn               | Tn               | Rn               | Tn               | Rn               | Tn               |
|        | $C_{in}/C_{out}$ | $C_{in}/C_{out}$ | $C_{in}/C_{out}$ | $C_{in}/C_{out}$ | $C_{in}/C_{out}$ | $C_{in}/C_{out}$ |
| 30     | 99%              | 1.62%            | 97%              | 0.65%            | 89%              | 0.16%            |
| 50     | 98%              | 0.97%            | 95%              | 0.39%            | 82%              | 0.10%            |
| 70     | 97%              | 0.69%            | 93%              | 0.28%            | 77%              | 0.07%            |
| 100    | 96%              | 0.49%            | 90%              | 0.19%            | 70%              | 0.05%            |

The following is recommended for the application of this method:

1. Choose the largest practically possible  $S/V$  ratio for the packaging;
2. Choose polyethylene membrane with thickness in the range 30-100  $\mu\text{m}$ . Small thicknesses should be preferred in order to decrease possible bias in the radon readings. Care should be taken to avoid perforations of the packaging which may compromise the thoron barrier;
3. Calibrate the packed detector for radon measurement at known temperature, which is close to the expected temperature during the measurement;
4. Use the diffusion model (e.g. Eq. A2) and the  $P(T)$  data in Annex XIII to evaluate the  $^{220}\text{Rn}$  transmission coefficient at that temperature and check if it is acceptable;
5. Estimate the expected range of temperature variation and using the solution of the diffusion model (e.g. Eq. A2) and the  $P(T)$  data in Annex XIII calculate the expected bias due to the temperature variation;
6. With a proper choice of  $S/V$ ,  $d$  and the calibration temperature, the temperature bias in the radon readings could be kept well below 10% in most cases. If applicable, the temperature-induced bias can be taken into account into the uncertainty budget of the measurement.

In order to illustrate the above approach, in Figure A2 we plot the influence of thoron and of the temperature on the radon signal of a detector which is packed in polyethylene. It is assumed that the packed detector is calibrated at  $20\text{ }^{\circ}\text{C}$  and exposed at  $30\text{ }^{\circ}\text{C}$  (left) and  $10\text{ }^{\circ}\text{C}$  (right). The results in the figure show, that the bias induced by measurement of radon at  $30\text{ }^{\circ}\text{C}$  with a detector packed and calibrated at  $20\text{ }^{\circ}\text{C}$  is less than 4 % in a very large interval of values of the parameter  $dS/V$ . The bias induced by measurement of radon at  $10\text{ }^{\circ}\text{C}$  with a detector packed and calibrated at  $20\text{ }^{\circ}\text{C}$  is less than 8 % in a very large interval of values of the parameter  $dS/V$ .

To bring the example one step further, in Table A5 we show the change in the radon concentration inside the packaging ( $C_{in}$ ) with the exposure temperature, relative to  $T=20\text{ }^{\circ}\text{C}$ . The table highlights the importance of the choice of  $S/V$ ,  $d$  and the calibration temperature for the minimization of the temperature-induced bias in the radon signal.

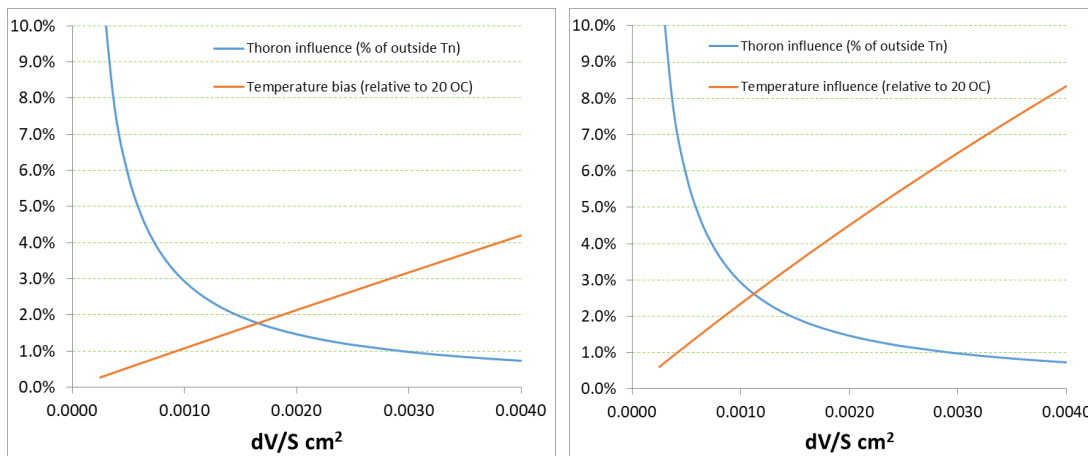


Figure A2. Illustration of the influence of temperature and thoron on the radon signal of a packed detector vs. the  $dS/V$  parameter of the packaging. Left: The detector is assumed to be calibrated for  $^{222}\text{Rn}$  measurement at  $20^\circ\text{C}$  and the measurement is assumed to be performed at  $30^\circ\text{C}$ . Right: The detector is assumed to be calibrated for  $^{222}\text{Rn}$  measurement at  $20^\circ\text{C}$  and the measurement is assumed to be performed at  $10^\circ\text{C}$  (the temperature influence is negative in this case and its absolute value is shown in the figure).

Table A5. Calculated bias in the radon signal of detectors, packed in packages with two  $S/V$  values and 4 thicknesses of the polyethylene. It is assumed that the detectors are calibrated (packed) at  $20^\circ\text{C}$  and long-term radon measurements are performed at *constant* temperatures equal to 5, 10, 15, 20, 25, 30 and  $35^\circ\text{C}$

|                   | $S/V=2\text{cm}^{-1}$                 | $S/V=0.8\text{cm}^{-1}$ |      |      |
|-------------------|---------------------------------------|-------------------------|------|------|
| d, $\mu\text{m}$  | 100                                   | 18                      | 40   | 97   |
| $T^\circ\text{C}$ | $C_{in} / C_{in}(T=20^\circ\text{C})$ |                         |      |      |
| 5                 | 82%                                   | 91%                     | 82%  | 68%  |
| 10                | 90%                                   | 95%                     | 90%  | 80%  |
| 15                | 96%                                   | 98%                     | 96%  | 91%  |
| 20                | 100%                                  | 100%                    | 100% | 100% |
| 25                | 103%                                  | 101%                    | 103% | 107% |
| 30                | 105%                                  | 102%                    | 105% | 112% |
| 35                | 107%                                  | 103%                    | 107% | 116% |

### III. Reduction of thoron influence by packing in polyethylene foils and performing differential measurements.

If the abovementioned method for reduction of the thoron bias is not applicable for some reason, we propose also the method of the differential measurements to reduce the thoron influence and account for the temperature-induced bias. The basic idea is to pack two identical passive detectors in polymer membranes with different radon diffusion properties – the most convenient way is to use membranes of the same material (polyethylene) with different thicknesses (see Fig. A3). Then, the diffusion model (Eq. A2) allows the activity concentration in the packed volumes to be estimated for the two packaging. Then, it is clearly seen that the ratio  $R=C_{in,pack1}/C_{in,pack2}$  is a function only of the parameters  $\lambda_d$  of the two packaging:

$$R(\lambda_{d1}, \lambda_{d2}) = \frac{C_{in,pack1}}{C_{in,pack2}} = \frac{\left(1 + \frac{\lambda}{\lambda_{d2}}\right)}{\left(1 + \frac{\lambda}{\lambda_{d1}}\right)} \quad (A3)$$

The ratio  $R(\lambda_{d1}, \lambda_{d2})$  depends only on the two parameters  $\lambda_{d1}$  and  $\lambda_{d2}$  and it is temperature dependent since  $\lambda_{d1}$  and  $\lambda_{d2}$  depend on the temperature. For a defined geometry of the packaging and known diffusion properties of the used membranes the temperature dependence of  $R$  could be estimated. Thus, if the ratio  $R$  is determined experimentally e.g. by the ratio of the net signal of the two detectors that were packed, the temperature could be estimated. Then the estimated temperature could be used to deduce the temperature correction for the detectors by Eq. A2.

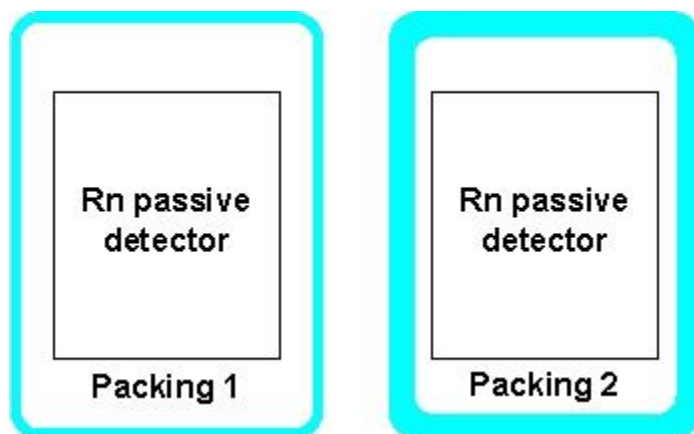


Figure A3. Two identical passive radon detectors packed identically in polymer membranes with different thickness

Using Eq. A3 the temperature sensitivity of the “detector couple” could be estimated *a priori* and some practical consideration could be drawn:

- The ratio  $R$  and the ratio  $C_{in} / C_{out}$  depend on the surface-to-volume ratio  $S/V$  of the packaging. The higher the  $S/V$  is, the smaller the temperature correction to  $C_{in} / C_{out}$  and the temperature sensitivity of  $R$  are. Varying the  $S/V$  ratio allows to modify the temperature sensitivity of the “detector couple”;
- It is better to use a “detector couple” with significant difference of  $\lambda_{d1}$  and  $\lambda_{d2}$ , resp. thicknesses of the packaging, which will improve the temperature sensitivity of  $R$ ;
- It is better one of the detectors to be packed in packaging with small  $\lambda_d$  ( $\lambda_d \ll \lambda$ ), thus the temperature correction would be smaller;

- Packaging with greater  $\lambda_d$  ( $\lambda_d$  comparable to or higher than  $\lambda$ ) would introduce decrease of the radon sensitivity of the packed detector.

Examples of the a priori estimation is shown in Table A6. We consider two types of devices: the diffusion chambers used in SUBG (cylindrical with radius  $r=3.5\text{cm}$  and height  $h=8\text{cm}$  and SSNTD Kodak Pathe LR115 II) packed in LDPE foil of different thickness (with the same  $S/V=0.8\text{cm}^{-1}$ ) and passive radon detectors with volume of  $10\text{-}20\text{ cm}^3$  (common volume for commercial devices) packed in  $100\mu\text{m}$  LDPE for which  $S/V=2\text{cm}^{-1}$  could be reached. It is seen that for some of the considered packed detectors the temperature influence is significant. With proper choice of the detector couple a good temperature sensitivity of  $R$  could be obtained. For the given example the ratio  $R(T)$  is estimated for the SUBG diffusion chambers packed in LDPE with thickness  $18\mu\text{m}$  and  $97\mu\text{m}$  and the estimated temperature sensitivity of  $R$  is about 1% per  $1^\circ\text{C}$ .

Table A6. Examples for the model estimation of the ratio  $R$  and the ratio  $C_{in} / C_{out}$  as a function of the temperature.

|                   | $S/V=2\text{cm}^{-1}$ | $S/V=0.8\text{cm}^{-1}$ |     |     |  |              |
|-------------------|-----------------------|-------------------------|-----|-----|--|--------------|
| $d, \mu\text{m}$  | 100                   | 18                      | 40  | 97  |  | 97:18        |
| $T^\circ\text{C}$ | $C_{in} / C_{out}$    |                         |     |     |  | $R(d_1:d_2)$ |
| 5                 | 74%                   | 87%                     | 75% | 55% |  | 63%          |
| 10                | 81%                   | 91%                     | 82% | 65% |  | 71%          |
| 15                | 87%                   | 94%                     | 87% | 73% |  | 78%          |
| 20                | 91%                   | 96%                     | 91% | 81% |  | 84%          |
| 25                | 94%                   | 97%                     | 94% | 86% |  | 89%          |
| 30                | 96%                   | 98%                     | 96% | 90% |  | 92%          |
| 35                | 97%                   | 99%                     | 97% | 93% |  | 95%          |

In order to validate the applicability of the differential method two experiments were carried out at SUBG. In the first experiment the diffusion chambers used in SUBG were packed in  $18\mu\text{m}$  LDPE and  $97\mu\text{m}$  LDPE and exposed to radon at different temperatures. The same type of diffusion chambers without packaging were also exposed. After the exposure at each temperature, the SSNTD were processed and counted and the ratio of the net track density  $n_0$  of the chambers packed in LDPE of the two different thicknesses was estimated as:

$$R(d_1, d_2) = \frac{n_0(d=97\mu\text{m})}{n_0(d=18\mu\text{m})} \quad (\text{A4})$$

The results are shown in Fig. A4. It is seen that a good agreement between the experimental and the model results for the ratio  $R$  is observed. Furthermore, the experimentally estimated  $R$  (shown in Fig. A4) was used to deduce the exposure temperatures, assuming that they were unknown and a good agreement with the actual exposure temperatures is observed (see Table A7). The estimated temperatures were used to estimate the transmission ratios  $R_{tr}$  (see Table A8) for the packed chambers by Eq. (A2) and to apply these ratios to correct the signal (net track density) of the packed chambers (see Table A9). It is seen in Tables A7-A9 that the temperature is estimated with relatively large uncertainty. This actually affects the uncertainties of the corrected signal of the detectors in the thicker packaging ( $d=97\mu\text{m}$ ), while the uncertainties of the detectors in thinner packaging ( $d=18\mu\text{m}$ ) are very slightly increased, which corresponds to the considerations mentioned earlier in that text. Additionally, there is very good agreement between the corrected signal and the signal of the "bare" (not packed)

chambers. This shows that, if the properties of the packaging material are known and the packaging dimensions are properly chosen, slight discrepancies between the estimated and the real exposure temperature could lead to negligible bias in the temperature correction.

Table A7. Net track density in the SSNTDs from diffusion chambers described in the text. The ratio  $R(d_1, d_2)$  is estimated by Eq. A4 and used to estimate the temperature.

| Exposure (real) temperature<br>$T_R$ °C | Net Track Density $n_0$ , $\text{cm}^{-2}$ |                     |                     | $R(d_1, d_2)$ , % | Estimated temperature<br>$T_E$ °C |       |
|---|--|---------------------|---------------------|-------------------|-----------------------------------|-------|
|   | bare                                       | $d_1=97\mu\text{m}$ | $d_2=18\mu\text{m}$ |                   |                                   |       |
| 10                                      | 7160(260)                                  | 4380(180)           | 6430(360)           | 68.1(48)          | =>                                | 9(3)  |
| 20                                      | 6360(240)                                  | 4940(250)           | 6100(240)           | 81.2(52)          | =>                                | 18(5) |
| 30                                      | 4700(210)                                  | 3870(190)           | 4400(200)           | 88.0(5.8)         | =>                                | 25(6) |

Table A8. Radon transmission ratios estimated for the packed chambers. The “bare” (not packed) chamber is assumed to have  $R_{tr}=100\%$

| Estimated temperature<br>$T_E$ °C | $R_{tr}=C_{in}/C_{out}(T_E, d)$ , % |                     |                     |
|-----------------------------------|-------------------------------------|---------------------|---------------------|
|                                   | bare                                | $d_1=97\mu\text{m}$ | $d_2=18\mu\text{m}$ |
| 9(3)                              | 100                                 | 61.0(60)            | 89.4(25)            |
| 18(5)                             | 100                                 | 76.5(64)            | 94.6(19)            |
| 25(6)                             | 100                                 | 85.2(73)            | 96.9(19)            |

Table A9. Comparison of the corrected net track densities for the packed chambers and the net track density in the bare chambers. Only chamber exposed at same temperatures should be compared.

| Estimated temperature<br>$T_E$ °C | Bare Track Density<br>$n_{0,corr}$ , $\text{cm}^{-2}$ | Corrected Track Density<br>$n_{0,corr}$ , $\text{cm}^{-2}$ |                     |
|-----------------------------------|---|--|---------------------|
|                                   |   | $d_1=97\mu\text{m}$  | $d_2=18\mu\text{m}$ |
| 9(3)                              | 7160(260)   | 7180(780)  | 7190(450)           |
| 18(5)                             | 6360(240)   | 6480(640)  | 6450(290)           |
| 25(6)                             | 4700(210)   | 4540(450)  | 4540(220)           |

It should also be noted that a systematic (but not statistically significant) bias is observed between the experimental values of  $R(T)$  and the model-estimated curve shown in Fig. A4. This could be attributed to differences in the diffusion properties of the LDPE foils used in the experiment and the one studied in Activity A2.3.2 (Annex XIII). That highlights again the importance of using characterised polymer membranes and foils.

The second experiment was carried out with the experimental setup with the CEA primary thoron system with a PIPs detector (the set-up is described in Annex XV). The permeation of two LDPE foils was studied at 26°C. The volume of the upper chamber of the PIPS system ( $V=15.64(18)\text{cm}^3$ ), the surface of the membrane ( $S=11.76(6)\text{cm}^2$ ) and the thickness of the membranes ( $d_1=91(1)\mu\text{m}$  and  $d_2=39(1)\mu\text{m}$ ) were measured precisely. The ratio  $R$  was

estimated by Eq. A2, using the  $K(T)$  and  $D(T)$  data shown in Annex XIII. The experimental value of  $R$  was estimated as:

$$R(d_1, d_2) = \frac{C_{in}/C_{out}(d=91\mu m)}{C_{in}/C_{out}(d=39\mu m)} \quad (A5)$$

where  $C_{in}(d_i)$  were measured radon concentration by the PIPS system and  $C_{out}(d_i)$  were measured by the AlphaGUARD. The results of the comparison are shown in Fig. A5.

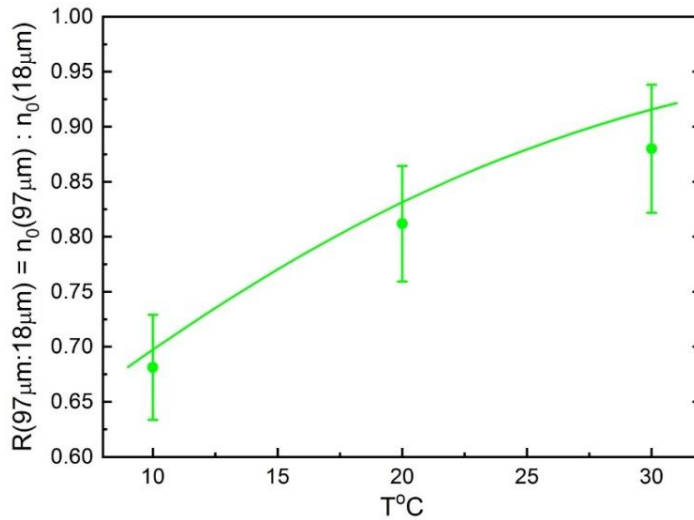


Figure A4. Comparison of the experimentally estimated ratio  $R$  for diffusion chambers packed in LDPE with two thicknesses (points) and the modelled estimation (solid line).

The example in Fig. A5 shows, that it is possible to estimate an effective radon temperature during the exposure with the differential method. It confirms the applicability of the differential method. This effective temperature can be used within Eq. A2 to correct the readings of both packed detectors for the temperature-induced bias during the measurement.

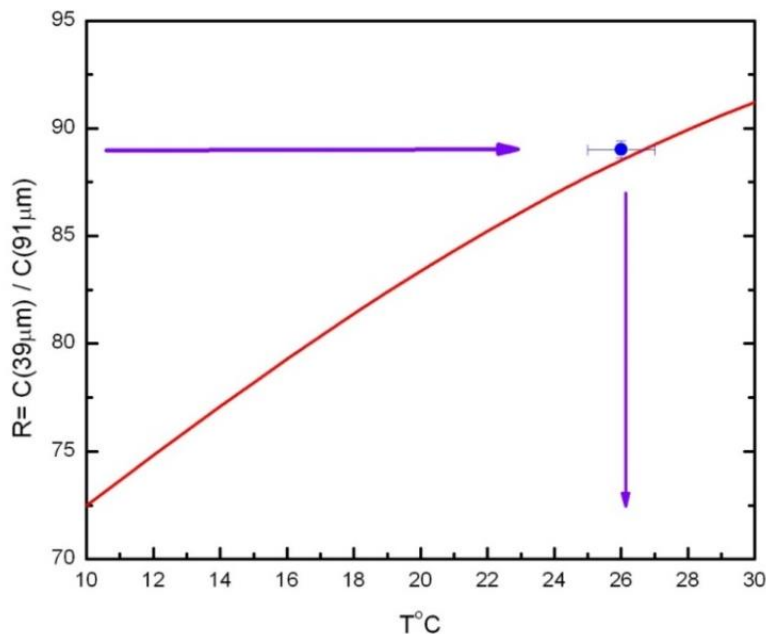


Figure A5. Comparison of the experimentally estimated ratio  $R$  for two LDPE membranes of different thicknesses separating the upper chamber of the PIPS system and the model-estimated ratio. The actual temperature was 26°C.

#### IV. Reduction of thoron influence of active instruments by packing in polyethylene foil and performing temperature correction.

This approach applies to active monitors which can record the temperature during the exposure. It is useful for monitors that apply passive radon sampling and cannot differentiate between radon and thoron by spectrometry.

The method is based on the fact that by knowing the temperature during the exposure and the  $K(T)$  and  $D(T)$  dependencies (see Annex XIII) one can apply the diffusion model and correct the temperature-induced bias in the radon signal.

In particular, if the time profile of the temperature during the exposure  $T(t)$  is known, where  $t$  indicates the time since the start of the radon measurement, then using Eq. A2 one can estimate the radon transmission factor :

$$R_{tr}(T) = \frac{C_{in}}{C_{out}} = \frac{1}{\left(1 + \frac{\lambda V d}{SP(T)}\right)}, \quad (A6)$$

where  $P(T)$  is the permeability of the polyethylene foil  $P(T)=K(T)D(T)$ . Note that knowing the temperature during the exposure means that we know the function  $T(t)$ , which implies that, for slow temperature changes, we can estimate the permeability variation with time  $P(t)$ . Substituting  $P(t)$  in Eq. A6 one gets:

$$R_{tr}(t) = \frac{C_{in}}{C_{out}} = \frac{1}{\left(1 + \frac{\lambda V d}{SP(t)}\right)} \quad (A7).$$

It follows that, if the monitor can make temperature records during the exposure ( i.e. if  $T(t)$  is known), we can estimate the time dependence of the transmission factor  $R_{tr}(t)$  and the time profile of the outside activity concentration  $C_{out}(t)$  by:

$$C_{out}(t) = \frac{C_{in}(t)}{R_{tr}(t)}, \quad (A8)$$

where  $C_{in}(t)$  is the measured radon activity concentration by the instrument at the moment  $t$  and  $R_{tr}(t)$  is calculated from Eq. A7.

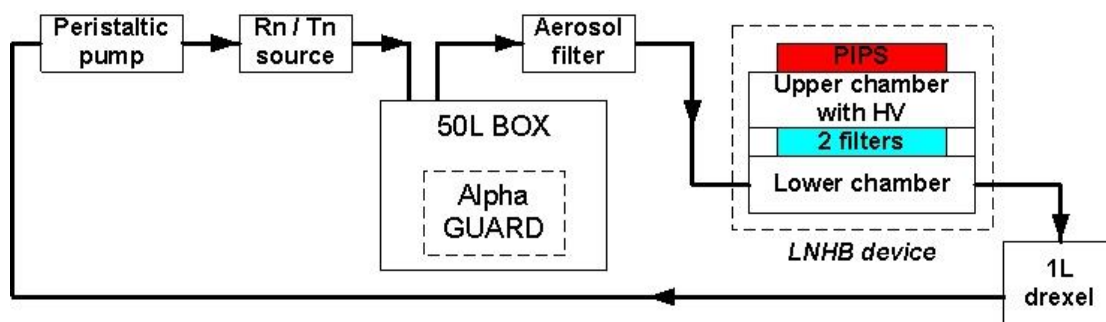


Figure A6 – Scheme of the experimental setup with the PIPS system. The PIPS detector and the upper chamber are effectively packed in the polyethylene membrane placed between the upper and the lower chamber.

The application of this approach is demonstrated using the experimental setup with the CEA primary thoron system with a PIPs detector (see Fig. A6). The upper chamber (the one with the PIPS detector) of the system was separated from the lower chamber with a LDPE foil with thickness  $d=91\mu\text{m}$  and radon with known activity concentration (measured by an AlphaGUARD) was continuously blown in the lower chamber. Thus, the upper chamber could be considered as an active monitor packed in LDPE foil. In order to make the example more illustrative, a thick foil ( $d=91\mu\text{m}$ ) was used, which introduced a significant delay in the diffusion

of radon in the upper chamber, resp. relatively small  $R_{tr}$ . Exposures at three different temperatures were carried out. Radon was promptly introduced in the system at the beginning of each exposure. The activity concentration of radon was continuously measured by the PIPS system – “the packed active monitor” and by the AlphaGUARD “outside the packaging”. The measurements at each temperature continued until equilibrium was reached. In Fig. A7 the results of the experiment are shown. The green line represents the AlphaGUARD measurement of the activity concentration “outside”, the light-blue – the PIPS measurement of the activity concentration “inside” and the dark-blue – the PIPS measurement of the activity concentration “inside” corrected by Eq. A8. A very good agreement is observed between the “outside” activity concentration and the temperature corrected measurements of the “packed” monitor, which proves the applicability of this approach.

It is worth to note that, due to the deliberated choice of the foil thickness the diffusion was seriously impeded. That was done to illustrate the potential delay in the response of an active monitor that a packing could introduce: the typical response of the PIPS system with nitrocellulose filter only is of the order of 10 minutes (time to reach equilibrium between Rn-222 and Po-218, as radon is measured by the alpha-particles of Po-218), while with the 91 $\mu$ m LDPE packing that time is increased to tens of hours.

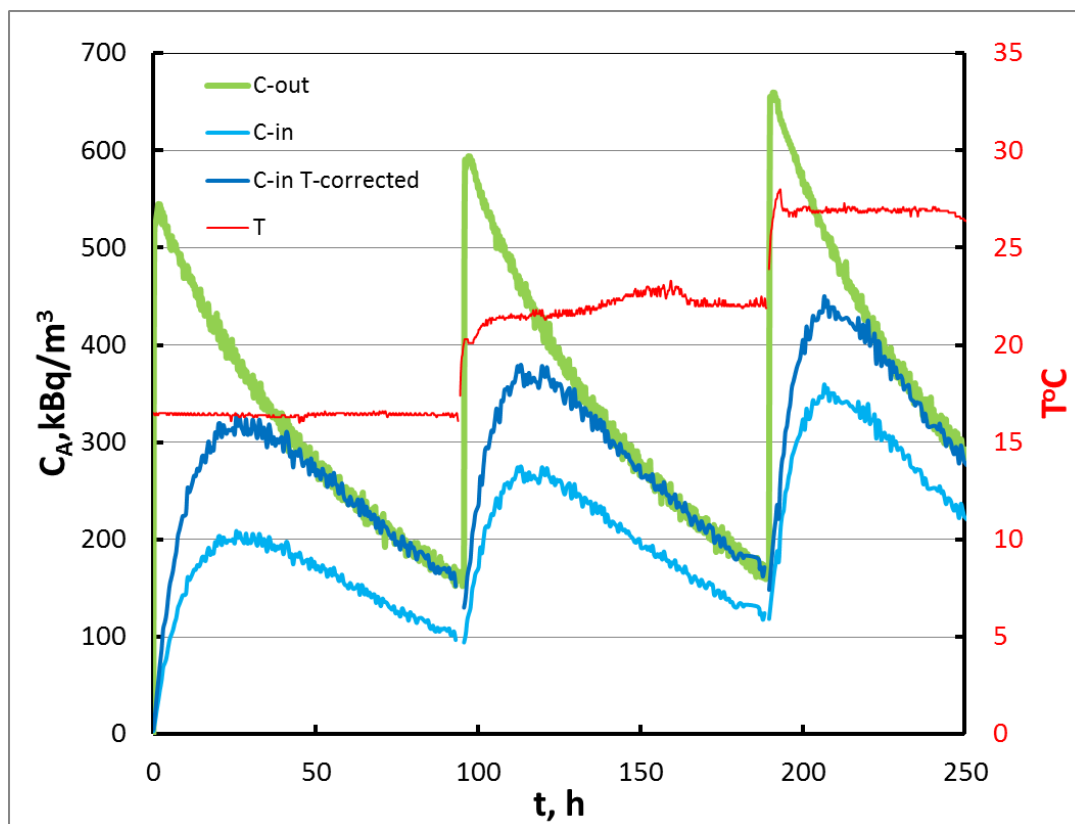


Figure A7. Example for the application of polyethylene packing of active monitor and temperature correction. The transmission ratios for the three temperatures are: 64% at 16°C, 73% at 21°C and 80% at 26°C.

The following is recommended for the application of this method:

1. Equation A8 can be used for slowly varying temperature during the measurement. For fast temperature variations the steady state diffusion equation cannot be used;
2. The largest practically possible  $S/V$  ratio for the packaging should be chosen. This will decrease the temperature-induced bias in the radon signal;
3. Polyethylene membrane with thickness in the range 30-100  $\mu\text{m}$  should be chosen. Small thicknesses should be preferred, in order to decrease the possible bias in the radon signal. Care should be taken to avoid perforations of the packaging which may compromise the thoron barrier;
4. The detector should be calibrated for radon measurement at known temperature.
5. The temperature readings of the packed detector should be used to correct the radon measurement signal by applying temperature correction of the transmission factor.